EFFECTS OF OSMOLYTES ON THE CONFORMATIONAL STABILITY AND HYDRODYNAMIC RADII OF IMMUNITY PROTEIN 9 AND HUMAN SERUM ALBUMIN

Chatuphon Charoenkitpaiboon

A thesis submitted in fulfilment of the requirements for

the Degree of Doctor of Philosophy

School of Pharmacy

University of East Anglia

2014

Abstract

Osmolytes affect protein stability through direct interactions with a protein, indirectly by perturbing the properties of the solvent water, and by a combination of these. In this thesis the conformational stability of the colicin E9 immunity protein (Im9) and Human serum albumin (HSA) were determined in the absence and presence of osmolytes (trehalose, sucrose, and glycerol) and their effective hydrodynamic radii measured in order to further explore the mechanism of stabilisation. $Urea_{1/2}$, the midpoint of the unfolding transition, and $\triangle G^{H2O}$, the free energy of unfolding, were measured in a urea-induced denaturation experiment and detected with fluorescence spectroscopy, and hydrodynamic radii (R_h) were measured with pulsed-field gradient NMR.

The unfolding curves of Im9 and HSA are shifted to higher urea concentration so that $Urea_{1/2}$ and $\triangle G^{H2O}$ increased, as the osmolyte concentration was increased indicating that Im9 and HSA are more stable in the presence of osmolytes. The R_h of Im9 and HSA increased in the presence of high concentration of trehalose and sucrose but glycerol produced a reduction. My data support the view that trehalose and sucrose act via a preferential hydration mechanism in which the water layer around the protein increases because osmolytes are excluded from the protein surface. In contrast, glycerol acts by interacting directly with the protein surface, and possibly by penetrating it, which causes the protein to become more compact as its void volume is reduced. This increase in compactness induces stabilisation.

In addition, HSA formulations were studied for their stability over 6 months under various conditions using trehalose, sucrose and glycerol as stabilisers instead of acetyltryptophan and sodium octanoate, which are used commercially. However, measurements of HSA esterase-like activity and heme binding, and its aggregation state with polyacrylamide gel electrophoresis and DLS showed the osmolytes cannot stabilize the protein under high storage temperatures.

Acknowledgement

My PhD journey has been challenging, and sometimes difficult to deal with. However, I have received support, respect, and love from my beloved people. I would like to acknowledge and give a sincere thank you to all for their love, caring, respect and compassion which I have received from them.

I would like to deeply express my sincere to my primary supervisor, Professor Geoffrey R. Moore, for working hard with me with understanding, kindness, and patience. My gratefulness also goes to my second supervisor, Professor Duncan Q. M. Craig.

Special thanks to my financial support, Government Pharmaceutical Organization (GPO), for giving me a chance to study in the UK. My gratitude goes to my colleagues who carried out my duties during the time of my study. My sincere appreciation goes to my friends at UEA, particularly my housemates, and friends in the Thailand for their support and encouraging me to undertake my study.

Lastly and the most important, I would like to thank family: father, mother, sisters, and brother who have encouraged and supported me since I started my PhD journey. Thank you all very much.

Table of Contents

List of Tables

List of Figures

Chapter 5

Abbreviations

$(NH_4)_2SO_4$	Ammonium sulphate
°C	degrees Celsius
1D ^{1}H NMR	One dimension proton NMR
A	Absorbances
Å	1Å=0.1 nm
AMPS	Ammonium per sulphate
CD	Circular dichroism
cP	Centipoise
D	Denatured state
DLS	Dynamic light scattering
DMSO	Dimethylsulphoxide
DOSY	Diffusion ordered spectroscopy
D_t	Translational diffusion coefficient
DTT	Dithiothreitol
E. coli	*Escherichia coli*
EDTA	Ethylenediaminetetraacetic acid
GdnHCl	Guanidine hydrochloride
HSA	Human serum albumin
I	Intermedaite state
ICH	International Conference on Harmonisation
Im9	E9 colicin-binding immunity protein 9
IPTG	Isopropyl-β-D-thiogalactopyranoside
K_2HPO_4	Dipotassium hydrogen phosphate
KCl	Potassium chloride
kDa	KiloDalton
KH_2PO_4	Potassium dihydrogen phosphate
k_{obs}	Pseudo-first-order rate constants or hydrolysis rate constants
LB	Luria-Bertani
M	Molar, unit of concentration (moles per litre)
m	Slope of the line which measures the dependence of $\triangle G$ on denaturant concentration
MD	Molecular dynamics

MW	Molecular weight
MWCO	Molecular weight cut-off
N	Native state
NaCl	Sodium chloride
N-Actrp	Sodium acetyltryptophan
Native-PAGE	Native or non-denaturing polyacrylamide gel electrophoresis
NP	*p*-nitrophenol
NPA	*p*-nitrophenyl acetate
Oct	Sodium octanoate
OD	Optical Density
PFG NMR	Pulsed-field gradient nuclear magnetic resonance
PMSF	Protease inhibitors
R_h	Hydrodynamic radius
RPM	Revolutions per minute
SASA	Solvent accessible surface area
SAXS	Small-angle X-ray scattering
SDS	Sodium dodecyl sulphate
SDS-PAGE	Sodium dodecyl sulphate – polyacrylamide gel electrophoresis
SEC	Size exclusion chromatography
TEMED	Tetramethylethylenediamine
TMAO	Trimethylamine-N-oxide
U	Unfolded state
$Urea_{1/2}$	Urea concentration at which 50 % of protein is unfolded
U.S. FDA	United states Food and Drug Administration
UV	Ultraviolet
v/v	Volume:volume ratio
ε	molar extinction coefficient
η	Viscosity of the solvent,
λ_{max}	Wavelength at which peak emission intensity occurs
$\triangle G$	Gibbs free energy levels
$\triangle G_{H2O}$	Conformational stability at zero molar concentration of urea

Chapter 1

General introduction

1.1 Globular proteins as therapeutic drugs

In recent years, a number of therapeutic drugs produced from biological products, such as insulin, plasma, collagen, fibrinogen, coagulation factors, monoclonal antibodies, and interferon, have been launched to the global pharmaceutical markets. Most of these products are purified proteins in a suitable formulation for delivery to patients. The protein monoclonal antibodies are the largest product category (Brekke and Sandlie 2003). However, the costs of these biological products are still high, because companies have to spend a lot of money on complex production processes and high production costs to improve their stability for storage with retained efficiency for a long time. The stabilisation and storage conditions are the most important factors in the formulation and manufacturing biological products. New techniques and stabilisers are used to improve the stability of biological products in both solid and liquid dosage forms. However, improved understanding about the interactions of proteins with their surrounding environment, such as temperature, pressure, pH, the presence of co-solutes, salts, preservatives, and surfactants, is required for further progress to be made in delivering proteins as drugs (Chi et al. 2003).

Loss of biological activity through denaturation or aggregation is often found in the formulation, production, and administration of these therapeutic drugs. Therefore, in the formulation process, the causes of aggregation and denaturation have to be indentified and alleviated by using any methods, such as process improvement, control of the environment, and the addition of stabilisers. It is important in protein stabilisation to reduce the molecular motions for reducing unfavourable conformational transitions. Water is the solvent which dominates molecular motions, protein structure and function, so the reduction in the molecular motions of the proteins are controlled by decreasing the water activity around the protein, such as removing it entirely, or exposing it to a co-solute to change its activity. It can be assumed that mechanisms for changing a protein stability are also based on surrounding water alteration.

Suitable stabilisation methods that have been proposed to modify the thermodynamic state of a protein by affecting its solvent include cooling, freezing and vitrification, or by removing most of the protein solvent, such as freeze-drying and desiccation. Each method has a different advantage, so it depends on the drug properties, drug application, or the required shelf-life of the drug which is adopted. However, most proteins lose their native configuration during harsh conditions including cooling, freezing, or desiccation. Therefore, stabilisers or osmolytes, such as sugars, polyols, and salts, are added into the protein formulation. The particular characteristics of these stabilisers are to modify the structure and the motions of water molecules, resulting in an improvement of the protein stabilisation.

1.2 Conformational stability of proteins

Normally, protein stability and protein function are studied together, although sometimes there are alterations in stability without major changes in activity. Therefore, many researchers employ methods which can detect alterations in protein-solution and protein-protein interactions that affect protein stability when changes in solution conditions that are not based on activity measurements. In addition, the results from these experiments can be used as a guideline to improve the formulation and estimate the results from changing solution or protein properties on protein stability.

Protein folding/unfolding is one of the indicators of protein stability. The conformational stability detected from the changes in a protein as it moves from its native to unfolded state is a critical approach to understanding protein stability. Normally, a lot of external factors can affect the stability of a protein such as temperature, pH, and the presence of denaturants. Therefore, conformational stability is a vital tool to determine the relationship between the structural changes and protein folding patterns.

Conformational stability can be measured and calculated from protein unfolding experiments which are the simplest methods for measuring the stability of folded conformations relative to the stability of unfolded conformations (Creighton 1997). Many factors can be used to denature the protein in this experiment, such as urea (Yao and Bolen 1995, Leggio et al. 2009), GdnHCl (Farruggia and Pico 1999), temperature (Jokiel, Klajnert and Bryszewska 2006), pH (Chalikian et al. 1997, Salahuddin 2008) or surfactant (Moriyama et al. 1996). These studies give much thermodynamic information on the forces and Gibbs free energy related to the folded/unfolded protein structure and protein compactness. Thermodynamic parameters can be evaluated from the protein folding equilibrium. The reversible folding equilibrium of a protein that follows a two-state mechanism – i.e. which folds without an intermediate state - can be written as in Equation 1.1

$$\text{Folded (Native, N)} \underset{k_f}{\overset{k_u}{\rightleftharpoons}} \text{Unfolded (Denatured, D)} \qquad \textit{Equation 1.1}$$

The transition between these conformations is determined thermodynamically by the difference in the Gibbs free energy levels (**△G**), between the two different states (folded/unfolded), which is written in Equation 1.2

$$\triangle G = G_d - G_n = \triangle H - T\triangle S \qquad \textit{Equation 1.2}$$

Equation 1.2 expresses the difference in the Gibbs free energy levels between two configurations (**△G**) as a function of the transition enthalpy (**△H**) and transition entropy (**△S**), where G_d and G_n are the Gibbs free energy of the protein in the unfolded (denatured) state and folded (native) state, respectively, and (T) is the absolute temperature.

The enthalpy of denaturation and the entropic contribution are significantly larger than the change in the Gibbs free energy and, therefore, the protein can transition spontaneously from a native to a denatured state with a slight shift in the entropic/enthalpic balance (Scharnagl, Reif and Friedrich 2005). Thus, any factor which affects one or the other can alter the free energy difference between the two states and will affect the stability of protein.

The Gibbs free energy of unfolding ($\triangle G_u$) and the equilibrium constant (K_u) for this reaction are related by Equations 1.3 and 1.4

$$\triangle G_u = -RT \ln K_u = -RT \ln (k_f/k_u) \qquad \textit{Equation 1.3}$$

$$K_u = f_U / f_F \qquad \textit{Equation 1.4}$$

where,

R is gas constant (1.987 cal mol^{-1} K^{-1});

T is the temperature in Kelvin (for 25 °C, it is 298 K).

k_f and k_u are the rate constants for folding and unfolding, respectively.

f_F and f_U are the concentrations of folded and unfolded protein, respectively.

1.3 Osmolytes and Chaotropes

Protein stability can be improved by the addition of osmolytes and this process is generally related to the shift of protein conformations toward more compact states and the inhibition of protein aggregation (Wang 1999). Moreover, the presence of osmolyte has been found to solubilise and stabilise protein in solution (Arakawa and Timasheff 1982). The choice of osmolytes is often based on previous experience, and on which osmolytes have been approved by the authorities e.g. Handbook of Pharmaceutical Excipients (Rowe 2009). However, what may be useful for one protein can have detrimental effects on another. Osmolytes are added to pharmaceutical formulations for several reasons such as anti-adsorption, oxidation protection, pH control, stabilisers, and tonicity control, and some of them may have more than one effect or purpose for being part of the formulation (Kamerzell et al. 2011).

There are many ways to categorise groups of osmolytes such as kosmotrope / chaotrope or compatible / counteracting osmolytes. Below I describe what these classifications mean.

1.3.1 Kosmotrope / chaotrope

The kosmotrope (order-maker) and chaotrope (order-breaking) are the osmolytes which stabilise or destabilise proteins, respectively. Normally, kosmotropes stabilise proteins and reduce the solubility of hydrophobic molecules, whereas chaotropes unfold proteins, increase the solubility of hydrophobic molecules, and destabilise aggregates of proteins. Moreover, the effect on the structure of water, increasing it (structure-making ions) or decreasing it (structure-breaking ions), are the effect of kosmotrope and chaotropes, respectively (Marcus 2009). Chaotropes are less polar than water and thus break hydrogen bonds between water molecules, suppressing water structure formation. In this group, compounds are classified into 2 subgroups: ionic and non-ionic kosmotrope / chaotrope.

1.3.1.1 Ionic kosmotropes and chaotropes

The behaviours of ionic kosmotropes/chaotropes are generally the same as the Hofmeister series. This series is named after the scientist who first rationalised (Hofmeister 1888, Kunz, Henle and Ninham 2004) the abilities of ions to affect the solubility of proteins in water. Small or multi-charged ions, i.e. those with a high charge density are kosmotropes, such as SO_4^{2-}, Mg^{2+}, Ca^{2+}, Li^+, Na^+, H^+, OH^-, and HPO_4^{2-}, have a stronger interaction with water molecules than water-water molecules, leading to their ability to break water-water hydrogen bonds. In contrast, large single charged ions with low charge density, such as SCN^-, $H_2PO_4^-$, HSO_4^-, HCO_3^-, I^-, Cl^-, NO_3^-, NH_4^+, Cs^+, K^+, $(NH_2)_3C^+$ and $(CH_3)_4N^+$ ions, have a weaker interaction with water than other water molecules, resulting in little effects to the hydrogen bonds of the surrounding water (Zhang and Cremer 2006).

1.3.1.2 Non-ionic kosmotropes and chaotropes

Non-ionic kosmotropes are very soluble; readily hydrated in aqueous solution, but have no net charge. Carbohydrates, polyols and most amino acids are non-ionic kosmotropes, as is urea.

1.3.2 Compatible / counteracting osmolytes

Compatible osmolytes, such as sugars and some amino acids, only affect protein stabilities, whereas counteracting osmolytes, such as trimethylamine-N-oxide (TMAO), betaine, and glycerophosphocholine, have an effect on both protein stability and function. Moreover, most of the osmolytes are categorized into three classes: polyols, amino acid, and methylamines.

A. Polyols

Many previous data on protein stabilisation (Arakawa and Timasheff 1982, Lee and Timasheff 1981, Timasheff 1993) has concerned polyols, which can stabilise proteins under harsh conditions; such as high or low temperature, acidic or basic pH, and elevated humidity. Sugars are usually used as pharmaceutical excipients to stabilise

proteins (Wang 1999). Among sugars, the disaccharides, sucrose and trehalose, are the most frequently used to protect and stabilise proteins.

B. Amino acids

The most widely used amino acids as protein stabilisers are histidine, arginine and glycine.

C. Methylamines

A commonly used methylamine to stabilise proteins is TMAO (trimethylamine-N-oxide)

1.3.3 Osmolytes used in this thesis

In this study, only sucrose, trehalose, and glycerol were chosen to be used as stabilisers because these are reported to be some of the most effective osmolytes for protein stabilisation (Shukla, Schneider and Trout 2011), and are already used in the pharmaceutical industry (Rowe 2009), and urea was used as the denaturant in unfolding experiments. The details of these osmolytes are shown in Table 1.1

Table 1.1 The details of osmolytes used in this thesis.

Chemical Name	Structure	Molecular Weight
Sucrose (α-D-glucopyranosyl-(1→2)-β-D-fructofuranoside)	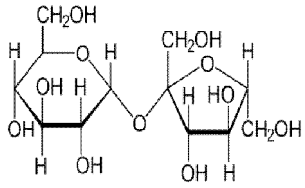	$C_{12}H_{22}O_{11}$ 342.3 g/mol (anhydrous)
Trehalose (α-D-glucopyranosyl α-D-glucopyranoside(α,α‐Trehalose)	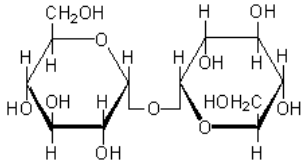	$C_{12}H_{22}O_{11} \cdot 2\ H_2O$ 378.33 g/mol (dihydrate)
Glycerol (Glycerine, 1,2,3-Propanetriol, 1,2,3-trihydroxypropane)	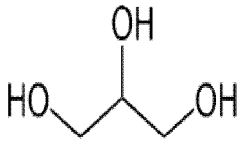	$C_3H_8O_3$ 92.09 g/mol
Urea (Carbonyl diamine)	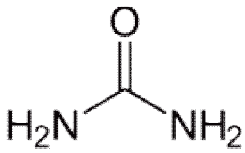	CH_4N_2O 60.06 g/mol

1.4 Measuring the conformational stability of proteins

The conformational stabilities of proteins can be measured from unfolding experiments. There are many techniques to follow the unfolding such as UV absorbance spectroscopy, fluorescence, circular dichroism (CD), NMR, and viscosity (Salahuddin 2008). In this study, fluorescence spectroscopy was used to monitor the changes in intrinsic tryptophan fluorescence in both Im9 and HSA in urea-induced denaturation transitions.

Denaturation experiments with urea as the chemical denaturant were used to study protein stability, which was calculated from the denaturation curves - a plot of Gibbs free energy as a function of the urea concentration - which allowed the stability of the proteins to be determined at zero molar concentration of urea ($\triangle G^{H2O}$).

The spectroscopic parameter reflecting the degree of unfolding was converted into the mole-fraction unfolded and plotted to give denaturation curves, which are separated into three parts - pre-transition, transition, and post-transition - as displayed in Figure 1.1. Transformation of the data of Figure 1.1 to a Gibbs free energy scale is shown in Figure 1.2. The method of estimating the conformational stability at zero molar concentration of urea ($\triangle G^{H2O}$) is to assume that the linear dependence in the transition region continues to zero urea concentration and to use a least-squares analysis of the data of $\triangle G_u$ as a function of urea concentration [Urea] to fit the data as displayed in Equation 1.5;

$$\triangle G_u = \triangle G^{H2O} - m\,[Urea] \qquad \textit{Equation 1.5}$$

where,

m is the slope of the line which measures the dependence of $\triangle G$ on denaturant concentration in cal mol^{-1} M^{-1}.

In terms of m-value, each group in the protein (i) has a free energy transfer from water to a urea solution when it is fully exposed to solvent. However, in the case of partial denaturation, only increases its exposure by a fraction (α), so the effective free energy change only in the denaturation group was calculated from this equation.

$$m = \Sigma\alpha_i\delta_i \qquad \textit{Equation 1.6}$$

The value of $\Sigma_i\alpha_i\delta_i$ can be calculated from standard values and α from the structure of the protein. A low m-value, compared with the calculated data, indicated that the protein does not become highly unfolded on denaturation. Therefore, the value of m can be used to a test for the degree of unfolding. In addition, m-value is related to the molecular size of a protein so that small proteins are less sensitive to solvent denaturation than larger ones (Fersht 1999). Small protein normally knows as a high stability protein or high resistance to the solvent denaturation, but in fact that only small change in the surface area on denaturation was usually found in small protein. In addition, the shapes of protein are the important factor of the surface area, such as native proteins in elongated-shaped have higher solvent exposure and correspondingly lower values of m-values.

As displayed in Figure 1.2, at low and high urea concentration, the conformational stability cannot be evaluated, because the very low concentration of the unfolded and folded protein produces large variations and uncertainties in equilibrium constant (K_u) at these urea concentrations. Moreover, the slope of the linear line from Equation 1.5 is termed its m-value which represents the change in the expansion of the solvent accessible surface area (SASA) between the folded and unfolded protein (Myers, Pace and Scholtz 1995).

These thermodynamic parameters ($\triangle G^{H2O}$, m-value, and $Urea_{1/2}$) are very useful to delineate the noncovalent forces stabilizing the different structural states and also can be related more directly to the structural arrangements of the protein and can provide a more detailed understanding of protein stability in co-solvents.

According to the two-step, three-state mechanism, an intermediate state (I) occurs in between the native and denatured states (N ⇆ I ⇆ D). Each step may be assumed to follow a two-state mechanism. Consequently, the fraction of the intermediate state (f_I) in the reaction N ⇆ I and the fraction of unfolded state (f_U) in the reaction I ⇆ D can be separately calculated from the experimental data (Muzammil, Kumar and Tayyab 2000, Salahuddin 2008, Varshney, Ahmad and Khan 2008).

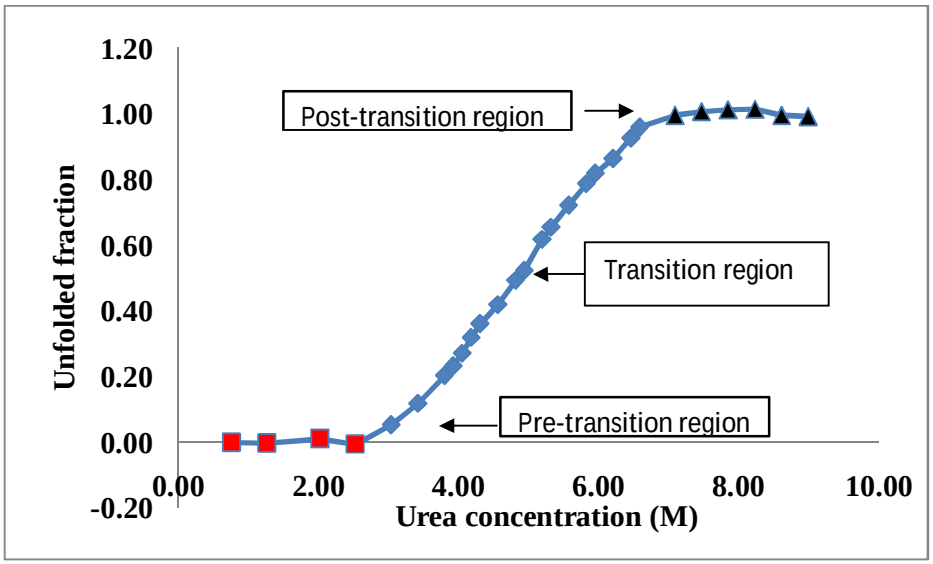

Figure 1.1 The unfolding curve of Im9 with increasing urea concentration detected by fluorescence spectroscopy at 25 °C. The excitation and emission wavelength were 295 and 340 nm, respectively. The excitation and emission slit widths were 10.0 nm each. Im9 solutions (0.21 μM) were prepared in 0.1 M phosphate buffer pH 7.0 at 25 °C with the addition of urea stock solution to obtain the desired concentrations (Pre-transition region (■), Transition region (◆), and Post-transition region (▲)).

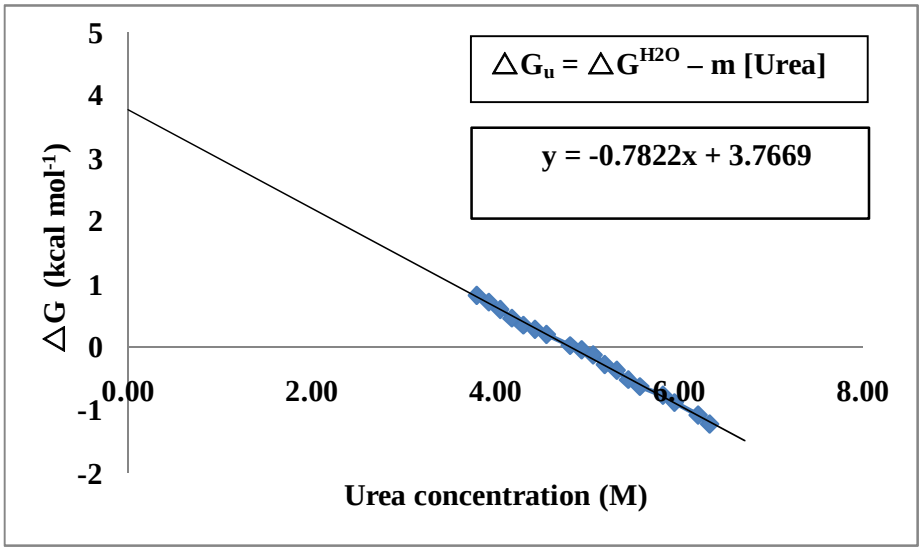

Figure 1.2 Transformation of the fluorescence data in Figure 1.1 to give a linear plot of the change in free energy versus urea concentration for urea-induced denaturation of Im9 in the absence of osmolyte.

1.5 Thermodynamic aspects to enhancing stability

To understand the conformational stability of proteins, the conformation of globular protein molecules in both their folded and unfolded states need to be characterised. The schematic view of Tanford displayed in Figure 1.3 shows a protein molecule to consist of peptide groups (rectangles) and side chains (circles) with some of them in contact with the solvent (black), and the rest within the globular structure and protected from the solvent (white). The native conformation (on the left side) is viewed as a rigid folded state, that surrounding solvent cannot access to penetrate to the interior of the folded molecule. The unfolded conformation (on the right side) looks like a random flexible coil, sufficiently extended so that most of its parts are in close contact with the surrounding solvent (Tanford 1962, Tanford 1964). Flexibility and solvent contact are two of the marked differences between the native and unfolded conformations. Since Tanford worked in 1962, many protein structures have been determined and his view has been shown to be true for many globular protein including Im9 and HSA.

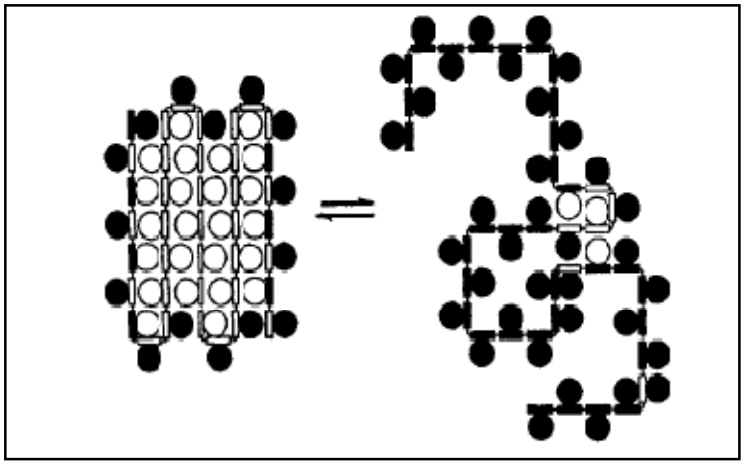

Figure 1.3 Schematic views from Tanford illustrating the changes in accessibility of protein molecule on protein unfolding. The native state (on the left side) is viewed as a rigid folded state, whereas the unfolded state (on the right side) looks like expansion state so that most of its parts are in close contact with the surrounding solvent. Rectangle-shapes are peptide groups and circle-shapes are side chains. The black colour represent groups in contact with the surrounding solvent, while the white colour represent groups shielded from the solvent by other parts of the protein molecule (Tanford 1964).

It is clear that the (unfavourable) solvophobic effect of transferring unfolded protein from buffer to osmolyte solution is critical to understanding the chemical origin of the stabilisation of proteins by protecting osmolytes. This requires the unfavourable effect of transferring unfolded protein from buffer to osmolyte solution to be considered. Using the transfer Gibbs energy measurement, the interaction between osmolytes on the protein structure in both the native and unfolded states can be explained by differences in the transfer free energies of the native and unfolded proteins from buffer to the osmolyte system, as displayed in Figure 1.4. There are four processes represented by in this diagram;

1. The unfolding reaction of the native protein in buffer solution without osmolyte ($\triangle G_1$)
2. The transfer of unfolded protein in buffer solution without osmolyte to unfolded protein in buffer solution with osmolyte ($\triangle G_2$)
3. The unfolding reaction of the native protein in buffer solution with osmolyte ($\triangle G_3$)
4. The transfer of native protein in buffer solution without osmolyte to native protein in buffer solution with osmolyte ($\triangle G_4$)

As seen in Figure 1.4, transferring native protein from buffer to osmolyte solution increase its Gibbs free energy ($\triangle G_4$), indicating to the increment in protein stabilisation by osmolyte (Liu and Bolen 1995). Moreover, the Gibbs free energy of the unfolded state ($\triangle G_2$) is increased much more than the Gibbs free energy of the folded state ($\triangle G_4$), indicating that protein molecules tend to disclose to the osmolyte solution (solvophobic process). $\triangle G_3$ is more positive than $\triangle G_1$, which means that protein unfolding in osmolyte solution is more unfavourable than unfolding in buffer solutions without osmolyte (Liu and Bolen 1995, Wang and Bolen 1997, Arakawa, Bhat and Timasheff 1990). Consequently, it can be assumed that protein stabilization by osmolytes mainly originates from destabilization of the unfolded states of proteins in osmolyte solution, and osmolytes do not materially affect the structure or functional activity of the proteins native state.

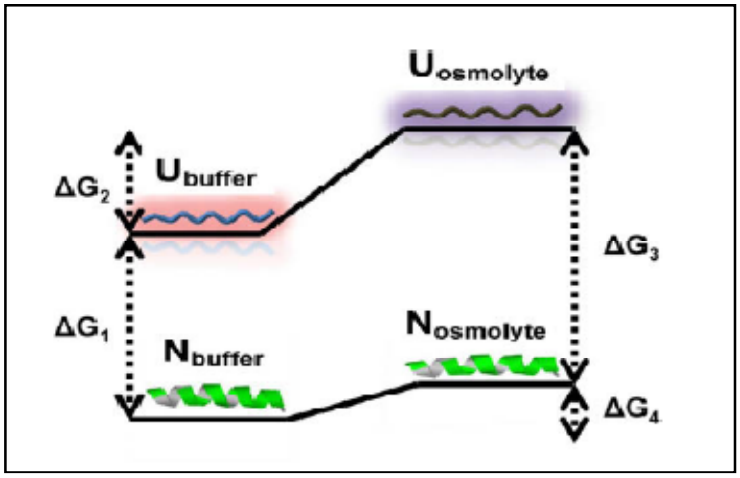

Figure 1.4 A schematic diagram (reproduced from Tanford 1964b) showing the effect of osmolytes on the protein denaturation according to the thermodynamic cycle model (Kumar 2009, Tanford 1964). Stabilisation of protein by osmolyte; the contact between the protein and osmolyte is unfavourable (positive) for both the native and denatured protein, but more positive in the denatured state.

1.6 Mechanism of enhancing stability

The mechanism of stabilisation of proteins by polyols has been primarily explained on the basis of the theory of preferential exclusion and is discussed in detail elsewhere (Gekko and Timasheff 1981a, Gekko and Timasheff 1981b, Lee and Timasheff 1981, Xie and Timasheff 1997). However, the reason for the molecular origin of such preferential exclusion is still under debate. Sugars, such as sucrose and trehalose increase the surface tension of water and are believed to be excluded from the protein domain because they increase the free energy at the protein water interface (Lin and Timasheff 1996). Glycerol on the other hand lowers the surface tension of water and has been hypothesised to preferentially hydrate proteins by enhancing the solvent ordering around the hydrophobic groups of the protein molecules (Gekko and Timasheff 1981b, Kaushik and Bhat 1998). Any increase in the hydrophobic surface area of proteins on unfolding would thus be rendered even more unfavourable in the presence of glycerol.

The interaction (both of weak and strong) are related to the interaction between osmolytes and proteins. The equilibrium dialysis experiments can explain these interactions and can be categorized into two different models as displayed in Figure 1.5. Preferential interaction (Figure 1.5A) indicated that high concentration of osmolyte was found at the protein surface more than in the bulk solution. On the other hand, preferential hydration or preferential exclusion (Figure 1.5B) showed that a number of water molecules were seen at the protein surface, but only a few molecules of osmolytes were found in the vicinity of the protein. Sugars normally do not interact chemically with the protein surface, but normally preferentially excluded from the protein surface or showed preferential hydration of the proteins (Timasheff 2002).

In addition, the mechanism of protein stabilisation by osmolytes can be explained in the interaction model: direct and indirect interaction. Direct interaction mostly is related to hydrogen bonds (H-bonds) and stabilises the native state, while indirect interaction is associated with changing the structure and dynamics of water in the solution, and enhancing the hydrophobic effect between non-polar groups. The osmolytes used in this thesis are trehalose, sucrose, and glycerol, therefore the indirect interactions, which are the main mechanism of protein stabilisation by these osmolytes, are considered in this chapter.

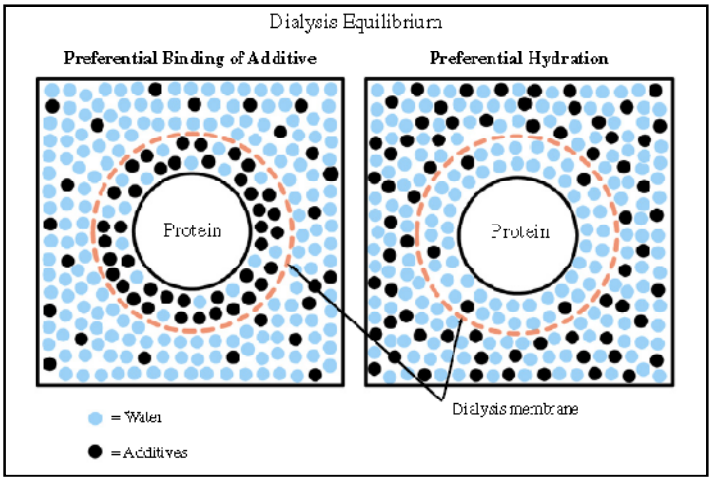

A). B).

Figure 1.5 Schematic presentation of solvent component distribution at dialysis equilibrium. A). preferential binding; at the end of experiment, the solution inside the bag has a higher concentration of the osmolyte than the bulk solution, and B). preferential exclusion or preferential hydration in a dialysis equilibrium experiment; the solution inside the bag has lower concentration of the osmolyte than the bulk solution. The white, black, and blue circles are protein, osmolyte and water molecules, respectively.

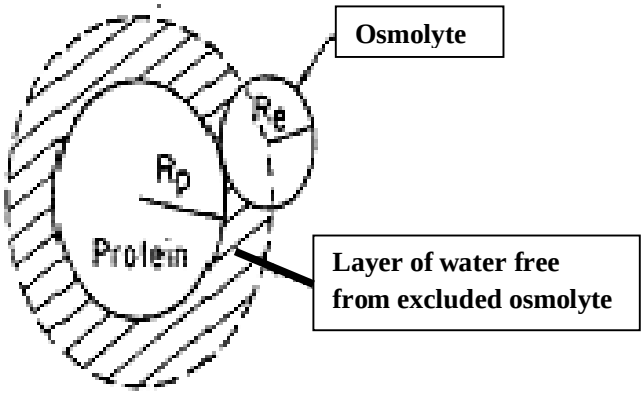

Figure 1.6 Schematic illustration of the steric excluded volume effect. R_p and R_e are the radius of the protein and the effective radius of the cosolvent, respectively. Steric exclusion is based on the difference in size between molecules of water and cosolvents. The cosolvent molecules are limited in their approach to the protein by the effective radius of the bulky cosolvent molecule. This effective shell, which is impermeable to the cosolvent for mechanism reasons, is filled with the smaller water molecules. The resulting excess of water in the vicinity of the protein is observed in dialysis equilibrium measurements as preferential exclusion of the cosolvent.

There are many possible mechanisms of protein stabilisation in liquid dosage form. However, only preferential hydration which involves the interaction with water is required to explain the effect of sugars and polyols on protein stabilisation. These mechanisms of preferential hydration (preferential exclusion) can be categorised into two parts (Timasheff 1997):

A). the mechanisms are totally independent of the chemical nature of the protein surface, so that the osmolytes and protein are inert toward each other: **Excluded volume effect (steric exclusion) and surface tension effect (cohesive force on water).**

B). the chemical properties of the protein surface are an important factor to control this mechanism, so the osmolyte can be have an interaction with the protein surface by attraction or repulsion, with repulsion often called **the solvophobic effect**.

Therefore, in this part, there are 2 sections to explain the mechanism of protein stabilisation and stabilisation mechanism of chosen osmolytes in this experiment.

1.6.1 Mechanism of protein stabilisation

1.6.1.1 Excluded volume effect (Steric exclusion)

The differences in particle size of osmolyte and water molecule are the basis of this effect. As shown in Figure 1.6, the protein surface can be considered impermeable to the osmolyte, so osmolyte cannot penetrate the protein structure. However, water molecules, which are smaller than the osmolyte, can pass through the osmolyte layer, so there are the excess of water at the protein surface that can form a hydration layer around the protein molecule.

The steric exclusion is thermodynamically unfavourable and repulsive so that when the protein surface area increases, this effect would be greater and more unfavourable. Thus, osmolytes can force the protein to the smallest solvent-exposed surface area in its equilibrium structure. Consequently, this mechanism is an important one to study and in this thesis it was achieved by measuring the effective hydrodynamic radius of stabilised and destabilised proteins.

1.6.1.2 Surface tension mechanism (Cohesive force on water)

Most stabilising osmolyte can increase the surface tension of the water. Timasheff and co-workers (Arakawa and Timasheff 1982, Lee and Timasheff 1981, Lin and Timasheff 1996, Xie and Timasheff 1997) have suggested that the ability of sugars to exert cohesive forces on water may explain their preferential exclusion from protein surfaces. The cohesive effect is reflected as surface tension increases when sugar concentration increases. Then, when the surface tension increases, the reduction of solute at the air-solution interface should be found. This surface tension effect is similar to the depletion of osmolyte near a solvated protein in the preferential hydration effect. The relationship between preferential hydration effects and surface tension increases led to the hypothesis that surface tension is the primary source of unfavourable interaction free energy between proteins and osmolytes. Therefore, it can be assumed that osmolyte-induced protein stabilisation results from the increase in solution surface tension when osmolyte is added to the solution.

1.6.1.3 Solvophobic effect

This mechanism is a type of exclusion which relies on the protein surface properties and is the cause of preferential hydration in polyols. Normally, polyols are compatible with the water lattice, and can form the hydrogen bonds which support the water interactions. Therefore, the interaction between nonpolar residues (hydrophobic) on protein surface and the polyol solution is more unfavourable than interactions with water; leading to the migration of glycerol from the protein surface and the protein becomes preferentially hydrated (Timasheff 1993).

In addition, this phenomenon is facilitated by the favourable interaction between water and the multiple hydroxyl groups found on polyols. Also this mechanism relies on the reduction of SAA of the protein to explain the enhanced protein stability.

1.6.2 Stabilisation mechanism of chosen osmolytes

1.6.2.1 Trehalose

Trehalose, a nonreducing disaccharide consists of two α, α (1→1) linked D-glucopyranose units. It has been found to be very effective in stabilising macromolecules in both solid (lyophilised products) and liquid dosage forms (Lin and Timasheff 1996, Xie and Timasheff 1997). There are three main hypotheses to explain protein stabilisation by trehalose in solution dosage forms; (1) the direct interaction between trehalose molecules and macromolecules via hydrogen bonds (water-replacement hypothesis); (2) enhancement of a hydration layer close to the protein surface (water-layer hypothesis); and (3) the entrapment of macromolecules in high viscosity trehalose or the clustering of trehalose molecules around the protein (mechanical-entrapment hypothesis).

Lerbret et al. (Lerbret et al. 2007) proposed that trehalose clusters in solution increase when the concentration of trehalose is increased because the water molecules become trapped in trehalose clusters, though even they said that they did not have sufficient data to support model. Roberto and co-workers (Roberto, Cristina and Philippe 2004) have studied their hypotheses by molecular dynamics simulations of lysozyme in the presence of 0.5 M trehalose at 25 °C and found that trehalose-trehalose and trehalose-water interactions can affect the protein-water interactions. When trehalose-trehalose hydrogen bonds increase, the trehalose-water and protein-water hydrogen bonding is decreased. Therefore, solvation properties of the hydration layer might be affected by the presence of trehalose molecules around the protein, leading to the enhancement of protein stabilisation via intra-protein effects.

Nevertheless, trehalose does not work as a universal stabiliser for all proteins. Trehalose can behave as a protein denaturant in specific proteins or in specific conditions (pH or concentration). For example, Stem bromelain was destabilised by trehalose (Habib, Khan and Younus 2007), trehalose act as denaturant in high pH condition of cutinase solution (Baptista et al. 2008), and high concentration of trehalose is also toxic to biological products (Melo et al. 2003).

1.6.2.2 Sucrose

Sucrose is one kind of sugar which increases the conformational stability of the native state of globular protein against denaturants. Lee and Timasheff (Lee and Timasheff 1981) stated from their studies of many proteins (chymotrypsin, chymotrypsinogen, ribonuclease, and tubulin) that sucrose is preferentially excluded from the protein surface and the degree of exclusion is proportionally related to the surface area of protein exposed to the solvent. In addition, only small conformational changes were proposed to occur to the protein structure detected by IR spectroscopy and near and far UV (Kendrick et al. 1997). The observed increased ordering in protein structure was not due to a large scale redistribution between secondary structure.

Sucrose and trehalose are both nonreducing disaccharides, so no chemical interaction with protein would be expected, but their efficiency of protein stabilisation manifests in different ways. Trehalose always shows a higher protein stabilisation ability than sucrose. Many researchers have studied this point and a common view is that it is likely to be because the interactions between trehalose with other molecules of trehalose and water are much better than the corresponding interactions of sucrose (Lerbret et al. 2007).

In the same way as trehalose, sucrose can behave as a protein denaturant in specific proteins, such as Stem bromelain (Habib et al. 2007) and Luciferase (Mehrabi, Hosseinkhani and Ghobadi 2008) were destabilised by sucrose.

The concentration of sucrose and trehalose used in this study are 0.25, 0.50, 0.75 M, because these are in the so-called effective range (Timasheff, Frederic M. Richards and Peter 1998) and a number of previous studies (Baptista et al. 2008) used these concentration to study the effects of osmolytes on the conformational stability of proteins.

1.6.2.3 Glycerol

Glycerol is the smallest molecule in the polyol group and is frequently used for stabilisation of macromolecules. The solvophobic effect is the basic principle of protein stabilisation due to the preferential hydration of glycerol, although the surface tension of water is reduced by glycerol and this may also be a factor (Gekko and Timasheff 1981a, Gekko and Timasheff 1981b).

Glycerol is hydrophilic molecule, which can interact favourably with water molecules (nonspecific interaction); therefore, glycerol molecules may penetrate into the solvation sheath of the protein. Moreover, the hydrophobicity of the protein can be increased in aqueous medium with glycerol. The hydrophobic residues on the protein surface would prefer to migrate into the interior of the protein to avoid contacting with the medium and can be covalently linked to the polypeptide chain of the protein, leading to tightly packing of the protein structure (Gekko and Timasheff 1981a).

Moreover, Gekko and co-workers (Gekko and Timasheff 1981a) also found that some glycerol molecules bound to the protein increasing with the glycerol concentration, and the total hydration is much smaller than the actual amount of hydration, suggesting that glycerol molecules may penetrate into the solvation shell. This might be because the complicated balance between repulsion and attraction forces from nonpolar and polar regions, respectively, of the protein surface. The preferential interactions of the hydrophobic (nonpolar) regions are different to those of hydrophilic (polar) regions, resulting in the differences in the hydration behaviour between the polar and nonpolar groups. Such as only glycerol can bind on the polar surfaces through the water hydration in the hydrophilic protein, whereas both of polar and nonpolar surfaces can be bound by glycerol in the hydrophobic proteins.

In the past few years, the mechanism of protein stabilisation by glycerol was intensely studied by molecular dynamic simulations (Vagenende, Yap and Trout 2009). They showed that electrostatic interactions, which come from the interaction of glycerol with the polar groups (N and O atoms) on the hydrophobic patches on the protein surface, are the main source of action of glycerol. Moreover, hydrogen bonding from polar sites, such as outer oxygen atoms, on the protein surface and glycerol molecules can be found in the simulation experiments. The excluded volume effect for this particular conformation is considerably larger as compared to randomly oriented

glycerol molecules. Therefore, the protein compaction resulting from preferential exclusion is significantly enhanced due to this additional excluded volume contribution. However, the protein compactness which is induced by glycerol is different from that induced by other polyols, because glycerol can decrease the volume and compressibility of protein, making the protein core denser. In addition, it is assumed that this reduction in the protein volume and compressibility is due to the release of water from the protein interior. These results are in excellent agreement with previous reports (Priev et al. 1996, Oliveira et al. 1994). Figure 1.7 displays the hypothetical structure of a solvated protein and considers it and its immediate surroundings to be composed of 6 regions. It was found that glycerol may reduce the total void volume of the protein core (region 3). This agreement leads me to believe that glycerol causes a reduction in the size of the void volume in the protein structure, which would otherwise accommodate water, leading to a decrease in the internal free volume and increasing protein compactness.

Nevertheless, while enhancement of protein stability by glycerol is true for some proteins it is not true for all, such as 6-phosphofructo-1-kinase in the presence of 37.5 % (v/v) glycerol showed lower biological activities than the control experiment under incubation at 50 °C (Faber-Barata and Sola-Penna 2005).

The concentrations of glycerol used in this thesis are 10, 20, and 30 % v/v or 1.37, 2.74, and 4.11 M. It means that the lowest % glycerol is about the highest trehalose/sucrose concentration. However, in the previous reports, these concentrations always use to compare with those concentrations (0.25, 0.50, and 0.75 M) of sucrose and trehalose.

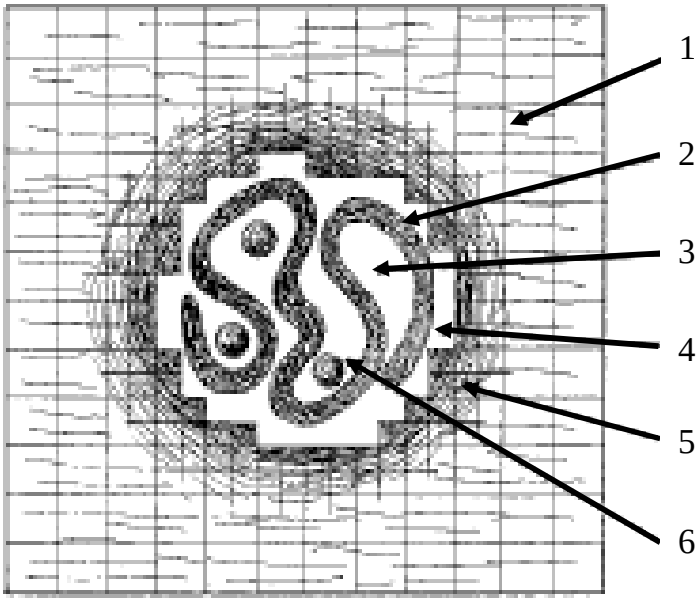

Figure 1.7 Schematic structure of a solvated protein. (reproduced from Priev 1996 (Priev et al. 1996)). This structure consists of 1). the bulk solvent; 2). the constitutive volume of the polypeptide chain itself; 3), voids or cavities formed by the polypeptide chain itself; 4), voids located at the interface between the protein and the solvents; 5), solvent at the protein-solvent interface with properties different from that of the bulk; 6), solvent molecules, which interact with the polypeptide chain only and are isolated from the solvent. Using this classification, the protein core consists of region 2+3+4, and the solvation region includes 5+6, however, the internal part of the protein can be identified with the region 2+3+6, while the surface includes region 4+5.

1.6.2.4 Urea

Urea, a small hydrophilic molecule, has been widely used as a protein denaturant in unfolding experiments, and there are a lot of studies about the mechanism of how urea denatures proteins (Frank and Franks 1968, TiradoRives, Orozco and Jorgensen 1997, Wallqvist, Covell and Thirumalai 1998, Bennion and Daggett 2003, Auton, Holthauzen and Bolen 2007, Stumpe and Grubmuller 2007). In spite of extensive studies, it has been difficult to analyse the origin of the denaturation of proteins by urea due to the small amount of the free energy transfer of globular proteins from water to aqueous urea solution. However, the current view about the action of urea in protein denaturation is that it occurs by two different mechanisms, the indirect and direct mechanisms, or a combination of them.

An “indirect mechanism” suggests that urea reduces the ability of hydrocarbon solute protein to make water structure around it, and when the water structure is disrupted, the hydrophobic interaction is weakened and the hydrophobic residues is less compact and more readily solvated, resulting in protein denaturation (Frank and Franks 1968, Zou et al. 2002).

On the other hand, a “direct mechanism” suggests that urea interact directly with the protein backbone by hydrogen bonds and other electrostatic interactions (Stumpe and Grubmuller 2007) or interact directly with amino acid residues by van der Waals attraction (Wallqvist et al. 1998, Hua et al. 2008), or both of them, leading to protein swelling and then protein denaturing. However, there is not a consensus about the predominant force that denatures proteins by this mechanism (O'Brien et al. 2007, Stumpe and Grubmuller 2007). Recently, Yang and co-workers (Yang et al. 2012) agreed with an earlier report (Hua et al. 2008) that showed that the direct interactions identified by molecular dynamics (MD) simulations of five proteins were predominantly dispersion interactions, while only a small amount of hydrogen bonds (electrostatic interaction) occurred in the denaturation process. However, some researchers (Bennion and Daggett 2003) suggest that urea denatures proteins both by means of a direct interaction on the protein backbone and indirect interaction by disrupting water structure, facilitating the exposure of nonpolar side chains to the solvent.

1.7 General aims of the thesis

In general, the addition of osmolytes, such as sugars and glycerol, to the protein solution enhances the stability of the native states of proteins over denatured states. Although there are many theories to support the mechanism of protein stabilisation by osmolytes, it is still not completely clear how they work. One approach is to understand how the particle size (hydrodynamic radius) of proteins in stabilised states by osmolytes is related to the particle size in the absence of osmolytes. As shown in the stabilisation mechanism (section 1.6.1), the formation of hydration layer was occurred in the protein in the presence of osmolytes. Therefore, the particle size of a protein in this situation would be increased when either higher concentration or larger osmolyte was added to the protein solution. This enhancement of particle size should be related to the proteins conformational stability. Furthermore, some capillary electrophoresis studies (O'Connor, Debenedetti and Carbeck 2004, O'Connor, Debenedetti and Carbeck 2007) have shown that the impact of sucrose and fructose on protein stability is related to the concentration and size of the osmolyte.

In this study, therefore, the relationship between conformational stability and hydrodynamic radius is the critical point to investigate the preferential exclusion of osmolytes in protein solution. Urea-induced denaturation and Pulsed-field gradient NMR (PFG-NMR) experiments were used to detect the stability and particle size of proteins, respectively. Moreover, two different kinds of protein (Immunity protein 9 (Im9) and Human serum albumin (HSA)) were chosen as a representative of single and multi domain protein, because the structure and stability are relatively well understood. In addition, only one tryptophan residue (Trp-74 and Trp-214) was found in Im9 and HSA, respectively, thereby simplifying their study by fluorescence spectroscopy. The results from these experiments are interpreted in terms of the interaction between protein and osmolyte. Trehalose, sucrose, and glycerol were selected as models of osmolytes. Both trehalose and sucrose are examples of non-reducing disaccharides, but trehalose is superior to sucrose as a stabiliser in protein solution. Moreover, glycerol is the smallest molecule in the polyols group. Therefore, the efficiency in protein stabilisation by these osmolytes compared to the protein stability in the absence of osmolyte should be revealing.

In addition, the stability of HSA with different osmolytes was studied to investigate the relationship between the protein stability and protein function in different storage temperatures (4, 25, and 37 °C) over long periods of time.

Consequently, these followings are the objectives and plan of the thesis:

1.7.1 To study the effects of osmolytes (trehalose, sucrose, and glycerol) on the conformational stability of Im9 and HSA by using fluorescence spectroscopy

1.7.2 To study the effects of osmolytes (trehalose, sucrose, and glycerol) on the hydrodynamic radii of Im9 and HSA using a PFG-NMR experiment

1.7.3 To study the relationship between conformational stability and hydrodynamic radii of Im9 and HSA under stabilising conditions with osmolytes.

1.7.4 To investigate whether single (Im9) and multi-domain (HSA) proteins behave differently with osmolytes

1.7.5 To study the stability of HSA in the presence of osmolytes in different storage conditions for 6 months.

Chapter 2
Materials and Methods

2.1 Materials

2.1.1 General chemicals

Tryptone, yeast extract, agar, tris base (ultrapure grade), dithiothreitol (DTT), isopropyl-β-D-thiogalactopyranoside (IPTG), and ampicillin were supplied by Formedium™, U.K. Sodium dodecyl sulphate (SDS) was supplied by Melford®, U.K. 1-4 dioxane (99.9 %, HPLC grade) was supplied by Aldrich®, U.K. Methanol (analytical grade) and urea (for molecular biology) were supplied by Sigma-Aldrich®, U.K. Trehalose and 4-nitrophenyl acetate were supplied by Sigma life science®, U.K. Hemin was supplied by Biochemika Fluka®, U.K. β-Mercaptoethanol was supplied by Acros organics®, U.K. Ultrapure protogel (30% Acrylamide:0.8% Bis-acrylamide) was supplied by National diagnostics®, U.K. Acetaldehyde (40 % solution in water) was supplied by SAFC®, U.K. Glycerol, Tetramethylethylenediamine (TEMED), sucrose, sodium chloride (NaCl), potassium chloride (KCl), ammonium persulphate (APS), Glycine, dipotassium hydrogen phosphate (K_2HPO_4), potassium dihydrogen phosphate (KH_2PO_4), and ammonium sulphate $(NH_4)_2SO_4$ were supplied by Fisher Scientific®, U.K.

2.1.2 Molecular biology

2.1.2.1 Im9

Unlabelled Im9 was prepared according to the method of (Wallis et al. 1992b) with a few modifications as shown in section 2.2.1. The Im9 concentrations were determined from the optical density of appropriate solutions using the extinction coefficient at 280 nm of 9530 M^{-1} cm^{-1} (Bijelic 2004).

2.1.2.2 Human serum albumin (HSA)

Human serum albumin was supplied by Sigma life science® as a freeze-dried powder in essentially fatty acid free grade (~99% agarose gel electrophoresis) and used without further purification. The HSA concentrations were determined from the optical

density of appropriate solutions using the extinction coefficient at 280 nm of 35700 M^{-1} cm^{-1}(Pace et al. 1995).

2.1.3 Buffers

2.1.3.1 TEM buffer: 1 mM EDTA, 50 mM Tris-HCl, 1 mM β-mercaptoethanol and adjusted pH to 7.5

2.1.3.2 Potassium phosphate buffer pH 7.0 (100 mM): 0.06 M potassium dihydrogen phosphate (KH_2PO_4), 0.04 M dipotassium hydrogen phosphate (K_2HPO_4) and adjusted to pH 7.0.

2.1.3.3 Potassium phosphate buffer pH 7.0 (50 mM): 0.03 M potassium dihydrogen phosphate (KH_2PO_4), 0.02 M dipotassium hydrogen phosphate (K_2HPO_4) and adjusted to pH 7.0.

2.1.4 Growth media

2.1.4.1 Luria-Bertani medium

Luria-Bertani medium was used for all cultures and prepared as follows:

Per litre,

Tryptone	10 g
Yeast extract	5 g
Sodium Chloride	10 g
Deionised water qs to	1 L

The medium was autoclaved at 121 °C / 15 psi for 20 min. Filter-sterilised ampicillin was added to cooled LB medium to obtain a final concentration of 100 µg/mL.

LB agar plates were prepared by adding 1.5 % agar to LB medium before autoclaving. During cooling down, filter-sterilised ampicillin was added to a final concentration of 100 µg/mL and then poured into petri dishes.

2.2 Methods

2.2.1 Protein preparation and purification of unlabelled Im9

Unlabelled Im9 was prepared according to the method of (Wallis et al. 1992b) with a few modifications. The processes which related to microbiological manipulations and growths were carried out under sterile conditions. The unlabelled Im9 was purified from 2.0 L of cell growth and the final product obtained was approximately 15 mg/L.

2.2.1.1 Transformation of cells

Competent *E. coli* JM109 cells (200 µL) were thawed on ice and plasmid pRJ345 encoding genes for Im9 added (1 µL). The mixture was gently mixed before being incubated on ice for 40 min, then heat shocked for 2 min at 42 ℃ and immediately returned to the ice for a further 5 min. After this step, 0.7 mL of warmed (37 ℃) LB medium (without antibiotic) was added and the cells were incubated at 37 ℃ for 45 min. Cells were then harvested by centrifugation in a Hermle Z 160 M microcentrifuge, spun at 10,000 rpm for 5 min. The supernatant (0.55 mL) was removed and discarded, and the cell pellet was resuspended in the rest of the supernatant. The resuspended cells (200 µL) were spread onto an LB agar plate containing ampicillin (100 µg/mL). The bacteria were allowed to grow at 37 ℃ overnight.

2.2.1.2 Cells growth, cells harvesting, and cells breakage

A single bacterial colony from the agar plate grown overnight was used to inoculate LB medium (5 mL) containing ampicillin (100 µg/mL). The cultures were grown for 7 hr at 37 ℃, with vigorous aeration from shaking at 200 rpm. The resulting 5 mL culture was then used to inoculate 40 mL of LB medium containing ampicillin (100 µg/mL), which was grown overnight (in a 250 mL conical flask) at 37 ℃ with vigorous aerating (200 rpm). The culture was used to inoculate 4 x 500 mL of LB medium (in 2 L of conical flask), containing ampicillin (100 mg/mL). These flasks were vigorous aerated at 37 °C, 200 rpm until the Optical Density (OD) at 600 nm reached about 0.6-0.8. Protein expression was induced at this step by the addition of filter-sterilised IPTG (1 mM final concentration) and allowed to grow for 3 hr. After this step, the resulting cells were harvested by centrifugation in a Beckman Avanti™ Centrifuge J-25 at 4 ℃ (15 min, 7000 RPM, JLA 9100). The supernatant was discarded and the pellets were resuspended in a small volume of supernatant. The cells were then harvested again by centrifugation at 4 °C (15 min, 8000 RPM, JA20). The supernatant was discharged, and a small volume (about 30 mL) of TEM buffer containing 1.2 mM Protease inhibitors (PMSF) was added to the pellet to resuspend.

The efficient cell lysis was achieved by sonicating 30 mL aliquots of the cell suspension on ice with power setting 50 % for 2 cycles of 8 min 20 sec (with 5 min rest on ice between each cycle). The protein solutions were clarified by centrifugation at 4 °C (45 min, 18500 RPM, JA20) to remove the crude cell lysate. The exact volume of

supernatant was used to calculate the amount of ammonium sulphate which used for protein precipitation at 50 % final saturation .The ammonium sulphate was slowly added to the supernatant with stirring in cold room and should allow it to dissolve before further addition. After that, the suspension kept stirring overnight in cold room. The unwanted precipitated proteins can be collected by centrifugation at 4 °C (45 min, 18500 RPM, JA20) and the supernatant containing Im9 was dialysed (by using SnakeSkin™ pleated dialysis tubing, 3500 MWCO) against 5 L of TEM buffer containing KCl (50 mM), pH 7.5 overnight in cold room to remove ammonium sulphate.

The fractions of protein in this step were identified by sodium dodecyl sulphate – polyacrylamide gel electrophoresis (SDS-PAGE) using Mini-PROTEAN® 3 Cell gel system (BIO-RAD®) apparatus (see section 2.2.1.5 for further explanation).

2.2.1.3 Anion-exchange chromatography

The first column purification step used anion exchange chromatography and was carried out at room temperature. The 5 mL anion-exchange column (HiTrap Q HP, GE Healthcare®), which was connected to an AKTAexplorer 100, GE Healthcare®, was equilibrated with five column volumes of TEM buffer containing 50 mM KCl. Then, the dialysed protein solution was filtered through a 0.45 µm Sartorius Minisart® syringe filter and was loaded onto the column. Im9 was eluted with step gradient method which consisted of potassium chloride 50 mM (low concentration) and 500 mM (high concentration) in TEM buffer. Fractions of 2.5 mL were collected and monitored by absorbance at 280. SDS-PAGE gels were run of fractions containing a high absorbance and the Im9-containing fractions were pooled and concentrated using an Amicon® Stirred Ultrafiltration Cells with YM3 membrane (MW 3000).

2.2.1.4 Gel filtration chromatography

The second column purification step used gel filtration chromatography. The concentrated Im9 solution was loaded onto a 300 mL gel-filtration column (Superdex® 75), that was previously equilibrated with potassium phosphate buffer (50 mM, pH 7.0) containing potassium chloride (200 mM), connected to an AKTAexplorer 100, GE Healthcare®, and eluted with flow rate 3 mL/min. Im9 fractions of 2.5 mL were pooled

and dialysed against deionised water overnight in cold room to remove salts before lyophilisation. The product obtained was stored at -60 °C.

2.2.1.5 Sodium dodecyl sulphate polyacrylamide gel electrophoresis

Sodium dodecyl sulphate polyacrylamide gel electrophoresis (SDS-PAGE) is a normally used technique to not only identify and characterize protein mixtures but also detect aggregation and estimate the relative molecular weight of proteins. Polyacrylamide gel at 15 % was prepared by using the Mini-PROTEAN® 3 Cell gel system (BIO-RAD®). The SDS-PAGE gels were consisted of resolving (separating) and stacking gel and the composition of these gels are shown in Table 2.1.

Table 2.1 Resolving and stacking gel components for SDS-PAGE.

Components	Resolving gel	Stacking gel
30 % Acrylamide:0.8 % Bis-acrylamide	2.50 mL	1.11 mL
1 M Tris, pH 8.8	1.87 mL	-
1 M Tris, pH 6.8	-	0.83 mL
10 % SDS	50 µL	66 µL
Deionised water	0.60 mL	4.64 mL
TEMED	3.30 µL	6.60 µL
10 % AMPS	33 µL	33 µL

Protein samples (10 µL) were diluted with 20 µL loading buffer (Tris, 1 M, pH 6.8; dithiothreitol, DTT, 200 mM; glycerol, 20 %; SDS, 4 %; bromophenol blue, 0.03 %) and boiled at 95 °C, for 5 min before loading onto the gel. Precision Plus Protein™ standards (unstained, BIO-RAD®) were used for reference markers. The gels were run with running buffer (Tris, 25 mM; glycine, 250 mM; SDS, 0.1 %) at a constant voltage of 200 V. Gels were stained with Coomassie brilliant blue solution (Coomassie brilliant blue, 0.1 % w/v; acetic acid, 10 % v/v; methanol, 50 % v/v, in water) and were destained with a solution containing acetic acid, 10 % v/v; and methanol, 10 % v/v, in water.

2.2.1.6 Protein concentration measurement

Protein concentration was determined with UV-Visible spectroscopy using a Lamda Bio^{+} spectrometer (Perkin Elmer®) and 1 mL quartz UV-vis cells with 1cm pathlength. Proteins in solution normally exhibit maximum UV absorbance at 280 and 200 nm because of aromatic rings and peptide bonds, respectively. Therefore, the absorption peak at 280 nm has been used for measuring protein concentration.

First, the reference buffer was placed into a cell and the spectrum recorded to ensure that the absorbance reading of the buffer at 280 nm was zero. Then, the protein solution was added to the sample cell. The cuvette was inverted several times to mix the content before the absorbance reading. After the absorption of the sample was established, the concentration of the protein was calculated from the Beer-Lambert Equation.

$$\mathbf{A} = \boldsymbol{\varepsilon}\,\mathbf{c}\,\mathbf{l} \qquad \textit{Equation 2.1}$$

where,

A is the absolute absorption of the protein at 280 nm;

ε is the extinction coefficient of the protein at 280 nm;

c is the molar concentration;

l is the path length in cm.

2.2.2 Conformational stability experiments

2.2.2.1 Preparation of Urea solution

Preparation of 10 M urea solutions was slightly modified from the literature (Creighton 1997). Urea was dissolved in 0.1 M phosphate buffer pH 7.0 and kept stirring at 40-50 °C for at least 1 hr until a clear solution was obtained. The pH of the urea solution was adjusted by the addition of 6 M HCl to pH 7.0. After that, this solution was sealed and left at 37 °C. Urea stock solution should be used on the day it was prepared because urea can degrade to cyanate which can interact with amino groups and affect protein stability, function and/or protein activity (Stark, Stein and Moore 1960).

The urea concentration was determined using the refractive index (detected by refractometer) of urea and solvent, as displayed in Equation 2.2 (Creighton 1997).

Urea Molarity = 117.66 (△N) + 29.753 (△N)^2 + 185.56 (△N)^3 *Equation 2.2*

where,

△N is the difference in refractive index between the urea solution and phosphate buffer.

2.2.2.2 Sample preparation for urea-induced denaturation experiments

In this work, HSA and Im9 were used as model proteins in experiments formulated by adding different concentrations of osmolytes (trehalose, sucrose, and glycerol) as displayed in Table 2.2. Each solution used for the unfolding experiment was prepared as a separate solution as shown in Table 2.3. These solutions were prepared volumetrically by firstly mixing a fixed volume of protein stock solution (15 μM HSA and 0.21 μM Im9) with the appropriate volumes of phosphate buffer solution (0.1 M, pH 7.0) and followed by the addition of urea stock solution to obtain the desired concentration. After that, each sample solution was thoroughly vortexed and incubated for 12-16 hr at room temperature (20-25 °C) or 10 °C prior to the fluorescence measurement at that temperature.

Table 2.2 Sample formulations for unfolding experiment.

	Type of Osmolytes		
	[Trehalose] (M)	**[Sucrose] (M)**	**[Glycerol] (% v/v)**
Model proteins	**MW = 378.33**	**MW = 342.29**	**MW = 92.09**
15 μM HSA at 25 °C	0.20	0.20	5.00
	0.25	0.25	10.00
	0.30	0.30	15.00
	0.40	0.40	20.00
	0.50	0.50	30.00
	0.75	0.75	
0.21 μM Im9 at 10 °C and 25 °C	0.25	0.25	10.00
	0.50	0.50	20.00
	0.75	0.75	30.00
	1.00	1.00	40.00

Table 2.3 The compositions of sample for unfolding experiment.

No.	Urea (mL)	Phosphate Buffer (mL)	Protein (mL)	Calculated Urea concentration (M)	Total (mL)
1	0.30	3.50	0.20	0.75	4.00
2	0.50	3.30	0.20	1.25	4.00
3	0.80	3.00	0.20	2.00	4.00
4	1.00	2.80	0.20	2.50	4.00
5	1.20	2.60	0.20	3.00	4.00
6	1.35	2.45	0.20	3.38	4.00
7	1.50	2.30	0.20	3.75	4.00
8	1.55	2.25	0.20	3.88	4.00
9	1.60	2.20	0.20	4.00	4.00
10	1.65	2.15	0.20	4.13	4.00
11	1.70	2.10	0.20	4.25	4.00
12	1.75	2.05	0.20	4.38	4.00
13	1.80	2.00	0.20	4.50	4.00
14	1.85	1.95	0.20	4.63	4.00
15	1.90	1.90	0.20	4.75	4.00
16	1.95	1.85	0.20	4.88	4.00
17	2.00	1.80	0.20	5.00	4.00
19	2.10	1.70	0.20	5.25	4.00
20	2.15	1.65	0.20	5.38	4.00
21	2.20	1.60	0.20	5.50	4.00
22	2.25	1.55	0.20	5.63	4.00
23	2.30	1.50	0.20	5.76	4.00
24	2.35	1.45	0.20	5.88	4.00
25	2.40	1.40	0.20	6.01	4.00
26	2.45	1.35	0.20	6.13	4.00
27	2.50	1.30	0.20	6.26	4.00
28	2.55	1.25	0.20	6.38	4.00
29	2.60	1.20	0.20	6.51	4.00
30	2.65	1.15	0.20	6.63	4.00
32	2.95	0.85	0.20	7.38	4.00
33	3.10	0.70	0.20	7.76	4.00
34	3.20	0.60	0.20	8.01	4.00
35	3.30	0.50	0.20	8.26	4.00
36	3.40	0.40	0.20	8.51	4.00

2.2.2.3 Urea-induced denaturation experiments and data analysis

Fluorescence spectroscopy was used to detect changes in the intrinsic protein fluorescence using Perkin Elmer LS55 Luminescence spectrometer with a scan speed of 400 nm per min. The proteins were excited at 295 nm and emission spectra were recorded in the range of 300-400 nm wavelength. The excitation and emission slit widths were 5 or 10 nm each and a 1 cm pathlength quartz cuvette was used for all the experiments. The temperature was regulated with water from water bath (Julabo^{TM} F25) and was calibrated by using digital thermometer. The sample solution was incubated at 10 ℃ or 25 ℃ for 5 min before the spectra were recorded at that temperature. Five continuous fluorescence reading was set and the average of these data was recorded.

The conformational stabilities of proteins can be measured and calculated from the unfolding experiment. The denaturation curves are separated into three parts; pre-transition, transition, and post-transition. According to the two-state mechanism (N ⇆ D), only the native state, N, and the denatured state, D, are present during unfolding, and $f_F + f_U = 1$, where f_F and f_U represent the fraction protein in the folded and unfolded state. Therefore, the protein fraction unfolded (f_U) can be calculated using the following Equation (Creighton 1997).

$$f_U = (Y_F - Y) / (Y_F - Y_U) \qquad \textit{Equation 2.3}$$

where,

Y is the measured fluorescence intensity of the protein at the given urea concentration;

Y_F is the measured fluorescence intensity of the folded states;

Y_U is the measured fluorescence intensity of the unfolded states.

The equilibrium constant (K_u) and the free energy change ($\triangle G_u$) can be estimated from the following thermodynamic Equations:

$$\triangle G_u = -RT \ln K_u \qquad \textit{Equation 2.4}$$

$$K_u = f_U / f_F = f_U / (1 - f_U) = (Y_F - Y)/(Y - Y_U) \qquad \textit{Equation 2.5}$$

where,

R is gas constant (1.987 cal mol^{-1} K^{-1});

T is the temperature in Kelvin (for 25 °C, it is 298 K).

The values of Y_F and Y_U were calculated by extrapolating a least-squares analysis from the pre- and post-transition regions, respectively. The method of estimating the conformational stability at zero molar concentration of urea ($\triangle G^{H2O}$) is to assume that this linear dependence continues to zero concentration and to use a least-squares analysis of the data of $\triangle G_u$ as a function of urea concentration [Urea] to fit the data as displayed in Equation 2.6;

$$\triangle G_u = \triangle G^{H2O} - m\,[Urea] \qquad \textit{Equation 2.6}$$

where,
m is the slope of the line which measures the dependence of $\triangle G$ on denaturant concentration in cal mol^{-1} M^{-1}.

In addition, the urea concentration at the midpoint of the unfolding curve, $[Urea]_{1/2} = \triangle G^{H2O} / m$. More details of conformational stability are discussed in Chapter 3.

According to the three-state mechanism, an intermediate state (I) occurs in between the native and denatured states (N ⇆ I ⇆ D). Each step may be assumed to follow a two-state mechanism. Consequently, the fraction of the intermediate state (f_I) in the reaction N ⇆ I and the fraction of unfolded state (f_U) in the reaction I ⇆ D can be separately calculated the thermodynamic data (Salahuddin 2008).

2.2.3 Nuclear magnetic resonance spectroscopy experiments

NMR measurements were recorded on Unity*Inova* 500 MHz (Varian Inc., U.S.A.) spectrometer with diffusion probe to produce magnetic field gradients in the z-direction. The temperature was set at 10 °C or 25 °C depending on the experiments. All experiments used 5 mm diameter Wilmad® NMR tube.

2.2.3.1 Sample preparation for NMR spectroscopy experiments

2.2.3.1.1 NMR studies of Stabilized protein

For Im9 native state, a solution containing 1 mM of Im9 was dissolved in 0.6 ml of 0.1 M phosphate buffer pH 7.0. In order to minimize water content, this solution was lyophilised until dried powder was obtained, and then dissolved again in 99.9 % D_2O.

For Im9 stabilized state, Im9 in the presence of osmolytes, as displayed in Table 2.4, were dissolved in 0.1 M phosphate buffer pH 7.0, lyophilised and then dissolved in 99.9 % D_2O.

For HSA, the preparation methods were different from Im9, because HSA is already in lyophilised state. HSA in the absence and the presence of osmolytes, as displayed in Table 2.4, were dissolved in deuterated phosphate buffer pH 7.0 (0.1 M).

Samples used for Pulsed-field gradient experiment were prepared by adding 40 µl of 1 % acetaldehyde in 99.9 % D_2O to the sample solutions as an internal radius standard.

Table 2.4 Sample formulations for NMR experiment.

	Type of Osmolytes		
	[Trehalose] (M)	**[Sucrose] (M)**	**[Glycerol] (% v/v)**
Model proteins	**MW = 378.33**	**MW = 342.29**	**MW = 92.09**
1 mM HSA at 25 °C	0.20	0.20	5.00
	0.25	0.25	10.00
	0.30	0.30	15.00
	0.40	0.40	20.00
	0.50	0.50	30.00
	0.75	0.75	-
1 mM Im9 at 10 °C and 25 °C	0.25	0.25	10.00
	0.50	0.50	20.00
	0.75	0.75	30.00

2.2.3.1.2 NMR studies of Unfolded protein

Urea at concentration of 8 M was used as a chemical denaturant in this experiment, because both HSA and Im9 were totally unfolded at this concentration (Farruggia and Pico 1999, Tezuka-Kawakami et al. 2006). The preparation of urea stock solution was different from that for an unfolding experiment. Urea was deuterated by dissolving in deuterated phosphate buffer pH 7.0 (0.1M) and lyophilised until a dried powder was obtained and dissolved again in 99.9 % D_2O. The urea concentration was determined by refractive index as described in section 2.2.2.1. In this experiment, only the highest concentration for each osmolyte (0.75 M trehalose, 0.75 M sucrose, and 30 % glycerol) was examined to determine the difference in free energy change of protein in the absence and the presence of osmolytes.

Samples used for Pulsed-field gradient experiment were prepared by adding 40 µl of 1 % acetaldehyde in 99.9 % D_2O to the sample solutions as an internal radius standard.

2.2.3.2 One dimensional proton NMR

1D ^1H NMR spectra of protein and osmolytes were recorded on Unity*Inova* 500 MHz (Varian Inc., U.S.A.) spectrometer at 10 °C or 25 °C. The water signal was suppressed with a pre-saturation field in all samples.

2.2.3.3 Pulsed Field Gradient NMR (PFG NMR) spectroscopy

In this work, PFG NMR diffusion measurement was used to evaluate the hydrodynamic radius of protein in the absence and presence of different concentration of osmolytes.

Hydrodynamic or Stokes radii can be determined via translational diffusion coefficient measurements by using different techniques such as dynamic light scattering (DLS) or PFG NMR. Translation diffusion or self-diffusion is movement in the liquid state has been called Translational motion or Brownian molecule motion (Price 2009). The translational diffusion coefficient (D_t) is inversely proportional to hydrodynamic radius as described by the Stokes-Einstein Equation:

$$D_t = kT / 6\pi\eta R_h \qquad \textit{Equation 2.7}$$

where,

k is the Boltzman constant;

T is temperature in Kevin;

η is the viscosity of liquid;

R_h is the hydrodynamic radius of the molecule.

A series of 1D ^{1}H NMR experiment with varied pulsed field gradients were done in PFG NMR experiment, as displayed in Figure 2.1. The percentages of diffusion gradients were optimized for each sample to give a total decay in the protein signal of between 80 % and 90 %. In Im9 experiment, 13 gradient strengths were shifted from 1.77 to 26.62 Gauss cm^{-1} and in HSA experiment, 11 gradient strengths were shifted from 1.77 to 31.06 Gauss cm^{-1}, as displayed in Table 2.5 A and B, respectively. The maximum strength can reduce protein intensities to 10 % to 20 %. Each measurement was repeated many scans to improve the signal to noise ratio. Over the series of the diffusion experiment, the intensities of protein and osmolytes will decay exponentially with the square of the gradient area according to Equation 2.8. The decay rates of the exponential curves for the protein and polyols are proportional to their diffusion coefficient. By taking the natural log of both sides of Equation 2.8, a linear equation results, and D is calculated from the slope.

$$I = I_o \exp\left[-D (\gamma\delta G)^2 (\Delta - \delta/3)\right] \qquad \textit{Equation 2.8}$$

where,

I_o = Intensity without magnetic field gradient;

I = Intensity with magnetic field gradient;

D = Diffusion coefficient;

γ = Gyromagnetic ratio;

δ = Pulse field gradient duration;

G = Gradient strength;

Δ = Time between the pulse field gradient pulses.

As displayed in Equation 2.7, viscosity of the solution is an important parameter in diffusion coefficient interpretation. In order to overcome this, an internal radius standard was chosen to use as a viscosity probe by adding to the protein solution, so protein and internal radius standard were placed in the measurement solution together. The measured diffusion coefficient for the protein was obtained by integrating the aromatic region and aliphatic region and converted to hydrodynamic radius by comparing with internal radius standard. The hydrodynamic radius for the protein can be calculated relative to known hydrodynamic radius of internal radius standard and the ratio between the measured diffusion coefficient of internal radius standard and protein, as in this Equation 2.9 (Wilkins et al. 1999).

$$\mathbf{R_{h\ protein}} = \frac{\mathbf{D_{ref}}}{\mathbf{D_{Protein}}} \mathbf{x}\ \mathbf{R_{h\ ref}} \qquad \textit{Equation 2.9}$$

where,

$\mathbf{R_{h\ protein}}$ = the hydrodynamic radius of the protein;

$\mathbf{R_{h\ ref}}$ = the hydrodynamic radius of the internal radius standard;

$\mathbf{D_{Protein}}$ = the diffusion coefficient of the protein;

$\mathbf{D_{ref}}$ = the diffusion coefficient of the internal radius standard.

From the literature, the effect of five internal radius standard (dioxane, alanine, acetic acid, dimethylsulphoxide (DMSO), and 2,2 dimethyl-2-silapentane-5-sulphonate (DSS)) on the diffusion rate of lysozyme were studied and it was found that dioxane did not have any significant interaction with the lysozyme. Therefore, dioxane is the best choice of internal radius standard in PFG experiment. Its hydrodynamic radius is 2.12 Å (Jones et al. 1997).

Unfortunately, dioxane cannot use as an internal radius standard in this experiment, because the chemical shifts of protein and osmolytes (trehalose, sucrose, and glycerol) were found at the same position of dioxane signal (3.53 ppm). Therefore, acetaldehyde, which has two chemical shifts at 1.2 and 9.5 ppm, was used as an internal radius standard instead of dioxane. However, we have to know the exact value of the hydrodynamic radius of acetaldehyde, which was determined by calibrating it with

dioxane and to study possible interactions between acetaldehyde and our model proteins (HSA and Im9). The effect of acetaldehyde on the diffusion coefficient of proteins can be determined from the diffusion rate constant (Lapham et al. 1997) which is the slope of the line of $-\ln(I/I_0)$ versus $(\gamma\delta G)^2(\Delta-\delta/3)$ (Equation 2.8).

In addition, DOSY (Diffusion ordered spectroscopy) was used for data processing. The data can be shown in a pseudo two dimensional (2D) NMR spectrum with chemical shift in x-axis and calculated diffusion coefficients in y-axis.

2.2.4 Stability study of HSA in aqueous solution

2.2.4.1 Sample preparation and long-term stability study protocols

HSA in the highest concentration of osmolytes were used to study long term stability. HSA at a concentration of 150 µM was prepared in 0.1 M phosphate buffer pH 7.0 as a control formulation. For testing formulations, trehalose, sucrose, and glycerol were added to the HSA solution in the concentration of 0.75 M, 0.75 M, and 30 % v/v, respectively. The equipments for this preparation were autoclaved and the sterile processes were done under the laminar air flow. All formulations were sterilized by using a 0.22 µm Sartorius Minisart® syringe filter and dispensed into borosilicate glass vials (type I class A) and sealed with black plastic screw cap.

These vials were stored at three different controlled temperatures; cold room (2-8 ℃), room temperature (20±3 ℃) and accelerated temperature (37±3 ℃) without humidity control. The samples were pulled at constant intervals (1, 2, 3, 4, 5, and 6 months), and analysed as described in the following sections (2.2.4.2 and 2.2.4.3).

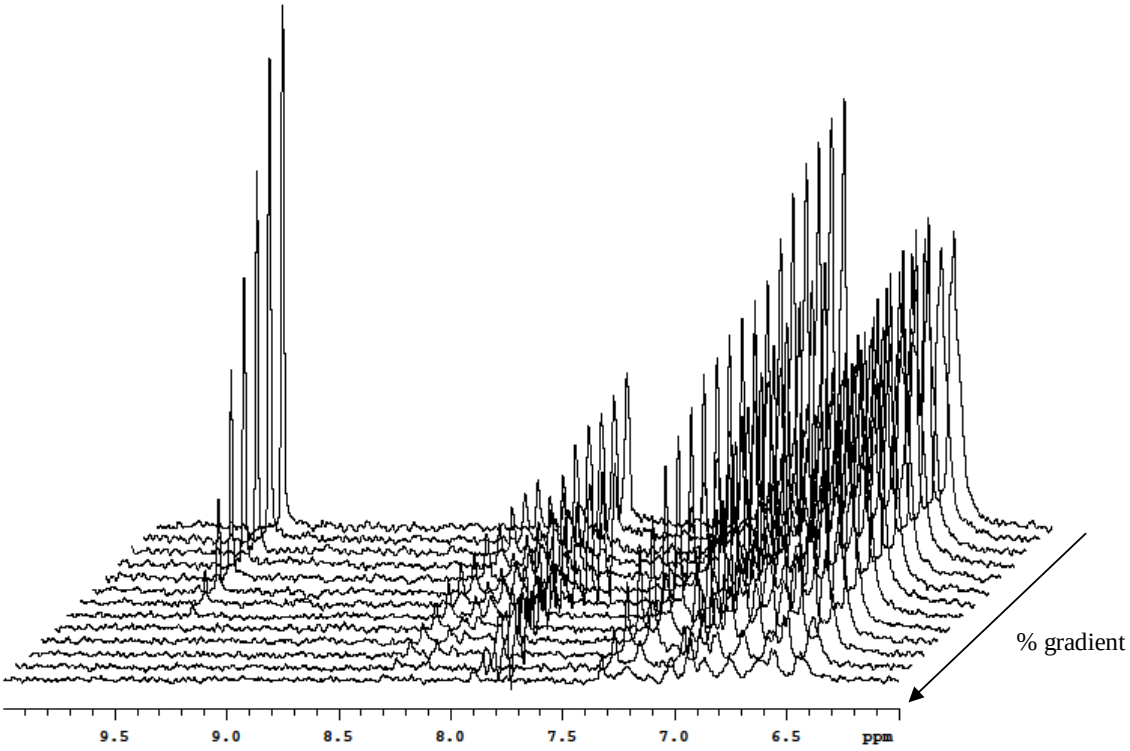

Figure 2.1 A series of 1D ^{1}H NMR diffusion spectra (expansion of the aromatic signal from 6.0 to 10.o ppm) obtained from Im9 in the presence of acetaldehyde. Im9 solution (1 mM) was prepared in deuterated phosphate buffer solution pH 7.0 with 40 µl of 1 % acetaldehyde and measured by Unity*Inova* 500 MHz spectrometer at 25 °C. The diffusion gradients were varied from minimum to maximum strength (1.77 to 26.62 G/cm). The Im9 signals (from 6.5 to 8.5 ppm) decay more slowly than the reference signal (at 9.5 ppm) as acetaldehyde diffuses more rapidly than the protein.

Table 2.5 The gradient strengths used for diffusion coefficient measurements

A) Im9

Gradient no.	Gradient strength (G/cm)	% Gradient strength
1	1.77	6.67
2	2.66	10.00
3	3.55	13.33
4	4.44	16.67
5	5.32	20.00
6	7.10	26.67
7	8.87	33.33
8	10.65	40.00
9	14.20	53.33
10	15.97	60.00
11	19.52	73.33
12	23.07	86.67
13	26.62	100.00

B). HSA

Gradient no.	Gradient strength (G/cm)	% Gradient strength
1	1.77	5.71
2	3.11	10.00
3	4.88	15.71
4	7.10	22.86
5	8.87	28.57
6	10.65	34.29
7	14.20	45.71
8	17.75	57.14
9	22.18	71.43
10	26.62	85.71
11	31.06	100.00

2.2.4.2 Biological activity

Ligand binding is one of the biological functions of HSA. In addition, it exhibits antioxidant activity, enolase-like activity, and esterase–like activity (Matsushita et al. 2004). In this work, we chose the esterase like activity and ligand binding to test the HSA biological activity in the different formulations throughout the stability testing.

2.2.4.2.1 UV Spectroscopy

Esterase-like activity can be evaluated by monitoring the appearance of *p*-nitrophenol, which was followed with time and detected by UV spectroscopy (LS35, Perkin Elmer) at 400 nm, from the reaction of *p*-nitrophenyl acetate with HSA in the absence and presence of osmolyte. The reaction was started by the addition of *p*-nitrophenyl acetate (in methanol solution, 5.5 mM) to HSA formulations in a 1 mL quartz UV-VIS cells with 1 cm pathlength at 25 °C. The reaction mixture contained 9.7 nM *p*-nitrophenyl acetate and 15 μM HSA in 0.1 M phosphate buffer, pH 7.0. The concentration of HSA should be used in excess quantity compared with *p*-nitrophenyl acetate to avoid complications because of the multiple reactive sites of HSA (Ikeda et al. 1979).

Under these conditions, pseudo-first-order rate constants or hydrolysis rate constants (k_{obs}) were determined from plots of log (A_∞-A_t) versus time, where A_∞ and A_t are the absorbances at the completion of the reaction and at time t, respectively (Kurono et al. 1992).

2.2.4.2.2 Fluorescence spectroscopy

Ligand binding property of HSA can be determined by using many techniques with different ligands such as hemin, diazepam, or billirubin (Varshney et al. 2008). In this study, hemin was chosen to use as a ligand to bind with HSA. The binding of Hemin to HSA was investigated using a fluorescence spectroscopy (Perkin Elmer LS55) technique. Hemin stock solution (1 mg/mL) was prepared daily in 10 mM NaOH and vigorously stirred until hemin totally dissolved, and was spectrophotometrically measured the absorbance at 385 nm for calculating the concentration.The molar extinction coefficient of hemin at 385 nm is 58.4 (Beaven et al. 1974).

In hemin titration experiment, a fixed volume (3 mL) of protein solution (3.5 uM) in 1 cm pathlength quartz cuvette was titrated with a small volume (1 μL) of

hemin stock solution at 25 °C and measured the fluorescence intensity at 340 nm after exciting the solution at 295 nm. After each addition, the contents in cuvette were stirred well and the spectra were collected after 10 min of the addition of hemin to protein solution. Emission and excitation bandwidth were set at 5 nm. Fluorescence data of hemin binding to HSA in the absence and presence of osmolytes were analyzed to obtain various binding parameters. The binding constant (K) and binding affinity was calculated according to Stern-Volmer equation (Lakowicz 2006a).

$$F_0 = F(1 + K[Q]) \qquad \textit{Equation 2.10}$$

$$\log [F_0 - F / F] = \log K + \log [Q] \qquad \textit{Equation 2.11}$$

where,
F_0 is the observed fluorescence intensity in the absence of hemin;
F is the observed fluorescence intensity in the presence of hemin;
[Q] is the hemin concentration.

By taking the log of both sides of Equation 2.10 (as displayed in Equation 2.11), log $[F_0-F / F]$ versus log [Q] were plotted and a least square analysis was used to calculate the binding parameters whose slope was equal to n (binding affinity) and the intercept on Y-axis was equal to log K (K=binding constant). Therefore, the standard free energy change ($\triangle G_0$) of the hemin binding to HSA can be calculated from the binding constant as displayed in Equation 2.12.

$$\triangle G_0 \text{ binding} = -2.303\, RT \log K \qquad \textit{Equation 2.12}$$

2.2.4.3 Aggregation testing

2.2.4.3.1 SDS PAGE

Aggregates were detected by SDS-PAGE which used the same processes as described in section 2.2.1.5

2.2.4.3.2 Native polyacrylamide gel electrophoresis

Native or non-denaturing polyacrylamide gel electrophoresis (Native PAGE) is one of the most powerful technique for studying the composition and structure of native

proteins. Proteins are sorted out in accordance with net charge, molecular size, and shape of their native structure because in this technique, proteins are not interacted with SDS and not heated in high temperature (Creighton 1997). The equipment used in Native PAGE are similar to SDS PAGE as described in section 2.2.15, but the compositions of resolving (separating) and stacking gel were different as shown in Table 2.6.

Protein samples (10 µL) were diluted with 20 µL loading buffer (Tris, 1 M, pH 6.8; glycerol, 20 %; bromophenol blue, 0.03 %) without boiling before loading onto the gel. Constant voltage, 80 V, was applied for stacking and resolving gel in running buffer (Tris, 25 mM and glycine, 250 mM in deionised water). Gels were stained with Coomassie brilliant blue (Coomassie brilliant blue, 0.1 %; acetic acid, 10 %; methanol, 50 %, in water) and were destained with a solution containing acetic acid, 10 %; and methanol, 10 %, in water.

Table 2.6 Resolving and stacking gel components for Native-PAGE

Components	Resolving gel	Stacking gel
30 % Acrylamide:0.8 % Bis-acrylamide	1.75 mL	1.11 mL
1 M Tris, pH 8.8	2.62 mL	-
1 M Tris, pH 6.8	-	0.83 mL
Deionised water	2.66 mL	4.7 mL
Tetramethylethylenediamine (TEMED)	4.6 µL	6.6 µL
Ammonium per sulphate (AMPS)	46 µL	33 µL

2.2.4.3.3 Dynamic light scattering

The particle size of proteins and aggregates were determined by dynamic light scattering (DLS) using a Malvern Zetasizer® Nano ZS instrument (Malvern Instrument Ltd., UK). This technique measures the scattered light from Brownian movement of the particles. The diffusion coefficient (D_t) was analysed and converted into a size distribution with the Stoke-Einstein equation as displayed in Equation 2.7. Viscosity and refractive index of protein samples needed for particle size evaluation which measured by using Rheometer (Rheolyst™ AR 1000-N, TA instruments) and Refractometer, respectively.

Protein samples were filtered through a 0.22 µm Sartorius Minisart® syringe filter (to remove dust particles) and placed in a low volume plastic disposable cuvette. Samples were measured five times at a temperature of 25 °C after a 2 min equilibration time to ensure that the samples reach thermal equilibrium and the average value is reported. The detection angle used was 173.0 degrees for backward scattering. The duration of measurement for each sample was automatically determined by the software to obtain optimal data quality.

Chapter 3

Effect of osmolytes on the conformational stability and hydrodynamic radii of Im9

3.1 Introduction

3.1.1 General background

As described in Chapter 1, protein denaturation is one of the primary ways to assess protein stability. The most frequently used chemical denaturants are urea and guanidine hydrochloride (GdnHCl). These denaturants have very different properties. GdnHCl is a more potent denaturant (Greene and Pace 1974) but, unlike urea, would have salting effects to the protein solution due to its charged ions, so the ionic strength of protein solutions with GdnHCl are difficult to control. Many previous works (Pace and Shaw 2000) indicate that urea has more advantages than GdnHCl as far as determining thermodynamic parameters are concerned. The free energy and enthalpy functions of both proteins and model compounds are more linear with urea than with GdnHCl; extrapolations of denaturant-dependent parameters to zero denaturant concentration are more reliable; and least squares analysis of the data is more stable. Consequently, in this study, urea was chosen to be the denaturant for determining the stabilities of Im9 (this Chapter) and HSA (Chapter 4).

The hydrodynamic radius of Im9, and HSA (Chapter 4), was studied, because it is directly related to the compactness of the protein, which is decreased on protein denaturation. We also considered that the hydrodynamic radius might be informative about how osmolytes affected protein structure as any major changes in solvation of the protein might show up in an altered hydrodynamic radius. In this study, a pulsed-field gradient NMR (PFG-NMR) experiment was used to measure the effective hydrodynamic radii of protein.

Im9 was used here as a model single domain protein whose structure and stability are relatively well understood. Two kinds of osmolytes were chosen to use as a stabilizer: sugars, represented by sucrose and trehalose (at concentrations of 0.25, 0.50,

and 0.75 M) and polyols, represented by glycerol, (at concentrations of 10, 20, and 30 % v/v of glycerol or at concentrations of 1.37, 2.74, and 4.11 M). In general, many researchers report that high concentration of osmolytes (more than 1.0 M) is useful for increases in protein stabilisation (Timasheff et al. 1998, Wang 1999). However, high concentrations of osmolytes cause higher viscosities of protein solutions, which might result in uncomfortable IV administration of a drug to the patient. Therefore, in this study, lower concentrations than the so-called effective range (Timasheff et al. 1998) were used to study the effects of osmolytes on the conformational stability and particle size of proteins in the absence and the presence of osmolytes.

3.1.2 Structure and properties of Im9

Im9 is a member of the E colicin binding immunity proteins, which inhibit the cytotoxic activity of the E colicin DNase killing domains. Im9 inhibits colicin E9, thus affording protection against it to cells producing Im9 (Wallis et al. 1992b, Wallis et al. 1992a). It is a single domain protein of 86 amino acid residues with a four helix bundle structure (Figure 3.1). The structure consists of three well-defined α-helices: helix I (Glu12-Cys23), helix II (Glu30-Thr44) (the longest one), helix IV (Ser65-A77), with an additional one-turn helix III (Asp51-Tyr55). Helices I and II are antiparallel (forming an angle of -150°) and are connected by a loop comprising six residues which is relatively ill-defined (Osborne et al. 1996). The side chains of these residues are situated at, or close to, the surface of Im9 and are therefore highly solvent accessible and in environments where they have relatively unrestricted motion compared to other regions of Im9.

The core of Im9 is stabilised by a large number of interactions involving hydrophobic side chains which, with the exception of some of the buried aromatic residues, are relatively well-defined. The core residues include the four isoleucines, four of the five valines, three of the five leucines, the three phenylalanines, the tryptophan, two of the three histidines, and one of the three tyrosines. Most of these residues tend to be located on the interior faces of the helices. Charged residues are located at the molecular surface, where they form favourable interactions with the solvent, but Lys4 and Asp9 appear to form a salt bridge. Although the long helices are generally

amphipathic, some of their residues are exceptions, most notably, the exposure of Ala25 on helix I and Val34 on helix II.

Im9 is an acidic protein (pI = 4.5), and salt has a major effect on its binding to the colicin E9 DNase domain (Wallis et al. 1995). Previous genetic and biochemical studies (Wallis et al. 1992a) in combination with earlier structural work (Osborne et al. 1994) have suggested that helices II and III of Im9 are important for this interaction, particularly Val34 which is located on the surface of the protein, which has now been validated by X-ray crystallography studies (Kleanthous et al. 1999).

It was found that the urea-induced unfolding of Im9 at pH 7.0, 10 °C (in 50 mM sodium phosphate and 2 mM DTT) follows a two-state mechanism in which only the native (N) and unfolded states (U) are populated. Moreover under stabilising conditions (0.4 M sodium sulphate), Im9 also folds in a two-state mechanism with altered thermodynamic parameters compared with in its absence. Single domain proteins normally fold in a simple two- state process (N⇆U) without a kinetically significant intermediate state (Jackson 1998) and thus Im9 is not unusual in this respect.

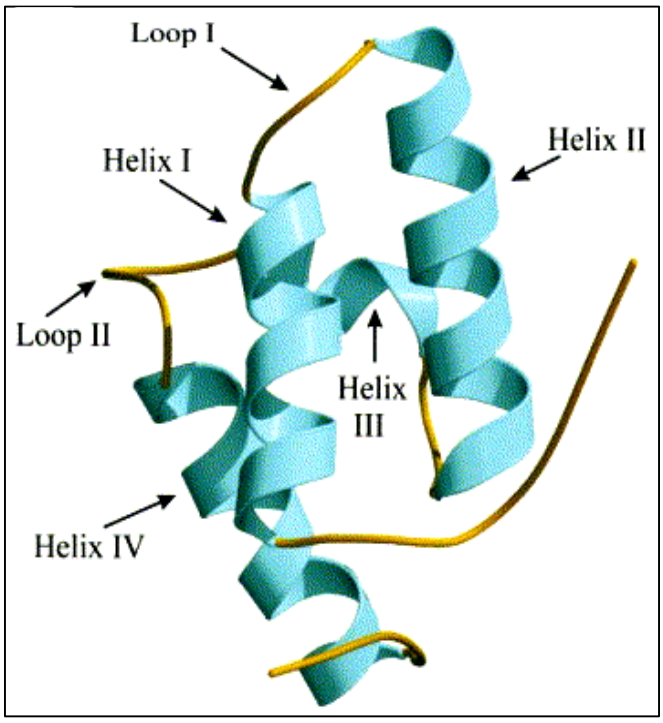

Figure 3.1 Ribbon diagram representation of the average NMR structure for Im9 (Osborne et al. 1996). The NMR structure of Im9 (PDB coordinates **P13479** IMM_9_ECOLX). Helix I (residues 12–21), helix II (residues 30–44), helix III (residues 51–55) and helix IV (residues 65–77) are shown.

3.2 Results and Discussion

Im9 used for the work described in this chapter was prepared as described in section 2.2.1.

3.2.1 Conformational stability of Im9 in the absence and in the presence of different concentration of osmolytes at 25 °C

3.2.1.1 Fluorescence spectrum

Determining protein stability is the first step in investigating the thermodynamic properties of proteins. The only requirement is that the protein establishes a reversible equilibrium between the folded and unfolded state. The unfolding of Im9 has been found to follow a two-state folding mechanism without any intermediate state (Ferguson et al. 1999), as shown in Equation 1.1

$$\text{Folded (Native, N)} \underset{k_f}{\overset{k_u}{\rightleftharpoons}} \text{Unfolded (Denatured, D)} \qquad \textit{Equation 1.1}$$

One common strategy for probing the tertiary structure of proteins is to measure the intrinsic fluorescence from aromatic residue such as tyrosine and tryptophan. The spectral parameters of tryptophan fluorescence such as I_{max}, $\lambda_{max,}$ the band shape, the anisotropy, the fluorescence lifetime and any energy transfer are dependent on the protein conformation in the vicinity of the Trp residues, the solvent polarity and the dynamic and electronic properties of the chromophore environment; hence fluorescence measurement has been extensively used to obtain information on the tertiary structural properties of proteins (Vivian and Callis 2001, Lakowicz 2006b). Im9 contains only one tryptophan residue (Trp 74) which can be specifically studied by selective excitation at wavelengths of 278-290 nm. In the native state, the fluorescence of the tryptophan of Im9 is quenched. The exact reason for this is not known but it has been suggested to be due to the proximity of the buried His 46 to the indole ring of the tryptophan (Osborne et al. 1996). In general, the fluorescence intensity of the native state of proteins is larger and blue shifted with respect to that of their unfolded state, Im9 being an exception to

this, and thus fluorescence emission is considered a sensitive tool to monitor the extent of unfolding/folding and to reveal local changes in protein conformation.

In order to establish whether the presence of urea has any influence on the structure of Im9, fluorescence spectroscopic measurements were performed in the absence of osmolytes at 25 °C, exciting fluorescence at 295 nm. In denatured state of Im9, the fluorescence spectrum of urea denatured protein at pH 7.0 was measured in the absence of osmolytes (Figure 3.2). The tryptophan fluorescence emission of native Im9 (0.1 M phosphate buffer, pH 7.0) is highly quenched while the tryptophan spectrum of denatured Im9 (8.0 M urea, 0.1 M phosphate buffer, pH 7.0) is considerably more intense and red-shifted with respect to that of the native state. Protein molecules in aqueous solution are normally covered by a hydration layer. Urea, the denaturant, tends to displace water molecules in both of hydration shell and interior of the protein. This phenomenon might change the interactions responsible for maintaining the native conformation of the protein. The fluorescence emission intensity of native Im9 is highly quenched compared with its denatured state; therefore a large increase in fluorescence intensity is observed when the protein is denatured upon the addition of urea as displayed in Figure 3.2.

Previous denaturation and stabilities studies of Im9 with urea were carried out using tryptophan emission fluorescence spectroscopy at 25 °C (Wallis et al. 1998) and showed that the λ_{max} shifted from 334 nm to 354 nm and the fluorescence intensity increased on denaturation, indicating the fluorescence emission of Trp 74 to be highly quenched in the native protein. The stability studies showed Im9 in the presence of osmolytes might be more stable than Im9 in the absence of osmolyte, because their fluorescence intensity is increased relative to Im9 and λmax is blue shifted, indicating lower exposure of Trp 74 to the solvent.

The fluorescence spectra of Im9 and stabilised Im9 (in the presence of 0.50 M trehalose, 0.50 M sucrose, and 20 % glycerol) in the native and denatured state were also measured and are displayed in Figure 3.3 A-D, respectively. It is seen from Figure 3.3 B-D that the fluorescence spectra of stabilised Im9 in both native and denatured states are slightly changed compared to that of Im9 in the absence of osmolyte from Figure 3.3 A. Different osmolytes may interact with proteins in different ways, depending on their physicochemical properties and concentration. Moreover, there

might be some partial-unfolding of Im9 in both of the absence and the presence of osmolytes. The incubation of protein sample for 12-16 hr at 25 °C before measurement might induce protein unfolding which related to the previous work of Ferguson stated that the stability of Im9 might be reduced at high temperature (25 °C) (Ferguson et al. 1999).

Thus, our assumption that osmolytes do not affect the structural characteristics of the two end-states of the process, N conformation ⇆ D conformation seems to be reasonable.

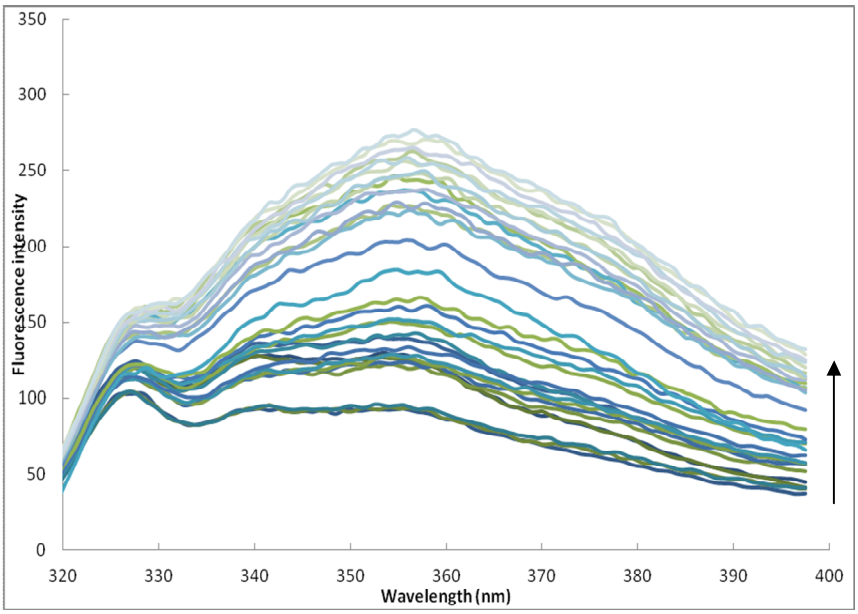

Figure 3.2 Fluorescence intensity of Im9 with urea (0 M to 8 M), at 25 °C. The arrow indicates the increase in fluorescence intensity with the increase in urea concentration. Im9 solutions (0.21 µM) were prepared in 0.1 M phosphate buffer solution pH 7.0 and then added to urea stock solutions to obtain the desired concentrations.

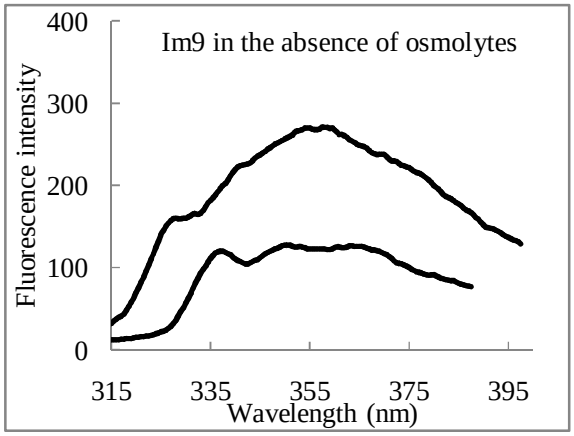

A).

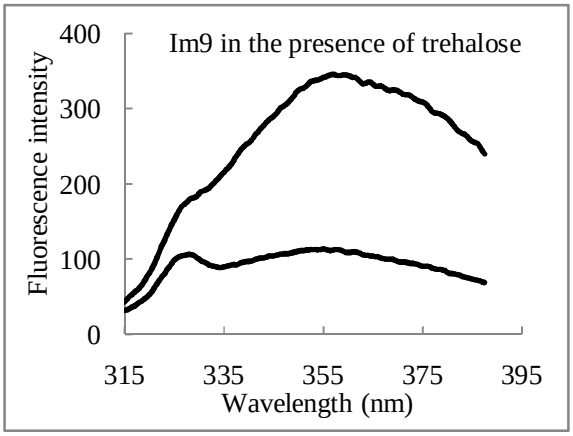

B).

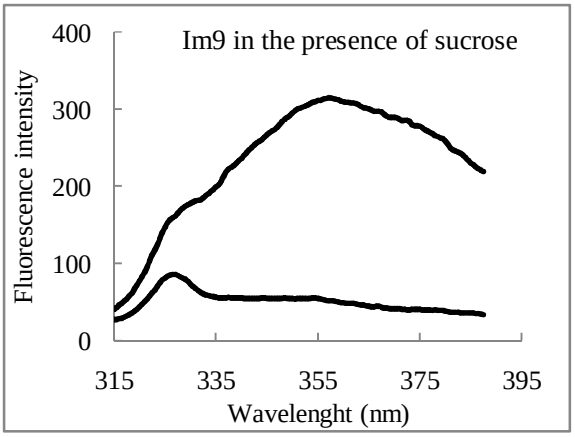

C).

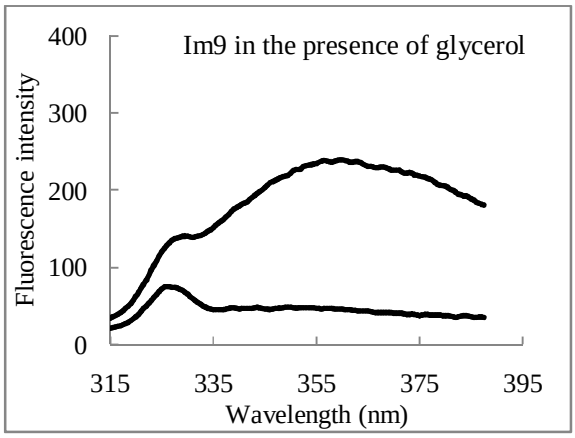

D).

Figure 3.3 The emission spectra (Trp fluorescence spectra) of native (solid line) and denatured (dashed line) Im9 in the absence and the presence of osmolytes at 25 °C. The emission spectra of native Im9 in the absence of osmolyte (A) and stabilised native Im9 in the presence of osmolytes (0.50 M trehalose (B), 0.50 M sucrose (C), and 20 % glycerol (D)). All samples contained 0.21 μM Im9 and were measured by using 1 cm pathlength cuvette, at pH 7.0 and at 25 °C.

3.2.1.2 Urea-induced denaturation

To gain insight into the conformational stability of Im9 in the absence and the presence of osmolytes, equilibrium denaturation methods, with urea as the chemical denaturant, were used to monitor the change in intrinsic tryptophan fluorescence upon unfolding. Im9 has only one tryptophan residue (Trp74), so tryptophan fluorescence was selected as a probe to detect this protein in urea-induced denaturation transition. The fluorescence spectrum of Im9 is displayed in Figure 3.4 A which shows that the intensity and emission maxima of Im9 changed in response to urea concentration.

Figure 3.4B displays the changes in the fluorescence intensity of Im9 at 340 nm when the urea concentration is increased. The fluorescence intensity slightly increases at low urea concentration and at high urea concentration starting around 2 M urea, there was a sharp increase in intensity. It has been suggested that the change in the fluorescence intensity of proteins in the pre- and post-transition regions is likely to be a result of the solvent perturbation or binding effect of the denaturants (Pace, Laurents and Thomson 1990, Johnson and Fersht 1995). The tryptophan emission maximum of the Im9 in phosphate buffer pH 7.0 was 340 nm and in low urea concentration (3.0 M) the Trp emission maximum was still nearly the same value. However, when the urea concentration increased to more than 4.0 M, a red-shift in Trp emission maximum occurred and the signal was shifted from 340 to 355 nm, indicating that the Im9 structure undergoes conformational changes in response to urea concentration. This is due to the exposure of the tryptophan to an aqueous environment as opposed to a hydrophobic protein interior.

The data from Figure 3.4 B were treated as described in Section 2.2.2.3, taking the fluorescence intensity at low and high urea concentration to be Y_F and $Y_{U,}$ respectively to yield the unfolding curve as displayed in Figure 3.4 C which plots the unfolded fraction against the urea concentration (M); the addition of urea to Im9 solution is to denature it and the transition region started from about 2.0 M urea and completely unfolded around 7.0 M urea concentrations. The unfolding curve (solid black line) was fitted well according to a two-state transition (N↔D) which agreed with previously reported data (Tezuka-Kawakami et al. 2006, Ferguson et al. 2001). The thermodynamic parameters were obtained from Equation 2.6:

$$\triangle G_u = \triangle G^{H2O} - m\,[Urea] \qquad \textit{Equation 1.5}$$

where,

m is the slope of the line which measures the dependence of $\triangle$G on denaturant concentration in kcal mol^{-1} M^{-1}; $Urea_{1/2}$, the midpoint of the unfolding transition; $\triangle G^{H2O}$, the difference in free energy between the native and denatured states in the absence of denaturant; and the m-value is a measure of the change in solvent-accessible surface area (SASA) between the native and denatured states. These parameters (Table 3.1) are useful to delineate the noncovalent forces stabilising the different structural states. Furthermore, these thermodynamic parameters can be related more directly to the structural arrangements of the protein and can provide a more detailed understanding of protein stability in co-solvents.

Our thermodynamic parameters values are different from the previous values (Ferguson et al. 2001). Experimental values of $\triangle G^{H2O}$ and m-value are significantly lower than those obtained by Ferguson. However, the midpoints of the unfolding transition ($Urea_{1/2}$) are nearly the same value (4.83 and 4.84 M) indicating that it is the slope of the transition region that differs. This difference can be attributed to the different experimental condition, such as composition in protein solution, which could give the different results. DTT is the only significant difference between ours and Ferguson's composition that might cause an alteration in unfolding property of Im9. The conformation of denatured proteins is often considered to be an extended chain, but denatured Im9 might not be fully extended if it is like urea-unfolded Im7 (Le Duff et al. 2006). Also the addition of different salts might affect the conformation. Therefore, in this work, I did not add any substance into Im9 solution other than buffer, because it might have some effects to the protein conformation and stabilization. Therefore, Im9 was prepared in only 0.1 M phosphate buffer solution pH 7.0 and these calculated thermodynamic parameters of Im9 can be used for comparing with those of Im9 in the presence of osmolytes to obtain the stabilizing effect of osmolytes on Im9.

Urea-induced denaturation curves of Im9 in the absence and presence of 0.25, 0.50, and 0.75 M each of trehalose and sucrose; and 10, 20, and 30 % (v/v) glycerol were also measured by following changes in fluorescence intensity as a function of the urea concentration at pH 7.0, 25 °C and are displayed in Figure 3.5 A, B, and C, respectively. These denaturation curves were also analyzed as two state transitions

because the main characteristics of the denaturation curve were not affected by the addition of osmolytes. Moreover, the profile of denaturation curves for Im9 in the presence of osmolytes was slightly shifted toward higher denaturation concentration at increasing osmolytes. The explanation of this mechanism is that normally urea destabilises protein by preferentially binding, therefore, when addition of urea to the protein in the presence of osmolyte, urea needed to overcome the stabilising effect of osmolyte. This is the reason why the midpoint concentration of urea increases with osmolyte concentration.

The thermodynamic parameters are presented in Table 3.2 and graphically displayed in Figure 3.6 A-C. Thermodynamic parameters of Im9 in its stabilised state are slightly increased compared with those of Im9 in its native state without osmolytes. The comparisons of thermodynamic parameters for each value ($Urea_{1/2}$, $\triangle G^{H2O}$, and m-value) under different conditions are graphically displayed in Figure 3.7 A-C, respectively. The results in Figure 3.7A obviously distinguish the change of $Urea_{1/2}$ values, which corresponds to the transition of Im9 to the unfolded state, as a function of osmolyte concentration. The highest concentration of osmolytes induces a shift of $Urea_{1/2}$ from 4.84 M to 5.28 M, 5.23 M, and 5.02 M for trehalose, sucrose, and glycerol, respectively. This enhancement is found here to be about 3.75 – 9.11 %, depending on the particular osmolyte concentration, indicating that these osmolytes can inhibit the chemical denaturation of Im9 by urea. Interestingly, the midpoint of unfolding transition order of the folding in osmolytes shows that trehalose as well as sucrose is the strongest stabiliser, while glycerol is only a mild stabiliser. However, the results of $\triangle G^{H2O}$ and m-value of Im9 in the presence of osmolytes, which are represented in Figure 3.7 B and C, respectively, are not related to those of $Urea_{1/2}$. Although these data increase as osmolyte concentration increase, the order of stabilising effect is different. Nevertheless, it can be seen that in the absence of osmolytes Im9 is less stable than in their presence.

The m-value is a parameter for indicating the degree of unfolding and characterises the change in accessible surface area on denaturation. This value is related to the molecular size of a protein so that small proteins are less sensitive to solvent denaturation than larger ones (Fersht 1999). Although the m-values of Im9 in this experiment increase when osmolyte concentration increases; only small changes are

seen, as displayed in Figure 3.7 C, results which are consistent with similar studies on other small proteins (O'Brien et al. 2008).

To further quantify the effect of osmolytes on Im9 stability, we follow the $\triangle\triangle G^{H2O}$, defined as the difference between $\triangle G^{H2O}$ measured in buffer and its value obtained in the presence of osmolytes. The comparison clearly showed that $\triangle\triangle G^{H2O}$ tend to increase with osmolyte concentration for all osmolytes tested, but not in a linear relationship, as displayed in Figure 3.6 D-F. From these values, it can be stated that the efficiency of stabilisation follows this order: trehalose > glycerol > sucrose.

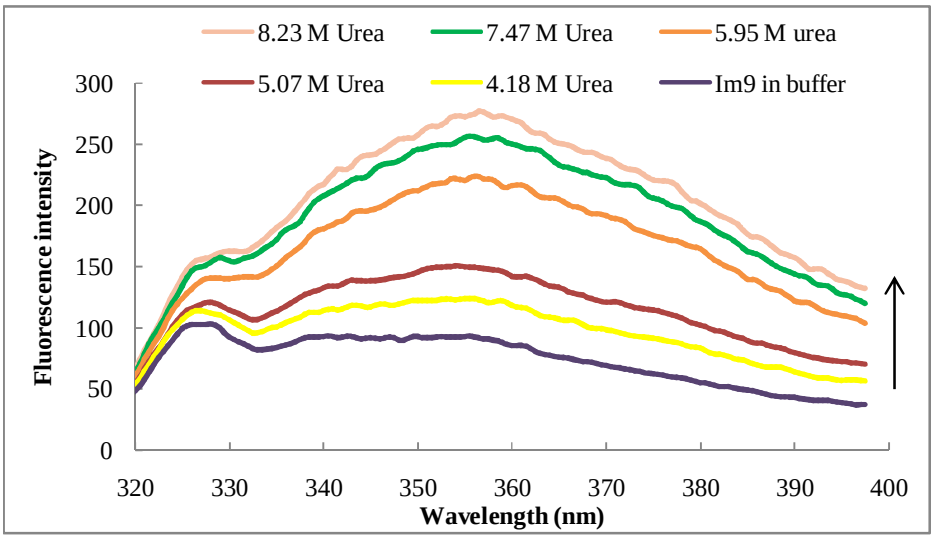

A).

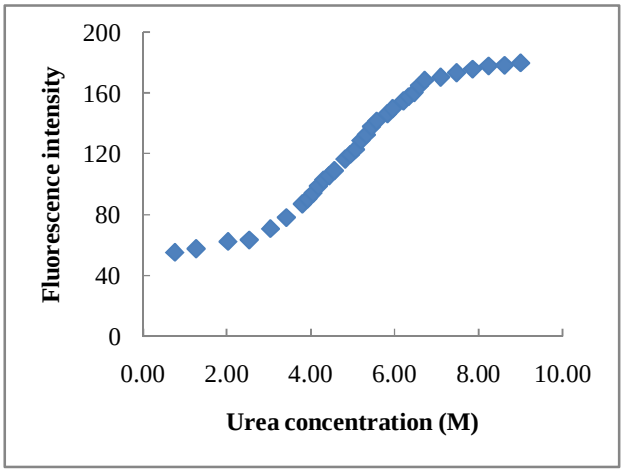

B).

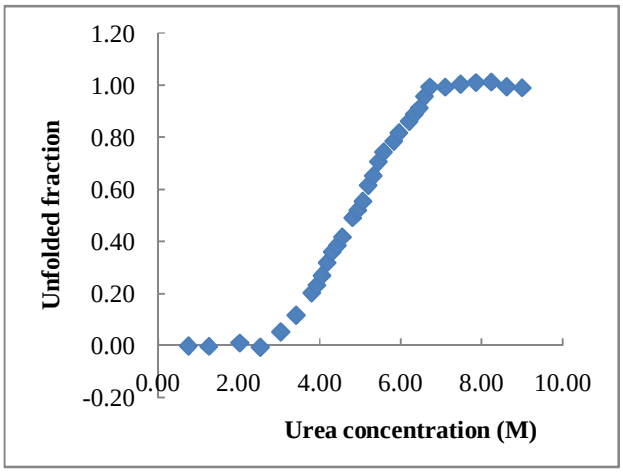

C).

Figure 3.4 Fluorescence intensity curve and unfolding curve of Im9 with urea at 25 °C. A). Fluorescence intensity of Im9 with urea (0 M to 8 M) at 25 °C. The arrow indicates the increase in fluorescence intensity with the increase in urea concentration. Im9 solutions (0.21 µM) were prepared in 0.1 M phosphate buffer solution pH 7.0 and then added to urea stock solutions to obtain the desired concentrations. The excitation wavelength was 295 nm. The excitation and emission slit widths were 10.0 nm each. B). Fluorescence intensity of Im9 at 340 nm versus urea concentration. C). The unfolding curve of Im9 with urea concentration detected by fluorescence spectroscopy at 25 °C.

A).

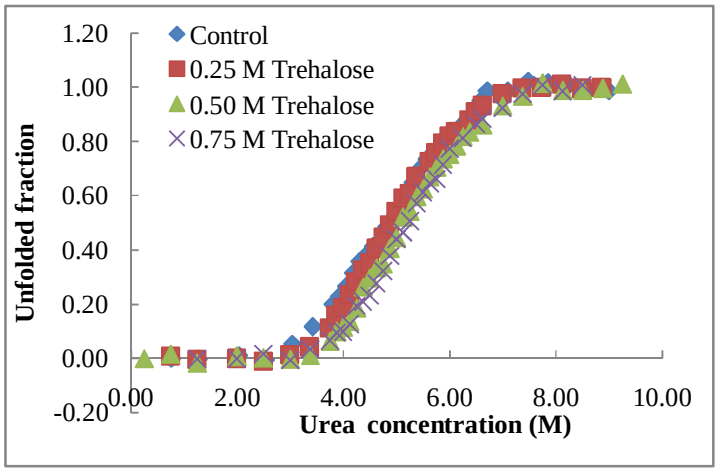

B).

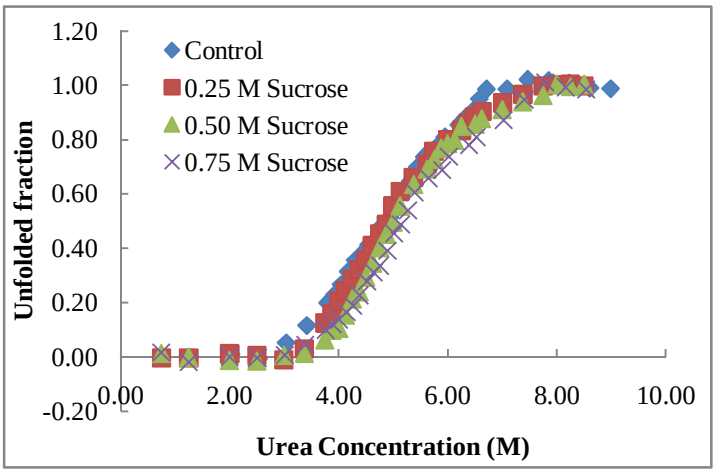

C).

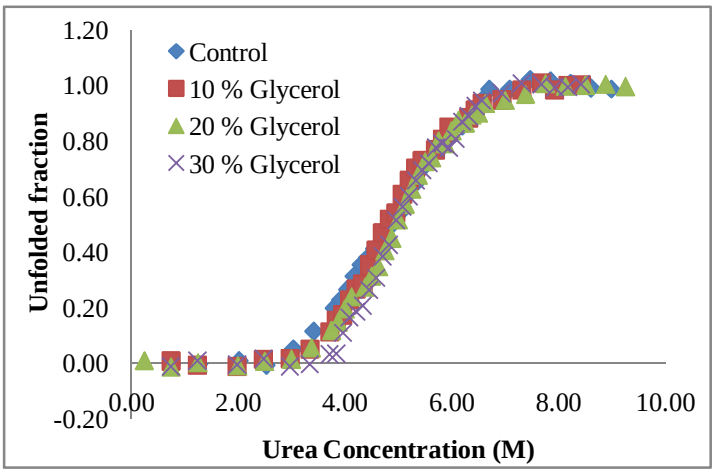

Figure 3.5 Urea-induced denaturation curves of Im9 in the absence and the presence osmolytes at 25 °C. Im9 solutions (0.21 µM) were prepared in 0.1 M phosphate buffer solution pH 7.0 in the absence and presence of 0.25, 0.50, and 0.75 M trehalose (A), 0.25, 0.50, and 0.75 M sucrose (B), and 10, 20, and 30 % (v/v) glycerol (C).

Table 3.1 Equilibrium unfolding parameters for native Im9 in the absence of urea 25 °C and pH 7.0.

Protein	Thermodynamic parameters		
	m-value (kcal mol^{-1} M^{-1})	**$\triangle G^{H2O}$ (kcal mol^{-1})**	**Urea $_{(1/2)}$ (M)**
Im9[a]	0.7712	3.73	4.8373
Im9[b]	0.9857 (4.13 ± 0.10 kJ mol^{-1} M^{-1})	5.14 21.52 ± 0.58 (kJ mol^{-1})	4.84 ± 0.02

a. Thermodynamic parameters from my experiment. The sample solutions were prepared containing 100 mM potassium phosphate buffer, pH 7.0 with a final concentration of 0.21 µM and monitored by fluorescence spectroscopy at 340 nm

b. Thermodynamic parameters from Ferguson (Ferguson et al. 2001). The sample solutions were prepared containing 50 mM sodium phosphate buffer, pH 7.0 and 2 mM DTT with a final concentration of 20 µM and monitored by far-UV CD at 225 nm.

Table 3.2 Thermodynamic parameters (m-value, $\triangle G^{H2O}$, $Urea_{1/2}$, and $\triangle\triangle G^{H2O}$) characterising the urea unfolding of Im9 in the presence of osmolytes at pH 7.0, 25 °C and R^2 values for the straight line relationship of $\triangle G$ and Urea concentration.

Protein	Osmolyte Concentration	Thermodynamic parameters				R^2
		m-value (kcal mol^{-1} M^{-1})	**$\triangle G^{H2O}$ (kcal mol^{-1})**	**$Urea_{1/2}$ (M)**	**$\triangle\triangle G^{H2O}$ (kcal mol^{-1})**	
Im9	Buffer (Control)	0.77	3.73	4.84	0.00	0.9973
Im9	0.25 M Trehalose	0.85	4.18	4.93	0.45	0.9956
	0.50 M Trehalose	0.92	4.79	5.21	1.06	0.9817
	0.75 M Trehalose	0.94	4.97	5.28	1.24	0.9918
Im9	0.25 M Sucrose	0.78	3.83	4.93	0.10	0.9950
	0.50 M Sucrose	0.84	4.30	5.11	0.57	0.9847
	0.75 M Sucrose	0.87	4.54	5.23	0.81	0.9916
Im9	10% Glycerol	0.89	4.30	4.84	0.57	0.9923
	20% Glycerol	0.94	4.68	4.98	0.95	0.9937
	30% Glycerol	0.98	4.90	5.02	1.17	0.9845

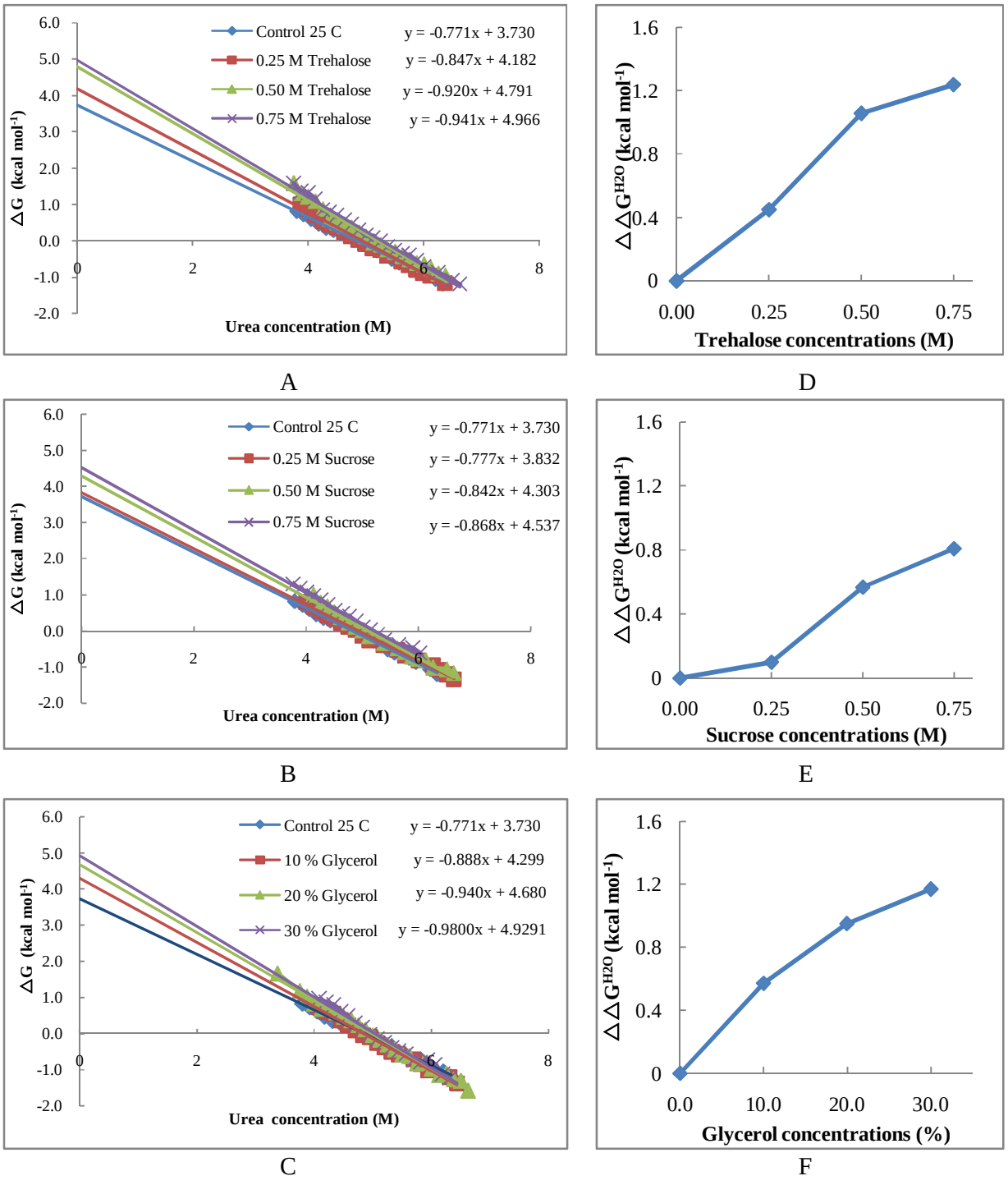

Figure 3.6 △G versus urea concentration plots and Value of $\triangle\triangle G^{H2O}$ measured in the absence and in the presence of osmolytes, for Im9 at 25 °C. A-C, Transformation of the fluorescence data to give a linear plot of change in free energy (△G) versus urea concentration for urea-induced denaturation of Im9 in the absence and presence of osmolyte. D-F, Value of $\triangle\triangle G^{H2O}$, the difference in $\triangle G^{H2O}$ measured in buffer and in the presence of osmolytes.

(A)

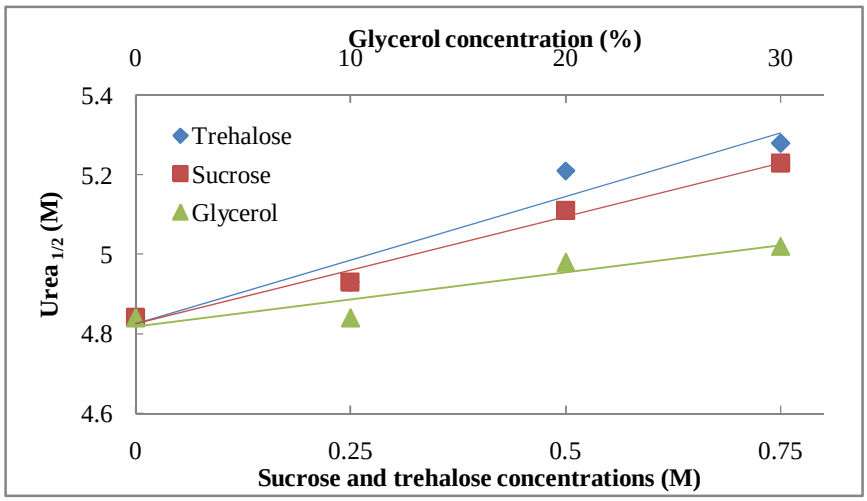

(B)

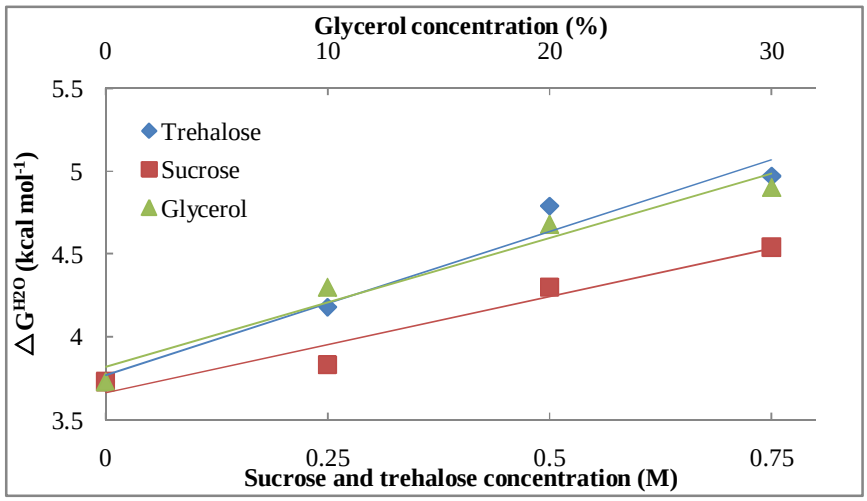

(C)

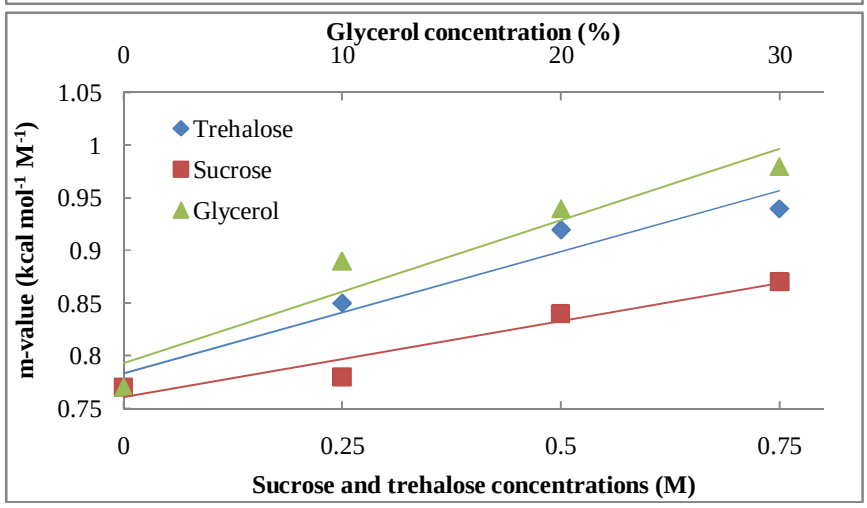

Figure 3.7 The influence of osmolytes on the thermodynamic stability and urea-induced denaturation of Im9, at 25 °C. The thermodynamic changes A-C ($Urea_{1/2}$, $\triangle G^{H2O}$, and m-value, respectively) in response to the transition of the Im9 to the unfolded state in osmolytes (trehalose (◆), sucrose (■), and glycerol (▲). The straight lines between each osmolyte concentrations were drawn by using a linear trend line in Excel.

3.2.2 Hydrodynamic radii of Im9 in the absence and in the presence of different concentration of osmolytes at 25 °C

From the results of the measurement of the conformational stability of Im9 in the absence and the presence of osmolytes, the m-value shows only the relative change in solvent accessible surface area, so it is more useful to know the dimensions of the protein structure to investigate whether there is preferential hydration of the protein in either the folded or unfolded state and to investigate how osmolytes affect the Im9 hydration shell. The aim of this experiment is to study the effect of osmolytes on the Im9 structure. A pulse-field gradient nuclear magnetic resonance (PFG-NMR) experiment was used to determine the hydrodynamic radii of Im9 in different states. In the preferential hydration or preferential exclusion theory, osmolytes mostly act indirectly on the protein by changing the structure and dynamics of water in the solution, resulting in enhancing the hydrophobic interaction. Water molecules in the hydration shell around the protein increase because the osmolyte molecules are excluded from the protein/solvent surface, and the protein compactness is also increased, thus influencing protein stability. Consequently, in order to see whether this is what happens to Im9 in its osmolyte-stabilised state, the particle size of Im9 was measured in the absence and the presence of 0.25, 0.50, and 0.75 M each of trehalose and sucrose; and 10, 20, and 30 % (v/v) glycerol by PFG-NMR experiment.

3.2.2.1 One-dimensional proton NMR (1D ^{1}H NMR)

To determine whether various osmolytes (trehalose, sucrose, and glycerol) in different concentrations affected the conformation of Im9, one-dimensional ^{1}H NMR spectra were recorded and are displayed in Figure 3.8. It was found that only small changes in the spectrum of Im9 were induced by the presence of osmolytes as far as resonance chemical shifts were concerned but there was a marked reduction in the signal noise ratio. This was most likely due to the increased viscosity accompanying increasing osmolyte concentrations causing slower rotational tumbling of the protein molecules which produced broader resonances. These results are in excellent agreement with those from the fluorescence spectroscopic experiment (Section 3.2.1), leading me to conclude that there is no indication of any major structure alteration in the protein itself produced by the osmolytes.

3.2.2.2 Pulsed-field gradient NMR (PFG-NMR) spectroscopy

PFG-NMR diffusion measurements have been used to determine the particle size of proteins by converting the diffusion coefficient into the hydrodynamic radius of the protein. Diffusion coefficients can be detected using a number of techniques, such as dynamic light scattering (Gast et al. 1998), small-angle X-ray scattering, gel filtration, analytical ultracentrifugation and pulsed-field gradient NMR (Wilkins et al. 1999). The PFG-NMR diffusion measurements are particularly suited to evaluating molecular size in both native and denatured states because it can measure the protein solutions, which are fully hydrated, under conditions that are identical to those used for structural prediction and it yields information about hydrodynamic radius in real particle size (Gounarides, Chen and Shapiro 1999). Moreover, this technique shows the potential to predict the diffusion phenomena for small molecules in solution better than DLS (Kato et al. 2006).

The diffusion coefficient can be calculated by two methods: the former is from the Stokes-Einstein equation (Equation 2.7), for which one has to know the temperature and viscosity of the protein solution.

$$D_t = kT / 6\pi\eta R_h \qquad \textit{Equation 2.7}$$

It is difficult to know the precise temperature and viscosity between different samples. Moreover, the strict definition of the radius defined by the Stokes-Einstein equation is that of a hard sphere that diffuses with the same speed as the molecule under investigation. Protein molecules in solution, however, are rarely spherical and are also dynamic and hydrated, and so the hydrodynamic radius is only a measure of the apparent size of the molecule.

The PFG-NMR method uses the diffusion of an inert internal standard molecule, for which the exact value of its hydrodynamic radius is known, as an internal reference so it is added to the protein solution. The hydrodynamic radius of the protein is obtained by comparison with the standard (Equation 2.9).

$$R_{h\ protein} = \frac{D_{ref}}{D_{Protein}} \times R_{h\ ref} \qquad \textit{Equation 2.9}$$

Therefore, the requirement of knowing the exact value of sample temperature and viscosity can be ignored since the measurements are made relative to an internal standard. The internal radius standard should not interact with the protein of interest and its spectrum should not overlap with the spectra of the protein and osmolytes. This method has been used to measure the hydrodynamic radii of the native and denatured state of several proteins (Jones et al. 1997, Wilkins et al. 1999). Consequently, we used this gradient NMR technique to compare the hydrodynamic radii of native and stabilised states of Im9, using acetaldehyde as an internal radius standard.

Normally, dioxane is used in the PFG-NMR experiment as an internal radius standard because the exact value of its hydrodynamic radius is known (2.12 Å) (Wilkins et al. 1999) and it also has low interactions with most proteins (Jones et al. 1997). In Figure 3.9, however, it was found that the dioxane signal (around 3.5 ppm) overlapped with signals of Im9 and the osmolytes (trehalose, sucrose, and glycerol). The chemical shifts of the osmolyte signals observed for 1D ^{1}H NMR spectra are listed at 6.0 to 2.0 ppm. Therefore, different kinds of reference molecules were investigated such as acetate (chemical shifts at 2.04 and 11.65 ppm), trifluoroacetate (chemical shifts at 11.50 ppm), 2,2-dimethyl-2-silapentane-5-sulphonate (DSS) (chemical shifts at 0.00 ppm), and acetaldehyde (chemical shifts at 1.2 and 9.5 ppm). However, it was found that high concentration (more than 10 % v/v) of acetate and trifluoroacetate needed to be added to the protein solution because in low concentration, their chemical shifts could not be detected in 1D ^{1}H NMR spectra of protein (data not shown). Therefore, acetate and trifluoroacetate were not used since the high concentrations needed might have caused pH changes of the protein solution leading to protein conformation changes, protein aggregation, or protein denaturation. In the case of DSS, only a small amount of DSS was added to the Im9 solution and was seen in 1D ^{1}H NMR, however, it was found that in the PFG NMR experiment, the DSS signal was slowly decreased when the gradient strength increased like the protein signal would be. Normally, the diffusion coefficient of the internal radius standard should sharply decrease and that of the protein should slowly decrease when the gradient strength increased. This suggests that the DSS

molecule diffuses more slowly than the normal situation indicating it binds to Im9. Therefore, it cannot be used in this experiment.

In this experiment, acetaldehyde, which consisted of two chemical shifts at 1.2 and 9.5 ppm, was chosen to use as an internal radius standard, because the chemical shift at 9.5 ppm was not overlapped with any signal of Im9 or osmolytes and only small amount (40 µl of 1% v/v acetaldehyde) was added to the protein solution and did not affect the solution pH. However, the hydrodynamic radius of acetaldehyde was not known exactly. Therefore, I calibrated the hydrodynamic radius of acetaldehyde with dioxane. Acetaldehyde was added to dioxane in deuterated phosphate buffer solution pH 7.0 and 1D ^{1}H NMR spectra of this mixture are displayed in Figure 3.10. The diffusion coefficients of acetaldehyde and dioxane were measured by PFG-NMR and the hydrodynamic radius of acetaldehyde was calculated by comparing with dioxane values using Equation 2.9. Consequently, the calculated hydrodynamic radius of acetaldehyde is 1.79 Å at pH 7.0, 25 °C.

Moreover, we have to show that acetaldehyde does not have any effect on the Im9 structure by studying the diffusion rate constant (Lapham et al. 1997) of Im9 on its own and with acetaldehyde. The region of the spectrum from 10.0 to 6.5 ppm, which corresponds to the aromatic region of Im9, was integrated, because this region gave a smooth baseline, as shown in Figure 3.11 and in the other regions osmolyte signals occurred at the same place as Im9 signals as displayed in Figure 3.9. The diffusion rate constant of Im9 in the absence and the presence of acetaldehyde in each protein signal around 7.5 to 6.8 ppm are shown graphically in Figure 3.12 and listed in Table 3.3. As it can be seen, these values were not significantly different in every protein signals (7.32, 7.21, 7.01, 6.93, and 6.86 ppm). Moreover, the diffusion coefficient rate constant of acetaldehyde was nearly the same in the absence and presence of Im9. Therefore, it can be concluded that acetaldehyde does not interact significantly with Im9 and can be used as an appropriate internal radius standard in this experiment.

The PFG-NMR experiment was used to determine the diffusion coefficient of Im9 in the absence and the presence of osmolytes in different concentrations by using DOSY software (Peresada et al. 1999) and the hydrodynamic radius of Im9 calculated by comparing with acetaldehyde data. Protein samples were magnetised in 13 gradient strengths (as displayed in Chapter 2, Table 2.5A), increased from 1.77 to 26.62 Gauss

cm^{-1} and protein intensity was attenuated to about 10-20 % comparing with the initial intensities (100 %) when the gradient strength increased to the maximum. As it can be seen in Figure 3.13, Im9 signals at 7.32, 7.21, 7.01, 6.93, and 6.86 ppm were decreased to about 10 %.

Hydrodynamic radii of Im9 can be calculated by two different methods: A). slope of protein signal attenuation, and B). a pseudo two-dimensional (2D) DOSY (Diffusion ordered spectroscopy) spectrum, compared with the internal radius standard data (Acetaldehyde data), as described in section 2.2.3.3. As can be seen in Table 3.4, the calculated hydrodynamic radii values of Im9 were not significantly different between the two methods, 19.29±0.91 and 20.57±0.60 Å, respectively. Consequently, the DOSY method was chosen to calculate the hydrodynamic radii of Im9 in this study, because it is an automatic function in the NMR operating software which should give more accurate measurements (i.e. a lower standard deviation) than calculations from the slope.

The hydrodynamic radii values of Im9 in the absence of osmolytes (triplicate measurement) are displayed in Table 3.5 and the average of hydrodynamic radius is 20.54±0.21 Å. The hydrodynamic radius of a protein in its native condition can be calculated by Equation 3.2, which was obtained from experimental data for native folded proteins assumed to be spherical concerning the molecular dimensions and the length of the polypeptide chain (Wilkins et al. 1999).

$$\mathbf{R_h} = \mathbf{(4.75 \pm 1.11)\, N^{0.29 \pm 0.02}} \qquad \textit{Equation 3.2}$$

where, N = number of residues.

The calculated hydrodynamic radius value of 17.28 Å for Im9 (86 amino acid residues) by Equation 3.2, is 18.8 % smaller than the experimental value of 20.54 Å. The structure of Im9 is non-spherical, so the result obtained from this equation might have some variations. Moreover, the hydrodynamic radii of Im9 from previous works (Bijelic 2004, Boetzel et al. 2003) were 18.28 and 18.6 Å, respectively, which were also slightly smaller than my experimental value. It might be because the composition of the Im9 solutions were slightly different (0.3 mM Im9 in 50 mM phosphate buffer pH 7.0,

100 % D_2O, 1.0 mM DTT (Bijelic 2004) and 1.5 mM Im9, 100 % D_2O (Boetzel et al. 2003) and 1.0 mM Im9 in 100 mM deuterated phosphate buffer pH 7.0 (my experimental formulation). However, as the results shown in Table 3.5, the range of hydrodynamic radii of Im9 is from 19.60-22.17 Å and the average is 20.54 ±0.21 Å. Consequently, it can be assumed that the particle size of Im9 in the native conditions I explored had a larger size than the previous works; however, it is reasonable to take this value as the reference to compare the hydrodynamic radii of Im9 in the presence of osmolytes and in the different equilibrium denatured states since all other solution parameters were the same.

The hydrodynamic radii of Im9 in the absence and the presence of 0.25, 0.50, and 0.75 M each of trehalose and sucrose; and 10, 20, and 30 % (v/v) glycerol were measured and are summarized in Figure 3.14 and Table 3.6. From the results, it was found that the hydrodynamic radii of Im9 in the presence of trehalose were larger than that with sucrose at the same concentration of osmolytes (0.50 M and 0.75 M). In particular, at 0.75 M concentration, hydrodynamic radii of Im9 in the absence and the presence of trehalose obtained in this work significantly differed by 21.42 %, suggesting that trehalose can produce a hydration shell around Im9 larger than sucrose did (increased by 14.26 %) at the same concentration. However, at 0.25 M concentration of trehalose and sucrose, only small increases in the hydrodynamic radius of Im9, compared with in the absence of sugar. These results are indicative of sucrose and trehalose increasing the solvation sphere around the protein, perhaps because they are excluded from the protein surface (Timasheff 1993).

In contrast, the hydrodynamic radius of Im9 in the presence of 20 % and 30 % glycerol decreased approximately 5.79 %, but only a 0.59 % reduction was observed for 10 % glycerol, showing that the hydrodynamic radius of Im9 in the absence and the presence of 10 % glycerol are practically identical. This indicates that Im9 in the presence of glycerol (20 and 30 %) were smaller or more compacted than Im9 in the absence of glycerol. This situation is the opposite from that of trehalose and sucrose, but it is in excellent agreement with previous reports (Priev et al. 1996, Vagenende et al. 2009) stating that glycerol can decrease the volume and compressibility of protein or make the protein core denser and less compressible, suggesting that glycerol may reduce the total void volume of the protein core. In addition, it can be assumed that this reduction in the protein volume and compressibility is due to the release of water from

the protein interior. Moreover, Oliveira and co-workers reported that glycerol dehydrates proteins by means of displacing water of hydration and preferentially hydrating the protein itself, which leads to a reduction in the protein volume and compressibility (Oliveira et al. 1994). This agreement leads me to believe that glycerol causes a reduction in the size of the void volume in the Im9 structure, which would otherwise accommodate water, leading to a decrease in the internal free volume and increasing protein compactness.

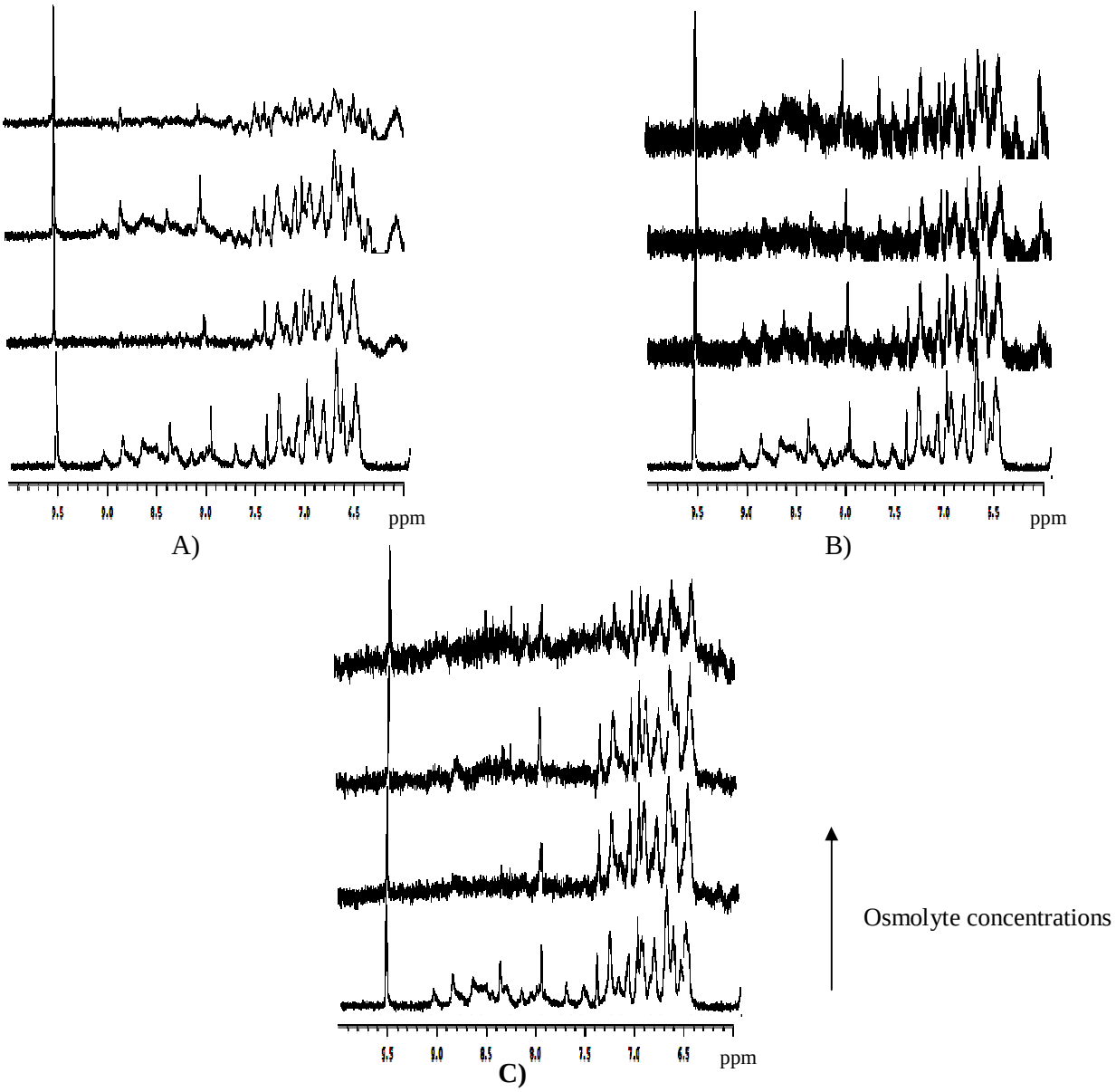

Figure 3.8 1D ^{1}H NMR spectra of Im9 in the absence and the presence of osmolytes. A) 1D ^{1}H NMR spectra of Im9 in the absence and the presence of trehalose from 0.25, 0.50, and 0.75 M, B) 1D ^{1}H NMR spectra of Im9 in the absence and the presence of sucrose from 0.25, 0.50, and 0.75 M, and C) 1D ^{1}H NMR spectra of Im9 in the absence and the presence of glycerol from 10, 20, and 30 % v/v glycerol (The arrow indicates the increase in osmolyte concentrations from bottom to top). Sample solutions (1 mM) were prepared in deuterated phosphate buffer solution pH 7.0 and measured by Unity*Inova* 500 MHz spectrometer at 25 °C. The decrease in signal: noise ratio is discussed in the text. Small differences in peak intensities in the region 8-10 ppm are a consequence of variable NH/ND exchange.

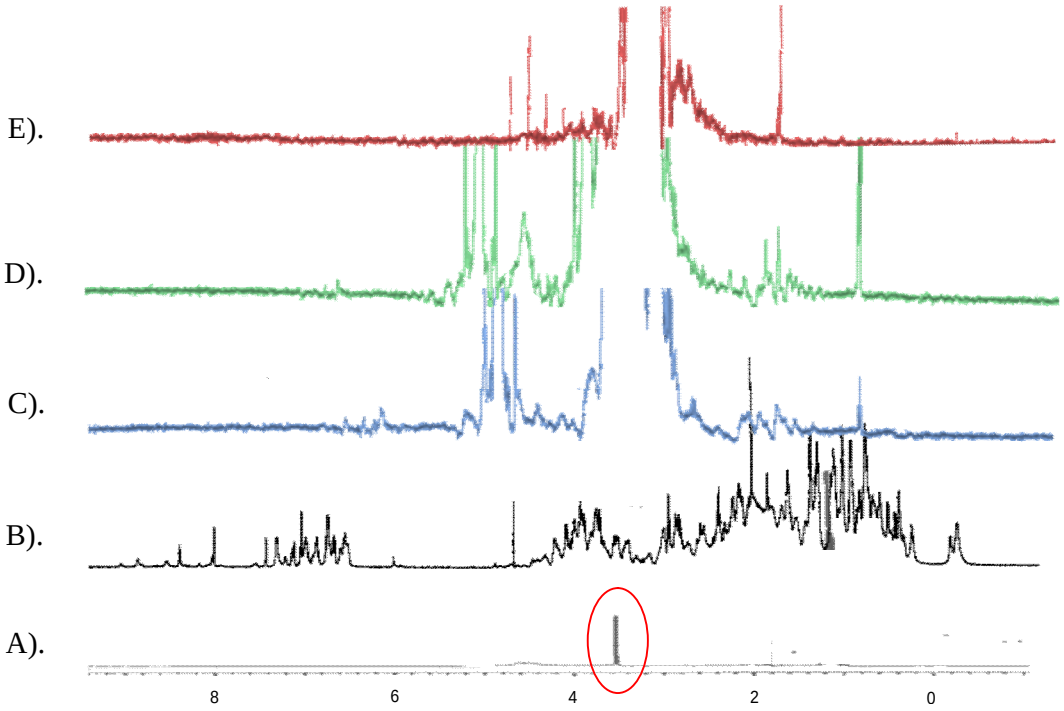

Figure 3.9 1D ^{1}H NMR spectra of dioxane, Im9, and osmolytes. A) 1% dioxane, B) Im9, C) 0.5 M trehalose, D) 0.5 M sucrose, and E) 20 % glycerol. Sample solutions were prepared in deuterated phosphate buffer solution pH 7.0 and measured by Unity*Inova* 500 MHz spectrometer at 25 °C.

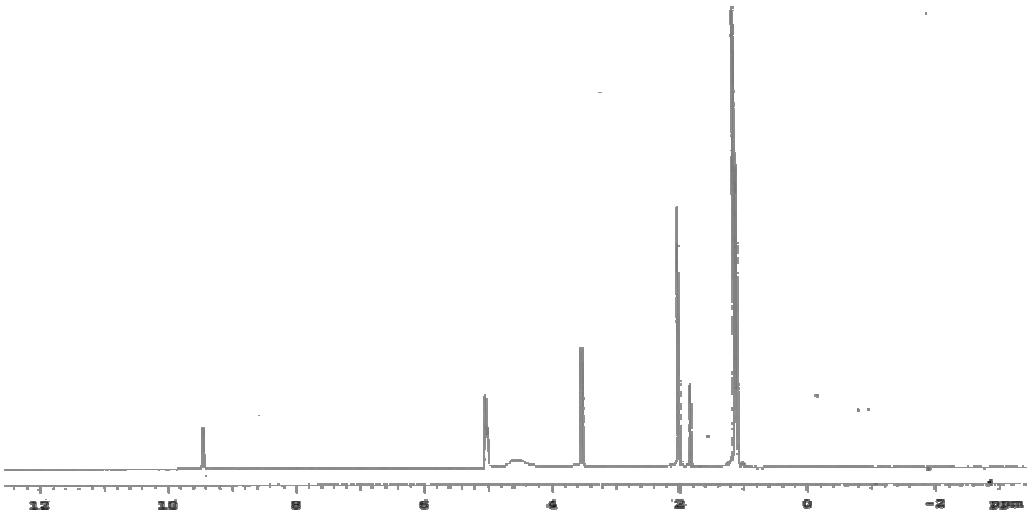

Figure 3.10 1D ^{1}H NMR spectrum of acetaldehyde (1.2 and 9.5 ppm) and dioxane (3.5 ppm) in deuterated phosphate buffer pH 7.0 was measured by Unity*Inova* 500 MHz spectrometer at 25 °C.

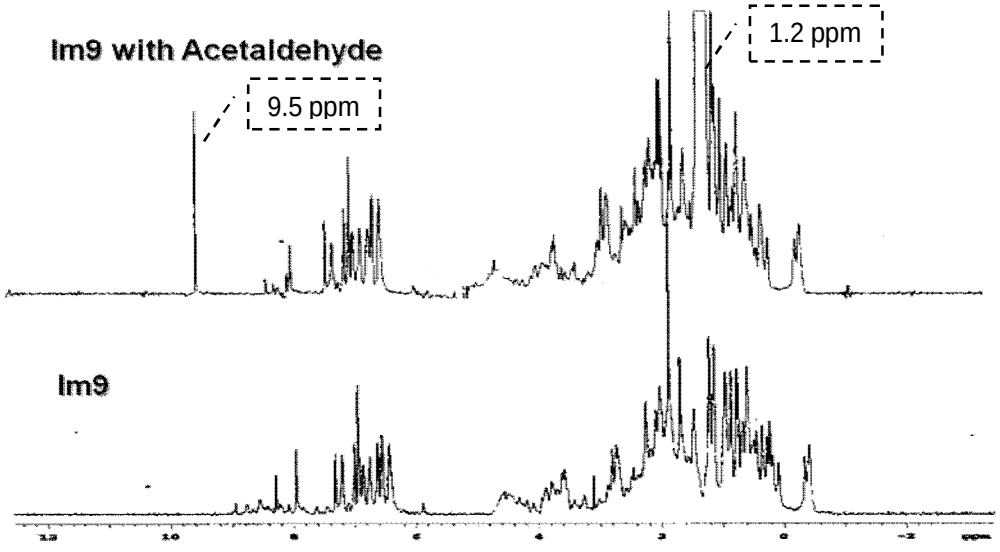

Figure 3.11 1D ^{1}H NMR spectra of Im9 in deuterated phosphate buffer pH 7.0 solution and Im9 in deuterated phosphate buffer solution pH 7.0 with 40 µl of 1 % acetaldehyde were measured by Unity*Inova* 500 MHz spectrometer at 25 °C.

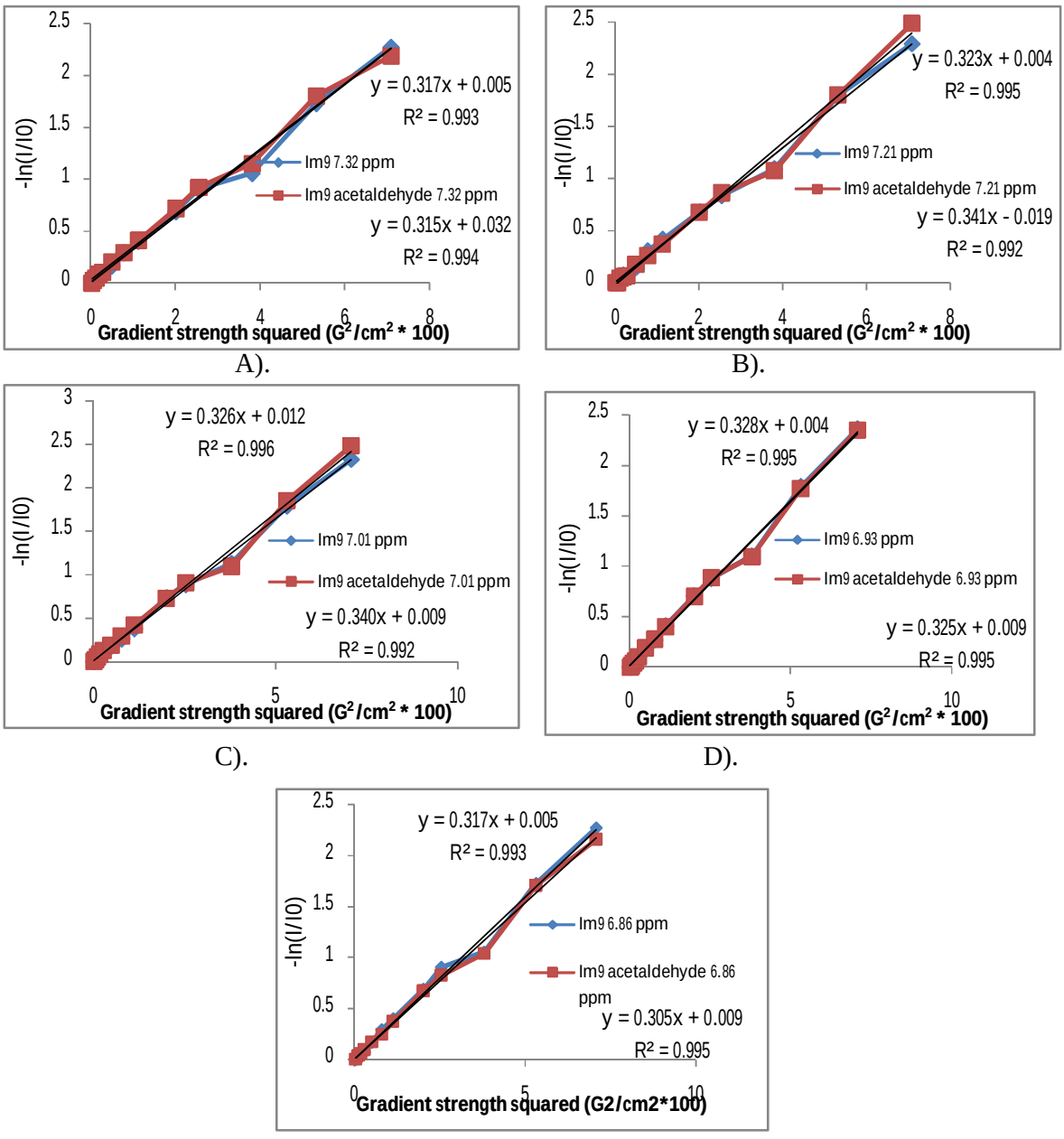

Figure 3.12 Diffusion coefficient rate constant measurements of Im9 with and without acetaldehyde in deuterated phosphate buffer pH 7.0, at 25 °C. The diffusion coefficient rate constants are the slope of straight line which drawn by using a linear trend line in Excel.

Table 3.3 Comparison of diffusion coefficient rate constant of Im9 in the absence and presence of acetaldehyde.

Chemical shift (ppm)	Diffusion coefficient rate constant (m^2/sec)	
	Im9	Im9 with acetaldehyde
7.32	0.3179	0.3151
7.21	0.3231	0.3410
7.01	0.3267	0.3404
6.93	0.3285	0.3257
6.86	0.3179	0.3056

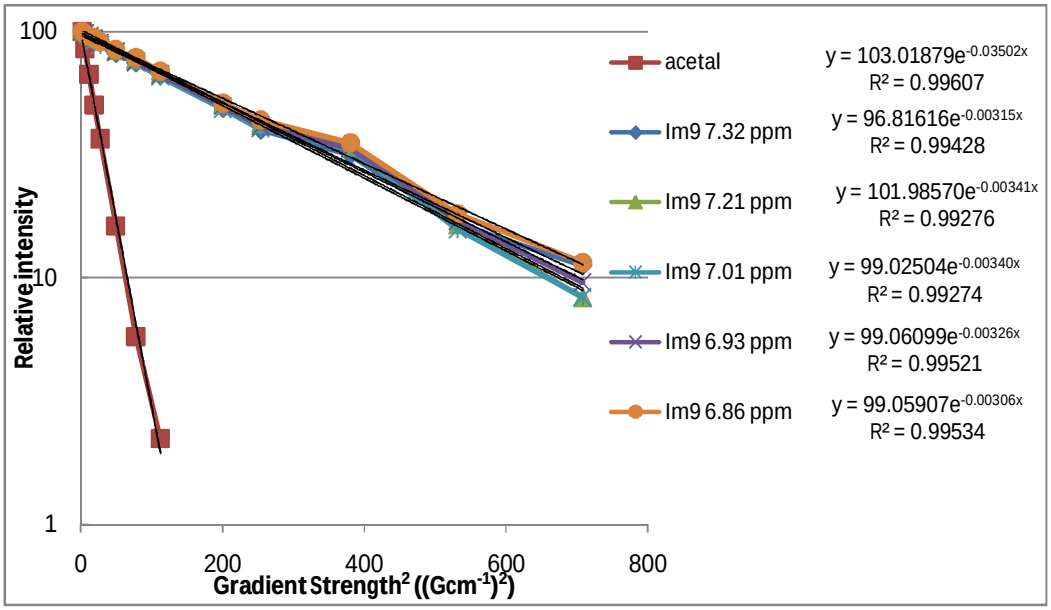

Figure 3.13 Signal attenuation caused by diffusion in PFG-NMR experiments for Im9 in the presence of acetaldehyde at 25 °C. The diffusion coefficient of acetaldehyde and each protein signals (7.32, 7.21, 7.01, 6.93, and 6.86 ppm) were measured and displayed as a slope in each exponential equation.

Table 3.4 Diffusion coefficient and hydrodynamic radius values of Im9 in each protein signals calculated by two methods;

Chemical shift (ppm)	Method A (Slope of signal attenuation)		Method B (DOSY)	
	Slope	Hydrodynamic radius (Å)	Diffusion coefficient (m^2/sec)	Hydrodynamic radius (Å)
7.32	0.00315	19.90	1.403	21.07
7.21	0.00341	18.38	1.508	19.60
7.01	0.00340	18.44	1.408	20.99
6.92	0.00326	19.23	1.423	20.77
6.86	0.00306	20.48	1.447	20.43
AVG	**0.00326**	**19.29**	**1.438**	**20.57**
SD	**0.00015**	**0.91**	**0.04**	**0.60**
% RSD	**4.71**	**4.75**	**2.98**	**2.90**

Method A: Slope of signal attenuation (The slope and hydrodynamic radius of acetaldehyde are 0.03502 and 1.79 Å, respectively)

Method B: DOSY (The diffusion coefficient and hydrodynamic radius of acetaldehyde are 16.512 m^2 / sec and 1.79 Å, respectively)

Table 3.5 The hydrodynamic radii values of Im9 calculated by DOSY in triplicate experiment.

	Measurement 1		Measurement 2		Measurement 3		Average value	
Chemical shift	**D_t**	**R_h**	**D_t**	**R_h**	**D_t**	**R_h**	**D_t**	**R_h**
(ppm)	**(m^2/sec)**	**(Å)**	**(m^2/sec)**	**(Å)**	**(m^2/sec)**	**(Å)**	**(m^2/sec)**	**(Å)**
7.32	1.403	21.07	1.500	19.96	1.535	20.41	1.479	20.48
7.21	1.508	19.60	1.441	20.78	1.486	21.08	1.478	20.49
7.01	1.408	20.99	1.527	19.61	1.546	20.27	1.494	20.29
6.92	1.423	20.77	1.475	20.30	1.518	20.64	1.472	20.57
6.86	1.447	20.43	1.498	19.99	1.413	22.17	1.453	20.86
AVG	**1.438**	**20.57**	**1.488**	**20.13**	**1.500**	**20.91**	**1.475**	**20.54**
SD	**0.04**	**0.60**	**0.03**	**0.44**	**0.05**	**0.77**	**0.01**	**0.21**
% RSD	**2.98**	**2.90**	**2.16**	**2.18**	**3.56**	**3.66**	**1.01**	**1.02**

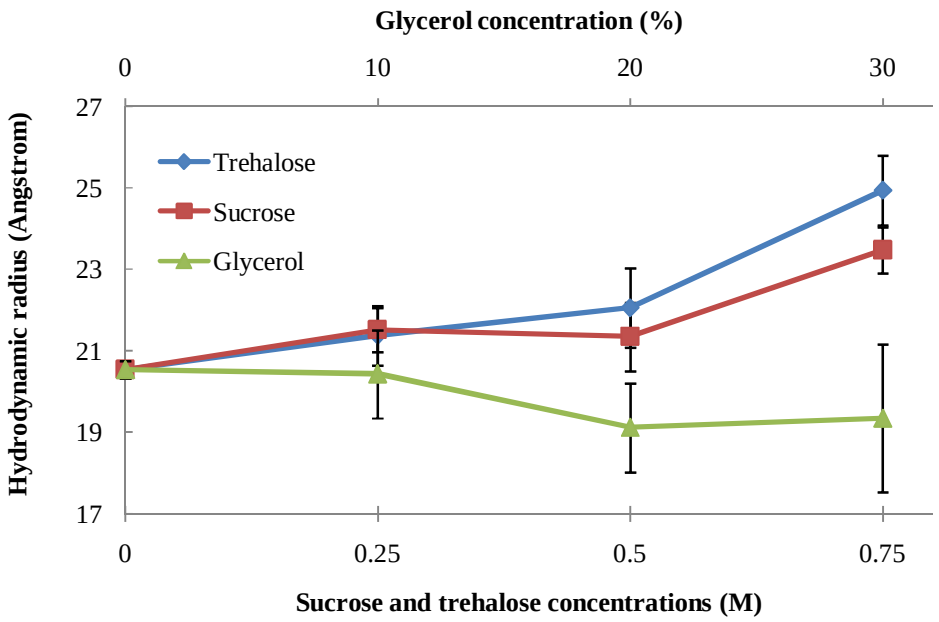

Figure 3.14 Comparison of hydrodynamic radii of Im9 in the absence and the presence of osmolytes at 25 °C. (trehalose (◆), sucrose (■), and glycerol (▲)). (Error bars are standard deviations n=3).

Table 3.6 Comparison of hydrodynamic radii of Im9 in the absence and presence of osmolytes (trehalose, sucrose, and glycerol) at 25 °C. (Error bars are standard deviations, n=3).

Conc	Trehalose		%	Sucrose		%	Glycerol		%	Conc
(M)	R_h (Å)	SD	Increased	R_h (Å)	SD	Increased	R_h (Å)	SD	Decreased	(%)
0.00	20.54	0.21	-	20.54	0.21	-	20.54	0.21	-	0.00
0.25	21.38	0.73	+4.09	21.52	0.54	+4.77	20.43	1.08	- 0.53	10.00
0.50	22.06	0.97	+7.40	21.35	0.84	+3.94	19.12	1.09	- 6.91	20.00
0.75	24.94	0.86	+21.42	23.47	0.57	+14.26	19.35	1.81	- 5.79	30.00

3.2.3 Hydrodynamic radii of urea-unfolded Im9

To investigate protein stability it is important to note that the interactions between solvent and protein in both the native and denatured state are of equal importance. The information about the denatured state should be studied, because the alteration in hydrodynamic radius upon denaturation is an important parameter to assess the effect of an osmolyte on protein stability.

In this study, PFG-NMR experiment has been used for measuring hydrodynamic radius of Im9 unfolded by 8M urea, frequently termed the fully denatured state (Tezuka-Kawakami et al. 2006), and can be considered as a reference value to compare with Im9 in its urea-denatured state in the presence of osmolytes. Many previous works also used PFG-NMR experiment to detect the hydrodynamic radius of proteins in denatured state ((Jones et al. 1997, Wilkins et al. 1999).

3.2.3.1 One dimensional proton NMR

1D ^{1}H NMR experiment was used to study the Im9 structure in both the native and denatured state and it was found that there are significantly differences between them, as displayed in Figure 3.15. These results are in excellent agreements with these from the fluorescence spectroscopic experiment in section 3.2.1.1; therefore, it can be assumed that urea has an interaction with Im9 both in the absence and the presence of osmolytes.

3.2.3.2 Pulsed-field gradient NMR (PFG-NMR) spectroscopy

PFG-NMR experiment was used to determine the diffusion coefficient of unfolded Im9 in the absence and the presence of osmolytes by using DOSY software and the hydrodynamic radius of Im9 was calculated by comparing with acetaldehyde data. The PFG-NMR experiments of Im9 in native and denatured state are very similar in the processes, except the sample preparation as displayed in Section 2.2.3.1.2.

The experimental hydrodynamic radius value of denatured Im9 is 31.34±1.68 Å. Hydrodynamic radii of proteins under denaturing conditions can be calculated by Equation 3.3, which is obtained from the experimental data between the molecular dimensions and the length of the polypeptide chain (Wilkins et al. 1999).

$$R_h = (2.21 \pm 1.07)\, N^{0.57 \pm 0.02} \qquad \textit{Equation 3.3}$$

where, N = number of residues.

The calculated hydrodynamic radius value for Im9 of 28.0 Å (86 amino acid residues) by Equation 3.3 is 10.94 % smaller than the experimental value of 31.34±1.68 Å. Moreover, the hydrodynamic radius of Im9 in 8 M urea from earlier work (Bijelic 2004) was 26.33 Å, which is also smaller than the experimental value. The explanation for these differences should be the same reasons as in the native state (Section 3.2.2.2), which stated that this might be due to the difference in protein composition. Therefore, it can be assumed that this experimental value would be used as the reference to compare with the hydrodynamic radii of unfolded Im9 in the presence of osmolytes.

In Table 3.7, the results show significant changes in the values of hydrodynamic radii for unfolded Im9 (8 M urea) in the absence and the presence of osmolytes. The hydrodynamic radius of fully unfolded Im9 is 53.48 % larger than that of its native state. Moreover, unfolded Im9 in the presence of osmolytes also has a large increment but in this case of about 80-95 % in its hydrodynamic radii. Unfolded Im9 in the presence of 0.75 M each of trehalose and sucrose has a larger hydrodynamic radius than in the presence of 30 % glycerol. In the case of trehalose and sucrose, the hydrodynamic radius of unfolded Im9 is about the same. However, the largest difference in hydrodynamic radius of unfolded Im9 in the absence and the presence of osmolytes is with glycerol. In unfolded conformation, the hydrophobic residues, which usually reside within the cleft of protein molecule, are expanded and the surface contacts with the surrounding solvent are increased in most of the hydrophobic residues, as described in Chapter 1, Figure 1.3. Moreover, as displayed in Figure 3.16, the structure of unfolded proteins in the presence of osmolytes can be more expanded than that of native state (O'Connor et al. 2004), and the expanded structure would be still covered with the hydration layer, resulting to the hydrodynamic radius of unfolded protein in the presence of osmolytes would be larger than that of native state in the presence of osmolytes. Although the hydrodynamic radii of Im9 in the presence of glycerol presented smaller size than the others, unfolded Im9 in the presence of glycerol showed the largest of % increment in hydrodynamic radius. This might be due to the fact that glycerol is more favourable to contact with hydrophilic than hydrophobic residue, but in

the unfolded state, hydrophobic residues stay on the surface of protein rather than in native state, so glycerol tends to stay outside, resulting in the large increment in hydration layer. Consequently, it can be concluded that a variation in solution conditions can affect the denatured state of Im9. However, some previous works (O'Connor et al. 2004, O'Connor et al. 2007) showed the opposite results to our study. No changes in the hydrodynamic radii of both RNase A and α-lactalbumin were seen in the denatured states upon the addition of sucrose and fructose. In this report the hydrodynamic radii of proteins in both the native and denatured state were measured by using the combination of capillary electrophoresis (CE) and protein charge ladders techniques. The explanation of these results is related to the disulfide bonds, which are present in RNase A and α-lactalbumin, but not in Im9, and these normally inhibit protein expansion upon denaturation. In these cases, an expansion still occurred upon denaturation, but a more compact denatured state was seen than in a protein, Im9, without disulfide bonds.

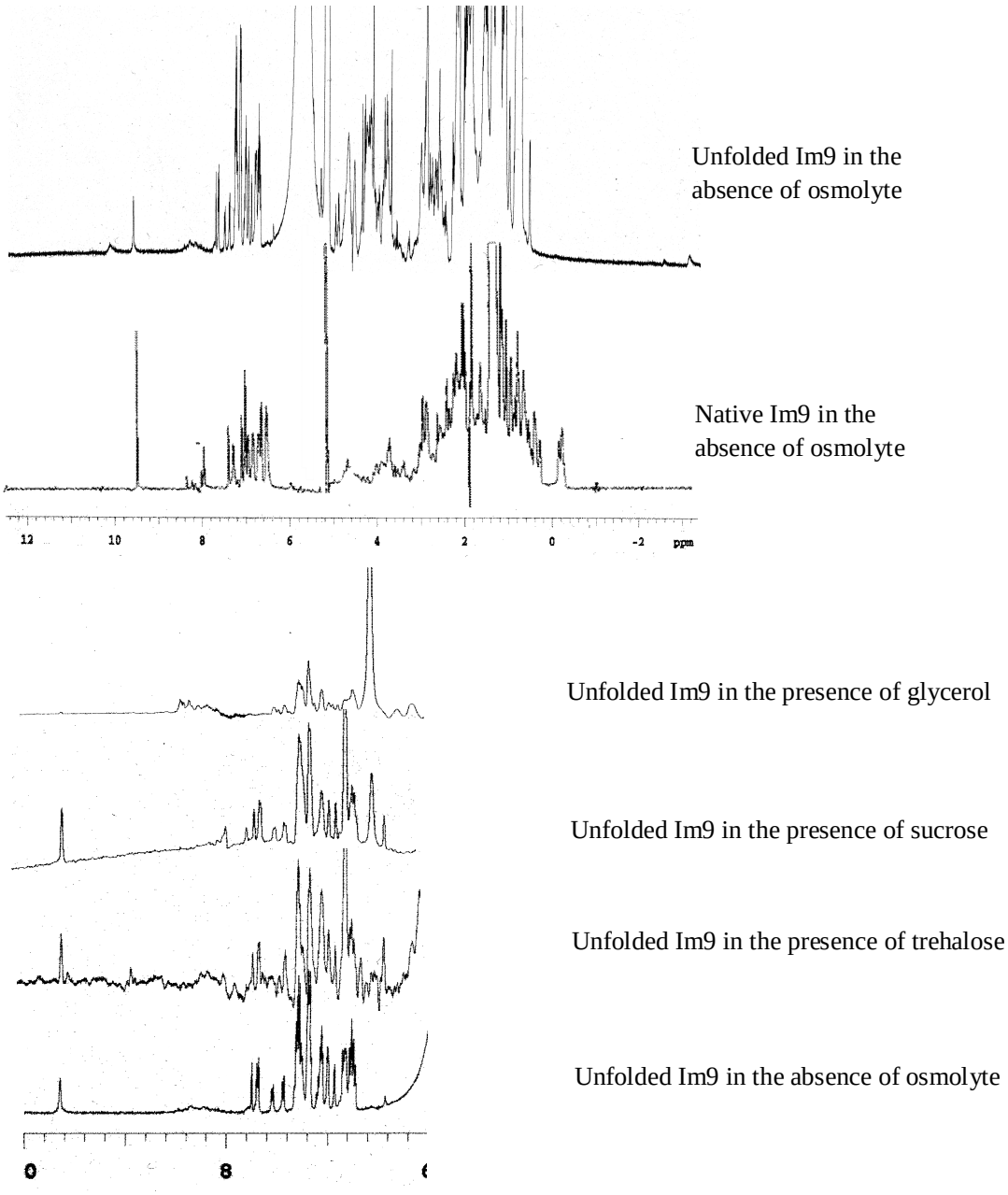

Figure 3.15 1D ^{1}H NMR spectra of native and unfolded Im9 in the absence and the presence of osmolytes (trehalose, sucrose, and glycerol). A). Full scale, chemical shift from -2 to 12 ppm and B). Some part of scale, chemical shift from 6 to 10 ppm. All unfolded protein solutions (1 mM protein concentration) were prepared in 8 M urea deuterated phosphate buffer solution pH 7.0 in the absence and the presence of osmolytes and measured by Unity*Inova* 500 MHz spectrometer at 25 °C.

Table 3.7 Hydrodynamic radii measured by PFG-NMR experiment of Im9 in the absence and the presence of osmolytes (0.75 M trehalose, 0.75 M sucrose, and 30% glycerol) in native and urea-unfolded state (8 M urea).

	R_h native (Å)	SD	R_h denatured (Å)	SD	$\triangle R_h$ (Å)	% increased
Control	20.42	0.26	31.34	1.68	10.92	53.48
0.75 M Trehalose	24.94	0.86	44.75	0.74	19.81	79.41
0.75 M Sucrose	23.47	0.57	41.58	1.14	18.11	77.14
30% Glycerol	19.35	1.81	37.87	1.05	18.52	95.68

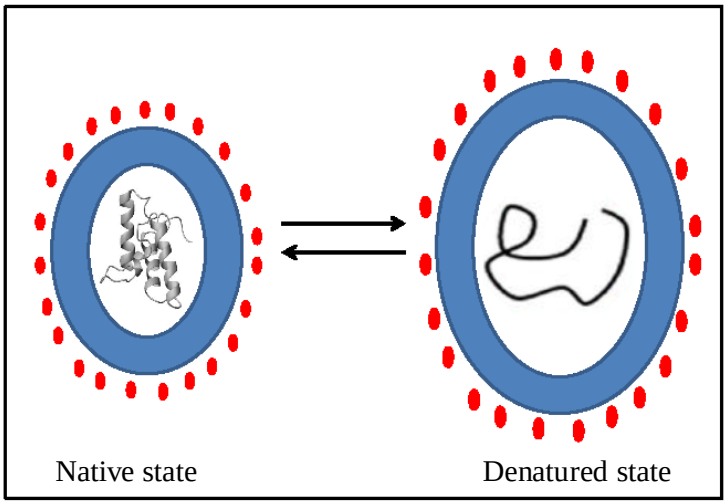

Figure 3.16 A model of a stabilised protein in the native and denatured state. A narrow hydration layer (blue circle around protein molecules) is formed around the protein in both native and denatured state, however the enhanced hydration layer was found in the denatured states, because the protein structure is more unstructured and expanded. In addition, osmolyte molecules (red filled circles) are preferentially excluded from the protein surface, resulting to the denatured protein is more enhanced hydration layer on the protein surface than the native protein.

3.2.4 Conformational stability of Im9 in the absence and in the presence of osmolytes at 10 °C

As can be seen from the previous work of Ferguson, the stability of Im9 is reduced at high temperature (Ferguson et al. 1999) and as a result, most of the reported unfolding experiments of Im9 are at 10 °C, (Ferguson et al. 1999, Gorski et al. 2001, Friel, Capaldi and Radford 2003, Cranz-Mileva, Friel and Radford 2005, Morton et al. 2007). In part, this was because they studied the equilibrium stability and folding/unfolding kinetics of Im9, measured by stopped-flow fluorescence, and this technique cannot detect rapid folding rates at higher temperature (25-40 °C) (Morton et al. 2007). Therefore, in this section, the temperature was changed from 25 to 10 °C so that the rate of folding should be reduced, resulting in easier to detect changes in thermodynamic properties of the protein that might be compared with data reported in the literature.

3.2.4.1 Fluorescence spectrum

In order to establish whether the presence of urea has any influence on the structure of Im9, fluorescence spectroscopic measurements were performed in the absence of osmolytes at 10 °C, exciting tryptophan fluorescence at 295 nm. For the denatured state of Im9, the fluorescence spectrum of urea denatured protein at pH 7.0 was measured in the absence of osmolytes (Figure 3.17). It was found that the intensities and Trp emission maxima of Im9 changed in response to urea concentration. The fluorescence spectra pattern are the same as detected at 25 °C, but the differences in intensity between native and denatured state are much higher than at 10 °C.

The effect of osmolytes on the protein structure has been investigated by taking fluorescence spectra versus osmolytes concentration in the range of 315-395 nm. The fluorescence of Im9 in the absence (Figure 3.18A) and in the presence of osmolytes (Figure 3.18 B-D for 0.5 M trehalose, 0.5 M sucrose and 20 % glycerol, respectively) at 10 °C were significantly different from those at 25 °C (Figure 3.3). The difference probably arises from more efficient quenching at 10 °C removing the low fluorescence emission seen at 25 °C as a consequence of reduced protein dynamics. Thus, I conclude

that Im9 retains its native structure and osmolytes don't have any effect on the Im9 structure at 10 °C, which is keeping with NMR data.

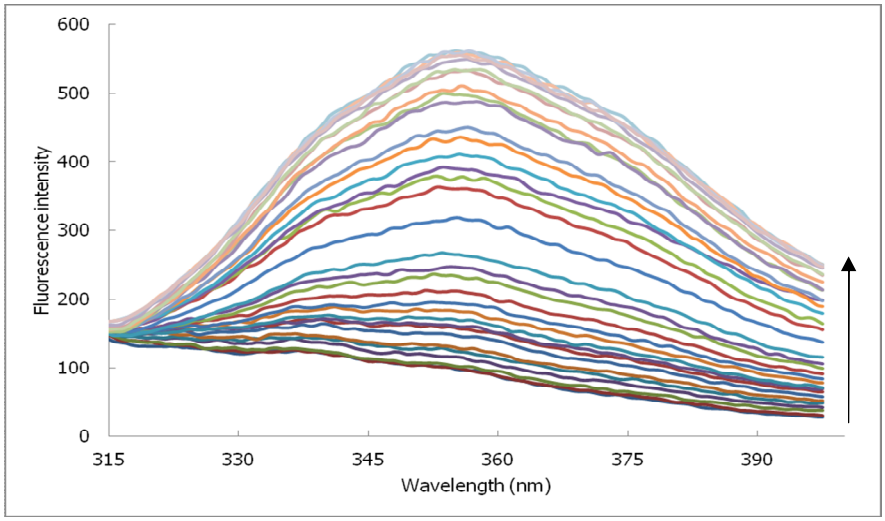

Figure 3.17 Fluorescence intensity of Im9 with urea (0 M to 8 M), at 10 °C. The arrow indicates the increase in fluorescence intensity with the increase in urea concentration. Im9 solutions (0.21 µM) were prepared in 0.1 M phosphate buffer solution pH 7.0 and then added with urea stock solution to obtain the desired concentration.

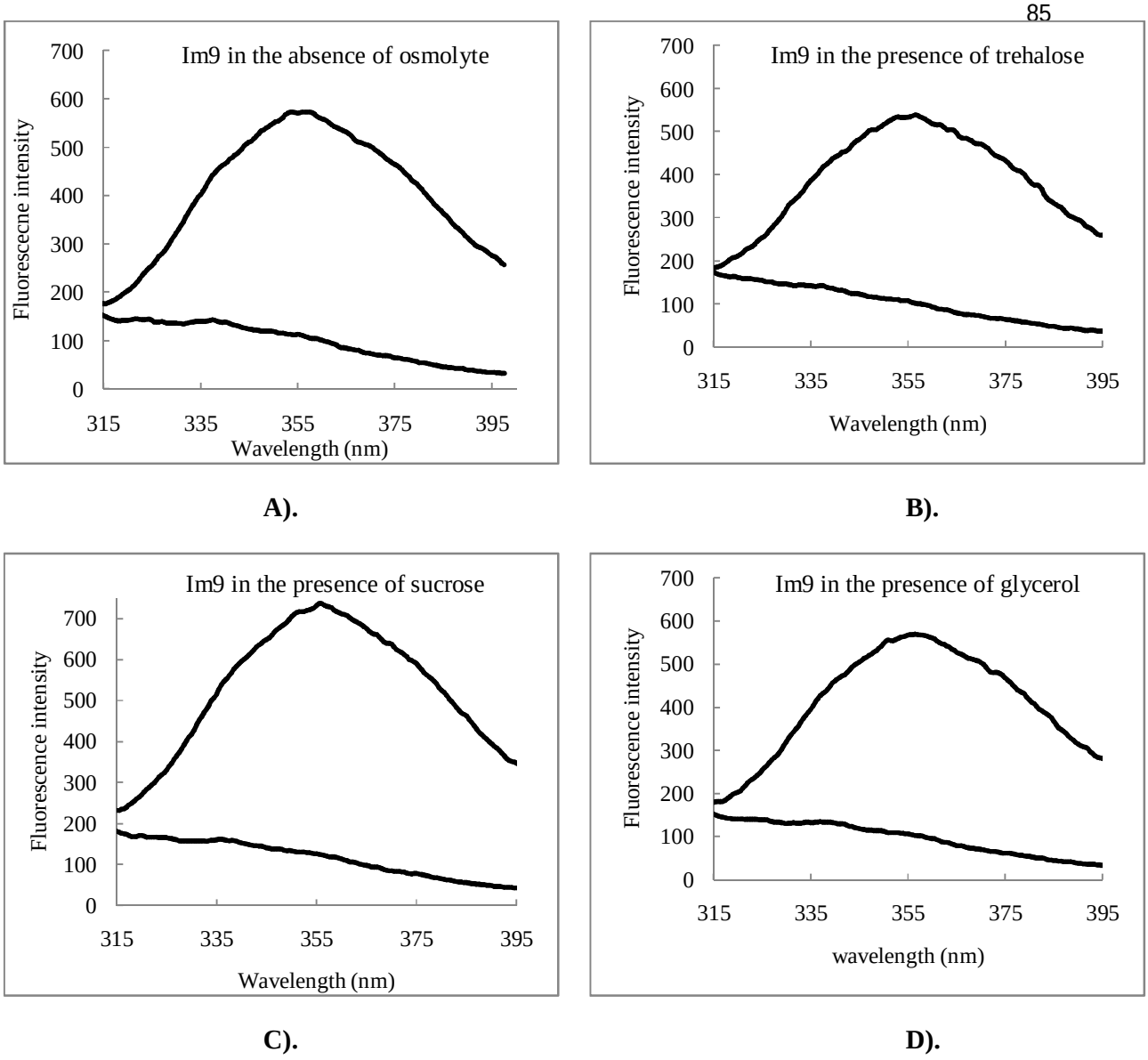

Figure 3.18 The emission spectra (Trp fluorescence spectra) of native (solid line) and denatured (dashed line) Im9 in the absence and the presence of osmolytes at 10 °C. The emission spectra of native Im9 in the absence of osmolyte (A) and stabilised native Im9 in the presence of osmolytes (0.50 M trehalose (B), 0.50 M sucrose (C), and 20 % glycerol (D)). All samples contained 0.21 μM Im9 and were measured by using 1 cm pathlength cuvette, at pH 7.0 and at 10 °C.

3.2.4.2 Urea-induced denaturation

Figure 3.19A displays the changes in the fluorescence intensity of Im9 at 340 nm when the urea concentration is increased. The pattern of unfolding curves were the same as when measured at 25 °C, but the fluorescence intensity in each spectrum were significantly higher. This situation generally occurs when the measuring temperature is decreased (Lakowicz 2006a). The emission intensities of Im9 at 340 nm in different urea concentrations were plotted against urea concentration, as displayed in Figure 3.19B. The urea-induced denaturation curves show that the addition of urea to Im9 denatures it; the transition region started from 3.0 M urea with Im9 completely unfolded around 8.0 M urea. Then the data from Figure 3.19B were treated as described in Section 2.2.2.3 to yield the unfolding curves displayed in Figure 3.19C. The thermodynamic parameters were calculated from this denaturation curve by using Equation 2.6 and are given in Table 3.8. The unfolding curve (solid black line) was fitted well according to a two-state transition (N↔D) which agreed with previously reported data (Gorski et al. 2001, Ferguson et al. 1999, Cranz-Mileva et al. 2005).

The thermodynamic parameters I obtained are significantly different from those previously reported (Ferguson et al. 1999, Gorski et al. 2001). Experimental values of $Urea_{1/2}$, $\triangle G^{H2O}$, and m-value are lower than those obtained from previous reports. These differences can be attributed to the different experimental conditions, such as composition in protein solution, which could give different values. In Gorski's formulation (Gorski et al. 2001), many substances were added to the protein solution, e.g. 20 mM sodium acetate, 20 mM sodium borate, 0.4 M sodium sulphate, and 1 mM EDTA. In particular, sodium sulphate is a stabilising salt that materially enhances protein stability (Tadeo et al. 2009, Cobos and Radford 2006).

Urea-induced denaturation curves of Im9 in the absence and presence of 0.25, 0.50, 0.75, and 1.00 M each of trehalose and sucrose; and 10, 20, 30, and 40 % (v/v) glycerol were also measured by following changes in the fluorescence intensity as a function of the urea concentration at pH 7.0, 10 °C and are displayed in Figure 3.20A, B, and C, respectively. The osmolyte concentrations were changed up to a maximum of 1.00 M, because at 25 °C, Im9 in the presence of the highest concentration of osmolytes (0.75 M and 30 % v/v) showed low $\triangle G^{H2O}$ values, comparing with Im9 in the absence of osmolyte. A two-state mechanism was also used for the analysis of the urea-induced

denaturation curves because the characteristics of the two-state transition of denaturation curve are not affected by the addition of osmolytes. As it can be seen in Figure 3.20A-C, the denaturation curves of Im9 in the presence of osmolytes at 10 °C were significantly shifted toward higher urea concentration at increasing osmolyte concentration except those of Im9 in the presence of glycerol. While the curve shifted to higher urea concentration for 10 % glycerol, only small changes were seen for 20, 30, and 40 % glycerol.

The thermodynamic parameters are presented in Table 3.9 and graphically displayed in Figure 3.21A-C. Thermodynamic parameters of Im9 in stabilised state are significantly increased compared to those of Im9 in its native state. The maximum $\triangle G^{H2O}$ values of Im9 in the presence of 0.75 M trehalose are high up to 6.40 kcal mol^{-1} compared with those values at 25 °C of 4.97 kcal mol^{-1}, indicating that Im9 at 10 °C are more stable than Im9 at 25 °C.

The comparisons of thermodynamic parameters for each value ($Urea_{1/2}$, $\triangle G^{H2O}$, and m-value) are graphically displayed in Figure 3.22A-C, respectively. The results in Figure 3.22A obviously distinguish the change of $Urea_{1/2}$ values. The highest concentration of osmolytes induces a shift of $Urea_{1/2}$ from 5.00 M to 5.99 M, 5.72 M, and 5.69 M for trehalose, sucrose, and glycerol, respectively. This enhancement is found here to be about 13.8 – 19.8 %, depending on the particular osmolyte concentration. Interestingly, the midpoint of unfolding transition order in osmolytes shows that trehalose is the strongest stabiliser. Only in low concentration is glycerol stronger than trehalose and sucrose, but at the highest concentration, sucrose changed to be a stronger stabiliser. Moreover, the results of $\triangle G^{H2O}$ and m-value of Im9 in the presence of osmolytes, which are represented in Figure 3.22B and C, respectively, related to those of $Urea_{1/2}$. It emerges from these figures that the $\triangle G^{H2O}$ values of Im9 in the presence of trehalose and sucrose significantly increased linearly as the osmolyte concentration increases, while in the presence of 10 % glycerol, $\triangle G^{H2O}$ values increased sharply and slightly increased when glycerol concentration increases to 20, 30, and 40 %. In addition, the m-values of Im9 are nearly constant in the presence of 0.25 M each of trehalose and sucrose comparing with Im9 in the absence of osmolyte and they significantly increased when the osmolytes concentration increased from 0.25 to 1.0 M.

As it can be seen for $\triangle\triangle G^{H2O}$, The comparison clearly showed that $\triangle\triangle G^{H2O}$ tend to increase with osmolyte concentration for all osmolytes tested, but not in a linear relationship, as displayed in Figure 3.21 D-F. Consequently, it can be assumed that these parameters increase as osmolyte concentration increases and the efficiency of stabilizing effects follows this order: trehalose > sucrose > glycerol.

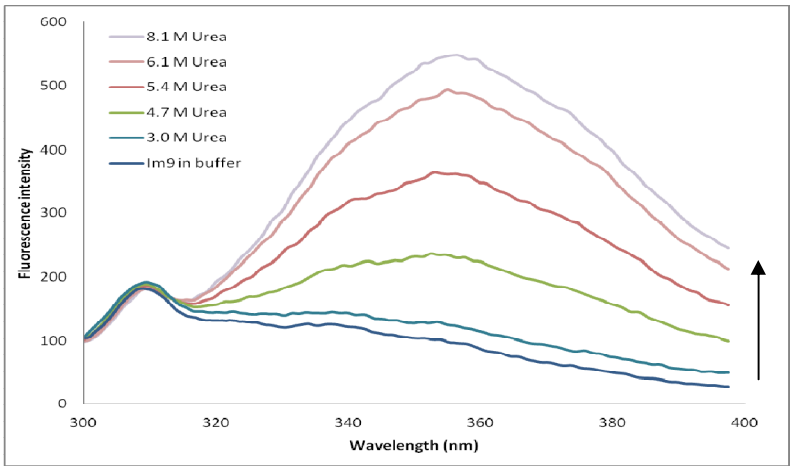

A).

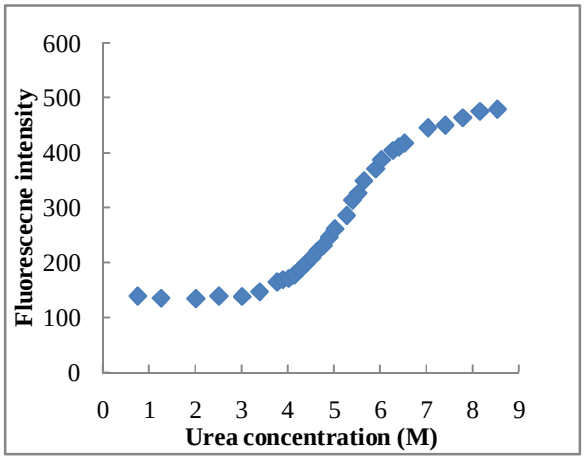

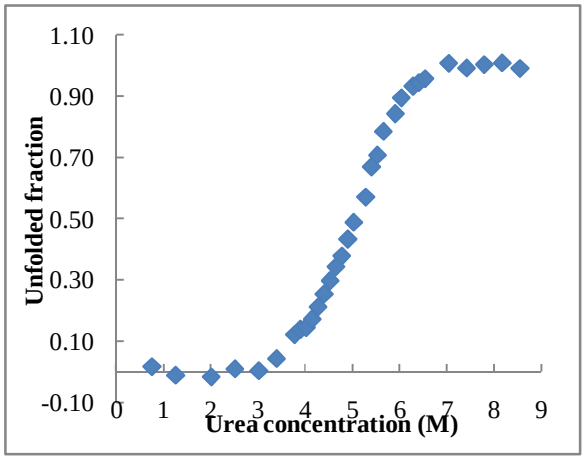

B). **C).**

Figure 3.19 Fluorescence intensity curve and unfolding curve of Im9 with urea at 10 °C. A). Fluorescence intensity of Im9 with urea (0 M to 8 M) at 10 °C. The arrow indicates the increase in fluorescence intensity with the increase in urea concentration. Im9 solutions (0.21 µM) were prepared in 0.1 M phosphate buffer solution pH 7.0 and then added to urea stock solutions to obtain the desired concentrations. The excitation wavelength was 295 nm. The excitation and emission slit widths were 10.0 nm each.

B). Fluorescence intensity of Im9 at 340 nm versus urea concentration.

C). The unfolding curve of Im9 with urea concentration detected by fluorescence spectroscopy at 10 °C.

Table 3.8 Equilibrium unfolding parameters for Im9 in native state at pH 7.0, 10 °C.

Protein	**Thermodynamic parameters**		
	m-value (kcal mol^{-1} M^{-1})	**$\triangle G^{H2O}$ (kcal mol^{-1})**	**Urea $_{1/2}$ (M)**
Im9[a]	1.03	5.17	5.01
Im9[b]	1.10 (4.62 ± 0.09 kJ mol^{-1} M^{-1})	6.23 26.1 ± 0.5 (kJ mol^{-1})	5.65
Im9[c]	1.06 (4.45 ± 0.10 kJ mol^{-1} M^{-1})	7.42 31.1 ± 0.6 (kJ mol^{-1})	6.99

a. Thermodynamic parameters from my experiment. The sample solutions were prepared containing 100 mM potassium phosphate buffer, pH 7.0 with a final concentration of 0.21 µM and monitored by fluorescence spectroscopy at 340 nm

b. Thermodynamic parameters from (Ferguson et al. 1999). The sample solution were prepared containing 50 sodium phosphate buffer, pH 7.0 and 2 mM DTT with a final concentration of 20 µM and monitored by far-UV CD at 225 nm

c. Thermodynamic parameters from (Gorski et al. 2001). The sample solution were prepared containing 20 mM sodium acetate, 20mM sodium phosphate, 20 mM sodium borate, 0.4 M sodium sulphate, 1 mM EDTA with a final concentration of 0.2mg/ml and monitored by Circular Dichroism at 222 nm

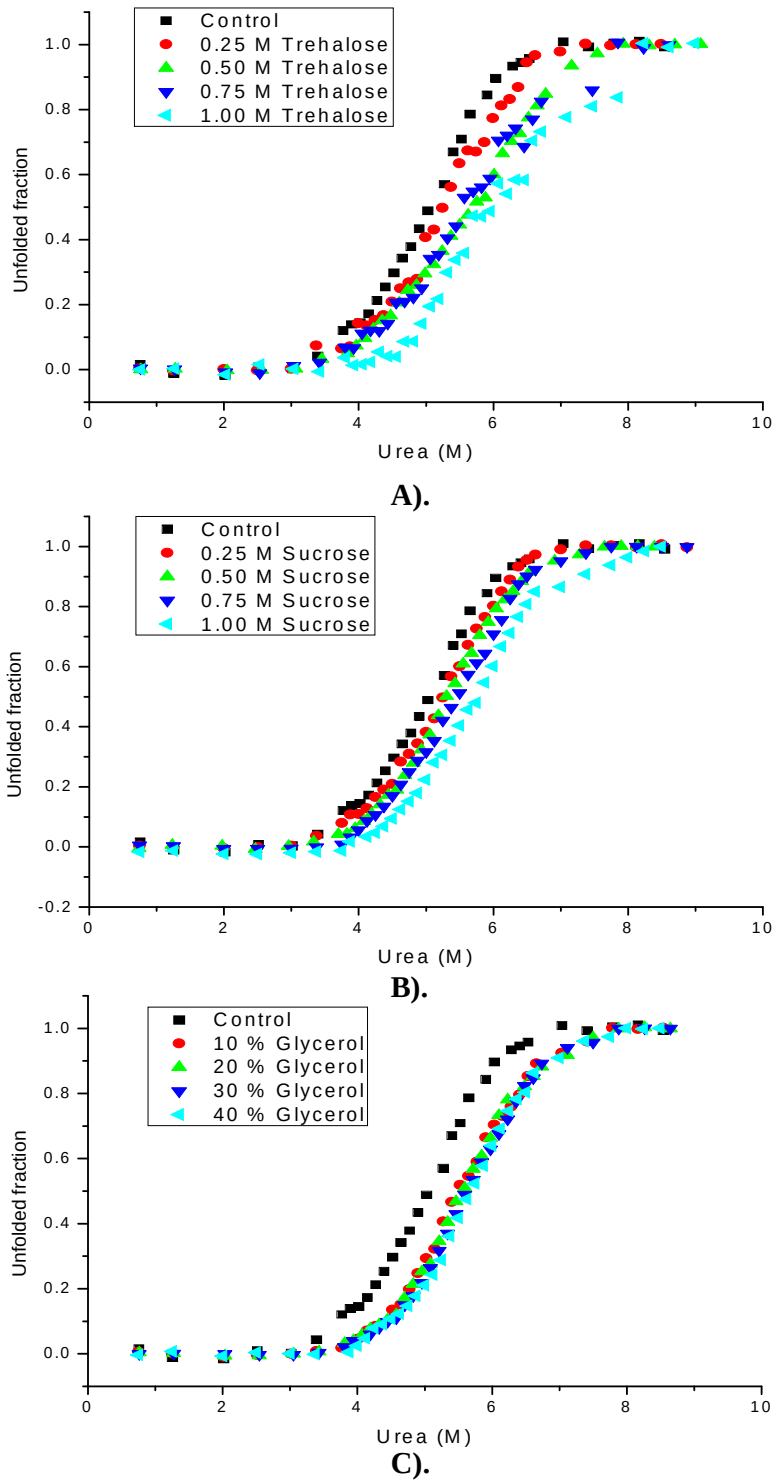

Figure 3.20 Urea-induced denaturation curves of Im9 in the absence and the presence osmolytes at 10 °C. Im9 solutions (0.21 μM) were prepared in 0.1 M phosphate buffer solution pH 7.0 in the absence and presence of 0.25, 0.50, 0.75, and 1.0 M trehalose (A), 0.25, 0.50, 0.75, and 1.0 M sucrose (B), and 10, 20, 30, and 40 % (v/v) glycerol (C).

Table 3.9 Thermodynamic parameters (m-value, $\triangle G^{H2O}$, $Urea_{1/2}$, and $\triangle\triangle G^{H2O}$) characterising the urea unfolding of Im9 in the presence of osmolytes at pH 7.0, 10 °C and R^2 values for the straight line relationship of $\triangle G^{H2O}$ and urea concentration.

Protein	Osmolyte Concentration	Thermodynamic parameters				R^2
		m-value (kcal mol^{-1} M^{-1})	$\triangle G^{H2O}$ (kcal mol^{-1})	$Urea_{1/2}$ (M)	$\triangle\triangle G^{H2O}$ (kcal mol^{-1})	
Im9 (Control)	0 M	1.03	5.17	5.01	0.00	0.9924
Im9	0.25 M Trehalose	1.04	5.49	5.29	0.32	0.9944
	0.50 M Trehalose	1.09	6.06	5.56	0.88	0.9926
	0.75 M Trehalose	1.12	6.40	5.71	1.23	0.9771
	1.00 M Trehalose	1.12	6.73	5.99	1.56	0.9733
Im9	0.25 M Sucrose	1.04	5.39	5.20	0.22	0.9942
	0.50 M Sucrose	1.08	5.75	5.33	0.58	0.9993
	0.75 M Sucrose	1.11	6.02	5.41	0.85	0.9910
	1.00 M Sucrose	1.12	6.42	5.72	1.25	0.9928
Im9	10% Glycerol	1.06	5.91	5.56	0.73	0.9940
	20% Glycerol	1.08	6.04	5.59	0.87	0.9975
	30% Glycerol	1.08	6.13	5.66	0.96	0.9987
	40% Glycerol	1.08	6.17	5.69	1.00	0.9975

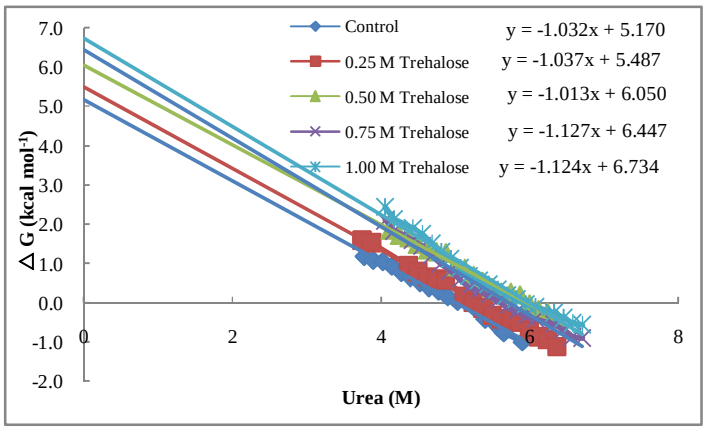

A

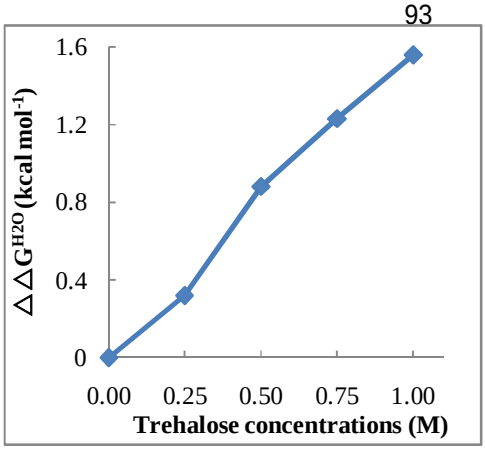

D

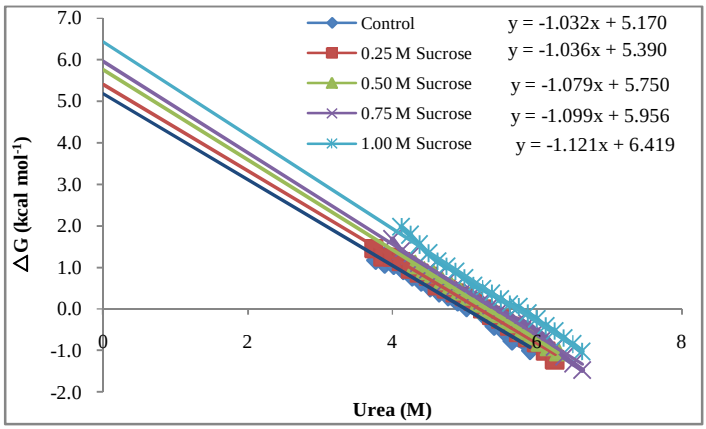

B

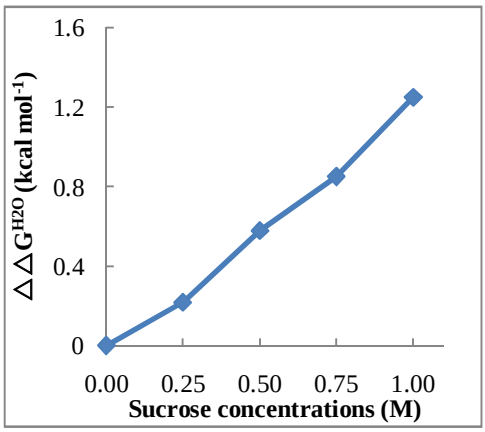

E

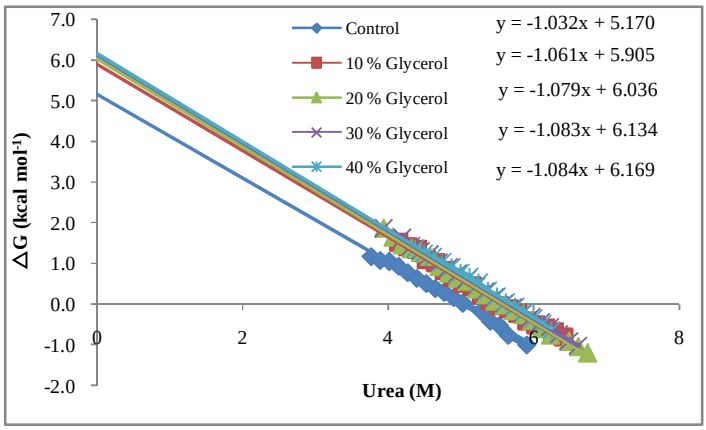

C

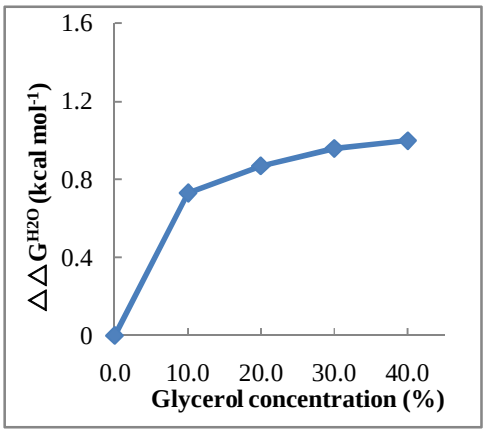

F

Figure 3.21 △G versus urea concentration plots and Value of $\triangle\triangle G^{H2O}$ measured in the absence and in the presence of osmolytes, for Im9 at 10 °C. A-C, Transformation of the fluorescence data to give a linear plot of change in free energy versus Urea concentration for urea-induced denaturation of Im9 in the absence and presence of osmolytes. D-F, Value of $\triangle\triangle G^{H2O}$, the difference in $\triangle G^{H2O}$ measured in buffer and in the presence of osmolytes.

(A)

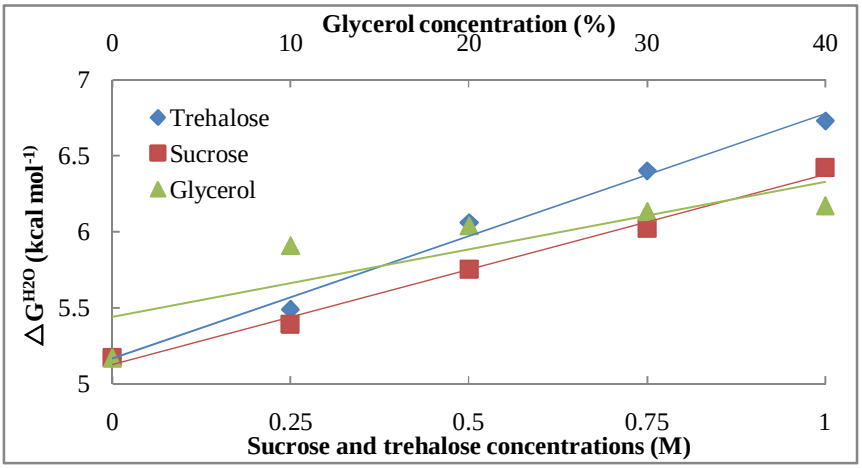

(B)

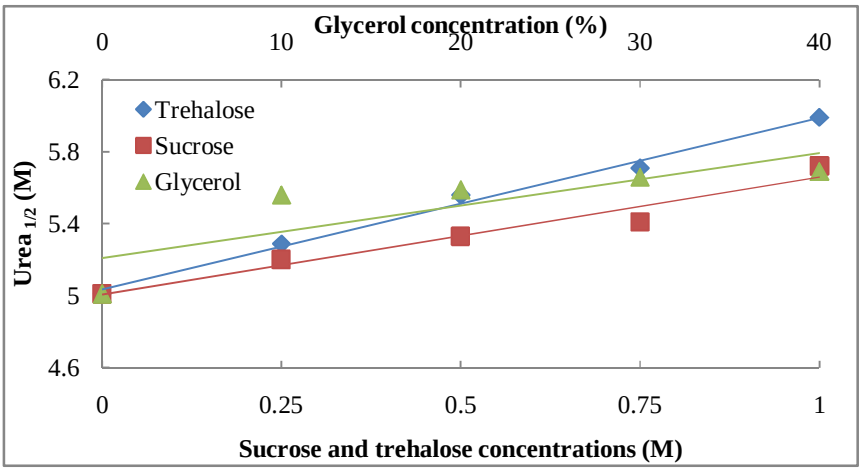

(C)

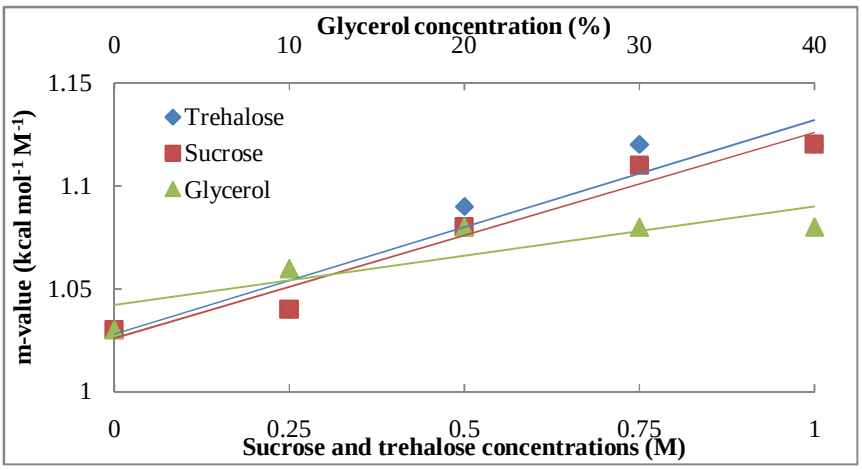

Figure 3.22 The influence of osmolytes on the thermodynamic stability and urea-induced denaturation of Im9, at 10 °C. The thermodynamic parameters A) $\triangle G^{H2O}$, B) $Urea_{1/2}$, and C) m-value.

3.2.5 Hydrodynamic radii of Im9 in the absence and in the presence of different concentration of osmolytes at 10 °C

3.2.5.1 One-dimensional proton NMR

1D ^{1}H NMR experiment was used to determine the interaction between Im9 and various osmolytes and it was found that only small changes in the spectra of Im9 in the presence of osmolytes comparing with Im9 on its own were found, though the signal to noise ratio decreased on addition of osmolytes (data not shown). These results are in excellent agreements with these from the fluorescence spectroscopic experiment in section 3.2.4.1. Therefore, it can be assumed that the osmolytes and lower temperature did not have any material effects on the Im9 structure.

3.2.5.2 Pulsed-field gradient NMR (PFG-NMR) spectroscopy

The hydrodynamic radii of Im9 in the absence and the presence of 0.25, 0.50, 0.75, and 1.0 M each of trehalose and sucrose; and 10, 20, 30, and 40 % (v/v) glycerol were measured and are summarized in Figure 3.23 and Table 3.10. The hydrodynamic radius of Im9 in the absence of osmolytes at 10 °C (17.65±0.18 Å) is significantly smaller than the value observed for Im9 at 25 °C (20.54±0.21 Å). In the case of the native state of the protein, the hydrodynamic radius should be the same in the absence of a structural change or solvation change. Therefore, the reduction in the hydrodynamic radius suggests the protein and its hydration sphere have become more compact at the lower temperature.

The hydrodynamic radii of Im9 in the presence of osmolytes at 10 °C showed the same pattern as the observed values at 25 °C. Sucrose and trehalose increased the hydrodynamic radii of Im9, but a reduction in particle size of Im9 occurred in the presence of glycerol when the osmolyte concentrations were increased. However, it was found that the maximum increment to the hydrodynamic radius of Im9 in the presence of trehalose and sucrose at 10 °C was significantly lower than at 25 °C. The highest concentration (0.75 M) of trehalose and sucrose increased the hydrodynamic radius of Im9 at 10 °C only 7.71 and 4.65 %, respectively, while at 25 °C, the particle size of Im9

were increased about 21.42 and 14.26 %, respectively. In contrast, the maximum reduction of hydrodynamic radii of Im9 in the presence of glycerol at 10 °C was significant higher than at 25 °C. The highest concentration (30 % glycerol) decreased the hydrodynamic radius of Im9 at 10 °C about 23.40 %, whereas at 25 °C, the particle size of Im9 were increased only 5.79 %.

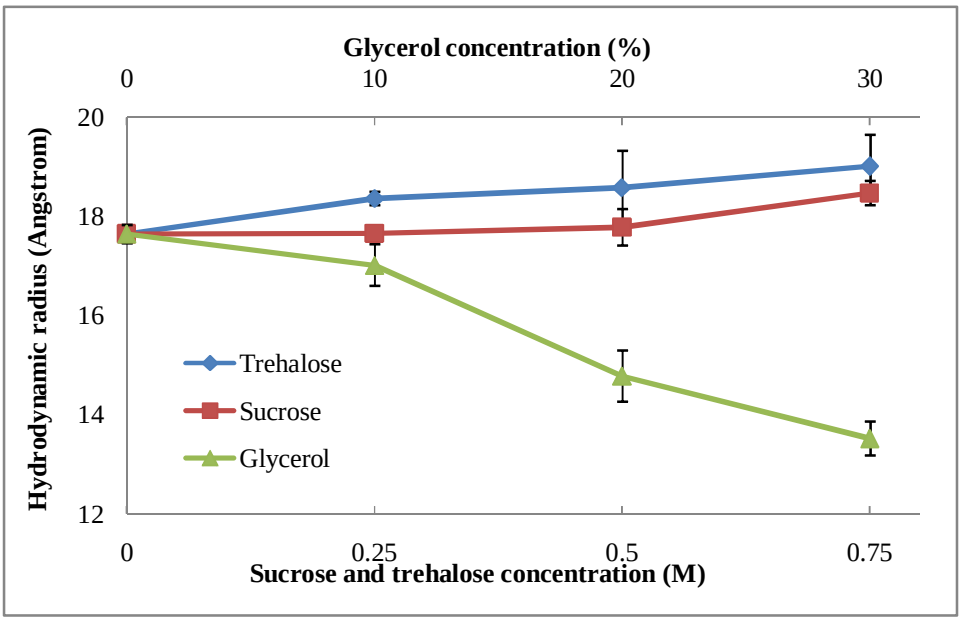

Figure 3.23 Comparison of hydrodynamic radii of Im9 in the absence and the presence of osmolytes at 10 °C (trehalose (◆), sucrose (■), and glycerol (▲). (Error bars are standard deviations n=2).

Table 3.10 Comparison of hydrodynamic radii of Im9 in the absence and the presence of osmolytes (trehalose, sucrose, and glycerol) at 10 °C (Error bars are standard deviations n=2).

Conc	Trehalose		%	Sucrose		%	Glycerol		%	Conc
(M)	R_h (Å)	SD	Increased	R_h (Å)	SD	Increased	R_h (Å)	SD	Decreased	(%)
0.00	17.65	0.18	-	17.65	0.18	-	17.65	0.18	-	0.00
0.25	18.36	0.14	4.02	17.66	0.05	0.06	17.02	0.42	-3.57	10.00
0.50	18.58	0.74	5.27	17.78	0.37	0.74	14.78	0.52	-16.26	20.00
0.75	19.01	0.64	7.71	18.47	0.25	4.65	13.52	0.34	-23.40	30.00

3.2.6 Comparison of conformational stability and hydrodynamic radii of Im9 in the absence and the presence of osmolytes at 10 and 25 °C

The comparison of thermodynamic parameters measured from the urea-induced denaturation experiments and hydrodynamic radii detected by PFG-NMR experiment of Im9 in the absence and the presence of osmolytes at 10 and 25 °C are displayed in Figure 3.24 and 3.25, respectively. The data show that Im9 in the absence and the presence of osmolytes at 10 °C is more stable than at 25 °C.

The hydrodynamic radius of Im9 on its own measured at 10 °C was significantly smaller than the value observed at 25 °C, suggesting that Im9 at 10 °C has a more compact shape than at 25 °C. Moreover, it is related to the conformational stability of Im9 at 10 °C which has higher values of $\triangle G^{H2O}$, m-value, and $Urea_{1/2}$ than Im9 at 25 °C.

In addition, at 25 °C, the hydrodynamic radii of Im9 in the presence of trehalose and sucrose showed significantly increased when the osmolyte concentrations are increased, but slightly increased at 10 °C. The explanations for these values related to the mechanism of protein stabilisation. The enhanced hydration layer on the protein surface by trehalose and sucrose, which can increase the surface tension of water, is the surface tension effect. When the surface tension increases, sugar concentration near a solvated protein is decreased, resulting to that osmolyte is preferentially excluded from the protein surface and the concentration of osmolyte near the protein surface is lower than in the bulk solution. However, the surface tension is dependent on temperature and tends to decrease with the increase of temperature. Consequently, the efficiency of sucrose and trehalose in the formation of hydration layer might be reduced in the lower temperature, resulting to the hydrodynamic radii of HSA in the presence of sucrose and trehalose at 10 °C showed lower increments than those of at 25 °C.

In contrast, the surface tension of water is reduced by glycerol, therefore in lower temperature (10 °C); glycerol might present higher efficiency in stabilisation than at 25 °C. The relation is in excellent agreement with the obtained results in hydrodynamic radii of Im9 in the presence of glycerol. A significant reduction in size was found upon the addition of glycerol concentration at 10 °C, but slightly decreased at 25 °C.

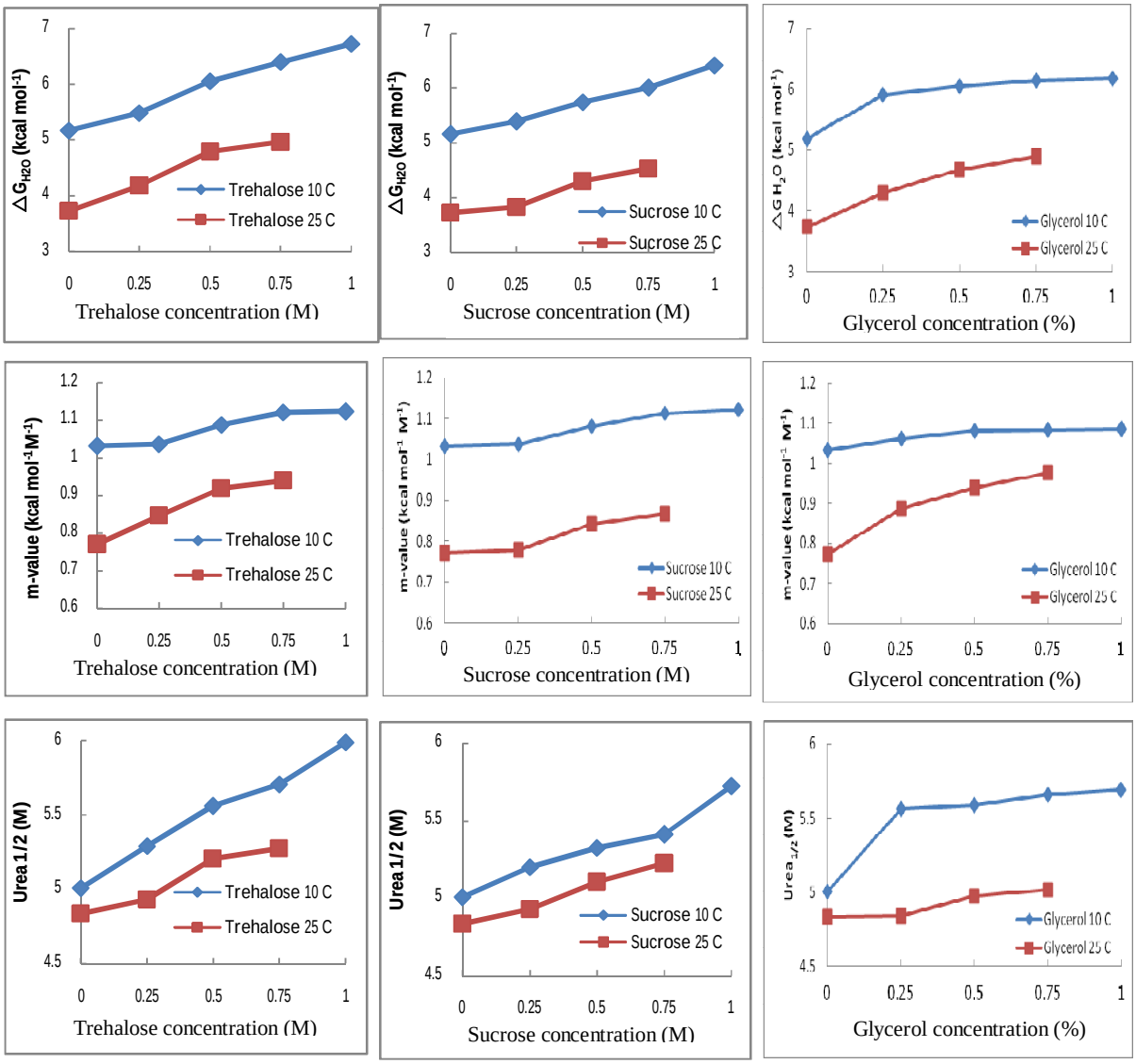

A). B). C).

Figure 3.24 Comparison of thermodynamic parameters ($\triangle G^{H2O}$, m-value, and $Urea_{1/2}$) of conformational stability of Im9 in the absence and the presence of osmolytes (Trehalose (A), sucrose (B), and glycerol (C)) at 10 and 25 °C.

(A)

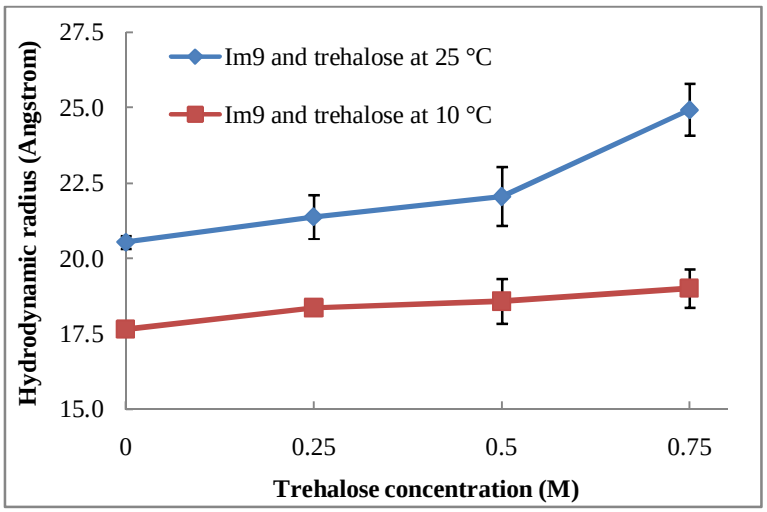

(B)

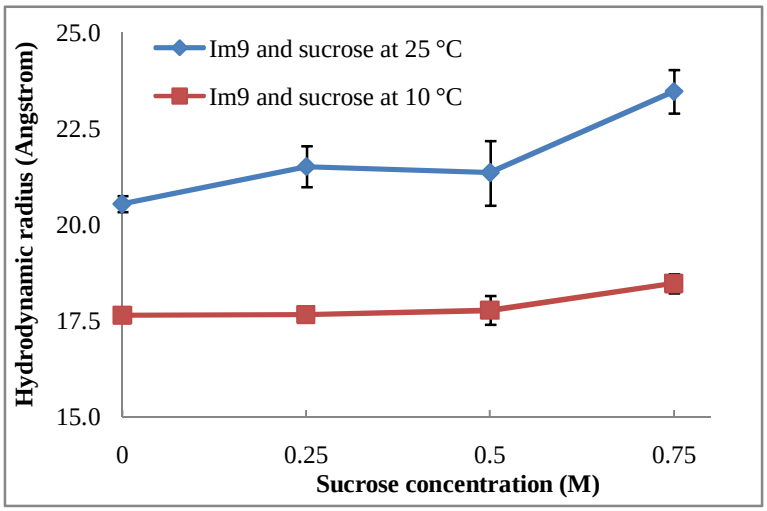

(C)

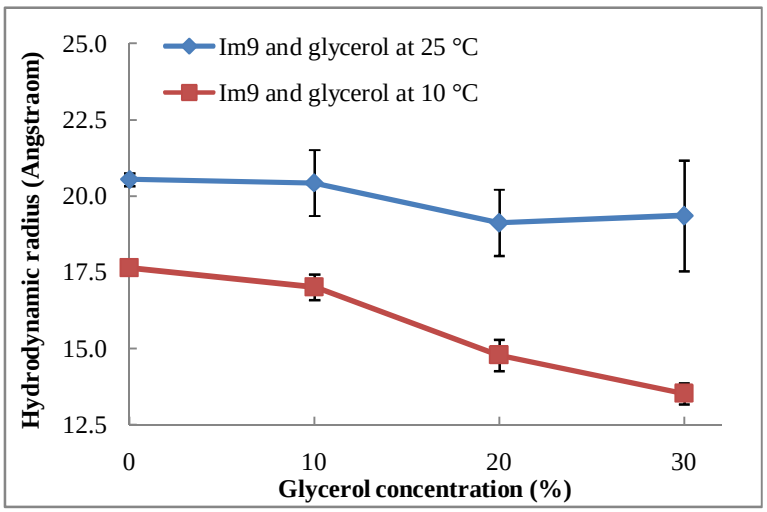

Figure 3.25 Comparison of hydrodynamic radii of Im9 in the absence and the presence of osmolytes at 10 and 25 °C. A) trehalose, B) sucrose, and C) glycerol.

3.3 General Discussion and Conclusions

Temperature is one of the most important parameters affecting protein stability and in this thesis experiments at 10 and 25 °C were carried out. The conformational stability of Im9 at 10 °C is greater than at 25 °C, whereas the native protein had a lower hydrodynamic radius at 10 °C than at 25 °C, indicating that protein stability and compactness could be related. Unfortunately, the hydrodynamic radius of unfolded Im9 was studied only at 25 °C, because urea was found to precipitate at high concentration (8 M urea) at 10 °C in the PFG-NMR experiments.

Our findings show that the conformational stabilities detected by urea-induced denaturation are in excellent agreement with the changes in hydrodynamic radii measured by the PFG-NMR experiment of Im9 in the absence and the presence of osmolytes. That means these two techniques are able to quantitatively describe the effects of osmolytes on the protein stabilisation and provide insight into the structural reasons for them. Both $\triangle\triangle G^{H2O}$ and the hydrodynamic radius of Im9 in the presence of osmolytes varies linearly with osmolyte concentration for all osmolytes tested (except glycerol), indicating that to obtain a higher stability osmolyte concentration should be increased. Im9 follows the Tanford model (Chapter 1, Figure 1.4) for the effect of osmolytes on protein stability since with increasing amounts of trehalose, sucrose or glycerol $\triangle G^{H2O}$ increases at both 10 °C and 25 °C. In terms of the Tanford model, $\triangle G^{H2O}$ increases because $\triangle G_3 > \triangle G_1$, which implies that the Gibbs free energy of the urea-unfolded state of Im9 is more affected than the Gibbs free energy of the folded state by the osmolytes.

The increase in particle size of Im9 in the presence of osmolytes (sucrose and trehalose), as shown by the hydrodynamic radius, is due to an increase in the hydration shell. Most sugars increase the surface tension of water (as described in Chapter 1, section 1.6.1.1). When the surface tension increases, sugar concentration near a solvated protein is decreased. Therefore, it can be assumed that due to this phenomenon (preferential hydration), osmolyte is preferentially excluded from the protein surface and the concentration of osmolyte near the protein surface is lower than in the bulk solution. Thus there is an enhanced hydration layer on the protein surface in osmolyte solution which affects the protein compactness and the stability (Lin and Timasheff 1996, Timasheff 1993).

In contrast to the effect of trehalose and sucrose, the particle size of Im9 decreases upon the addition of glycerol. Glycerol is a polar molecule which can form hydrogen bonds with water as well as polar residues on the protein surface, so glycerol can interact favourably with water, but effectively repel nonpolar substances. It can be assumed that glycerol will be preferentially repelled from the nonpolar residues on the protein surface, leading to redistribution of water and glycerol molecules around nonpolar groups to minimise unfavourable contacts. Therefore, glycerol might have effects on Im9 due to both preferential exclusion and direct interaction (hydrogen bonds) between the protein surface and glycerol. Moreover, some researchers (Gekko and Timasheff 1981a) stated that there are some penetrations of glycerol molecules to the protein and increasing penetration with increasing glycerol concentration, resulting from the low values of the preferential hydration relative to the total hydration. Nevertheless, other researchers (Priev et al. 1996, Oliveira et al. 1994) have another mechanism to explain the effects of glycerol; namely, that glycerol leads to a reduction in the size and number of voids in the protein structure which normally accommodate water, thereby decreasing internal free volume and increasing protein rigidity, resulting in more compactness and enhanced stability. Consequently, it can be concluded that the mechanism of protein stabilisation by glycerol is markedly different from that by sucrose and trehalose and shows a more complicated pattern. Sugars (sucrose and trehalose) strongly hydrate the protein backbone and are also excluded from the protein surface. In contrast, The formation of hydration layer of glycerol are different from those of trehalose and sucrose, because both water and osmolyte were excluded from the protein surface and the direct interaction between glycerol and polar residues on the surface of protein might be occurred, leading to only small changes in hydration layer were found (Auton, Bolen and Rosgen 2008).

In the case of the denatured state of Im9 in the absence and the presence of osmolytes, there are large increases in its hydrodynamic radius upon the addition of osmolytes. Im9 in its denatured state can be a fully extended peptide chain because it has no intramolecular disulfide bonds. Therefore the particle size of Im9 in its denatured state is obviously greater than that of its native state, in excellent agreement with the Tanford model (Chapter 1, Figure 1.3) which states that denatured proteins are more expanded than their native states. When the osmolyte solution was added to the denatured protein, the expanded protein structure would be covered by a hydration

layer, resulting in larger hydrodynamic radius than the native state, for the same reasons as the native state, as discussed above. However, because the denatured state has a greater solvent accessible surface area than the native state, the hydration layer is greater leading to the denatured state being more affected by osmolytes than the native state.

In summary, the impact of osmolytes on the conformational stability of Im9 and the hydrodynamic radii of its native and urea-denatured states fit well with expectations based on previous work concerning the effects of osmolytes on proteins. The data were generally straightforward to interpret, partly because Im9 is a single domain protein with no disulfide bonds. In the next chapter, Human serum albumin, a multi-domain protein with many disulfide bonds, was used as a more complicated system to investigate the effect of osmolytes.

Chapter 4

Effect of osmolytes on the conformational stabilities and hydrodynamic radii of Human serum albumin

4.1 Introduction

4.1.1 General background

The understanding of protein folding/unfolding phenomenon is more complex in multi-domain protein because each domain can fold and unfold independently. Nowadays, it has now become clear that the folding phenomenon in many proteins may process through intermediate states. Albumin denaturation with urea (Leggio et al. 2009), GdnHCl (Farruggia and Pico 1999), heat (Jokiel et al. 2006), pH (Salahuddin 2008) or surfactant (Moriyama et al. 1996) has been widely studied by many workers and is relatively well understood in both its structural and thermodynamic aspects.

In the present work, HSA was used here as a model multi-domain protein, whose structure and stability are relatively well understood, to characterise the relationship between conformational stability and particle size of the protein. Two kinds of osmolytes were chosen to use as a stabilizer: sugars, represented by sucrose and trehalose (at concentrations of 0.20, 0.25, 0.30, 0.40, 0.50, and 0.75 M) and polyols, represented by glycerol (at concentrations of 5, 10, 15, 20, and 30 % v/v of glycerol or at concentrations of 0.68, 1.37, 2.05, 2.74, and 4.11 M).

4.1.2 Structure and properties of Human serum albumin (HSA)

HSA is a monomeric, multi-domain globular protein of 66.5 kDa that is a multifunctional plasma carrier protein which aids in the transportation and distribution in serum of exogenous and endogenous molecules such as fatty acids, hormones, nutrients and various drugs. In addition, HSA can be used as a stabiliser in pharmaceutical products to protect protein against harsh conditions (Ruiz et al. 2006). HSA contains 585 amino acid residues, 17 disulfide bridges, one free cysteine in

position 34, and one tryptophan residue in position 214. The tertiary structure of HSA is composed of three structurally homologous domains, I (residues 1-195), II (residues 196-383), and III (residues 384-585), each containing two separate helical subdomains, A and B (He and Carter 1992, Sugio et al. 1999), as displayed in Figure 4.1. The tryptophan residue has an important structural role in the subdomain IIA binding site by limiting solvent accessibility. It acts as a fluorophore in optical studies of proteins and is located in a cleft or in a hydrophobic fold in HSA (Bell and Brenner 1982) and its fluorescence is sensitive to the ligands bonded nearby. Hence, it is often used as a probe to investigate the binding properties of HSA.

Aromatic and heterocyclic ligands are found to bind within two hydrophobic pockets in subdomains IIA and IIIA, which are designated as site I and site II, respectively. There are seven fatty acid binding sites in each HSA molecule with different affinities (fatty acid sites 2, 4, and 5 are high affinity, while site 1, 3, 6 , and 7 are low affinity fatty acid binding sites), which can bind medium and long chain fatty acids, located in different domains, IB, IIIA, IIIB (Curry et al. 1998). The transportation of fatty acid by HSA is very important because some diseases, such as acute anxiety or myocardial infarction, might occurred due to a lack of this transport (i.e the fatty acid to HSA ratio increases) (Cistola and Small 1991). The binding of fatty acids to HSA molecules is known to markedly affect their conformational stability (Simard et al. 2006).

In the case of multi-domain proteins, intermediate states are generally found in the unfolding pathway. Urea-induced denaturation of HSA has been widely studied, but conflicting results were found. The unfolding of HSA has been found to follow both a one-step, two-state transition without any intermediate state (N ⇆ D) and a two-step, three-state transition with an intermediate state (N ⇆ I ⇆ D). For example the one-step, two-state transition was found by Gonzalez and co-workers (Gonzalez-Jimenez and Cortijo 2002) detected by tryptophan fluorescence spectroscopy (excitation wavelength at 295 nm), whereas the two-step, three-state transition was detected by tryptophan fluorescence spectroscopy (excitation wavelength at 280 nm) by Muzammil and co-workers (Muzammil et al. 2000), however, different solutions conditions were used in these experiments as well as different excitation wavelengths. From the previous reports, it can be stated that the intermediate state of HSA in the absence of osmolyte was detected by intrinsic fluorescence measurement, indicating the environment of the

sole Trp residue was significantly affected or the accumulation of hydrophobic patches occurred at that urea concentration where the intermediate was detected (Muzammil et al. 2000).

In other denaturation processes, no intermediate state was found with GdnHCl-induced denaturation (Wallevik 1973), which resulted in the positive preferential salt binding for guanidinium ion (Arakawa and Timasheff 1984), while intermediate state was found in urea-induced denaturation detected by viscosity measurement (Salahuddin 2008).

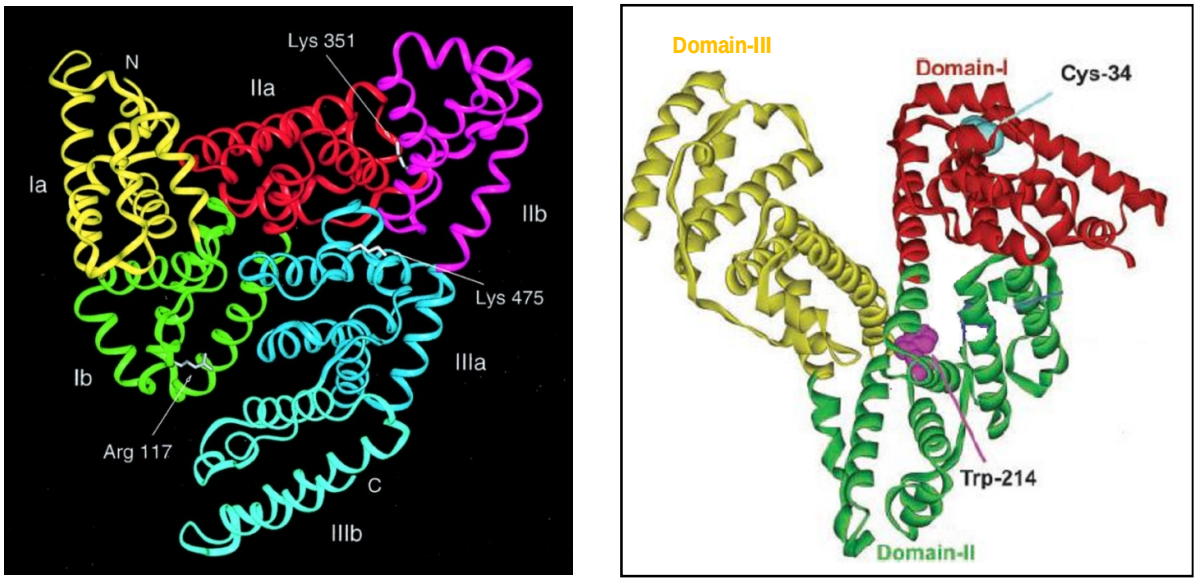

A). B).

Figure 4.1 Schematic drawing of the HSA molecule. A). HSA molecule is reproduced from Sugio et al 1999, PDB coordinates 1BM0. Each subdomain is marked with a different colour (yellow for subdomain Ia; green, Ib; red, IIa; magenta, IIb; blue, IIIa; and cyan, IIIb). N- and C-termini are marked as N and C, respectively. Arg117, Lys351 and Lys475, which may be binding sites for long-chain fatty acids, are white-coloured (Sugio et al. 1999). B). HSA molecule shown Trp-214 and Cys-34 is reproduced from Kamal et al 2004, PDB coordinate 1HA2 (Kamal, Zhao and Zewail 2004).

4.2 Results and discussions

HSA used for the work described in this chapter was supplied by Sigma life science® in essentially fatty acid free grade (~99% agarose gel electrophoresis) and used without further purification. The fatty acid free HSA was chosen to use in this experiment, because it is easier to evaluate the interaction between HSA with other osmolytes, even though in the physiological condition, HSA is present as various fat-containing forms.

4.2.1 Conformational stability of HSA in the absence and in the presence of different concentration of osmolytes at 25 °C

4.2.1.1 Fluorescence spectrum

HSA contains only one tryptophan residue (Try 214) which can be specifically studied by selective excitation at wavelengths of 278-290 nm. In the native state, the fluorescence intensity of the tryptophan of HSA is larger and blue shifted with respect to that of their unfolded state and thus fluorescence emission is considered a sensitive tool to monitor the extent of unfolding/folding and to reveal local changes in protein conformation.

In order to establish whether the presence of urea has any influence on the structure of HSA, fluorescence spectroscopic measurements were performed in the absence of osmolytes at 25 °C, exciting fluorescence at 295 nm. In the denatured state of HSA, the fluorescence spectrum of urea denatured protein at pH 7.0 was measured in the absence of osmolytes (Figure 4.2). The tryptophan fluorescence emission of denatured HSA (8.0 M urea, 0.1 M phosphate buffer, pH 7.0) is highly quenched while the tryptophan spectrum of native HSA (0.1 M phosphate buffer, pH 7.0) is considerably more intense and blue-shifted with respect to that of the denatured state. This quenching is a common effect occurring during denaturation as a result of de-excitiation of the excited state of Trp by collisions with solvent molecules. Previous denaturation and stabilities studies of HSA with urea were carried out using tryptophan emission fluorescence spectroscopy at 25 °C (Galantini et al. 2010) and showed that the

λ_{max} shifted from 345 nm to 355 nm and the fluorescence intensity decreased on denaturation, indicating a greater exposure of the fluorophores to the solvent.

The fluorescence spectra of HSA and stabilised HSA (in the presence of 0.30 M each of trehalose and sucrose and 15 % glycerol) in the native and denatured state were also measured and are displayed in Figure 4.3A-D, respectively. It is seen from Figure 4.3 B-D that the fluorescence spectra of stabilised HSA in both native and denatured states are only slightly changed Figure 4.3A, indicating that there are negligible alterations in the environment of the tryptophan in the presence of osmolytes. Thus, our assumption that osmolytes do not affect the structural characteristics of the two end-states of the process, N conformation ⇆ D conformation seems to be reasonable.

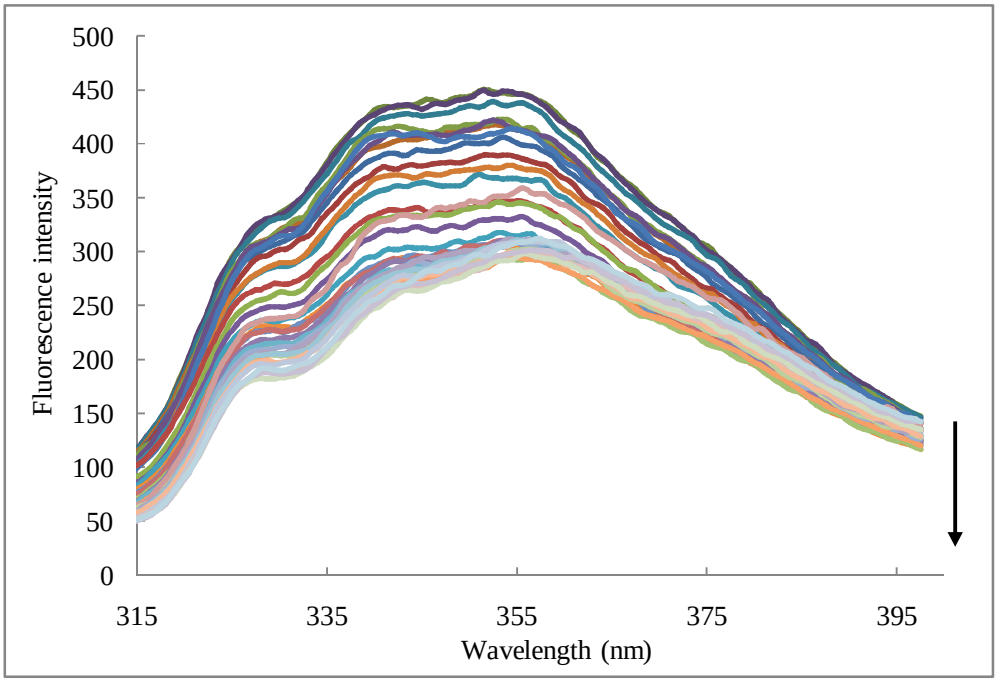

Figure 4.2 Fluorescence intensity of HSA with urea (0 M to 8 M), at 25 °C. The arrow indicates the decrease in fluorescence intensity with the increase in urea concentration. HSA solutions (15 µM) were prepared in 0.1 M phosphate buffer solution pH 7.0 and then added to urea stock solutions to obtain the desired concentrations.

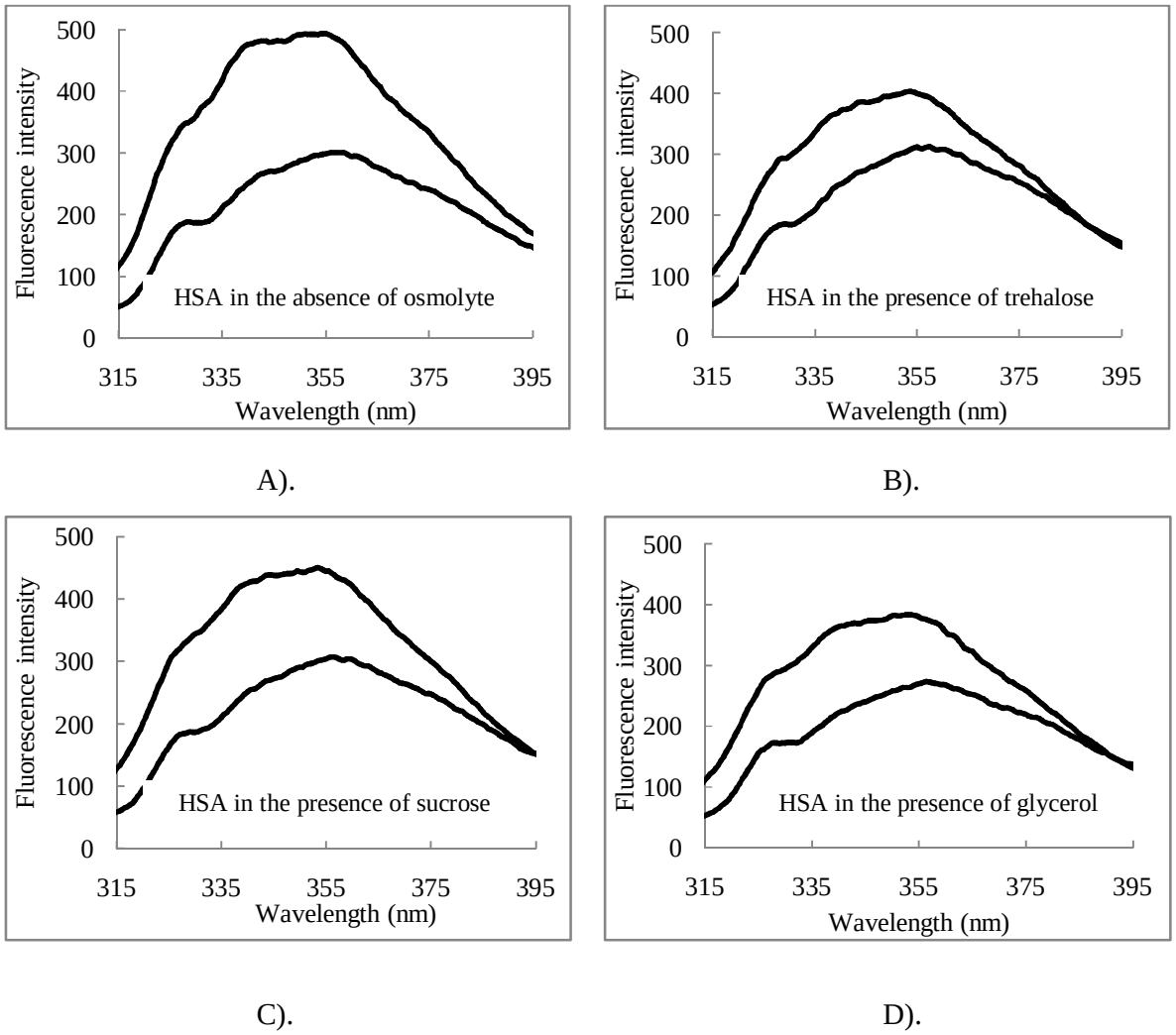

Figure 4.3 The emission spectra (Trp fluorescence spectra) of native (solid line) and denatured (dashed line) HSA in the absence and the presence of osmolytes at 25 °C. The emission spectra of native HSA in the absence of osmolyte (A) and stabilised native HSA in the presence of osmolytes (0.50 M trehalose (B), 0.50 M sucrose (C), and 20 % glycerol (D)). All samples contained 15 μM HSA and were measured by using 1 cm pathlength cuvette, at pH 7.0 and at 25 °C.

4.2.1.2 Urea-induced denaturation

To gain insight into the conformational stability of HSA in the absence and the presence of osmolytes, equilibrium denaturation with urea as the chemical denaturant was used with the change in intrinsic tryptophan fluorescence upon unfolding being monitored. HSA has only one tryptophan residue (Trp214), so tryptophan fluorescence was selected as a probe to detect this protein in urea-induced denaturation transition. The fluorescence spectrum of HSA is displayed in Figure 4.4A which shows that the intensity and emission maxima of HSA changed in response to urea concentration.

Figure 4.4B displays the changes in the fluorescence intensity of HSA at 340 nm when the urea concentration is increased. The fluorescence intensity slightly decreases at low urea concentration and at high urea concentration there was a sharp decrease in intensity. It has been suggested that the change in the fluorescence intensity of proteins in the pre- and post-transition regions is likely to be a result of the solvent perturbation or binding effect of the denaturants (Pace et al. 1990, Johnson and Fersht 1995). As can be seen from the Figure 4.4B, the transition is a single step with no apparent intermediate state, which agrees with previously reported data (Ahmad et al. 2004). The presence of the intermediate was not detectable when detected by tryptophan fluorescence measurement, excited at 295 nm where only tryptophan contributes towards the protein absorption, indicated that the Trp residue environment was not markedly affected (Muzammil et al. 2000). However, the intermediate state can be found in the urea-induced denaturation curve when monitored by intrinsic fluorescence measurement, excited at 280 nm (Muzammil et al. 2000).

The data from Figure 4.4B were treated as described in Section 2.2.2.3, taking the fluorescence intensity at low and high urea concentration to be Y_F and $Y_{U,}$ respectively to yield the unfolding curve as displayed in Figure 4.4C which plots the unfolded fraction against the urea concentration (M); the addition of urea to HSA solution is to denature it and the transition region started from about 3.0 M urea and completely unfolded around 7.0 M urea concentrations with a midpoint occurring at 4.48 M urea concentration. The alteration in fluorescence intensity observed after exciting the protein at 295 nm resulted from conformational changes in domain II (Trp-214). Therefore, it can be assumed that there is no structural change in domain II in the range of 0-3.0 M urea concentration that affects Trp-214. The unfolding curve

(solid black line) was fitted well according to a two-state transition (N↔ D). The thermodynamic parameters were obtained from Equation 2.6:

$$\triangle G_u = \triangle G^{H2O} - m\,[Urea] \qquad \textit{Equation 2.6}$$

Our thermodynamic parameters values are different from the previous values (Farruggia and Pico 1999). Experimental values of $\triangle G^{H2O}$ and m-value are significantly higher than those obtained by Farruggia and co-workers. However, the midpoints of the unfolding transition ($Urea_{1/2}$) are nearly the same value (4.48 and 4.46 M) indicating that it is the slope of the transition region that differs. This difference can be attributed to the different preparations of HSA and experimental condition, such as composition in protein solution, method of measurement, or solution conditions, which could give the different results. Farruggia and co-workers used 0.08 M phosphate buffer pH 7.4 as a medium solution and also used the intrinsic fluorescence measurement at 20 °C, however, in this thesis, HSA was prepared in 0.1 M phosphate buffer solution pH 7.0 and so these differences might result in different thermodynamic values. Nevertheless, the thermodynamic parameters of HSA determined in this thesis can be used for comparison with those of HSA in the presence of osmolytes.

Urea-induced denaturation curves of HSA in the absence and presence of 0.20, 0.25, 0.30, 0.40, 0.50, and 0.75 M each of trehalose and sucrose; and 5, 10, 15, 20, and 30 % (v/v) glycerol were measured by following changes in fluorescence intensity as a function of the urea concentration at pH 7.0, 25 °C and are displayed in Figure 4.5 A, B, and C, respectively. As seen in Figure 4.5A-C, the unfolding curves showed that the intermediate state which was found around 5.2-6.1 M urea concentration is not well defined as it appears from the unfolding curves that the appearance of the denatured state starts before the native state has all converted to the intermediate, so the one-step, two-state transition calculation was used to analysed these curves. Unfortunately, the calculated thermodynamic parameters for the two-state fits fluctuate in a manner (data not shown) that suggests the either the raw data contain errors or the two-state fitting procedure is at fault. The attempt to fit the data to a two-step, three-state transition calculation (N ⇆ I ⇆ D, where N, I, and D are the native, intermediate, and denatured states, respectively) (Figure 4.6 and Table 4.2) yields apparently good fits but the $\triangle G^{H2O}$ values are unreasonably high. Therefore, for this multi-domain protein, I have used the $Urea_{1/2}$ values as a guide to stability changes rather than the derived $\triangle G^{H2O}$.

For example, the urea denaturation curve of HSA in the presence of 0.3 M trehalose is displayed in Figure 4.6A. The first transition which corresponded to the transformation of the N state to the I state started from about 3.0 M urea and completed at 5.0 M urea concentration with a midpoint occurring at 4.46 M urea. The intermediate state was stable in the urea concentration range 5.4-5.9 M. The second transition, which corresponded to the unfolding of the I state, started from about 6.0 M urea and finally sloped off to the D state at around 8.4 M urea with a midpoint occurring at around 6.78 M urea concentration. In the other curves of HSA in the presence of osmolytes (trehalose, sucrose, and glycerol), the intermediate states were also found in this range of 5.2-6.1 M urea concentration, whereas the earlier report (Muzammil et al. 2000) used HSA under different conditions with KCl as a stabiliser. It was found that the formation of the intermediate state of HSA was abolished by the addition of high KCl concentration (1 M) when monitored by intrinsic fluorescence measurement. This is because salt was found to stabilise the intermediate transition (N ⇆ I), while the unfolded transition (I ⇆ D) showed no alteration. However, the mechanism of protein stabilisation by salts and osmolytes is thought to be significantly different: the former occurring by preferential binding, while the latter probably by preferential hydration (Timasheff 1993).

The profile of denaturation curves for HSA in the presence of osmolytes was shifted toward higher denaturant concentration at increasing osmolyte concentrations. One explanation for this is that normally urea destabilises proteins partly by preferentially binding to them (Bennion and Daggett 2003, Auton et al. 2007, Hua et al. 2008) therefore, when urea is added to the protein in the presence of osmolytes, it needs to overcome the stabilising effect of osmolyte.

The denaturation curves in the presence of osmolytes were analysed as a two-step, three-state transition (N ⇆ I ⇆ D) which is similar to the one-step, two-state transition, but separated into two sections (N ⇆ I and I⇆ D) (Muzammil et al. 2000, Varshney et al. 2008, Salahuddin 2008). Each step may be assumed to follow a one-step, two-state transition. The fraction of intermediate state, f_I in the reaction, N ⇆ I can be obtained from this Equation:

$$f_I = (Y_F - Y) / (Y_F - Y_I) \qquad \textit{Equation 4.1}$$

Where $f_I + f_N = 1$

Similarly, the fraction of denatured state, f_D in the reaction, I ⇆ D can be calculated from the relation:

$$f_D = (Y_F - Y) / (Y_F - Y_U) \quad \textit{Equation 4.2}$$

Where $f_D + f_I = 1$

The equilibrium constant and the free energy for the above transitions may be calculated from the following relationships:

For N ⇆ I transition,

$$K_I = f_I / (1 - f_I) \quad \textit{Equation 4.3}$$

And $$\triangle G_I = -RT \ln K_I \quad \textit{Equation 4.4}$$

For I ⇆ D transition,

$$K_u = f_U / (1 - f_U) \quad \textit{Equation 4.5}$$

and $$\triangle G_u = -RT \ln K_u \quad \textit{Equation 4.6}$$

Least square analyses of the data treated according to Equations 4.4 and 4.6 as a function of denaturation concentration were used to fit the data to the following equation for the determination of $\triangle G_I^{H2O}$ and $\triangle G_U^{H2O}$, the free energy change in the absence of urea.

$$\triangle G_I = \triangle G_I^{H2O} - m\,[Urea] \quad \textit{Equation 4.7}$$

$$\triangle G_u = \triangle G_U^{H2O} - m\,[Urea] \quad \textit{Equation 4.8}$$

As seen in Figure 4.6A, the urea denaturation curve was normalized assuming two-step transition by plotting f_I and f_U values obtained by using Equation 4.1, and 4.2, respectively against urea concentration. Assuming both the transitions shown in Figure 4.6B to follow two-state mechanisms, the fraction of intermediate state (f_I, solid line) and fraction of denatured state (f_D, dashed line) were plotted against urea concentration of HSA for N ⇆ I and I ⇆ D transition, respectively. Then, we calculated the free energy of unfolding of HSA for the transition of N ⇆ I and I ⇆ D, ($\triangle G_I$ and $\triangle G_U$, respectively) as a function of urea concentration as described in Equation 4.4 and 4.6 and are displayed in Figure 4.6C. A least squares analysis was used to fit the data using Equation 4.7 and 4.8 to $\triangle G_I^{H2O}$ (solid line) and $\triangle G_U^{H2O}$ (dashed line), the free energy of unfolding in the absence of urea.

The comparisons of thermodynamic parameters for each value ($Urea_{1/2}$, $\triangle G^{H2O}$, and m-value) under different conditions are graphically displayed in Figure 4.6 A-C, respectively. Thermodynamic parameters of HSA in its stabilised state are markedly increased compared with those of HSA in its native state without osmolytes as shown in Table 4.2.

As stated earlier, $Urea_{1/2}$ values were used as a guide to study conformational stability changes in this experiment rather than the derived $\triangle G^{H2O}$. The results in Figure 4.7A obviously distinguish the change of $Urea_{1/2}$ values, which corresponds to the transition of HSA to the unfolded state, as a function of osmolyte concentration. The highest concentration of osmolytes induces a shift of $Urea_{1/2}$ from 4.48 M to 5.70 M, 6.06 M, and 5.67 M for trehalose, sucrose, and glycerol, respectively. This enhancement is found here to be 26.26-35.27 %, depending on the particular osmolyte concentration, indicating that these osmolytes can inhibit the chemical denaturation of HSA by urea. Therefore, it can be seen that in the absence of osmolytes HSA is less stable than in their presence. Interestingly, the midpoint of the unfolding transition order shows that trehalose and glycerol are mild stabilisers, while sucrose is the strongest stabiliser. In the same manner, the results of $\triangle G^{H2O}$ and the m-value of HSA in the presence of osmolytes, which are represented in Figure 4.7B and Table 4.2, respectively, are related to those of $Urea_{1/2}$.

To further quantify the effect of osmolytes on HSA stability, we follow the $\triangle Urea_{1/2}$ defined as the difference between $Urea_{1/2}$ measured in buffer and its value obtained in the presence of osmolytes. The comparison clearly showed that $\triangle Urea_{1/2}$ tend to increase with osmolyte concentration for all osmolytes tested, but not in a linear relationship, as displayed in Figure 4.8. From these values, it can be stated that the efficiency of stabilisation follows the order: sucrose > trehalose > glycerol.

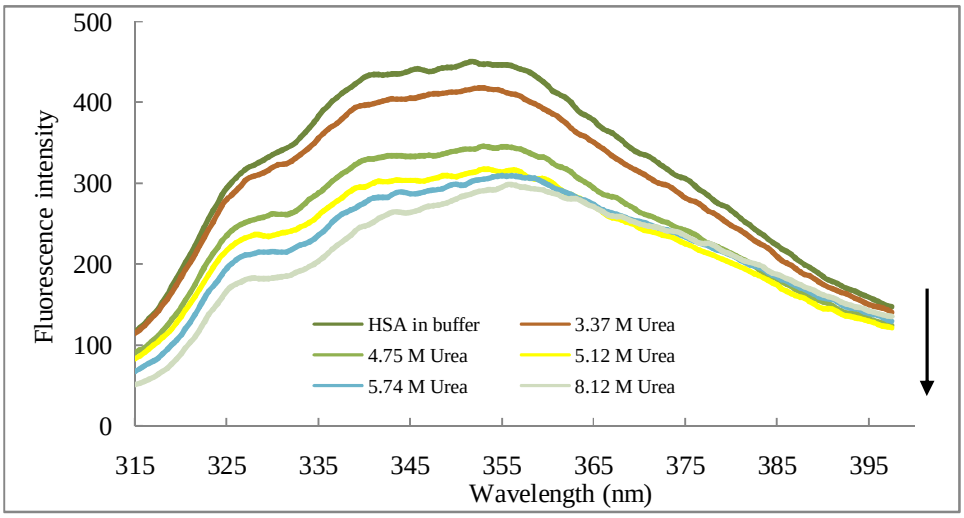

A).

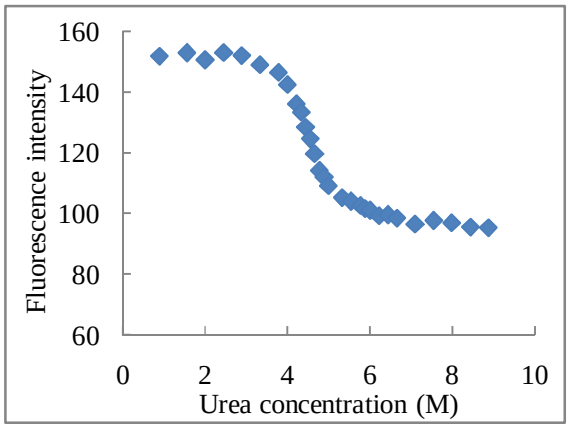

B).

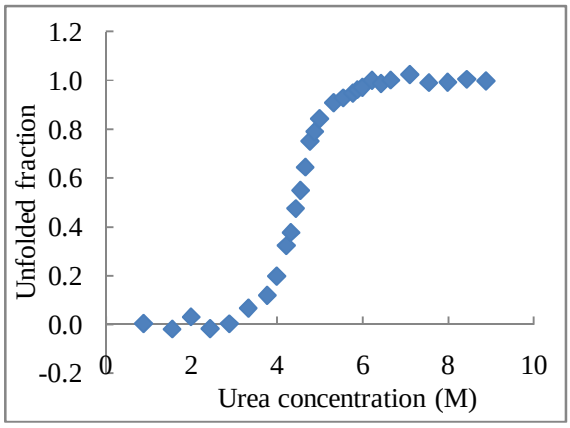

C).

Figure 4.4 Fluorescence intensity curve and unfolding curve of HSA with urea. A). Fluorescence intensity of HSA with urea (0 M to 8 M) at 25 °C. The arrow indicates the decrease in fluorescence intensity with the increase in urea concentration. HSA solutions (15 µM) were prepared in 0.1 M phosphate buffer solution pH 7.0 and then added to urea stock solutions to obtain the desired concentrations. The excitation wavelength was 295 nm. The excitation and emission slit widths were 10.0 nm each. B). Fluorescence intensity of HSA at 340 nm versus urea concentration. HSA solutions (15 µM) were prepared in 0.1 M phosphate buffer pH 7.0 at 25 °C with the addition of urea stock solution to obtain the desired concentrations. C). The unfolding curve of HSA with urea concentration detected by fluorescence spectroscopy at 25 °C.

A).

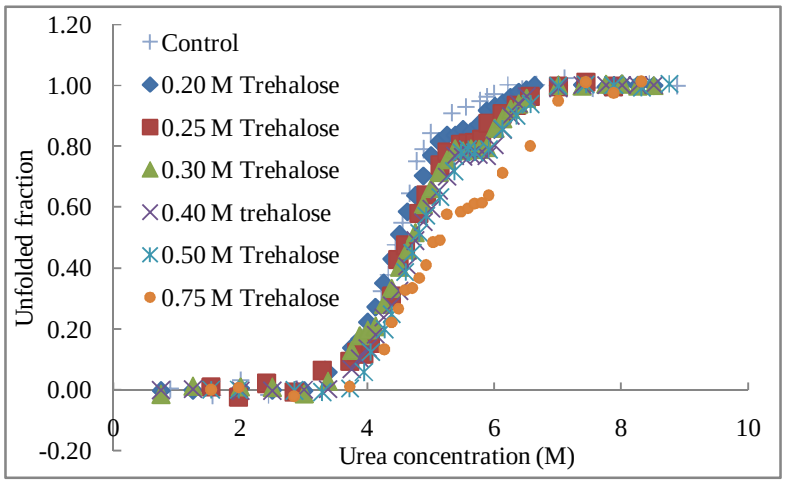

B).

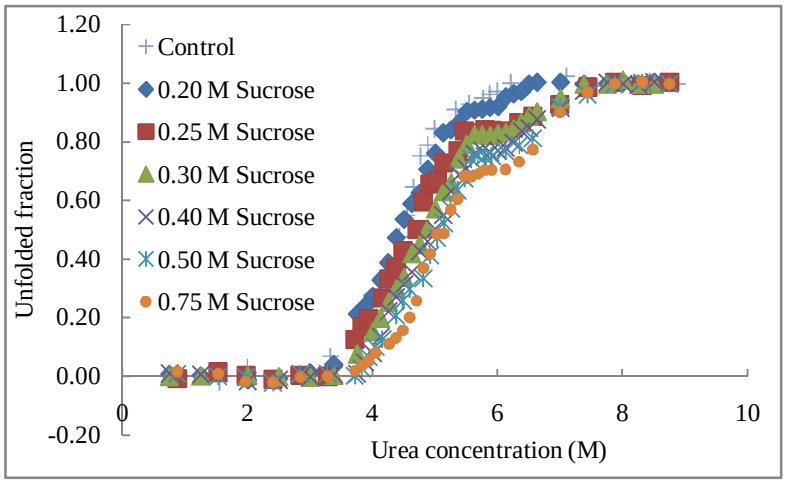

C).

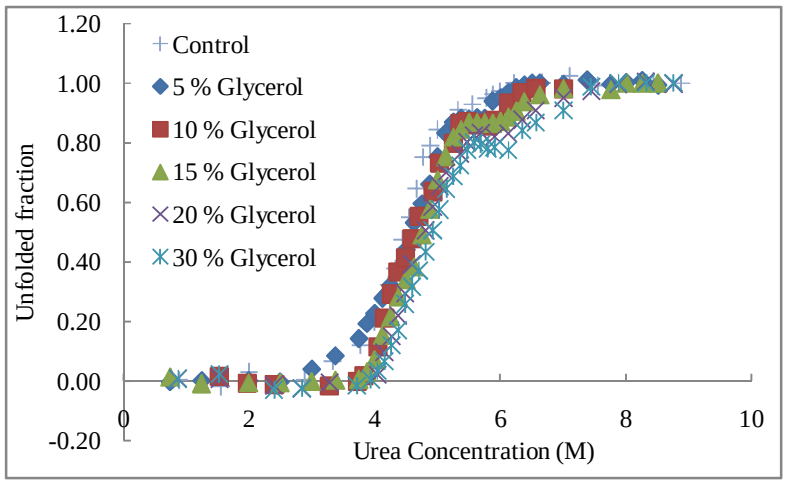

Figure 4.5 Urea-induced denaturation curves of HSA in the absence and the presence of osmolytes at 25 °C. A). 0.20, 0.25, 0.30, 0.40, 0.50, and 0.75 M trehalose B). 0.20, 0.25, 0.30, 0.40, 0.50, and 0.75 M sucrose and C) 5, 10, 15, 20, and 30 % (v/v) glycerol.

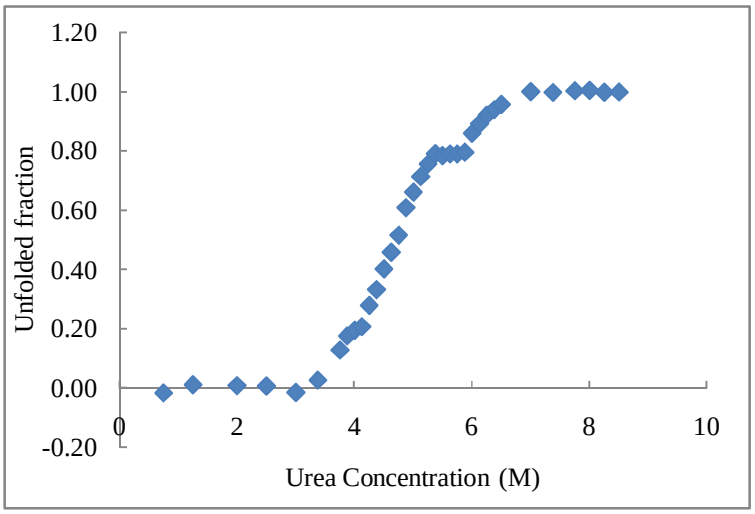

A).

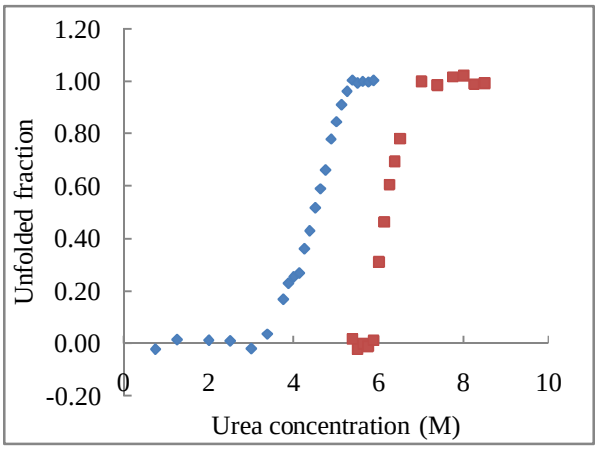

B).

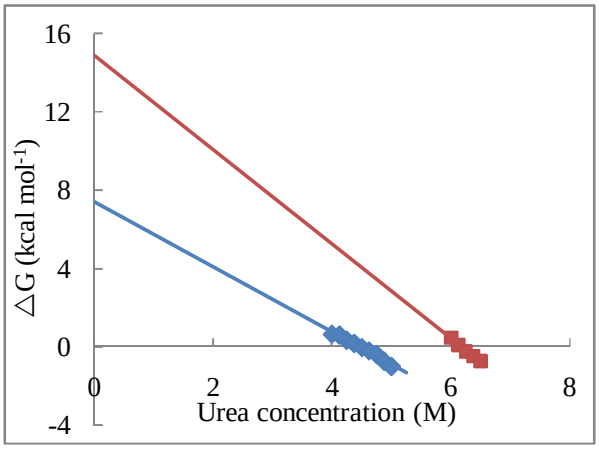

C).

Figure 4.6 Urea-induced denaturation of HSA in the presence of 0.30 M trehalose.

A) Transition curve of HSA in the presence of 0.30 M trehalose.

B) A plot between fraction of intermediate (f_I, blue-coloured line) and fraction of denatured (f_D, red-coloured line) versus urea concentration of HSA for N ⇆ I and I ⇆ D transition, respectively.

C) A plot between △G versus urea concentration of HSA for the transition of N ⇆ I (blue-coloured line)) and I ⇆ D (red-coloured line). A least square analysis of the data of △G as a function of denaturant concentration was used to fit the data using the relation shown by Equation 4.7 and 4.8.

Table 4.1 Equilibrium unfolding parameters for native HSA in the absence of urea 25 °C and pH 7.0

Protein	Thermodynamic parameters						
	m-value 1	**m-value 2**	**Total m-value (kcal mol^{-1} M^{-1})**	**$\triangle G^{H2O}$ 1**	**$\triangle G^{H2O}$ 2**	**Total $\triangle G^{H2O}$ (kcal mol^{-1})**	**Urea $_{(1/2)}$ (M)**
HSA[a]	1.48	0.00	1.48	6.62	0.00	6.62	4.48
HSA[b]	0.982	0.00	0.982	4.10	0.00	4.10	4.46

a. Thermodynamic parameters from my experiment. The sample solutions were prepared containing 100 mM potassium phosphate buffer, pH 7.0 with a final concentration of 15 µM and monitored by fluorescence spectroscopy at 340 nm.

b. Thermodynamic parameters from Farruggia (Farruggia and Pico 1999). The sample solutions were prepared containing 0.08 M phosphate buffer, pH 7.4 at 20 °C and monitored by fluorescence spectroscopy with excitation and emission wavelength at 280 and 345, respectively.

Table 4.2 Thermodynamic parameters (m-value, $\triangle G^{H2O}$, and $Urea_{1/2}$) characterising the urea unfolding of HSA in the presence of osmolytes at pH 7.0, 25 °C.

Protein	Osmolyte Concentration	Thermodynamic parameters							
		m-value 1	m-value 2	$\triangle G^{H2O}$ 1	$\triangle G^{H2O}$ 2	Total $\triangle G^{H2O}$ (kcal mol^{-1})	$\triangle\triangle G^{H2O}$ (kcal mol^{-1})	$Urea_{1/2}$ (M)	$\triangle Urea_{1/2}$ (M)
HSA	0 M (Control)	1.48	0.00	6.62	0.00	6.62	0.00	4.48	0.00
HSA	0.20 M Trehalose	1.69	1.77	7.28	10.69	17.97	11.35	5.19	0.71
	0.25 M Trehalose	1.72	1.78	7.66	11.03	18.69	12.07	5.34	0.86
	0.30 M Trehalose	1.66	2.41	7.40	14.89	22.29	15.67	5.48	1.00
	0.40 M Trehalose	1.74	2.37	7.90	14.62	22.51	15.89	5.49	1.01
	0.50 M Trehalose	1.92	2.18	8.86	13.83	22.68	16.06	5.53	1.05
	0.75 M Trehalose	1.85	2.31	8.37	15.32	23.69	17.07	5.70	1.22
HSA	0.20 M Sucrose	1.59	1.85	6.81	11.64	18.45	11.83	5.36	0.88
	0.25 M Sucrose	1.74	1.76	7.67	11.87	19.53	12.91	5.57	1.09
	0.30 M Sucrose	1.47	2.17	6.45	14.34	20.79	14.17	5.71	1.23
	0.40 M Sucrose	1.75	1.97	8.14	13.50	21.65	15.03	5.81	1.33
	0.50 M Sucrose	1.71	2.22	8.16	15.59	23.76	17.14	6.05	1.57
	0.75 M Sucrose	1.83	2.62	8.72	18.29	27.01	20.39	6.06	1.58
HSA	5 % Glycerol	1.51	1.95	6.68	11.60	18.28	11.66	5.28	0.80
	10% Glycerol	1.67	1.84	7.63	11.16	18.79	12.17	5.36	0.88
	15 % Glycerol	2.02	1.77	9.35	10.95	20.30	13.68	5.37	0.89
	20% Glycerol	2.26	1.72	10.54	10.98	21.52	14.90	5.41	0.93
	30% Glycerol	2.14	2.01	10.22	13.29	23.51	16.89	5.67	1.19

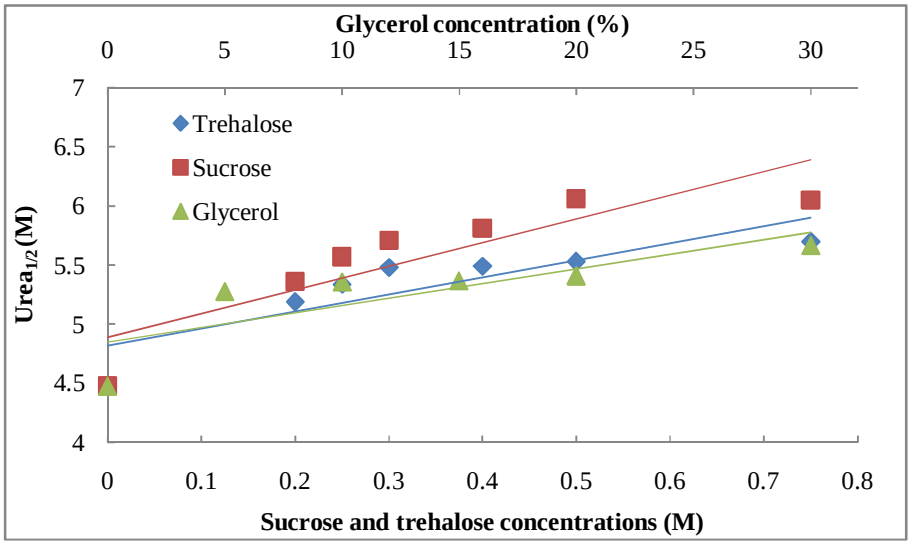

A).

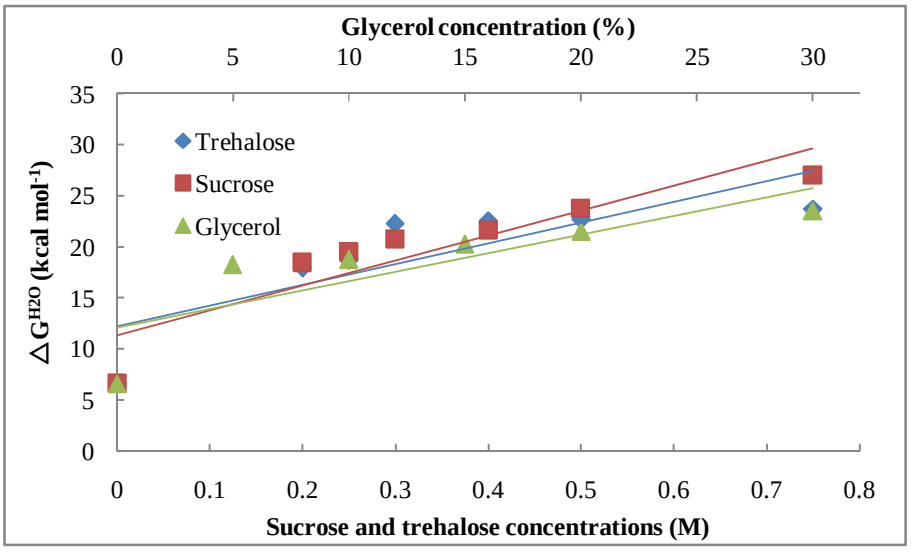

B).

Figure 4.7 The influence of osmolytes on the thermodynamic stability and urea-induced denaturation of HSA, at 25 °C. The thermodynamic changes A) $Urea_{1/2}$ and B) $\triangle G^{H2O}$ in response to the transition of the HSA to the unfolded state in osmolytes (Trehalose (◆), sucrose (■), and glycerol (▲)). The straight lines between each osmolyte concentrations were drawn by using a linear trend line in Excel.

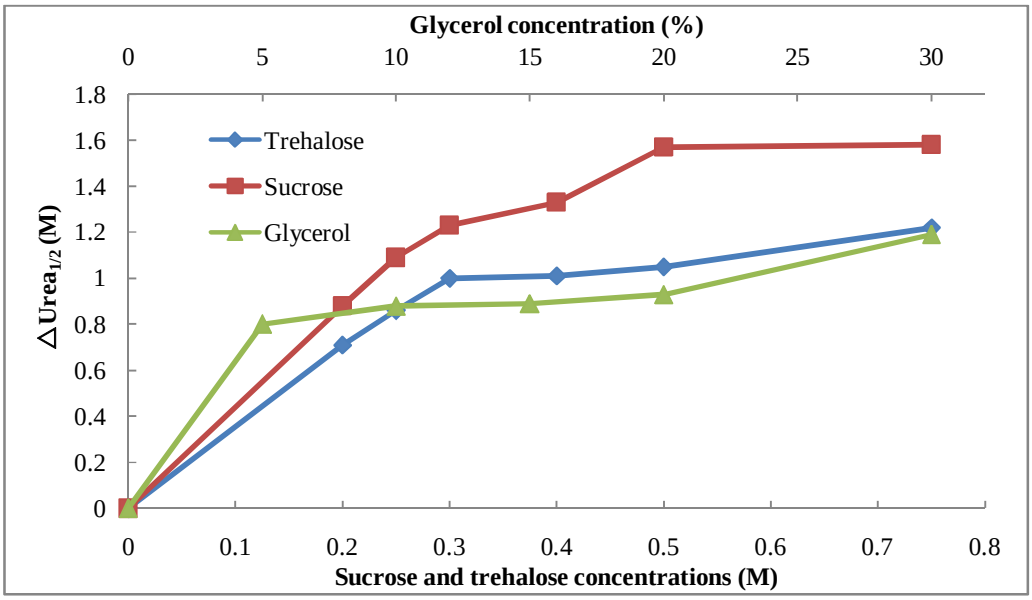

Figure 4.8 Value of △Urea$_{1/2}$, the difference in Urea$_{1/2}$ measured in buffer and in the presence of osmolytes, for HSA at 25 °C. (Trehalose (◆), sucrose (■), and glycerol (▲)).

4.2.2 Hydrodynamic radii of HSA in the absence and in the presence of different concentration of osmolytes at 25 °C

The aim of this experiment was to study the effect of osmolytes on the size of HSA. A pulse-field gradient nuclear magnetic resonance (PFG-NMR) experiment was used to determine the hydrodynamic radii of HSA in different states. Consequently, the particle size of HSA was measured in the absence and the presence of 0.20, 0.25, 0.30, 0.40, 0.50 and 0.75 M each of trehalose and sucrose; and 5, 10, 15, 20, and 30 % (v/v) glycerol by PFG-NMR experiment.

4.2.2.1 **One-dimensional proton NMR** (1D ^{1}H NMR)

To determine whether the various osmolytes (trehalose, sucrose, and glycerol) in different concentrations affected the conformation of HSA, one-dimensional ^{1}H NMR spectra were recorded and are displayed in Figure 4.9. It was found that only small changes in the spectrum of HSA were induced by the presence of osmolytes as far as resonance chemical shifts were concerned but there was a marked reduction in the signal noise ratio. This was most likely due to the increased viscosity accompanying increasing osmolyte concentrations causing slower rotational tumbling of the protein molecules which produced broader resonances. These results are in excellent agreement with those from the fluorescence spectroscopic experiment (Section 4.2.1), leading me to conclude that there is no indication of any major structure alteration in the protein itself produced by the osmolytes.

4.2.2.2 **Pulsed-field gradient NMR (PFG-NMR) spectroscopy**

PFG-NMR diffusion measurements have been used to determine the particle size of proteins by converting the diffusion coefficient into the hydrodynamic radius of the protein and this technique was described in section 3.2.2.2. Acetaldehyde was used as the internal radius standard instead of dioxane and the hydrodynamic radius of acetaldehyde, which was calibrated against dioxane, is 1.79 Å at pH 7.0, 25 °C as described in section 3.2.2.2. Moreover, I have to show that acetaldehyde does not have any effect on the HSA structure by studying the diffusion rate constant (Lapham et al.

1997) of HSA on its own and with acetaldehyde. The region of the spectrum from 10.0 to 6.5 ppm, which corresponds to the aromatic region of HSA, was integrated and in the other regions osmolyte signals occurred at the same place as HSA signals as displayed in Figure 4.10. Although, the aromatic regions in 1D ^{1}H NMR spectra of HSA showed broad peaks, in PFG-NMR experiment, the PFG-NMR spectra were sharper and easier to interpret than in 1D ^{1}H NMR as displayed in Figure 4.11A and B. The diffusion rate constant of HSA in the absence and the presence of acetaldehyde in each protein signal around 7.7 to 6.8 ppm are shown graphically in Figure 4.12 and listed in Table 4.3. As it can be seen, these values were not significantly different for protein signals at 7.57 and 6.98 ppm, and were only slightly different at 7.66 ppm. Moreover, the diffusion coefficient rate constant of acetaldehyde was nearly the same in the absence and presence of HSA. Therefore, it can be concluded that acetaldehyde does not interact significantly with HSA and can be used as an appropriate internal radius standard in this experiment.

The PFG-NMR experiment was used to determine the diffusion coefficient of HSA in the absence and the presence of osmolytes in different concentrations by using DOSY software (Peresada et al. 1999) and the hydrodynamic radius of HSA calculated by comparing with acetaldehyde data. Protein samples were magnetised in 11 gradient strengths (as displayed in Chapter 2, Table 2.5B), increasing from 1.77 to 31.06 Gauss cm^{-1} and intensities of protein peaks was attenuated to about 10-20 % comparing with the initial intensities (100 %) when the gradient strength increased to the maximum. Hydrodynamic radii were calculated by a pseudo two-dimensional (2D) DOSY (Diffusion ordered spectroscopy), and compared with the internal radius standard data (Acetaldehyde data) because it is an automatic function in the NMR operating software which should give more accurate values (lower standard deviation), as discussed in section 3.2.2.2.

As it can be seen in Figure 4.13, HSA signals at 7.66, 7.57, and 6.98 ppm were decreased to only 20-30 % for these gradient strength series rather than 10% because of the limitations of the NMR equipment. Higher gradient strengths cannot be used for the probe of the Unity*Inova* 500 MHz spectrometer (Varian Inc., U.S.A.), because it would damage it during the long measurement times. However, the average experimental hydrodynamic radii of HSA in the absence of osmolytes (38.29±2.21 Å, Table 4.4) are not significantly different from the previous reports (Galantini, Leggio and Pavel 2008)

which were 36.5 and 35.2 Å from experimental (measured by DLS measurement) and calculated hydrodynamic radii by HYDROPRO® software, respectively, and also are in agreement with my experimental DLS values (40.51±0.06 Å) in chapter 5. Therefore, it is reasonable to take this set of gradient strength conditions to measure the diffusion coefficient of HSA in the absence and the presence of osmolytes and to take this value as the reference to compare the hydrodynamic radii of HSA in the presence of osmolytes and in the different equilibrium denatured states since all other solution parameters were the same.

The hydrodynamic radii of HSA in the absence and the presence of 0.20, 0.25, 0.30, and 0.40 M each of trehalose and sucrose; and 5, 10, 15, and 20 (% v/v) glycerol were measured and are summarized in Figure 4.14 and Table 4.5. The osmolyte concentrations in this experiment were different from those with Im9, because the hydrodynamic radii of HSA in the presence of high concentrations of osmolytes (0.50 and 0.75 M each of trehalose and sucrose, 30 % glycerol) could not be measured by the PFG-NMR experiment because most of the protein signals could not be detected. Presumably the tumbling of the protein was so slow that the signals were considerably broadened leading to poor spectra with noisy base lines and low intensity signals. The numbers of repeated scans were changed from 1024 to 2048 scans to improve the signal to noise ratio, but a significant improvement was not seen in the HSA spectra (data not shown).

From the results, it was found that the hydrodynamic radii of HSA in the presence of osmolytes showed a different profile than Im9 did (Chapter 3) when the osmolyte concentrations increased. A large increment (increased by 25.06 %) was found in the particle size of HSA in 0.2 M trehalose, but no significant difference was observed with higher concentration of trehalose (increased by 22.73 % (0.25 M), 24.35 % (0.30 M), and 23.07 % (0.40 M)). Hydrodynamic radii of HSA in the presence of sucrose markedly increased to begin with 38.19±0.36 Å to 51.35±1.66 Å, but no difference in hydrodynamic radii was observed between 0.30 and 0.40 M sucrose concentration (51.35±1.66 and 51.17±1.36 Å, respectively). Therefore, it can be implied that sucrose can produce a hydration layer around HSA larger than trehalose did at the same concentration (except at 0.20 M concentration). These results are indicative of

sucrose and trehalose increasing the solvation sphere around the protein, perhaps because they are excluded from the protein surface (Timasheff 1993).

In contrast, the hydrodynamic radius of HSA in the presence of a low concentration (5 % v/v) of glycerol increased approximately 14.04 %, but a reduction in its hydrodynamic radius was found at higher concentrations (10, 15, and 20 % v/v) of glycerol. This indicates that HSA in the presence of glycerol (10, 15, and 20 % v/v) were smaller or more compact than HSA in the absence of glycerol and the presence of 5 % glycerol. This situation is the opposite from that of trehalose and sucrose, but it is in excellent agreement with previous reports (Priev et al. 1996, Vagenende et al. 2009, Oliveira et al. 1994) stating that glycerol can decrease the volume and compressibility of protein or make the protein core denser and less compressible, suggesting that glycerol may reduce the total void volume of the protein core. It is assumed that this reduction in the protein volume and compressibility is due to the release of water from the protein interior (Priev et al. 1996), as described in Chapter 1, section 1.6.2.3. Moreover, Oliveira and co-workers reported that glycerol dehydrates proteins by means of displacing water of hydration and preferentially hydrating the protein itself, which leads to a reduction in the protein volume and compressibility (Oliveira et al. 1994). This leads me to believe that glycerol causes a reduction in the size of the void volume in the HSA structure, which would otherwise accommodate water, leading to a decrease in the internal free volume and increasing protein compactness.

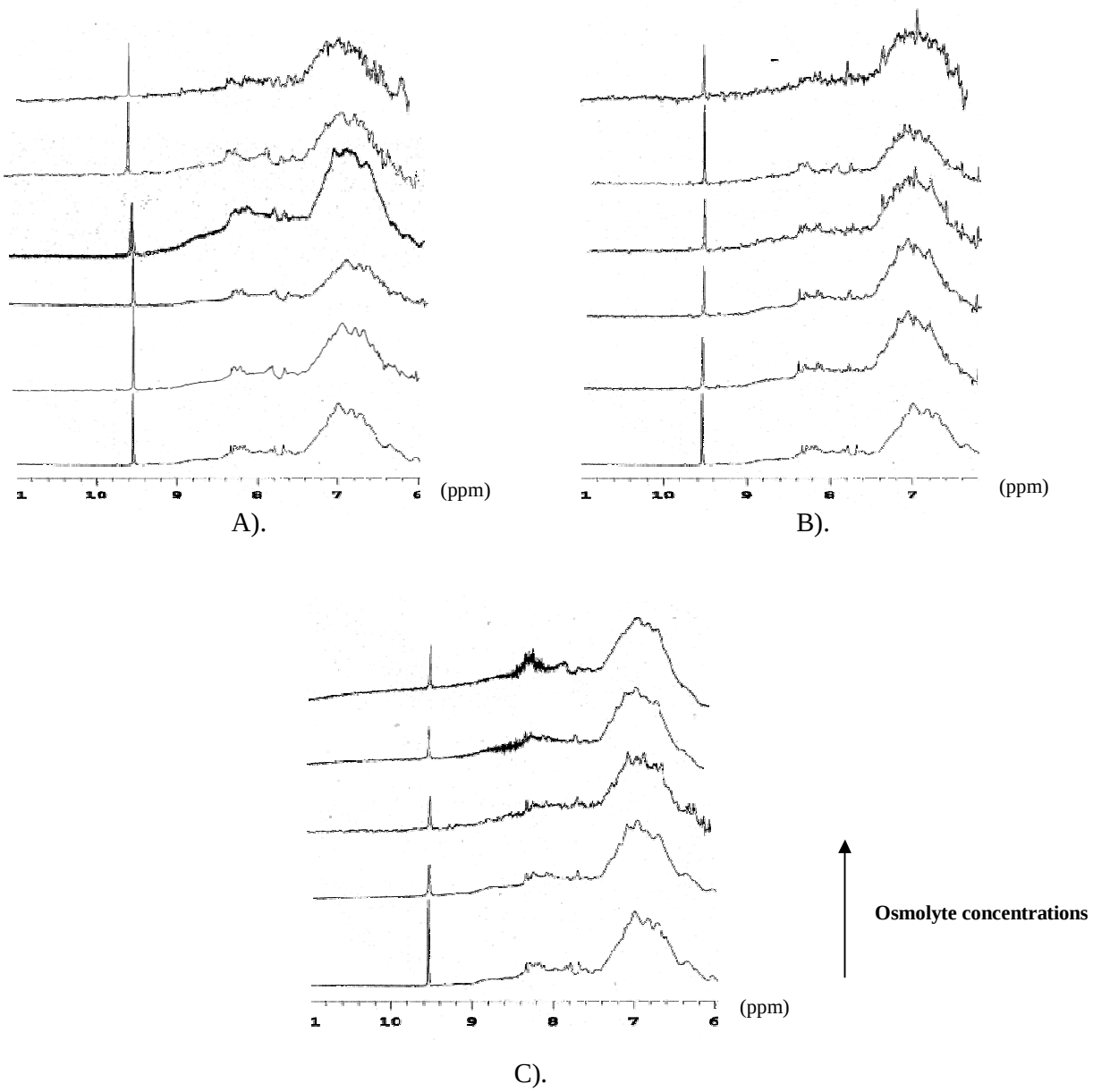

Figure 4.9 1D ^{1}H NMR spectra of HSA in the absence and the presence of osmolytes. A) 1D ^{1}H NMR spectra of HSA in the absence and the presence of trehalose from 0.20, 0.25, 0.30, 0.40, and 0.50 M, B) 1D ^{1}H NMR spectra of HSA in the absence and the presence of sucrose from 0.20, 0.25, 0.30, 0.40, and 0.50 M, and C) 1D ^{1}H NMR spectra of HSA in the absence and the presence of glycerol from 5, 10, 15, and 20 % v/v glycerol (The arrow indicates the increase in osmolyte concentrations from bottom to top). All of these sample solutions were prepared in deuterated phosphate buffer solution pH 7.0 and measured by Unity*Inova* 500 MHz spectrometer at 25 °C.

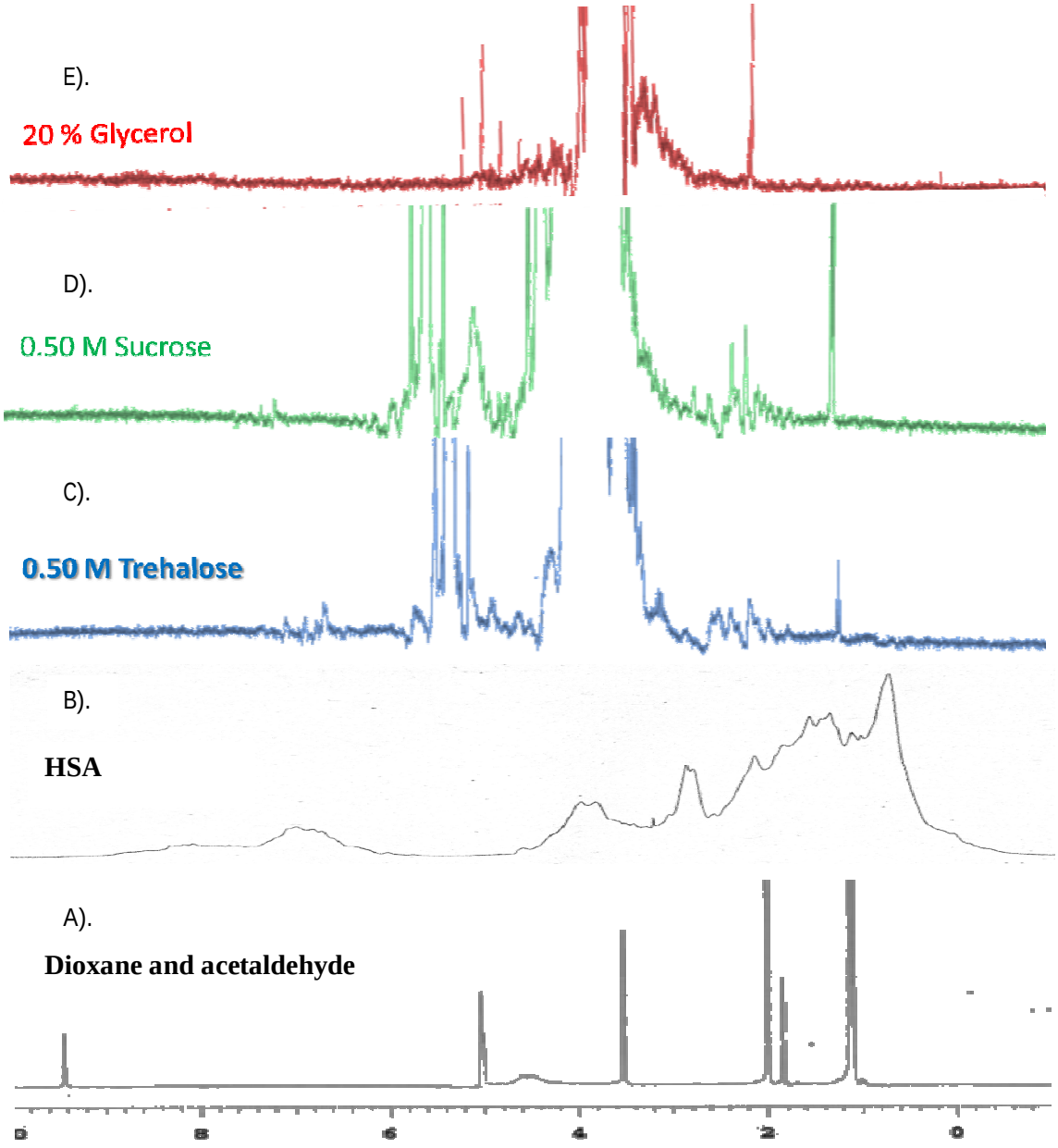

Figure 4.10 1D ^{1}H NMR spectra of dioxane/acetaldehyde, HSA, and osmolytes. 1D ^{1}H NMR spectra of A) 1% dioxane and acetaldehyde, B) HSA, C) 0.5 M trehalose, D) 0.5 M sucrose, and E) 20 % glycerol. All of these sample solutions were prepared in deuterated phosphate buffer solution pH 7.0 and measured by Unity*Inova* 500 MHz spectrometer at 25 °C.

A).

B).

C).

D).

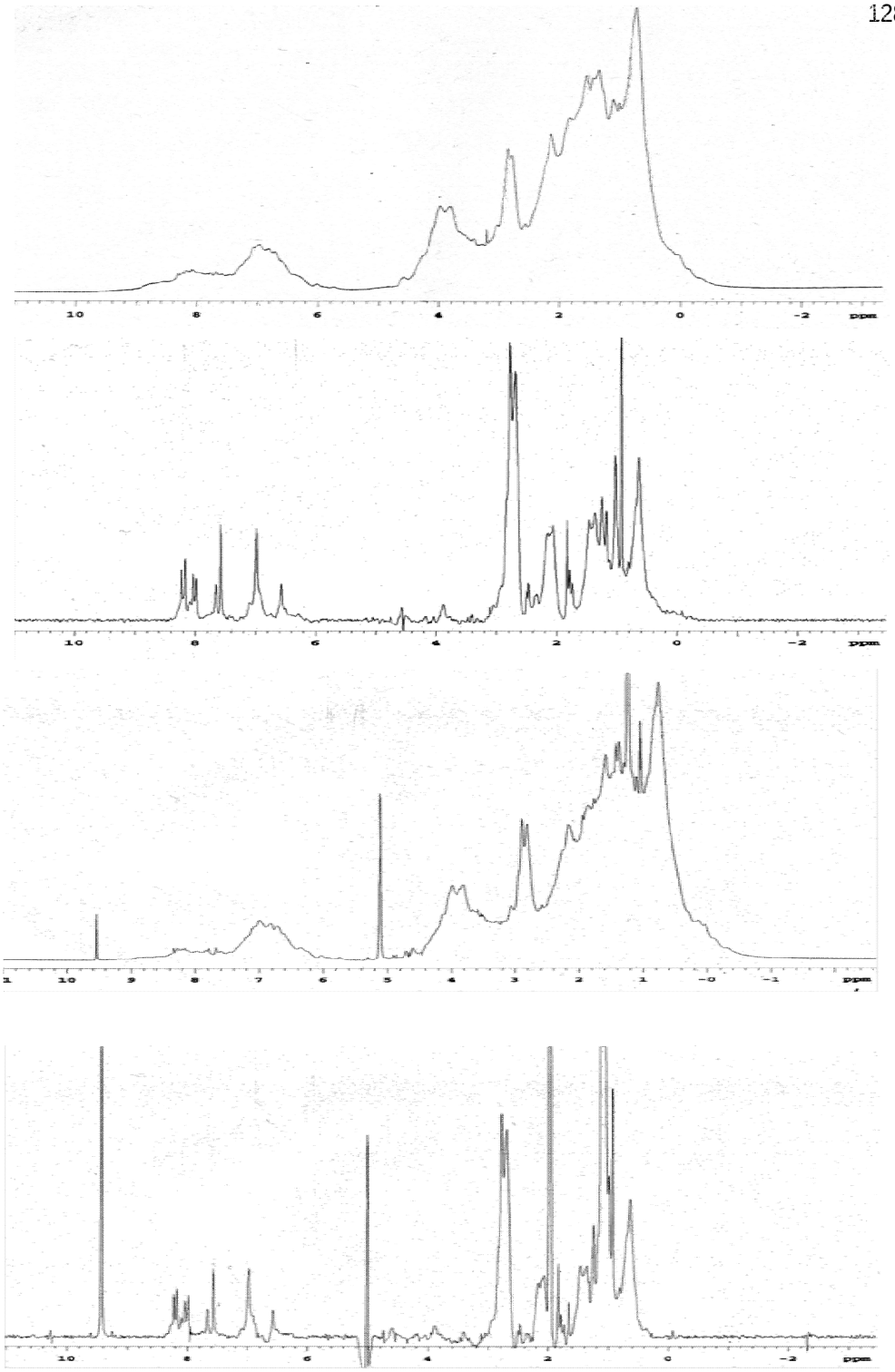

Figure 4.11 The comparison of 1D ^{1}H NMR and PFG NMR spectra of HSA. 1D ^{1}H NMR (A and C) and PFG NMR spectra (B and D) of HSA in the absence and presence of acetaldehyde (40 µl of 1 % acetaldehyde) in deuterated phosphate buffer pH 7.0 solutions and measured by Unity*Inova* 500 MHz spectrometer at 25 °C.

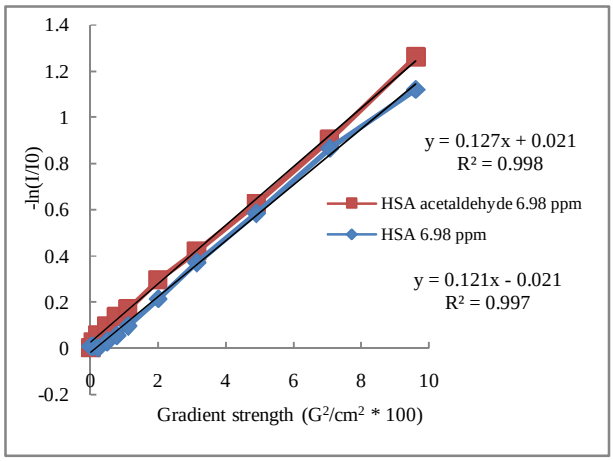

A).

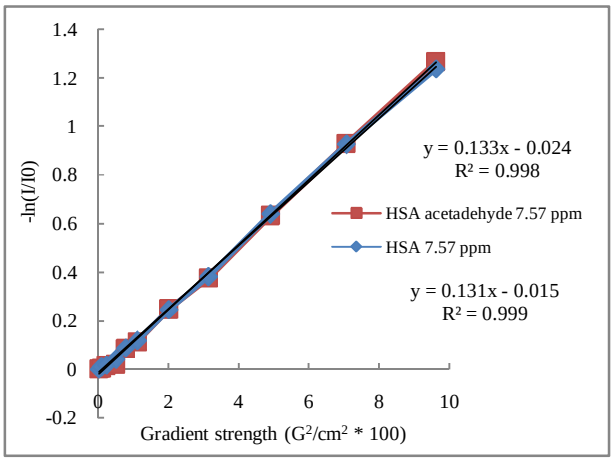

B).

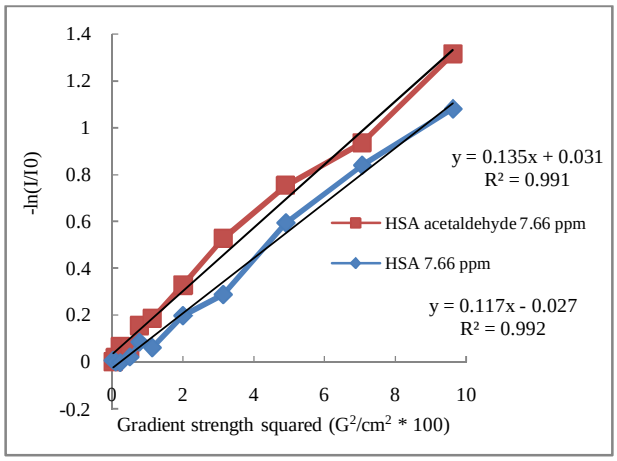

C).

Figure 4.12 Diffusion coefficient rate constant measurements of HSA with and without acetaldehyde in deuterated phosphate buffer pH 7.0, at 25 °C. The diffusion coefficient rate constants are the slope of straight line which drawn by using a linear trend line in Excel.

Table 4.3 Comparison of diffusion coefficient rate constant of HSA pure and HSA in the presence of acetaldehyde.

Chemical shift (ppm)	Diffusion coefficient rate constant (m^2/sec)	
	HSA pure	HSA with acetaldehyde
7.66	0.1176	0.1353
7.57	0.1312	0.1339
6.98	0.1213	0.1273

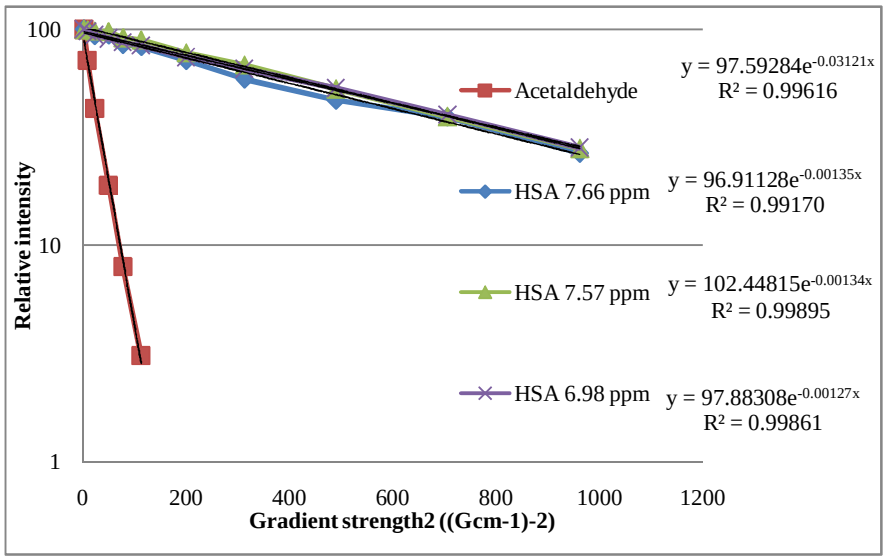

Figure 4.13 Signal attenuation caused by diffusion in the PFG-NMR experiment for HSA in the presence of acetaldehyde at 25 °C. The diffusion coefficient of acetaldehyde and each protein signals (7.66, 7.57, and 6.98 ppm) were measured and displayed as a slope in each exponential equation.

Table 4.4 The hydrodynamic radii values of HSA calculated by DOSY in duplicate experiment.

	Measurement 1		Measurement 2		**Average value**	
Chemical shift	**D_t**	**R_h**	**D_t**	**R_h**	**D_t**	**R_h**
(ppm)	**(m^2/sec)**	**(Å)**	**(m^2/sec)**	**(Å)**	**(m^2/sec)**	**(Å)**
7.66	0.65	35.87	0.66	35.42	**0.66**	**35.75**
7.57	0.59	39.52	0.60	39.02	**0.60**	**39.38**
6.98	0.58	39.93	0.60	39.35	**0.59**	**39.75**
AVG	**0.61**	**38.44**	**0.62**	**37.93**	**0.61**	**38.29**
SD	0.04	2.23	0.04	2.18	0.04	2.21
% RSD	6.00	5.81	5.93	5.74	5.97	5.77

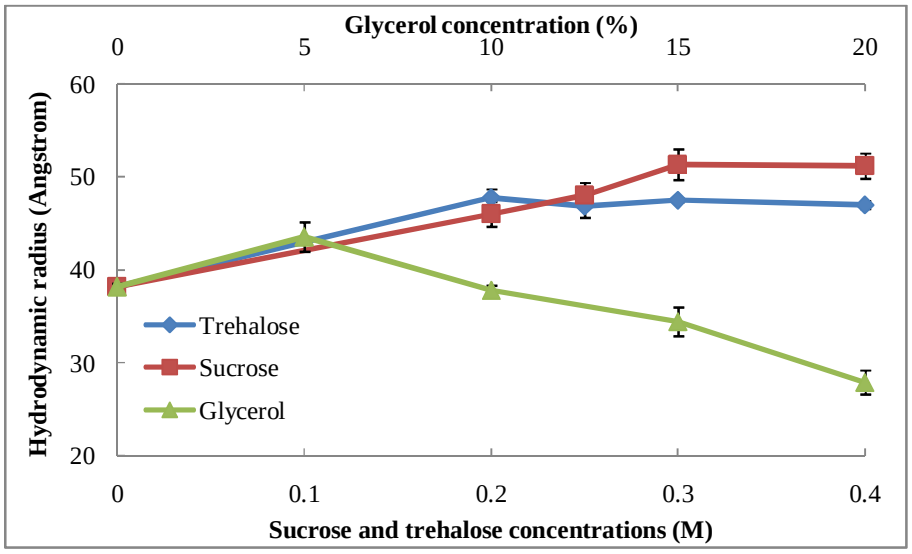

Figure 4.14 Comparison of hydrodynamic radii of HSA in the absence and the presence of osmolytes at 25 °C. (◆; trehalose, ■; sucrose, and ▲; glycerol). Error bars are standard deviations n=2.

Table 4.5 Comparison of hydrodynamic radii of HSA in the absence and presence of osmolytes (trehalose, sucrose, and glycerol). (Error bars are standard deviations n=2)

Conc	Trehalose		%	Sucrose		%	Glycerol		%	Conc
(M)	R_h (Å)	SD	Increased	R_h (Å)	SD	Increased	R_h (Å)	SD	Decreased	(%)
0.00	38.19	0.36	-	38.19	0.36	-	38.19	0.36	-	**0**
0.20	47.76	0.92	25.06	46.02	1.34	20.50	43.55	1.58	14.04	**5**
0.25	46.87	1.22	22.73	48.04	1.33	25.79	37.81	0.53	-1.00	**10**
0.30	47.49	0.21	24.35	51.35	1.66	34.46	34.46	1.56	-9.77	**15**
0.40	47.00	0.41	23.07	51.17	1.36	33.99	27.92	1.30	-26.89	**20**

4.2.3 Hydrodynamic radius of urea-unfolded HSA

In this study, PFG-NMR experiment has been used for measuring the hydrodynamic radius of HSA unfolded by 8 M urea, frequently termed the fully denatured state (Tezuka-Kawakami et al. 2006), and it can be considered as a reference value to compare with Im9 in its urea-denatured state in the presence of osmolytes.

4.2.3.1 One dimensional proton NMR

1D ^{1}H NMR experiment was used to study the HSA structure in both the native and denatured state and it was found that there are significant differences between them, as displayed in Figure 4.15A. In addition, the NMR spectra of denatured HSA in the presence of osmolytes (trehalose, sucrose, and glycerol), displayed in Figure 4.15B, are in excellent agreement with these from the fluorescence spectroscopic experiment in section 4.2.1.1 in showing the protein is unfolded and therefore, it can be stated that urea has an interaction with HSA both in the absence and the presence of osmolytes.

4.2.3.2 Pulsed-field gradient NMR (PFG-NMR) experiment

PFG-NMR experiment was used to determine the diffusion coefficient of unfolded HSA in the absence and the presence of osmolytes by using DOSY software and the hydrodynamic radius of HSA was calculated by comparing with acetaldehyde data. The experimental hydrodynamic radius value of unfolded HSA is 104.04±6.0 Å. However, from the earlier work (Leggio et al. 2009) the hydrodynamic radius of HSA in 9 M urea detected by DLS was only 58.7 Å, which smaller than the experimental value. Nevertheless, my experimental value can be used as the reference point to compare with the hydrodynamic radii of unfolded HSA in the presence of osmolytes since all other experimental conditions are the same. Unfortunately, in the presence of even small concentrations of osmolytes the NMR signals of HSA could not be detected due to a number of technical problems, such as the NMR spectra of unfolded HSA in the presence of osmolytes showed broad peaks and a rough baseline, resulting from the high viscosity of the HSA solution in the presence of osmolyte and 8 M urea as displayed in 4.15B.

In Table 4.6, the results show significant changes in the values of hydrodynamic radii for unfolded HSA (8 M urea) in the absence of osmolytes. The hydrodynamic radius of fully unfolded HSA is 172.43 % larger than that of its native state. Even though the hydrodynamic radii of unfolded HSA in the presence of osmolyte cannot be measured, the particle sizes should be increased as in the Im9 experiment.

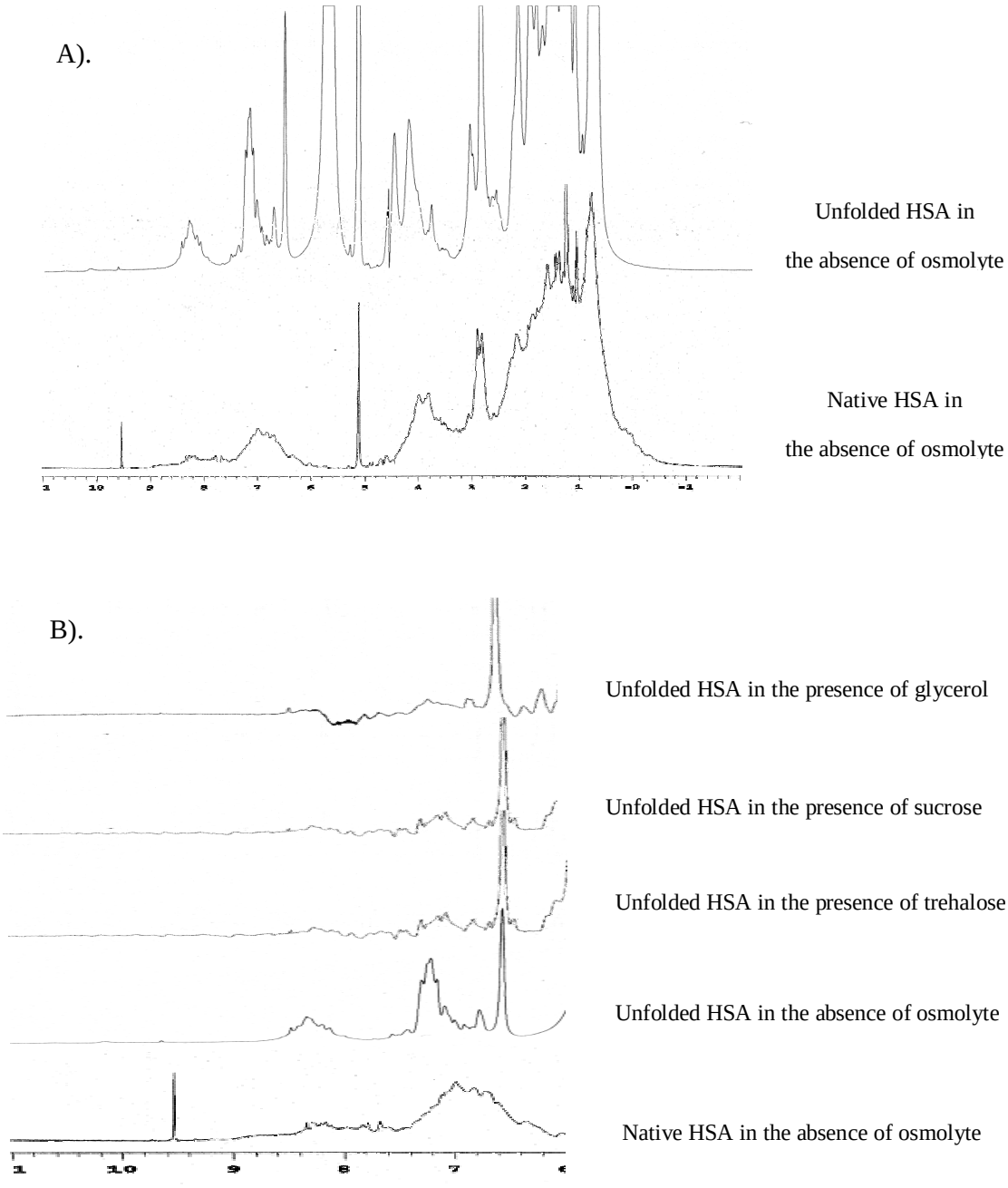

Figure 4.15 1D ^{1}H NMR spectra of native and unfolded HSA in the absence and presence of osmolytes (trehalose, sucrose, and glycerol). A). Full scale, chemical shift from -2 to 11 ppm and B). Some part of scale, chemical shift from 6 to 11 ppm. All protein solutions were prepared in 8 M urea deuterated phosphate buffer solution pH 7.0 and measured by Unity*Inova* 500 MHz spectrometer at 25 °C.

Table 4.6 Hydrodynamic radii of HSA in the absence of osmolyte in native and denatured state.

	R_h native (Å)	**SD**	**R_h denatured (Å)**	**SD**	**$\triangle R_h$ (Å)**	**% increased**
Control	38.19	0.36	104.04	6.00	65.85	172.43

4.3 General Discussion and Conclusions

Our findings show that a one-step, two-state transition was detected in the urea-denaturation of HSA in the absence of osmolyte, but an intermediate, which is not well defined, appears in the urea-denaturation of HSA in the presence of osmolytes. The one-step, two-state transition calculation could not be used to give a guide to the relevant $\triangle G^{H2O}$ values because of the fluctuating results obtained, so these curves were analysed with a two-step, three-state transition calculation and yielded apparently good fits. However, the $\triangle G^{H2O}$ values are unreasonably high and therefore, for this multi-domain protein I have used the $Urea_{1/2}$ values as a guide to stability changes rather than the derived $\triangle G^{H2O}$. $Urea_{1/2}$ values increase when osmolyte concentration is increased indicating that these osmolytes can inhibit the chemical denaturation of HSA by urea and also shows that sucrose is the strongest stabiliser, while trehalose and glycerol are mild stabilisers.

In what follows it is important to note that although HSA has many binding sites for small molecules, there is no evidence to show that the osmolytes used in this experiment have any specific binding to the binding sites. The trends in conformational stabilities detected by urea-induced denaturation are in excellent agreement with the changes in hydrodynamic radii measured by the PFG-NMR experiment of HSA in the absence and the presence of osmolytes. The increase in particle size of HSA in the presence of osmolytes (sucrose and trehalose), as shown by the hydrodynamic radius, is due to an increase in the hydration layer, resulting from preferential hydration and surface tension (Timasheff 1993, Lin and Timasheff 1996). Thus there is an enhanced hydration layer on the protein surface in osmolyte solution which affects the protein compactness and the stability. These stabilisation efficiency results of PFG-NMR experiment are in excellent agreement with the results of conformational stability experiment which stated that the $Urea_{1/2}$ is the highest values in HSA in the presence of sucrose. Therefore, protein type dependent might be the plausible reason for this explanation.

In this experiment, the hydrodynamic radii of HSA in the presence of trehalose showed smaller size than those of HSA in the presence of sucrose. Although the $Urea_{1/2}$ of HSA in the presence of trehalose and sucrose increased upon the addition of osmolytes, the particle size of HSA only sharply increased in the first addition (0.20 M)

of osmolytes and kept nearly the same size at higher concentration (0.25, 0.30, and 0.40 M). The explanation for this non-linear behaviour is the compactness of HSA structure. The higher the osmolyte concentration, the higher the compactness that occurred. Thus as the protein molecule becomes more compact, the hydration layer increases so that the net effect is that the particle size seems about the same with increasing osmolyte concentration after the initial increase.

In contrast to the effect of trehalose and sucrose, the particle size of HSA decreases upon the addition of glycerol after a small increase (from 38.19 to 43.55 Å) following the first addition (5 %) of glycerol. As described in Chapter 1, the formation of a hydration layer with glycerol is different from those of trehalose and sucrose, because both water and osmolyte were excluded from the protein surface and the direct interaction between glycerol and polar residues on the surface of protein might occur. Moreover, the total void volume of the protein core can be decreased by the addition of glycerol (Priev et al. 1996), leading to a reduction in the particle size of the stabilised protein. The reduction in size of HSA at 20 % glycerol concentration (the highest concentration) is substantial at 26.89 %. This might be because HSA is a large macromolecule consisted of three structurally homologous domains, as displayed in Figure 4.1, so the large reduction in size could partly be because the domains are forced to move closer together by glycerol as well as the internal void volume being reduced.

Consequently, it can be concluded that the mechanism of protein stabilisation by glycerol is markedly different from that by sucrose and trehalose and shows a more complicated pattern. Sugars (sucrose and trehalose) strongly hydrate the protein backbone and are also excluded from the protein surface. In contrast, indirect (glycerol excludes both water and osmolyte from the protein surface), direct interaction (direct interaction between glycerol and polar residues on the surface of protein), and a reduction in total void volume at the protein core, resulting in only small changes in hydration layer were found (Auton et al. 2008)..

In the case of the denatured state of HSA in the absence of osmolytes, there is a marked increase in its hydrodynamic radius (increased 65 Å), even though HSA in its denatured state cannot be a fully extended peptide chain because of its 17 disulfide bridges. As shown in previous work (Leggio et al. 2009), the hydrodynamic radii of native and urea-unfolded HSA measured by small-angle X-ray scattering (SAXS) and

DLS are 36.5 and 58.7 Å, respectively. It is unclear why the NMR measurement should be so different and this requires further study. However, it is important to note that the conclusions regarding the effect of osmolytes on the stability of HSA do not depend on the NMR measurement of its hydrodynamic radius in the presence of urea.

In summary, the impact of osmolytes on the conformational stability of HSA and the hydrodynamic radii of its native and urea-denatured states showed complicated and unexpected behaviour compared with Im9 (Chapter 3), likely a consequence of its multi-domain character and its possession of 17 intramolecular disulfide bridges. In the next chapter, HSA was used as a model to investigate the stability studies in different storage conditions for 6 months.

Chapter 5

Storage and stability of Human serum albumin in aqueous solution

5.1 Introduction

5.1.1 General background

In clinical application, a number of Human serum albumin (HSA) derivatives are used in surgery and to treat shock trauma. HSA from donated blood might lead to blood transmission diseases. Therefore, HSA for pharmaceutical products is manufactured with a pasteurizing process (60 °C for several hours) to demolish pathogenic viruses, such as HIV and hepatitis. Stabilisers are important ingredients in HSA formulations to prevent aggregation of HSA during heating. Many kinds of compounds have been studied to stabilise HSA from these harsh conditions, such as glycine, valine, tyrosine, tryptophan, and phenylalanine (Mackay and Martin 1957), but sodium acetyltryptophan (N-Actrp) and sodium octanoate (Oct) are the most effective and widely used in HSA formulations (Anraku et al. 2004). HSA solutions approved by the US FDA (U.S. Food and Drug Administration, http://www.fda.gov) for the pharmaceutical market - Buminate®, AlbuRx®, and Albumarc® - have HSA concentrations of 5, 20, and 25 % and use N-acetyltryptophan and sodium octanoate as protein stabilisers in the formulation. Moreover, there is no need to use any preservative in these formulations because sterile-filter technique was used in the manufacturing process.

Sugars and polyols, which are widely used as stabilisers in protein formulations, have rarely been studied with respect to their effect on the conformational stability of HSA in both thermal and urea-induced denaturations, and the long-term stability of HSA in the presence of these osmolytes is not understood. Consequently, in the present study, the osmolytes (trehalose, sucrose, and glycerol) were examined as a potential alternative to sodium acetyltryptophan (N-Actrp) and sodium octanoate (Oct) to stabilise HSA in long-term stability tests performed under various storage conditions for

6 months. The samples were stored in three different controlled temperatures without humidity control: cold room temperature (2-8 °C), room temperature (20±3 °C), and high temperature (37±3 °C). HSA was used as a representative multi-domain protein model because HSA is a stable protein and has a number of biological activities to measure during the stability test.

The storage temperatures used in this stability test were selected from the ICH (International Conference on Harmonisation) guidelines (the International Conference on Harmonisation of Technical Requirements for Registration of Pharmaceuticals for Human Use, www.ich.org) (ICH 2003). ICH Topic Q1 A (R2) stated that drug products intended for storage in a refrigerator should be studied at two different storage conditions: 5±3 ℃ and 25±2 ℃. However, in this study, we adapted the temperatures in this regulation to match our facilities. Therefore, we considered room temperature at 20±3 ℃ as an appropriated temperature instead of at 25±2 ℃ and also added a higher temperature (37±3 ℃) in order to study HSA under harsher conditions. Although HSA concentrations in the pharmaceutical market are at 0.75 mM (5% albumin), 3.0 mM (20% albumin), and 3.76 mM (25 % albumin), the HSA concentration used in this experiment was only 0.15 mM (1 % albumin) in 0.1 M phosphate buffer pH 7.0, due to the high cost of the raw material. However, this concentration is in the range of normally used (0.1-10 %) in other pharmaceutical products in the market. This concentration was also different from those used in urea-induced denaturation (15 µM) and PFG-NMR (1mM) experiments. The osmolyte concentrations used in this study were chosen from the results of the investigation of the conformational stability of HSA in the presence of osmolytes described in Chapter 4. The highest concentrations used (0.75 M trehalose, 0.75 M sucrose, and 30 % v/v glycerol) showed the most efficiency in stabilising HSA, indicating that the concentrations of these osmolytes can significantly inhibit the chemical denaturation by urea at these concentrations.

5.1.2 Biological activities of HSA

As described in Chapter I, HSA is a multi-domain protein consisting of three homologous domains (I, II, and III) (Fasano et al. 2005), and has many functions throughout the human body, such as ligand binding (Beaven et al. 1974), enzymatic properties (Matsushita et al. 2004), and antioxidant properties (Anraku et al. 2001). HSA binds and transports many kinds of substances such as bilirubin, steroids, bile salts, tryptophan, vitamins, hemin, metal ions, and a number of drugs (Kraghhansen 1981). Consequently, in this study, each one of the most prominent properties of HSA (hemin binding and esterase-like activity, as representatives of ligand binding and enzymatic properties, respectively) was chosen to evaluate the HSA biological activity in the different formulations throughout the stability testing.

5.1.2.1 Esterase-like activity

To elucidate the esterase-like activity of HSA, the reaction of *p*-nitrophenyl acetate (NPA) with HSA was investigated kinetically, because it was previously reported (Kurono et al. 1979) that albumin presents esterase-like activity toward phenyl esters and the active site related to this reaction was found to be one of the most important drug binding sites on HSA, which is located in subdomain IIIA; site II near Arg-410 and Tyr-411 amino acid residues (Watanabe et al. 2000). Moreover, only weak esterase activity was found in domain I, and no esterase-like activity was detected in domain II (Matsushita et al. 2004). In addition, the subdomain IIIA binding site is related to the hydrolysis of prodrugs through its esterase-like activity and is the binding sites for fatty acid and some drugs, such as Ketoprofen and Ibuprofen (Galantini et al. 2010).

Esterase-like activity can be evaluated by monitoring the appearance of *p*-nitrophenol (NP), which results from the deacetylation reaction between *p*-nitrophenyl acetate (NPA) and HSA, as shown in Figure 5.1. This deacetylation reaction occurs very rapidly and involves multiple sites responsible for the ester cleavage of NPA in the HSA structure. The concentration of HSA in the assay mixtures

is usually in excess compared with that of NPA to allow the highly reactive site of HSA to dominate the kinetics (Means and Bender 1975).

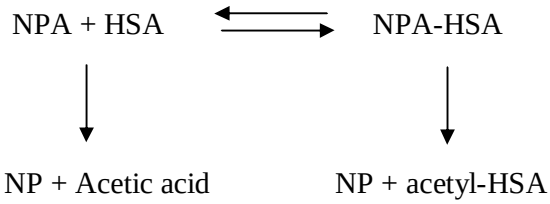

Figure 5.1 The reaction of *p*-nitrophenyl acetate (NPA) and HSA (Ikeda et al. 1979).

In this reaction, NPA-HSA and acetyl-HSA are the non-covalent complex of NPA with HSA and the acetylated form of HSA, respectively. The reaction rate was followed by monitoring changes in UV absorption at 400 nm due to the appearance of the *p*-nitrophenol (NP). The pseudo-first-order rate constants or hydrolysis rate constants (k_{obs}) were determined from plots of log (A_∞-A_t) versus time, where A_∞ and A_t are the absorbances at the completion of the reaction and at time t, respectively (Kurono et al. 1992). The release of NA was followed spectrophotometrically in the absence and the presence of osmolytes in this stability test.

5.1.2.2 Hemin binding

Hemin is an important iron-containing component of haemoglobin that binds to HSA under physiological conditions to form a complex known as methaemalbumin (Rosenfeld and Surgenor 1950), where met means the iron is in the ferric state. From the kinetics of hemin binding to HSA, Adam and Berman (Adams and Berman 1980) inferred that the formation of methaemalbumin is a two stage, single intermediate (I) process as displayed in Figure 5.2.

Hemin + HSA ⟷ I ⟷ Methaemalbumin

Figure 5.2 The methaemalbumin formation process (Adams and Berman 1980)

The X-ray crystal structures of HSA in a fatty acid free state and with bound hemin have been determined (Sugio et al. 1999, Wardell et al. 2002) and are displayed in Figures 5.3A and B, respectively. The HSA-hemin complex has shown a single binding site for hemin on domain I (Kraghhansen 1981, Zunszain et al. 2003). Hemin is a large planar molecule that sterically displaces fatty acids from fatty acid site I, therefore, it can be used as a probe for monitoring the effect of fatty acid on the binding properties of domain I.

Consequently, in this study, the binding of hemin to HSA in the absence and the presence of osmolytes was studied with a fluorescence quenching technique. The binding of hemin to HSA quenches the protein fluorescence, which progressively changes in character from a tryptophan type to a tyrosine type, so the hemin at the primary site strongly quenches the tryptophan fluorescence specifically (Beaven et al. 1974).

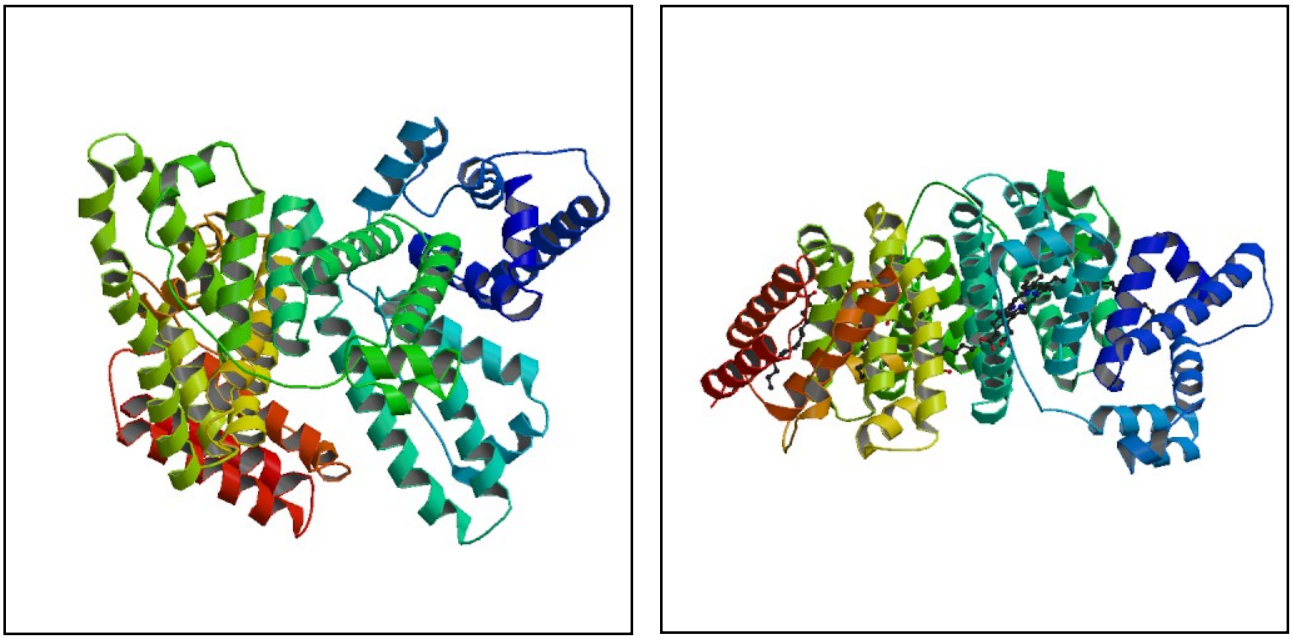

A). B).

Figure 5.3 Crystal structures of HSA in the absence and the presence of hemin (PDB coordinates 1AO6 and 1N5U, respectively) A). HSA (Sugio et al. 1999) and B). HSA binding with hemin (Wardell et al. 2002)

5.1.3 Aggregation testing

Many proteins are stable in solution under controlled temperatures such as at 2-8 °C, but alterations in protein conformation might occur under stress conditions such as high temperature, high pressure, or harsh conditions in the processing. Aggregation is an important problem for long-term stability and it can cause adverse reactions and difficulties for administration of therapeutic proteins. Therefore, aggregation should be minimized during processing, storage, and shipping of pharmaceutical proteins. Many techniques can be used to detect the aggregation in protein formulations, such as Size exclusion chromatography (SEC) (Wang 1999), Dynamic light scattering (DLS), and Native polyacrylamide gel electrophoresis (Native-PAGE) (Lin et al. 2009) In this study the extent of aggregation of HSA in the absence and the presence of osmolytes were monitored with SDS-PAGE, Native-PAGE and DLS techniques.

5.2 Results and Discussions

Liquid formulations of HSA in the absence and the presence of osmolytes (0.75 M trehalose, 0.75 M sucrose, and 30 % v/v glycerol), all in 0.1 M phosphate buffer at pH 7.0, were chosen for the study of the long-term stability of HSA under various storage conditions: cold room temperature (2-8 °C), room temperature (20±3 °C), and high temperature (37±3 °C) for 6 months. During this storage period, the stored solutions were sampled at regular intervals (1, 2, 3, 4, 5, and 6 months), and analysed for their biochemical activities (Esterase-like activity and hemin-binding activity) and aggregation (SDS-PAGE, Native PAGE, and dynamic light scattering).

5.2.1 Visual appearance of solutions

In the British Pharmacopoeia 2010, the specification of human albumin solutions is given as:

Characters : A clear, slightly viscous liquid; it is almost colourless, yellow, amber or green.

pH : 6.7-7.3

Storage : Stored at room temperature (not exceed 30 °C), and protected from light

The solutions in this study were yellowish and without suspended solids. The pH was maintained between 6.7 and 7.0, throughout the stability test.

5.2.2 Biochemical activities

5.2.2.1 Esterase-like activity

The appearance of *p*-nitrophenol from the reaction of *p*-nitrophenyl acetate with HSA in the absence and presence of osmolytes was followed with time and detected by UV spectroscopy at 400 nm, as displayed in Figure 5.4A. The pseudo-first-order rate constants or hydrolysis rate constants (k_{obs}) of these samples are the slopes of the line of log (A_∞-A_t) versus time, as displayed in Figure 5.4B and Table 5.1.

My hydrolysis rate constant values of HSA in the absence of osmolyte are different from the previously reported values (Matsushita et al. 2004), most probably because we used different types of HSA; here, fatty acid free HSA from Sigma, and recombinant HSA in the earlier work.

To quantify the effect of osmolytes on the esterase-like activity of HSA, we follow the slope of the line (hydrolysis rate constants), as graphically presented in Figure 5.4B for freshly prepared samples. The comparison clearly shows that hydrolysis rate constants of HSA in the absence and the presence of trehalose and sucrose (6.05, 5.99, and 5.92 sec, respectively) are nearly the same indicating that trehalose and sucrose do not perturb the esterase-like activity. However, those of HSA in the presence of glycerol (5.61 sec) are slightly decreased compared to the others. This could be because the glycerol led to a marked change in solution viscosity which affected the rate at which substrate and HSA interacted. Since the important issue with this experiment is that the freshly prepared glycerol solution acts as a control for the long-term stability tests the small reduction in rate was not investigated further.

These hydrolysis rate constants were changed to % esterase-like activity for easy comparison with the stability data under various storage conditions, as displayed in Table 5.2 and Figure 5.5. In this experiment, an in-house specification was created to easily interpret the biological activity of HSA during this stability test. The acceptance range for % biological activity (Esterase-like activity) of my products is not less than 70 %. The esterase-like activity of HSA in the absence and the presence of osmolytes decreased throughout the stability testing when the samples were kept at 37±3 °C. Since the first month of stability test, the significant reductions were occurred in all formulations, especially in glycerol formulations, the remaining activity was only

46.20 %. Although the esterase-like activity of trehalose and sucrose formulations was still acceptable (70-80 % activity) in the first month, after that the activity significantly decreased over the period. The 20±3 °C data showed that the formulation without osmolyte and trehalose formulation maintained their activity for 6 months (about 70 %), but the sucrose formulation lose its activity after 4 month (less than 70 %). In addition, the activity of glycerol formulation reduced to 50 % since the first month of storage time. However, in case of HSA in the absence and the presence of osmolytes (trehalose and sucrose) under 2-8 °C, HSA was found to be relative stable since the first month. The esterase-like activity slightly decreased to 70-80 % at the end of the study test. In contrast, glycerol formulation still showed poor stability in this storage temperature.

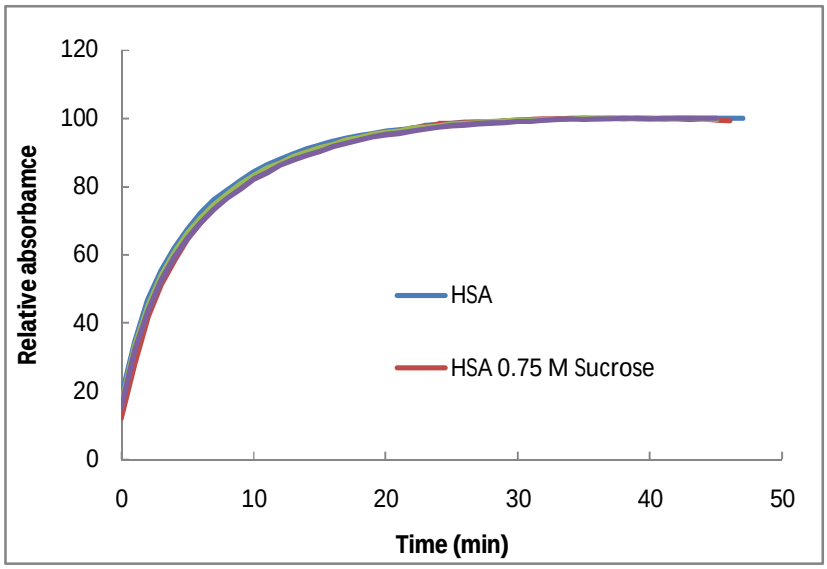

A).

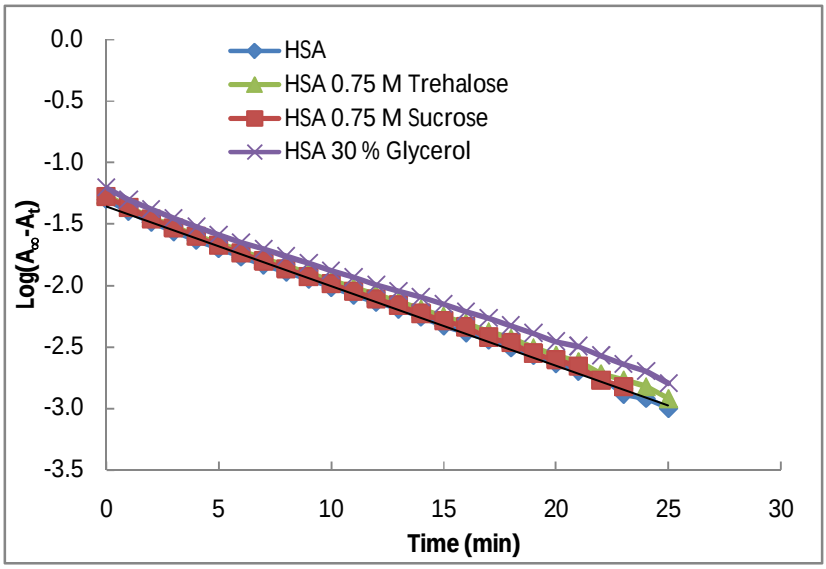

B).

Figure 5.4 Plots of *p*-nitrophenol occurrence by relative absorbance and first order reaction. A). The relative absorbance at 400 nm of *p*-nitrophenol which occurred from the reaction of *p*-nitrophenyl acetate with HSA in the absence and presence of osmolytes (trehalose, sucrose, and glycerol) versus time.

B). First order plots of log (A_∞-A_t) versus time, where A_∞ and A_t are the absorbances at the completion of the reaction and at time t, respectively.

Table 5.1 Hydrolysis rate constant (k_{obs}) for *p*-nitrophenyl acetate of HSA in the absence and the presence of osmolytes. The reaction mixtures contained 9.7 nM *p*-nitrophenyl acetate and 15 μM HSA in the absence and the presence of osmolytes (0.75 M Trehalose, 0.75 M sucrose, and 30 % glycerol) in 0.1 M phosphate buffer pH 7.0. The samples were pulled at constant intervals over the storage period and the reactions were analysed at 25 °C. All values are expressed as mean (n=2) ± standard deviation in the parentheses.

	Hydrolysis rate constant, k_{obs} (sec x 10^{-2})						
Storage time (month)	**Initial**	**1**	**2**	**3**	**4**	**5**	**6**
HSA at 2-8°C	6.05 (0.099)	5.35	5.18	4.96	5.35	5.09	4.98
		(0.099)	(0.198)	(0.255)	(0.276)	(0.177)	(0.106)
HSA at 20 ± 3 °C		4.46	4.13	4.63	4.72	4.80	4.55
		(0.113)	(0.255)	(0.247)	(0.354)	(0.049)	(0.410)
HSA at 37 ± 3 °C		5.35	5.18	4.96	5.35	5.09	4.98
		(0.049)	(0.198)	(0.134)	(0.092)	(0.219)	(0.191)
HSA 0.75 M Trehalose at 2-8°C	5.99 (0.226)	5.71	5.18	5.54	5.15	4.95	4.99
		(0.226)	(0.085)	90.170)	(0.148)	(0.106)	(0.212)
HSA 0.75 M Trehalose at 20 ± 3 °C		4.66	4.27	4.41	4.32	4.44	4.26
		(0.297)	(0.113)	(0.276)	(0.226)	(0.240)	(0.163)
HSA 0.75 M Trehalose at 37 ± 3 °C		4.29	4.06	3.88	4.06	3.98	3.65
		(0.361)	(0.177)	(0.035)	(0.269)	(0.170)	(0.233)
HSA 0.75 M Sucrose at 2-8°C	5.92 (0.226)	5.64	5.30	4.99	4.88	4.47	4.30
		(0.163)	(0.240)	(0.177)	(0.212)	(0.262)	(0.354)
HSA 0.75 M Sucrose at 20 ± 3 °C		5.31	4.89	4.91	4.36	3.82	3.59
		(0.106)	(0.269)	(0.057)	(0.156)	(0.132)	(0.134)
HSA 0.75 M Sucrose at 37 ± 3 °C		4.83	4.52	4.07	3.60	3.37	3.55
		(0.269)	(0.148)	(0.007)	(0.078)	(0.148)	(0.170)
HSA 30 % Glycerol at 2-8°C	5.61 (0.184)	4.50	4.55	3.88	3.42	3.46	3.11
		(0.339)	(0.240)	(0.191)	(0.212)	(0.276)	(0.099)
HSA 30 % Glycerol at 20 ± 3 °C		3.26	3.32	2.87	2.66	2.46	2.51
		(0.134)	(0.134)	(0.240)	(0.269)	(0.156)	(0.134)
HSA 30 % Glycerol at 37 ± 3 °C		2.80	2.73	2.44	2.25	2.34	2.29
		(0.332)	(0.205)	(0.106)	(0.156)	(0.099)	(0.113)

Table 5.2 % Esterase-like activity of HSA in the absence and the presence of osmolytes which calculated from Table 5.1. All values are expressed as mean (n=2) ± standard deviation in the parentheses. The unacceptable values (less than 70 % esterase-like activity) are in the red-coloured.

	% Esterase-like activity						
Storage time (month)	**Initial**	**1**	**2**	**3**	**4**	**5**	**6**
HSA at 2-8°C	100.00 (1.64)	88.35	85.62	81.98	88.35	84.05	82.23
		(5.49)	(3.27)	(4.21)	(4.56)	(2.92)	(1.75)
HSA at 20 ± 3 °C		73.72	68.26	76.45	78.02	79.26	75.21
		(1.87)	(4.21)	(4.09)	(5.84)	(0.82)	(6.78)
HSA at 37 ± 3 °C		**64.21**	**65.79**	**69.17**	**66.36**	**62.56**	**58.43**
		(0.82)	(3.27)	(2.22)	(1.52)	(3.62)	(3.16)
HSA 0.75 M Trehalose at 2-8°C	100.00 (3.78)	94.38	85.62	91.57	85.04	81.74	82.48
		(3.78)	(1.42)	(2.83)	(2.48)	(1.77)	(3.54)
HSA 0.75 M Trehalose at 20 ± 3 °C		77.02	70.58	72.81	71.4	73.39	70.33
		(4.96)	(1.89)	(4.60)	(3.78)	(4.01)	(2.72)
HSA 0.75 M Trehalose at 37 ± 3 °C		70.83	**67.02**	**64.05**	**67.11**	**65.79**	**60.25**
		(6.02)	(2.95)	(0.59)	(4.49)	(2.83)	(3.90)
HSA 0.75 M Sucrose at 2-8°C	100.00 (3.82)	93.14	87.6	82.4	80.66	73.8	71.07
		(2.75)	(4.06)	(2.99)	(3.58)	(4.42)	(5.97)
HSA 0.75 M Sucrose at 20 ± 3 °C		87.69	80.83	81.16	72.07	**63.08**	**59.26**
		(1.79)	(4.54)	(0.96)	(2.63)	(2.23)	(2.27)
HSA 0.75 M Sucrose at 37 ± 3 °C		79.83	74.63	**67.19**	**59.42**	**55.62**	**58.68**
		(4.54)	(2.51)	(0.12)	(1.31)	(2.51)	(2.87)
HSA 30 % Glycerol at 2-8°C	100.00 (3.28)	74.38	75.21	**64.05**	**56.53**	**57.11**	**51.4**
		(6.05)`	(4.29)	(3.40)	(3.78)	(4.92)	(1.76)
HSA 30 % Glycerol at 20 ± 3 °C		**53.8**	**54.79**	**47.44**	**43.97**	**40.66**	**41.4**
		(2.39)	(2.39)	(4.29)	(4.79)	(2.77)	(2.39)
HSA 30 % Glycerol at 37 ± 3 °C		**46.2**	**45.04**	**40.25**	**37.19**	**38.68**	**37.85**
		(5.92)	(3.66)	(1.89)	(2.77)	(1.76)	(2.02)

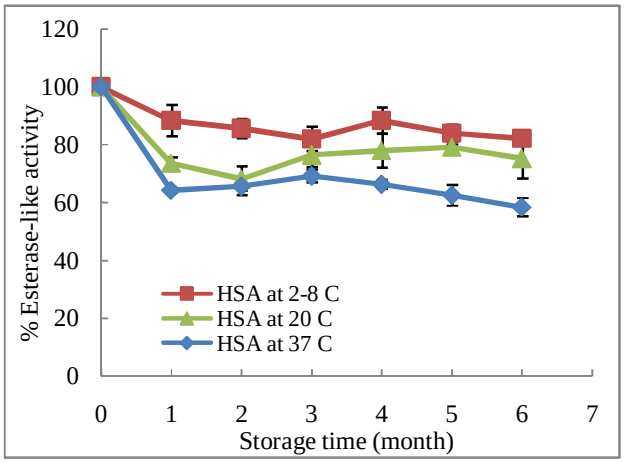

A).

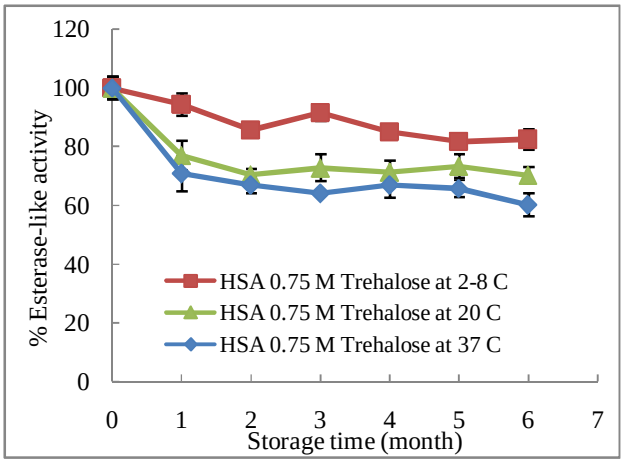

B).

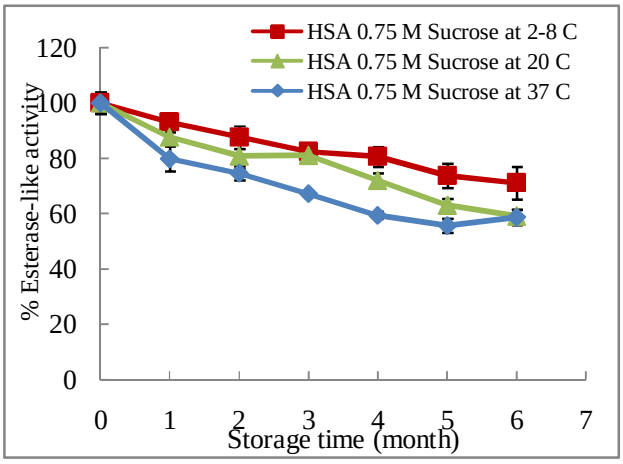

C).

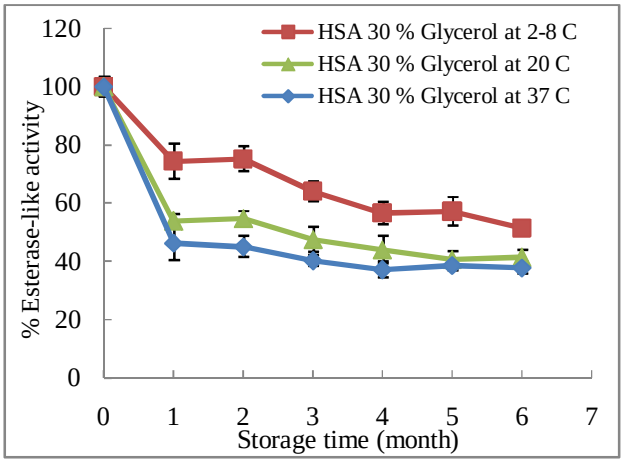

D).

Figure 5.5 % Esterase-like activity of HSA in the absence and the presence of osmolytes over the storage period (6 months) at different temperatures.

5.2.2.2 Hemin-binding activity

The quenching of fluorescence intensity of HSA in the absence of osmolytes when titrated by hemin solution is displayed in Figure 5.6. Figure 5.7A displays the binding isotherm of hemin obtained with HSA in the absence and the presence of osmolytes. In equilibration of HSA with hemin, the intrinsic fluorescence intensity was significantly quenched when hemin was titrated, indicating hemin binding to HSA. These quenching data were analysed to obtain various ligand binding parameters by plotting log [F_0-F / F] versus log [Q], where F_0 and F are the observed fluorescence intensity in the absence and the presence of hemin, respectively, and [Q] is the hemin concentration, as shown in Figure 5.7B, and calculating the binding parameters, as listed in Table 5.3, via least square analysis of the straight line relationship: the slope was equal to n (binding affinity) and the intercept on the Y-axis was equal to log K (K = association constant). Therefore, the standard free energy change ($\triangle$G) of the hemin binding to HSA can be calculated from the binding constant as displayed in Equation 2.12.

$$\triangle G_{binding} = -2.303\ RT \log K \qquad \textit{Equation 2.12}$$

The binding parameters of HSA in the absence of osmolyte are different from previously reported data (Varshney et al. 2008). All of our values are lower than those obtained by Varshney and co-workers, as displayed in Table 5.4. These differences could be attributed to the different experimental conditions, such as different preparations of HSA and/or different hemin stock solution preparation, which could give different values. In Varshney's method, hemin stock solution was prepared to 4.0 mM concentration. Firstly, I tried to use this concentration in my experiment, but the results fluctuated greatly. This might be because hemin was not totally dissolved in 10 mM NaOH or might have aggregates in hemin solution. To prevent this complexity, therefore, lower concentrations (1.8-2.1 μM) of hemin stock solution were used to maintain monomeric hemin and HSA undenatured in this environment.

To quantify the effect of osmolytes on hemin binding to HSA, we followed fluorescence quenching titration curves, as graphically presented in Figure 5.7 A and B, and determined the binding parameters (Association constant, $\triangle G_{binding}$, and number of binding site), as presented in Table 5.3. The comparison clearly showed that the addition of osmolytes decreased the binding parameters comparing to those of HSA

without osmolyte. This reduction correlates well with the solution viscosity. HSA containing glycerol (the highest viscosity) showed the lowest values of binding parameters, while HSA containing trehalose (the lowest viscosity) showed the highest values, except for HSA without osmolyte. This could be because the osmolytes led to a marked change in solution viscosity which affected the rate at which substrate and HSA interacted. The formation of hydration layers originating from the interaction between osmolytes and water, totally covered the protein structure; and hence hemin access to the protein was perturbed.

As it can be seen for binding constant and free energy change in binding, the comparison clearly showed that Association constant and $\triangle G_{binding}$ of HSA in the absence and the presence of osmolytes significantly decreased since the first month in all the storage temperatures, except in the trehalose and sucrose formulations under 2-8 °C, these values were relatively constant in the first month and slightly decreased in the next months, as displayed in Table 5.3A and B. The relationships between these two parameters are displayed in Equation 2.12: the higher the association constant, the larger the $\triangle G_{binding}$. In contrast, the number of binding (n), or binding capacity of HSA in the absence and the presence of osmolytes slightly affected throughout the stability testing in all of storage temperatures. The values are in the range of 1.20 – 1.65. These parameters reflect binding at the tight binding site detected crystallographically (Figure 5.3) and binding at a number of unidentified weaker binding sites. These latter sites, sometimes called adventitious binding sites, are most likely to be regions of the surface to which hemin can adhere.

In conclusion, however, HSA have a high-affinity binding site and an unknown number assumed to be large of weaker binding sites (Beaven 1974). The weaker binding sites are usually regarded as being adventitious binding of hemin to the protein surface with the high-affinity binding being at the site identified by X-ray crystallography, as displayed in Figure 5.3 (Wardell 2002). In this experiment, I have followed the procedure of Antika and co-workers (Ankita, 2008) in increasing an apparent association constant (K) for hemin binding and the number of binding sites (n) while this does not provide a site-specific binding constant for the high-affinity binding, therefore, in these results, free and total hemin in the solution cannot be distinguished, however, these results allows me to compare samples in the stability test which alter with values as relevant literature.

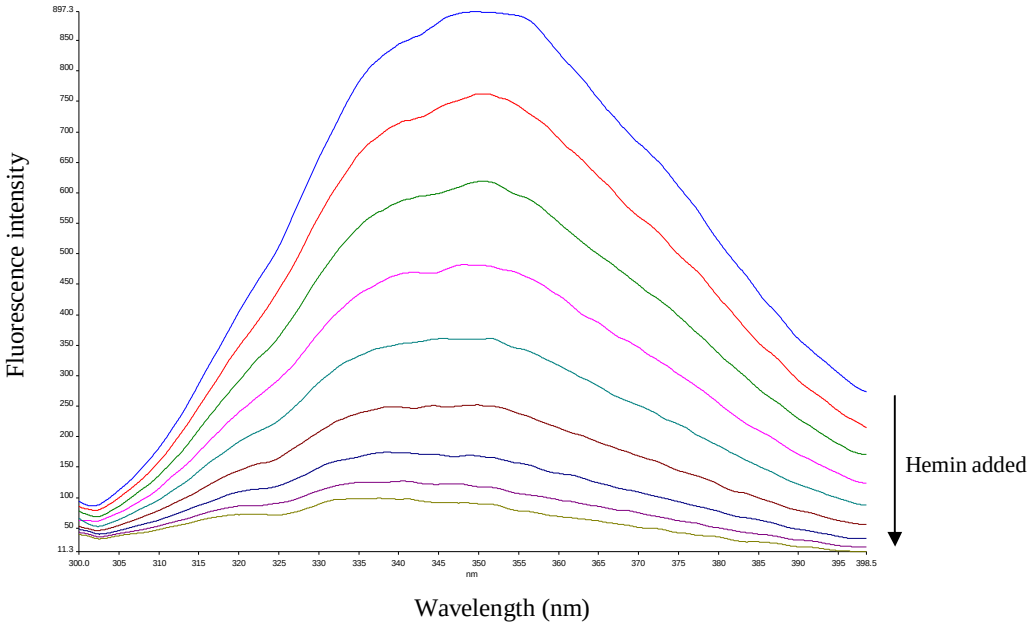

Figure 5.6 Fluorescence spectra of Hemin titrated binding to HSA, showing quenching, and significant changes. Hemin was titrated to HSA solutions (3.5 μM HSA) in 0.1 M phosphate buffer, pH 7.0. Excitation and emission wavelength were 295 and 340 nm and emission and excitation bandwidth were set at 5 nm.

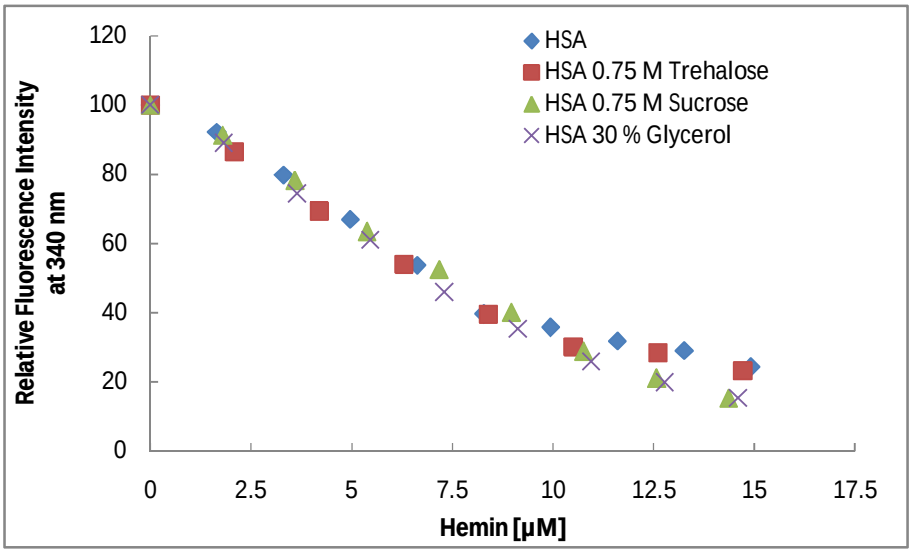

A).

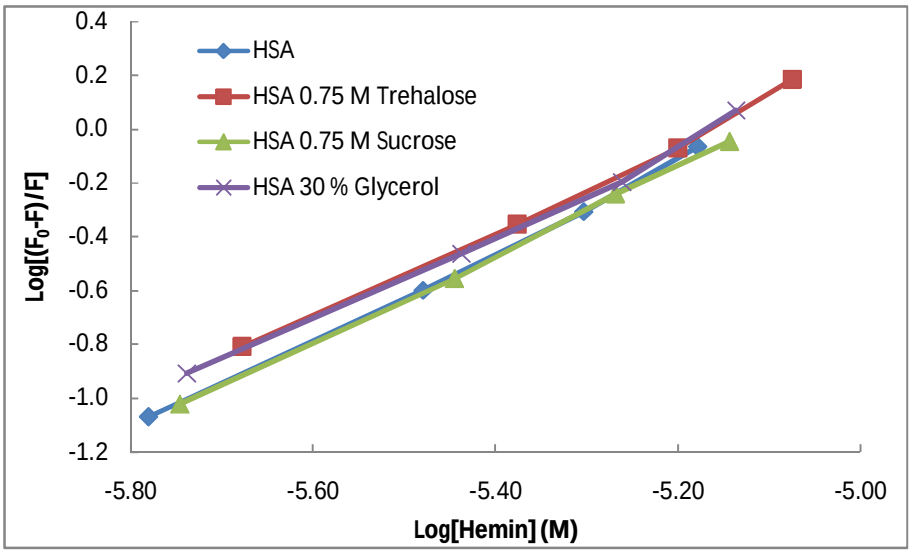

B).

Figure 5.7 The binding isotherm of hemin obtained with HSA. A). Fluorescence quenching titration results of hemin binding to HSA in the absence (◆) and the presence of osmolytes (Trehalose (■), sucrose (▲), and glycerol (×)). B). Log[(F_0-F)/F] versus Log[Hemin] plots HSA conformations for association constants and binding sites.

Table 5.3 Ligand binding parameters (Association constant, $\triangle G_{binding}$, and number of binding sites) of HSA in the absence and the presence of osmolytes

A).	Association constant, K ($x10^7$)(M^{-1})						
Storage time (month)	**Initial**	**1**	**2**	**3**	**4**	**5**	**6**
HSA at 2-8°C	29.50	1.58	0.96	0.74	0.66	0.86	0.52
HSA at 20 ± 3 °C		1.41	0.83	0.69	0.59	0.48	0.41
HSA at 37 ± 3 °C		0.79	0.63	0.56	0.49	0.33	0.32
HSA 0.75 M Trehalose at 2-8°C	25.70	26.30	15.80	7.08	3.47	2.09	1.74
HSA 0.75 M Trehalose at 20 ± 3 °C		5.62	2.57	1.82	1.20	0.71	0.66
HSA 0.75 M Trehalose at 37 ± 3 °C		1.35	1.05	0.74	0.62	0.51	0.44
HSA 0.75 M Sucrose at 2-8°C	22.40	22.40	10.70	6.03	2.63	1.62	1.02
HSA 0.75 M Sucrose at 20 ± 3 °C		6.92	4.07	2.69	1.29	0.44	0.42
HSA 0.75 M Sucrose at 37 ± 3 °C		1.62	1.38	0.58	0.37	0.41	0.35
HSA 30 % Glycerol at 2-8°C	16.20	0.71	0.31	0.47	0.24	0.13	0.12
HSA 30 % Glycerol at 20 ± 3 °C		0.15	0.09	0.05	0.03	0.04	0.06
HSA 30 % Glycerol at 37 ± 3 °C		0.12	0.05	0.06	0.03	0.02	0.01

	$\triangle G_{binding}$ (kcal mol^{-1})						
Storage time (month)	**Initial**	**1**	**2**	**3**	**4**	**5**	**6**
HSA at 2-8°C	-11.56	-9.82	-9.52	-9.37	-9.30	-9.46	-9.16
HSA at 20 ± 3 °C		-9.76	-9.44	-9.33	-9.24	-9.11	-9.02
HSA at 37 ± 3 °C		-9.41	-9.28	-9.21	-9.12	-8.89	-8.88
HSA 0.75 M Trehalose at 2-8°C	-11.47	-11.49	-11.19	-10.71	-10.29	-9.99	-9.88
HSA 0.75 M Trehalose at 20 ± 3 °C		-10.57	-10.11	-9.91	-9.66	-9.35	-9.30
HSA 0.75 M Trehalose at 37 ± 3 °C		-9.73	-9.58	-9.37	-9.26	-9.15	-9.06
HSA 0.75 M Sucrose at 2-8°C	-11.39	-11.39	-10.96	-10.61	-10.12	-9.84	-9.56
HSA 0.75 M Sucrose at 20 ± 3 °C		-10.70	-10.38	-10.14	-9.70	-9.06	-9.03
HSA 0.75 M Sucrose at 37 ± 3 °C		-9.84	-9.74	-9.22	-8.96	-9.02	-8.92
HSA 30 % Glycerol at 2-8°C	-11.20	-9.35	-8.85	-9.10	-8.70	-8.34	-8.30
HSA 30 % Glycerol at 20 ± 3 °C		-8.43	-8.12	-7.82	-7.49	-7.57	-7.85
HSA 30 % Glycerol at 37 ± 3 °C		-8.28	-7.74	-7.93	-7.39	-7.22	-6.99

Table 5.3 (cont.) Ligand binding parameters (Association constant, $\triangle G_{binding}$, and number of binding sites) of HSA in the absence and the presence of osmolytes.

C).	Number of binding sites (n)						
Storage time (month)	**Initial**	**1**	**2**	**3**	**4**	**5**	**6**
HSA at 2-8°C	1.65	1.45	1.38	1.31	1.20	1.29	1.29
HSA at 20 ± 3 °C		1.52	1.43	1.49	1.37	1.35	1.29
HSA at 37 ± 3 °C		1.55	1.47	1.36	1.22	1.45	1.26
HSA 0.75 M Trehalose at 2-8°C	1.63	1.42	1.34	1.28	1.36	1.27	1.30
HSA 0.75 M Trehalose at 20 ± 3 °C		1.56	1.48	1.45	1.41	1.42	1.39
HSA 0.75 M Trehalose at 37 ± 3 °C		1.46	1.42	1.37	1.32	1.29	1.34
HSA 0.75 M Sucrose at 2-8°C	1.63	1.44	1.37	1.33	1.21	1.32	1.27
HSA 0.75 M Sucrose at 20 ± 3 °C		1.53	1.39	1.47	1.32	1.44	1.36
HSA 0.75 M Sucrose at 37 ± 3 °C		1.51	1.45	1.37	1.29	1.34	1.28
HSA 30 % Glycerol at 2-8°C	1.59	1.38	1.37	1.29	1.25	1.33	1.23
HSA 30 % Glycerol at 20 ± 3 °C		1.41	1.33	1.27	1.24	1.32	1.26
HSA 30 % Glycerol at 37 ± 3 °C		1.36	1.32	1.34	1.28	1.33	1.20

Table 5.4 Ligand binding parameters (Association constant, number of binding sites, and $\triangle G_{binding}$) of HSA in the absence osmolytes compared to the previous data.

Proteins	**Binding parameters**		
	Association constant, K ($x10^7$)(M^{-1})	**Number of binding sites (n)**	**$\triangle G_{binding}$ (kcal mol^{-1})**
HSA[a]	29.5	1.65	-11.56
HSA[b]	43.02	1.83	-11.85

a. Binding parameters from my experiment. The sample solutions were prepared containing 3.5 μM HSA titrated by hemin (1.8-2.1 μM stock solution and were monitored by fluorescence spectroscopy (excitation and emission wavelength were 295 and 340 nm, respectively). The spectra were recorded after 10 min of the addition of hemin to HSA solution.

b. Binding parameters from Varshney (Varshney et al. 2008). The samples solution were prepared containing 3.5 μM HSA titrated by hemin (4.0 mM stock solution) and were monitored by fluorescence spectroscopy (excitation and emission wavelength were 280 and 340 nm, respectively). The spectra were recorded after 15-20 min of the addition of hemin to HSA solution.

5.2.2.3 Aggregation testing

5.2.2.3.1 SDS-PAGE and Native PAGE

Native or non-denaturing PAGE is a suitable technique to detect aggregation. SDS is not used in this technique, so the conformation and mobility of the native protein molecule is maintained. The electrophoretic mobility of proteins in Native-PAGE depends on both their charge and size, while in SDS-PAGE; the electrophoretic mobility depends only the molecular mass of the protein molecules as there is an approximately constant ratio of charge to amino acid residue: two SDS per residue.

At the initial stage of the stability test, HSA in the absence and the presence of osmolytes was studied with SDS and Native-PAGE, as displayed in Figure 5.8A and B. Two dilutions of samples were used in this study: without dilution (left hand side) and 10 times dilution (right hand side). However, in case of the detection of trace amounts of aggregates and impurities, samples should not have any dilutions, because the soluble aggregates might be dissolved in the adding solution. Therefore, concentrated HSA samples (samples without dilution) were intentionally loaded to sample wells for both SDS and Native-PAGE experiments. From these results, it showed that there were no significant changes in HSA integrity in both SDS and Native-PAGE at the initial stage arising from the presence of the osmolytes, notwithstanding the observation of associated forms of HSA under native conditions. Therefore, it can be assumed that osmolytes do not have any effect on the formation of aggregates in freshly prepared protein samples.

The Native-PAGE of HSA in the absence and the presence of osmolytes, at the initial stage, exhibit three intense bands, corresponding to monomer, dimer, and higher order aggregates. After the stability test had run for 6 months, all formulations displayed the electrophoretic pattern almost identical to the initial stage, as displayed in Figure 5.9A-F. No additional band was found in each month under various storage conditions, suggesting that no aggregation occurred in the stability test.

The SDS-PAGE results in this stability test, as displayed in Figure 5.10A-F, showed that the gel pattern is identical to the initial stage in the first month under various storage conditions, but intense bands at the top of each lane occurred in the presence of sucrose and trehalose from the second month of the test to the final 6 month

sample. These intense bands must be aggregated material unable to enter the gel but since similar behaviour was not seen with the native gels the aggregation was not simply a consequence of the age of the sample or the presence of osmolytes.

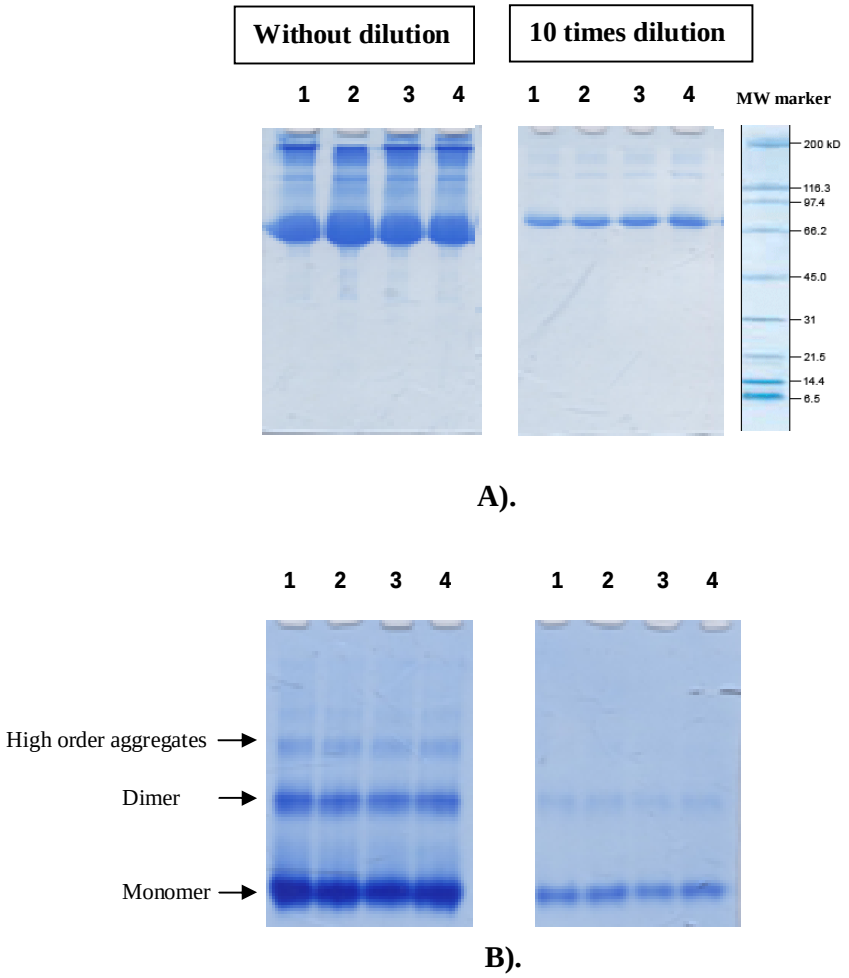

Figure 5.8 SDS-PAGE and Native-PAGE of HSA in the absence and the presence of osmolytes in the initial stage (before the stability test). A). SDS-PAGE and B). Native-PAGE (1; HSA, 2; HSA 0.75M Trehalose, 3; HSA 0.75 M Sucrose, and 4; HSA 30 % Glycerol).

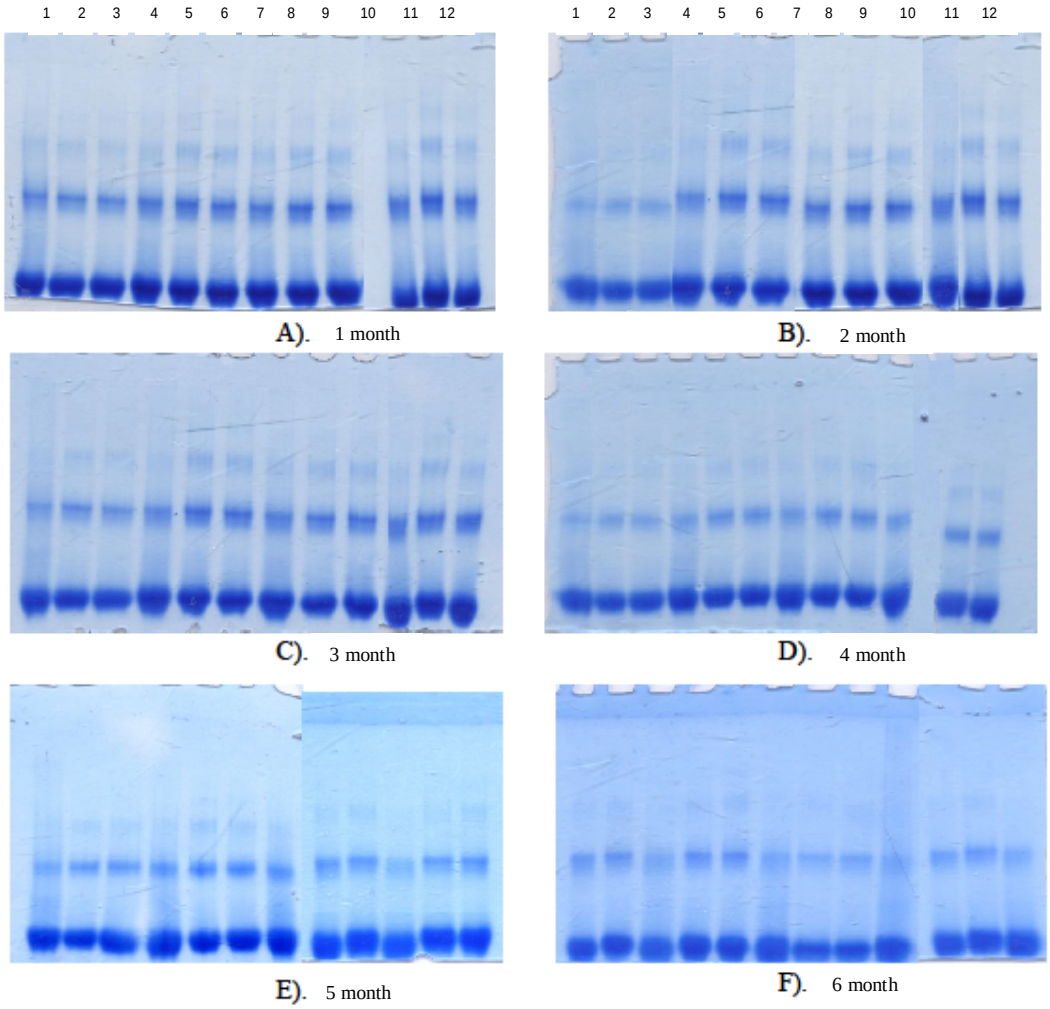

Figure 5.9 Native-PAGE of HSA in the absence and the presence of osmolytes under various storage conditions (37±3 °C, 2-8°C, and 20±3 °C) throughout 6 months stability test (A-F: 1-6 month): Lane 1; HSA at 37±3 °C, Lane 2;HSA at 2-8°C, Lane 3; HSA at 20±3 °C, Lane 4; HSA 0.75 M Trehalose at 37±3 °C, Lane 5; HSA 0.75 M Trehalose at 2-8 °C, Lane 6; HSA 0.75 M Trehalose at 20±3 °C, Lane 7; HSA 0.75 M Sucrose at 37±3 °C, Lane 8; HSA 0.75 M Sucrose at 2-8 °C, Lane 9; HSA 0.75 M Sucrose at 20±3 °C, Lane 10; HSA 30 % Glycerol at 37±3 °C, Lane 11; HSA 30 % Glycerol at 2-8 °C, and Lane 12; HSA 30 % Glycerol at 20±3 °C.

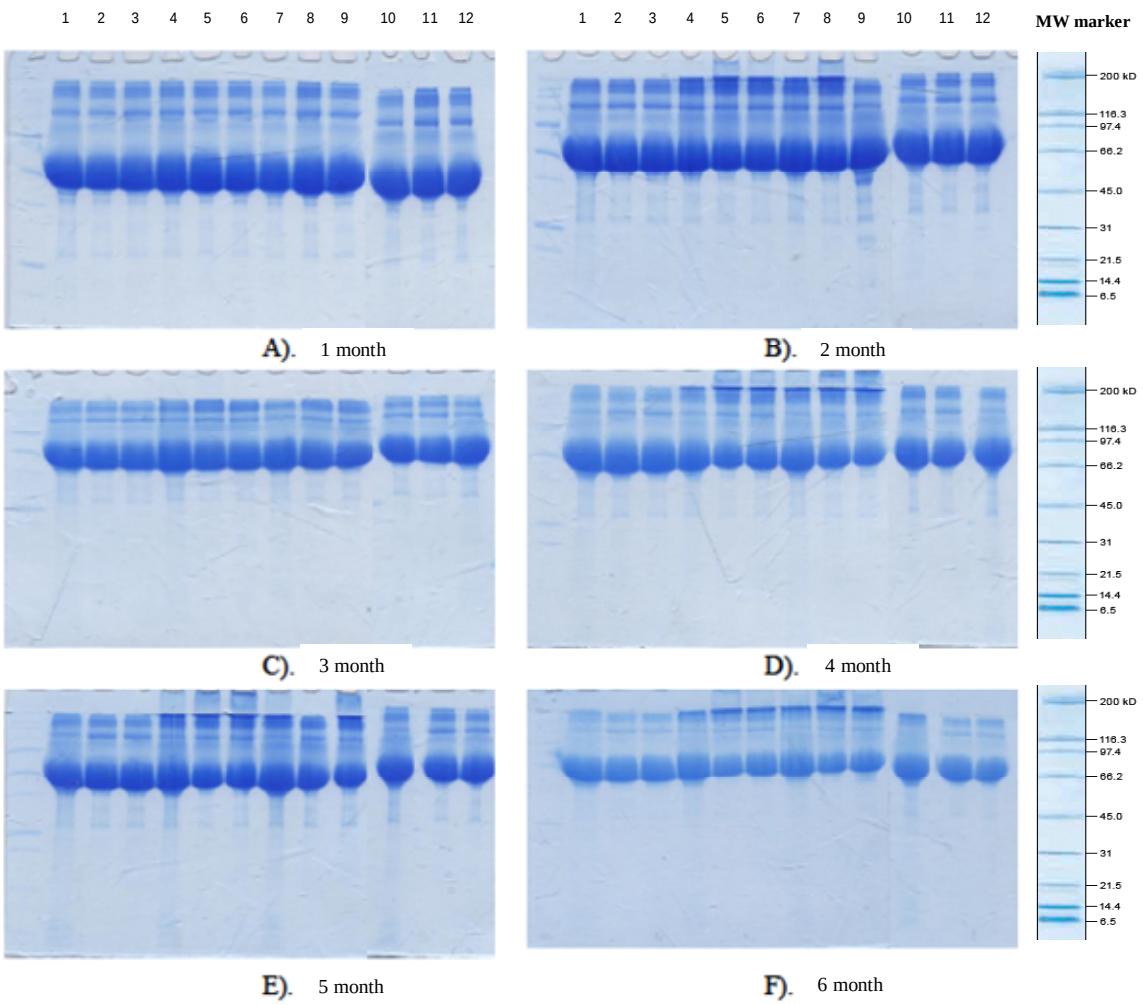

Figure 5.10 SDS-PAGE of HSA in the absence and the presence of osmolytes under various storage conditions (37±3 °C, 2-8°C, and 20±3 °C) throughout 6 months stability test (A-F: 1-6 month): Lane 1; HSA at 37±3 °C, Lane 2;HSA at 2-8°C, Lane 3; HSA at 20±3 °C, Lane 4; HSA 0.75 M Trehalose at 37±3 °C, Lane 5; HSA 0.75 M Trehalose at 2-8 °C, Lane 6; HSA 0.75 M Trehalose at 20±3 °C, Lane 7; HSA 0.75 M Sucrose at 37±3 °C, Lane 8; HSA 0.75 M Sucrose at 2-8 °C, Lane 9; HSA 0.75 M Sucrose at 20±3 °C, Lane 10; HSA 30 % Glycerol at 37±3 °C, Lane 11; HSA 30 % Glycerol at 2-8 °C, and Lane 12; HSA 30 % Glycerol at 20±3 °C.

5.2.2.3.3 Dynamic light scattering

The particle size of proteins and aggregates were determined by dynamic light scattering (DLS). The diffusion coefficient was detected and converted into the hydrodynamic radius of the protein and its size distribution by the Stoke-Einstein equation. The advantage of this technique is that it is one of the most sensitive methods for detecting the presence of soluble aggregates (Katayama et al. 2006).

Figure 5.11A shows the normal size distribution of HSA in the absence of osmolytes which yields a hydrodynamic radius (R_h) of 4.138±0.12 nm. This average experimental hydrodynamic radii of HSA in the absence of osmolytes is not significantly different from previous reports (Galantini et al. 2008) which were 36.5 and 35.2 Å from experimental (measured by DLS measurement) and calculated hydrodynamic radii by HYDROPRO® software, respectively. In addition, the hydrodynamic radius of HSA measured by PFG-NMR experiment from Chapter 4 is 3.819±0.036 nm. Consequently, it can be assumed that the particle size of HSA in the native conditions I explored had a larger size than in the previous works; however, it is reasonable to take this value as the reference to compare the hydrodynamic radii of HSA in the presence of osmolytes and in the stability experiment since all other solution parameters were the same.

To quantify the effect of osmolytes on size distribution of HSA, therefore, the comparison of distribution curves between HSA and HSA with osmolytes (0.75 M Trehalose, 0.75 M Sucrose, and 30 % Glycerol) is displayed in Figure 5.11 A-D, and hydrodynamic radii of HSA in the absence and the presence of osmolytes in different concentrations are showed in Table 5.5 and Figure 5.12. As can be seen from these Figures and Table, extra peaks (less than 1 nm and higher than 100 nm, i.e. both smaller and larger than HSA peak) occurred in osmolyte solution (Figure 5.11B-D) but not found in the protein solution (Figure 5.11A) for the initial, because these peaks are the typical size distributions of their osmolytes (Kaszuba et al. 2008).

The hydrodynamic radii of HSA in the presence of trehalose and sucrose varies linearly with osmolyte concentration (0.25, 0.50, and 0.75 M), and the hydrodynamic radii of HSA in the presence of trehalose were larger than that with sucrose at the same concentration of osmolytes. At 0.75 M concentration, the hydrodynamic radius of HSA in the absence and the presence of trehalose obtained in this work significantly differed by 21.85 %, suggesting that trehalose can produce a hydration shell around HSA larger than sucrose did (increased by 10.75 %). These results are indicative of sucrose and trehalose increasing the solvation sphere around the protein, perhaps because they are excluded from the protein surface (Timasheff 1993) and are also in agreement with the values obtained from the PFG-NMR experiment (Chapter 4), although the increase in hydrodynamic radii of HSA in the presence of osmolytes are not same.

In contrast to the effect of trehalose and sucrose, the particle size of HSA in the presence of glycerol only slightly changes (2.71-4.30 %) to begin with and then has a constant value upon the addition of further glycerol. The formation of hydration layer with glycerol is different from with trehalose or sucrose, because both water and osmolyte are excluded from the protein surface and a direct interaction between glycerol and polar residues on the surface of protein might occur (Auton et al. 2008).

In the stability test, at 37±3 °C, the hydrodynamic radii of HSA in all of the formulations significantly increased throughout the storage periods, especially in osmolyte formulations, where the size of HSA increased up to about 6.6 nm. However, HSA without osmolyte showed only a slight increment in size from 4.1 nm to about 4.3 nm. In contrast, at 2-8 °C and 20±3 °C the values obtained showed that the formulations in the presence of osmolytes slightly increased their particle size, but the particle size of HSA without osmolyte showed the same size as the initial stage throughout the storage periods, as shown in Table 5.6 and Figure 5.13.

The explanations for these stability data are that when HSA is stored at high temperature (37 °C), denaturation might occur. When a protein denatures, the hydrophobic residues (non-polar regions) buried in the interior of the native structure become exposed to solvent and promotes aggregation of the protein. In the absence of the osmolytes any such aggregation might be reversible but just as osmolytes can stabilise native structure perhaps they can also stabilise partially unfolded aggregates. Therefore, the particle size of protein in the denatured state might be larger than the

native state, especially in stabilised denatured state by osmolyte. These results are in excellent agreement with those from the PFG-NMR experiment (Chapter 3 and 4). The hydrodynamic radii of denatured Im9 and HSA in the presence of osmolytes also show a larger size than the native state.

In all formulations at 37±3 °C storage temperature, the extra peaks with a smaller size (less than 1 nm) were seen as well as the larger (higher than 100 nm) at 6 month storage time were greater than the initial stage, as displayed in Figure 5.14A-D. The larger peaks must have arisen from aggregates as described above, and the smaller peaks presumably came from fragments of HSA generated when some of the molecules had their polypeptides broken. Though this normally requires a catalyst some amino acid sequences are particularly prone to fragmentation, especially at elevated temperatures for long periods of time.

Nevertheless, the aggregates were detected only in DLS experiment, but not found in gel electrophoresis. This is because the DLS technique measures time-dependent fluctuations in the scattering intensity arising from particles undergoing random Brownian motion (dynamic), but Native-PAGE use the static measurement to detect the aggregates, so the aggregates might not be found in the this experiment.

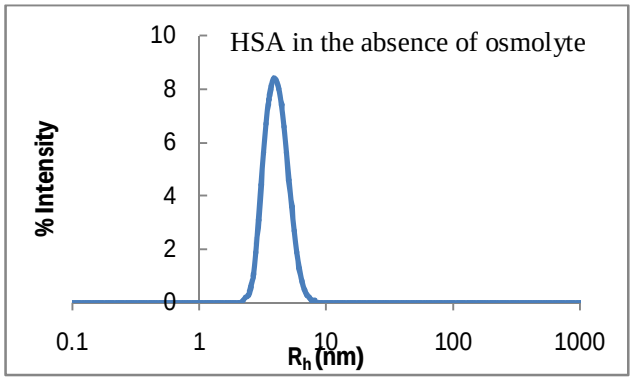

A).

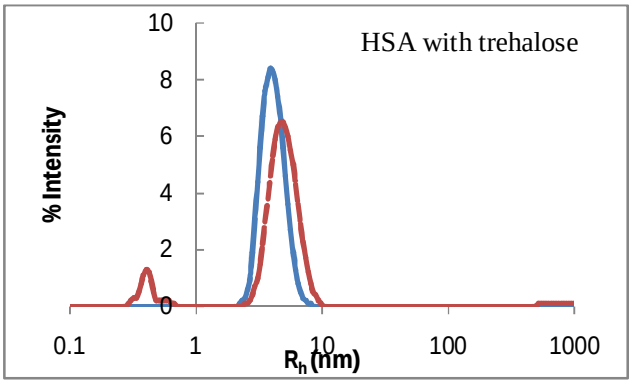

B).

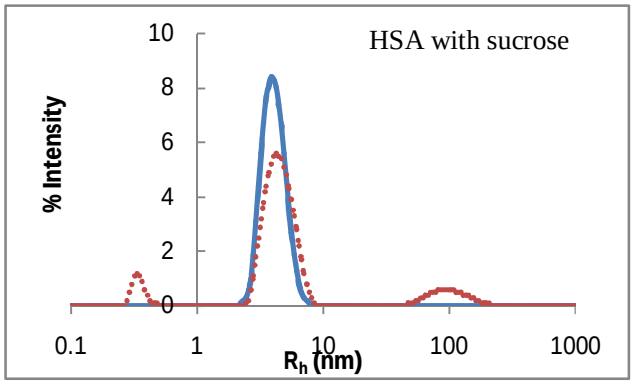

C).

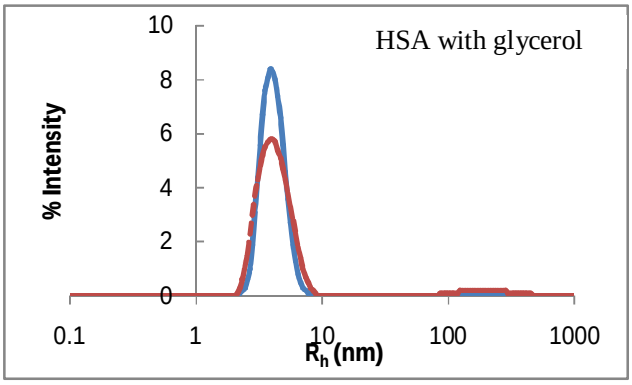

D).

Figure 5.11 Size distribution for HSA solution in the absence (solid line) and in the presence of osmolytes (0.75 M trehalose (dashed line)), 0.75 M sucrose (round dot line), and 30% glycerol (square dot line)) in 0.1 M phosphate buffer, pH 7.0 were measured by DLS at 25 °C. Extra peaks (both smaller than 1 nm and larger size than 100 nm) are the typical size distribution of these osmolytes.

Table 5.5 Hydrodynamic radii of HSA in the absence and the presence of osmolytes in different concentrations from DLS and PFG-NMR experiments. The DLS and PFG-NMR results are expressed as mean (n=1 with 5 scans and n=2, respectively) ± standard deviation.

	DLS		PFG-NMR	
Proteins	**R_h (nm)**	**SD**	**R_h (nm)**	**SD**
HSA	4.138	0.121	3.819	0.036
HSA 0.25 M Trehalose	4.526	0.088	4.687	0.122
HSA 0.50 M Trehalose	4.916	0.200	-	-
HSA 0.75 M Trehalose	5.042	0.154	-	-
HSA 0.25 M Sucrose	4.343	0.187	4.804	0.133
HSA 0.50 M Sucrose	4.466	0.079	-	-
HSA 0.75 M Sucrose	4.583	0.108	-	-
HSA 10 % Glycerol	4.266	0.143	3.781	0.053
HSA 20 % Glycerol	4.316	0.051	-	-
HSA 30 % Glycerol	4.250	0.121	-	-

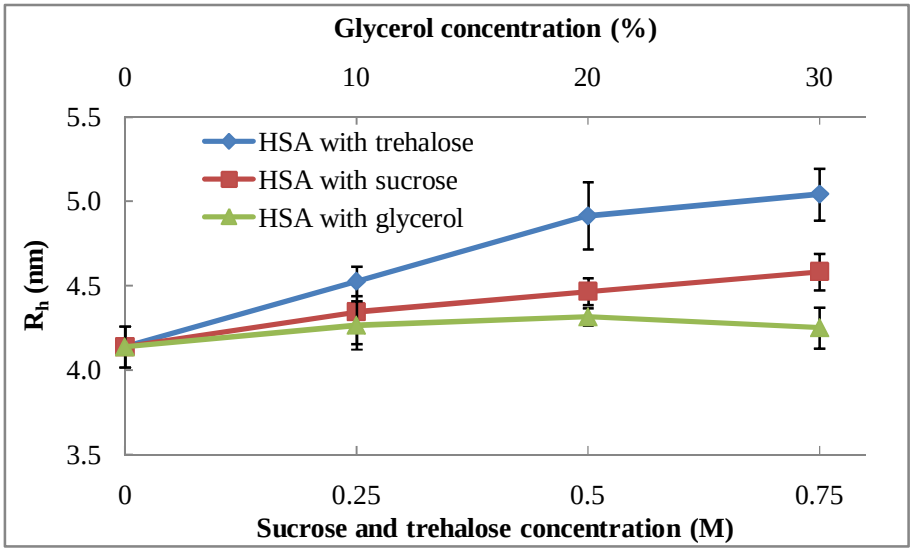

Figure 5.12 Hydrodynamic radii of HSA in the absence and the presence of osmolytes (Trehalose (◆), sucrose (■), and glycerol (▲)) in different concentrations (0.25, 0.50, 0.75 M trehalose and sucrose, and 10, 20, 30 % glycerol, respectively). The results measured by DLS at 25 °C are expressed as mean (n=1 with 5 scans) ± standard deviation.

Table 5.6 Hydrodynamic radii of HSA in the absence and the presence of osmolytes (0.75 M trehalose, 0.75 M sucrose, and 30 % glycerol) in 0.1 M phosphate buffer pH 7.0 under various storage conditions (2-8 °C, 20±3 °C, and 37±3 °C). The samples were analysed by DLS at 25 °C. All values are expressed as mean (n=1 with 5 scans) ± standard deviation in the parentheses.

	Hydrodynamic radius (nm)						
Storage time (month)	**Initial**	**1**	**2**	**3**	**4**	**5**	**6**
HSA at 2-8 °C	4.138 (0.12)	4.209	4.049	4.129	4.13	4.135	4.073
		(0.10)	(0.10)	(0.07)	(0.15)	(0.09)	(0.14)
HSA at 20±3 °C		4.015	4.101	4.084	4.049	4.097	4.136
		(0.08)	(0.14)	(0.08)	(0.07)	(0.08)	(0.08)
HSA at 37±3 °C		4.195	4.141	4.113	4.233	4.286	4.302
		(0.18)	(0.12)	(0.08)	(0.07)	(0.11)	(0.11)
HSA 0.75 M Trehalose at 2-8 °C	5.042 (0.15)	5.313	5.331	5.429	5.427	5.372	5.445
		(0.11)	(0.09)	(0.05)	(0.15)	(0.16)	(0.15)
HSA 0.75 M Trehalose at 20± 3 °C		5.394	5.284	5.386	5.473	5.699	5.728
		(0.13)	(0.10)	(0.16)	(0.13)	(0.25)	(0.22)
HSA 0.75 M Trehalose at 37±3 °C		5.569	5.621	5.928	6.43	6.539	6.667
		(0.17)	(0.10)	(0.13)	(0.15)	(0.20)	(0.26)
HSA 0.75 M Sucrose at 2-8 °C	4.583 (0.11)	4.906	4.826	4.857	4.848	4.88	4.837
		(0.10)	(0.09)	(0.08)	(0.13)	(0.18)	(0.20)
HSA 0.75 M Sucrose at 20±3 °C		4.788	4.609	4.881	4.954	5.072	5.211
		(0.11)	(0.11)	(0.06)	(0.13)	(0.15)	(0.17)
HSA 0.75 M Sucrose at37±3 °C		4.928	5.151	5.522	5.425	6.501	6.584
		(0.09)	(0.20)	(0.15)	(0.13)	(0.16)	(0.35)
HSA 30 % Glycerol at 2-8 °C	4.25 (0.12)	4.392	4.322	4.376	4.289	4.422	4.414
		(0.10)	(0.09)	(0.07)	(0.10)	(0.16)	(0.16)
HSA 30 % Glycerol at 20±3 °C		4.197	4.329	4.268	4.349	4.343	4.415
		(0.06)	(0.11)	(0.11)	(0.11)	(0.12)	(0.14)
HSA 30 % Glycerol at 37±3 °C		4.599	4.678	4.765	4.99	5.361	5.413
		(0.13)	(0.09)	(0.14)	(0.08)	(0.24)	(0.26)

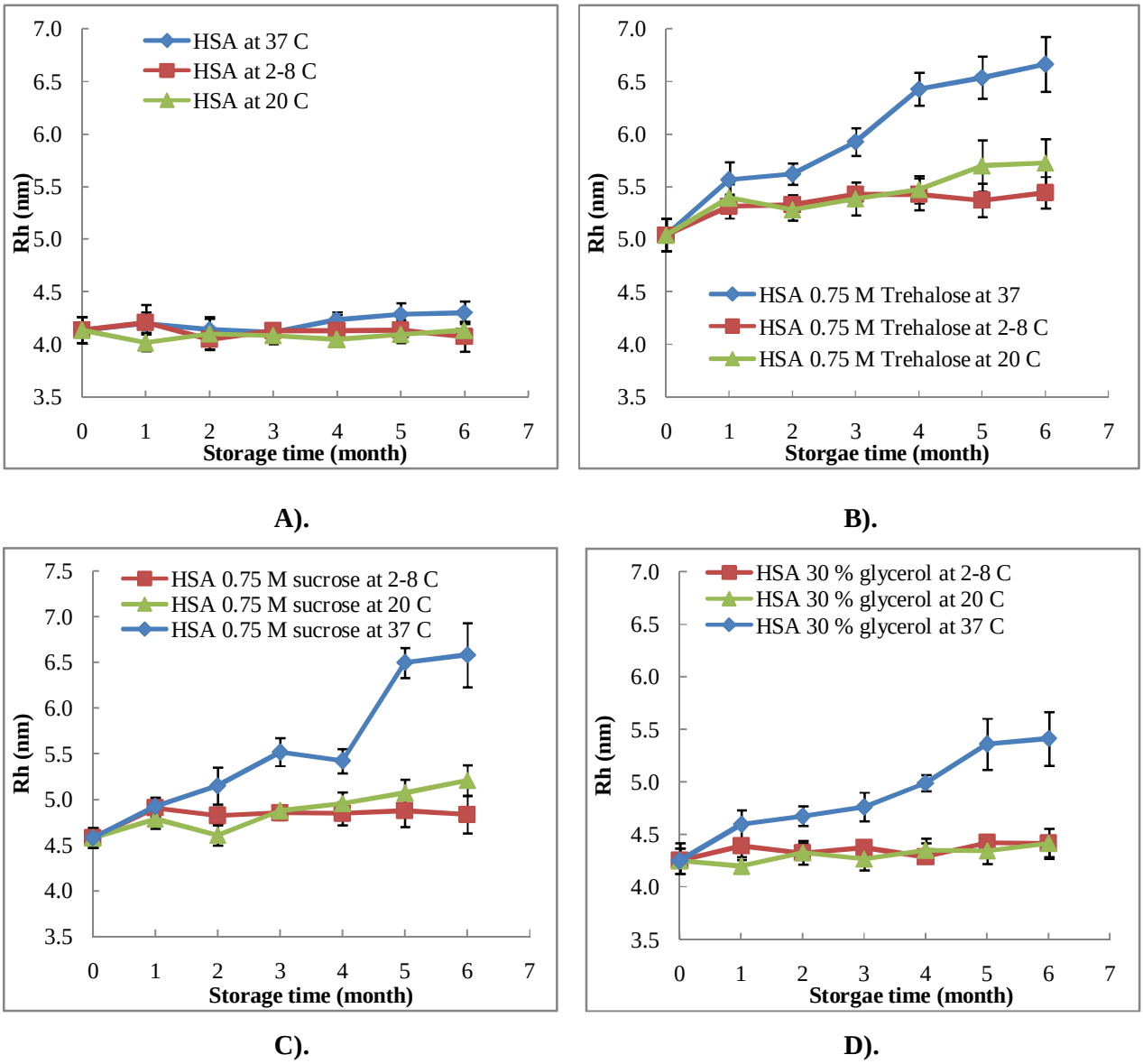

Figure 5.13 Plot of hydrodynamic radii of HSA in the absence and the presence of osmolytes (0.75 M Trehalose, 0.75 M sucrose, and 30 % glycerol) versus storage time under various storage conditions (2-8 °C, 20±3 °C, and 37±3 °C). The samples were analysed by DLS at 25 °C. All values are expressed as mean (n=1 with 5 scans) ± standard deviation in the parentheses.

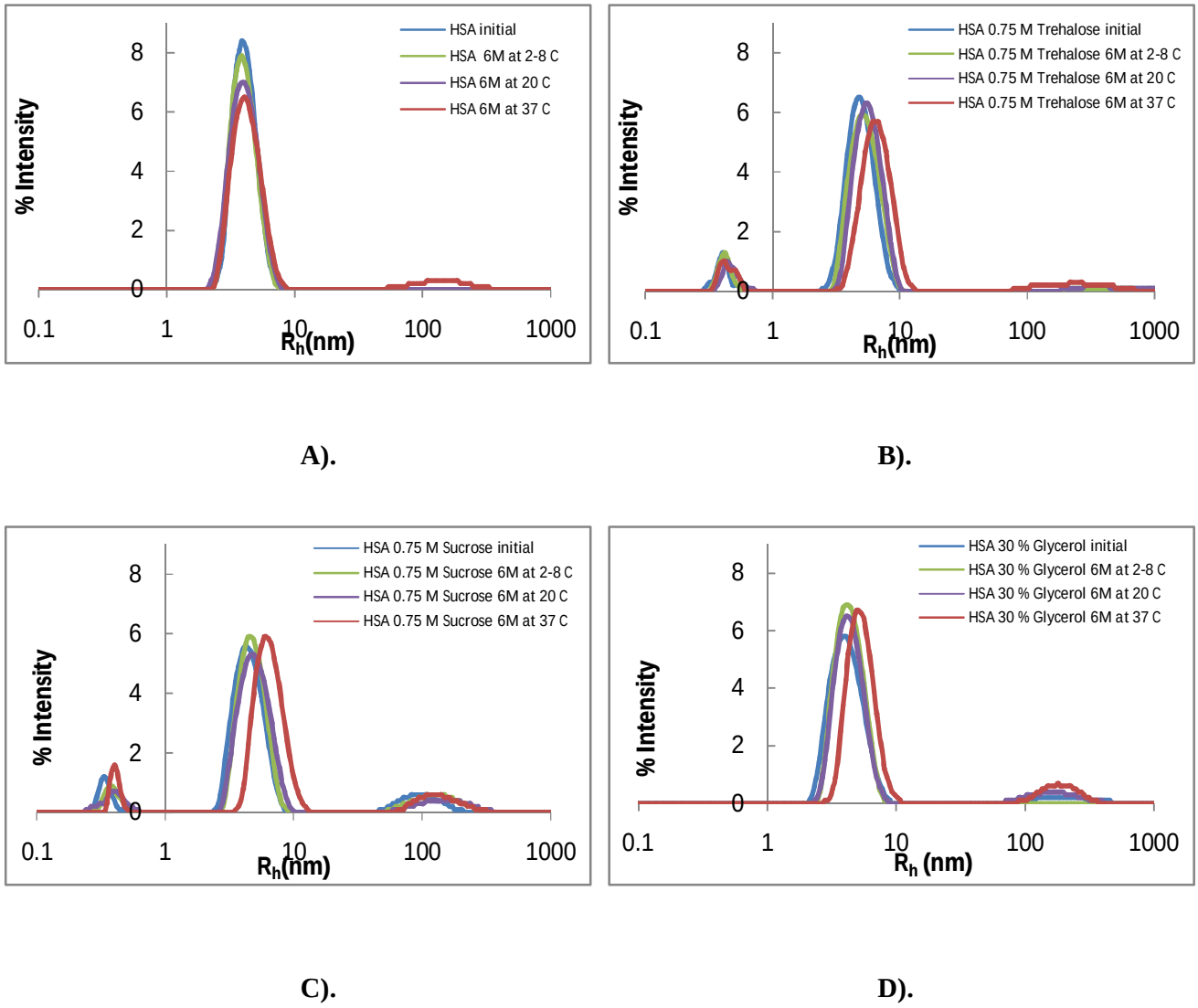

Figure 5.14 Overlays of the size distributions for HSA in the absence and the presence of osmolytes (0.75 M Trehalose, 0.75 M sucrose, and 30 % glycerol) between the initial stage and 6 month stability testing under various storage conditions (2-8 °C, 20±3 °C, and 37±3 °C). The samples were analysed by DLS at 25 °C.

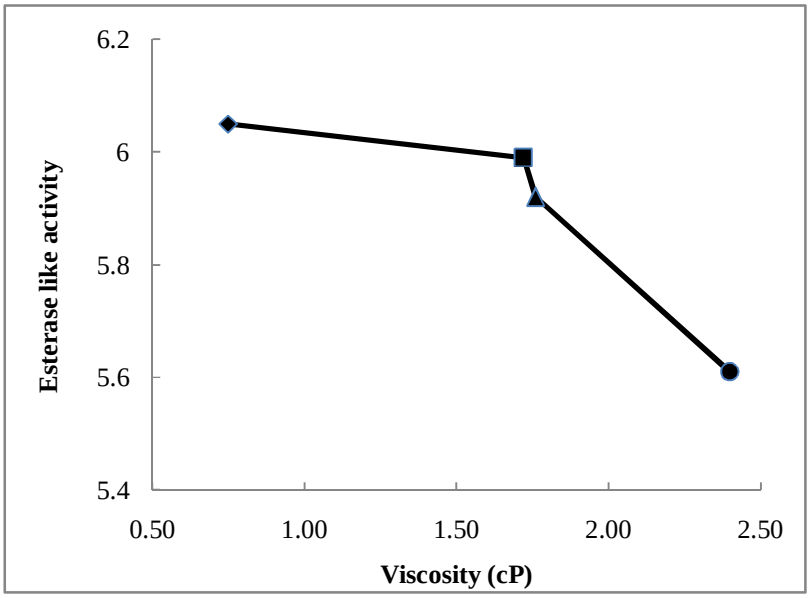

Figure 5.15 The relationship between esterase-like activity of HSA in the absence and the presence of osmolytes and solvent viscosity. (◆, buffer; ■, 0.75 M trehalose; ▲, 0.75 M sucrose; and ●, 30 % glycerol)

5.3 General Discussion and Conclusions

Normally, HSA formulations in current pharmacological use have sodium acetyltryptophan (N-Actrp) and sodium octanoate (Oct) as stabilisers and are able to maintain stability in high temperature (60 °C) for several hours. In my stability study, the stabilisers were changed to trehalose, sucrose, and glycerol and the formulations were examined in long-term stability tests performed under various storage conditions for 6 months. Although the visual appearance of HSA solution in the absence and the presence of osmolyte remained clear and yellowish without any suspended solids, the biological activities of the samples showed a significant reduction and aggregates were found in some formulations in long-term high temperature storage.

As can be seen in the results of esterase-like activity, the activity of HSA in the absence of osmolyte formulation showed high values, but lower values were found in the HSA in the presence of osmolytes. I considered this could be because of the effect of viscosity on the reaction rate of HSA with NPA. High viscosity osmolytes have been shown to slow down kinetic coefficients of ligand-protein binding interactions and biochemical processes (Almagor, Yedgar and Gavish 1992, Uribe and Sampedro 2003) and might inhibit some enzyme reactions (Jacob and Schmid 1999). This phenomenon is supported by the equation from Jacob and Schmid (Jacob and Schmid 1999), as shown in Equation 5.1;

$$k = \eta^{-1} \exp(-\triangle U/RT) \qquad \textit{Equation 5.1}$$

where k is the rate constant for the reaction, η is the viscosity of the solvent, R is the gas constant (8.314 J K^{-1} mol^{-1}), T is the absolute temperature and U is the free energy barrier imposed by solvent friction. However, as displayed in Figure 5.15, the relationship between esterase-like activity of HSA and the solvent viscosity is not linear suggesting that in addition to the viscosity effect some other factor(s) affect the rate.

The interaction of *p*-nitrophenyl acetate (NPA) and HSA on domain I and III might be perturbed by the hydration layers originating from the interaction between osmolytes and water, which totally cover the protein structure. However, since NPA is a small polar molecule it should still pass through the hydration layer to have an interaction with HSA, though this would take time and might be sufficient to slow the overall reaction. In particular, glycerol-containing samples showed poorer activity than

the other osmolytes. Besides the high viscosity of glycerol, it might be because, as noted previously (Chapter 4), glycerol is a polar molecule which has an interaction with water and polar residues at the surface of protein, so the hydration layer would be more compacted, resulting in the productive interaction between NPA and HSA being harder to achieve than with other formulations.

In the case of ligand binding property (hemin binding), the reduction of ligand binding parameters was found when the osmolytes were added to the HSA solution, suggesting this reduction correlates well with the solution viscosity, as shown in the esterase-like activity. Moreover, it was found that all formulations in every storage conditions showed low values in $\triangle G_{binding}$ and association constant (K) comparing to the initial data. A possible explanation is that hemin is a large planar nonpolar molecule, so it is difficult to access the hydration layer (polar molecules) which totally covers the HSA structure. As with the esterase-activity, the effect of glycerol on the binding of hemin is more pronounced than with trehalose and sucrose, presumably because glycerol makes the HSA more compact than other formulations.

In conclusion, the storage temperature at 2-8 °C is the most suitable condition for HSA in the absence and the presence of trehalose formulations, but not good enough for HSA in the presence of sucrose and glycerol formulations. However, the results from these stability testings still showed low values. For more accurate data, the market products, which use sodium acetyltryptophan (N-Actrp) and sodium octanoate (Oct) as stabilisers, should be studied the stability along with in-house formulations in the future. Consequently, it can be assumed that osmolytes (trehalose, sucrose, and glycerol) might not be suitable to stabilise the HSA due to the stabilisation mechanisms, although the conformational stability increases upon the addition of osmolytes, as shown in Chapter 4.

Chapter 6

General discussions and conclusions

6.1 General discussions and conclusions

In the present work, I have used two independent experimental methodologies, fluorescence spectroscopy and PFG-NMR, to investigate the conformational stabilities and the hydrodynamic radii of two proteins in order to investigate how certain osmolytes enhance protein stability. The proteins studied are Im9, a single domain protein without disulphide bridges, and HSA, a multi-domain protein with 17 intramolecular disulphide bridges. Different concentrations of the osmolytes trehalose, sucrose, and glycerol were investigated for their effect on the stabilities of Im9 and HSA towards denaturation by urea. My goal was to understand how these osmolytes influence the protein stability. Since previous works (Chapter 1) indicated that they can influence hydration layers around proteins I employed measurements of hydrodynamic radii to study this. According to previous work (Chapter 1), all of the osmolytes I used enhance protein stability by a preferential hydration or preferential exclusion mechanism, but trehalose and sucrose do so by affecting the surface tension of water, glycerol does so by a solvophobic effect coupled to a direct interaction with the protein surface.

The comparison of conformational stabilities of Im9 and HSA in the absence and the presence of osmolytes has shed new light on how trehalose, sucrose and glycerol function to enhance stability. For both Im9 (Chapter 3) and HSA (Chapter 4), unfolding curves are shifted to higher urea concentration as the osmolyte concentration increased consistent with the presence of osmolytes enhancing protein stability.

In chapter 3 I showed that the stability of Im9 was enhanced because trehalose, sucrose, and glycerol interact with the unfolded state of Im9 more than with the folded state, as indicated by the change in hydrodynamic radii of the native and denatured states. Presumably this is a consequence of the denatured state having a greater surface area than the native state. In chapter 4 I showed that the stability of HSA was also enhanced by trehalose, sucrose, and glycerol but for this protein it was less certain by

what mechanism. This is partly a consequence of its size and complexity: the tryptophan fluorescence may not have been monitoring the formation of the fully unfolded state as two of the three domains do not contain tryptophan residue, and the urea-denatured state would not have been fully extended as a consequence of the 17 disulphide bonds in the protein, though I was unable to get confirmation of this by PFG-NMR as the protein signals became too broad for accurate measurement. However, it is clear that the native state of HSA increased in size with trehalose and sucrose and decreased with glycerol similar to Im9.

$Urea_{1/2}$, which is more accurate than $\triangle G^{H2O}$, was used to compare the conformational stability of Im9 and HSA at 25 °C. $\triangle Urea_{1/2}$ of HSA with 0.75 M trehalose and 0.75 M sucrose (1.22 M and 1.58 M, respectively) were higher than that of Im9 in the same conditions (0.44 M and 0.39 M, respectively). If the increase in stability is a consequence of the greater effect of trehalose and sucrose on the denatured state than the native state, as we deduced above for Im9, then it seems likely that trehalose and sucrose affect the denatured state of HSA considerably even though I was unable to unambiguously demonstrate this as trehalose and sucrose affect $\triangle Urea_{1/2}$ for HSA more they do for Im9. The same phenomenon was also found in the presence of glycerol. $\triangle Urea_{1/2}$ of HSA with 30 % glycerol (1.19 M) was higher than that of Im9 (0.18 M), and glycerol increased the hydrodynamic radius of Im9 considerably while making the radius of native Im9 slightly smaller, implying glycerol has more impact on the denatured state of HSA than its native state as well.

The hydrodynamic radii of native Im9 and HSA were increased by increasing amounts of trehalose and sucrose due to an increased hydration layer as described by the preferential hydration model (Figure 1.5B), while glycerol caused a reduction in particle sizes of the native proteins, most likely, resulting from an indirect solvophobic effect and direct interaction of glycerol with the protein, leading to the penetration of glycerol into the protein surface and the reduction of the internal free volume of the protein, the so-called void volume (Figure 1.7). It would be interesting in future work to do this experiment with a highly hydrophobic protein to confirm this glycerol stabilisation mechanism. This is because Im9 and HSA are hydrophilic proteins, so more penetration of glycerol across the protein surface is expected, but with a hydrophobic protein glycerol might be repelled from the protein surface so that any reduction in size would be less than for Im9 and HSA.

HSA had a greater decrease in size than Im9 at high glycerol concentration (26.89 % and 6.91 %, respectively at 20 % v/v glycerol). This might be because HSA is a large macromolecule composed of three structurally homologous domains, so the large reduction in size could partly be because the domains are forced to move closer together by glycerol as well as the internal void volume being reduced, while Im9 is a small polypeptide chain that has less space inside the structure.

The impact of temperature on the protein stability showed that both $Urea_{1/2}$ and $\triangle G^{H2O}$ of Im9 at 10 °C are higher than at 25 °C, whereas the hydrodynamic radius of Im9 on its own measured at 10 °C was significantly smaller than the value observed at 25 °C, indicating that Im9 at 10 °C has a more compact shape than at 25 °C. In addition, the hydrodynamic radii of Im9 in the presence of trehalose and sucrose at 10 °C (7.71 % and 4.65%) showed a smaller increase in size than at 25 °C (21.42 % and 14.26 %, respectively), while a significant reduction in size was found upon the addition of glycerol at 10 °C (-23.4%), and a smaller decrease at 25 °C (-5.79 %). This might be because the formation of hydration layers around the protein was significantly different at these two temperatures resulting from changes in a number of parameters, such as the surface tension and density of water, and hydrogen bonding of both water and osmolyte molecules. Surface tension, which is an important factor in the stabilisation mechanism of sugars, is dependent on the temperature and tends to decrease with an increase of temperature. Moreover, the tumbling of sugars is slowed down at lower temperature, which will change the dynamics of how osmolyte molecules interact with water, and perhaps resulting in a more compact hydration layer. Finally, the density of water is higher at lower temperatures, and increase from 997.0479 to 999.7026 kg/m^3 from 25 °C to 10 °C (Lide 1990). This is only small change, but it might be sufficient to contribute to the reduction in size of stabilised protein due to dense hydration layer at 10 °C.

Furthermore, the increase of hydrodynamic radii of urea-unfolded Im9 and HSA in the absence of osmolytes is in excellent agreement with expectations from previous research (Chapter 1). The conformation of a polypeptide chain in the denatured state is greater or more expanded than that of its native state and also requires a greater number of water molecules for hydration. Im9 in its denatured state can be a fully extended peptide chain because it has no intramolecular disulphide bonds and even though the

denatured state of HSA retains considerable structure as a result of its disulphide bonds distributed throughout the protein structure, which limit the freedom of expansion of the polypeptide coil, it is still expanded compared to the native state. Possibly this disulphide-bonded HSA in the presence of urea has a partially folded structure that can interact more extensively with the osmolytes and water than can the denatured state of Im9. It would have been interesting to repeat the experiments set out in chapter 4 with HSA in which the disulphide bonds had been reduced with DTT. However, this would not be a trivial exercise as it is likely to require unfolding experiments to be carried out anaerobically.

Importantly, the denatured state has a greater solvent accessible surface area than the native state; the hydration layer is greater leading to the denatured state being more affected by osmolytes than the native state, especially in glycerol which is more favourable to contact with hydrophilic than hydrophobic residues, but in the denatured state, hydrophobic residues stay on the surface of protein rather than being buried as they generally are in the native state, so glycerol tends to stay in bulk solution, resulting in a large increase in the hydration layer. NMR results of urea-unfolded Im9 with glycerol are in accord with this hypothesis and showed that urea-unfolded Im9 with glycerol has the highest increase in hydrodynamic radius comparing with trehalose and sucrose (95.68 %, 79.41, and 77.14 % increment, respectively).

In summary, protein stabilisation mechanism by osmolytes can be explained as displayed in Figure 6.1. The two-state folding mechanisms (native state ⇆ unfolded state) are displayed in 3 categories related to the stabilisation mechanism: A). Protein in the absence of osmolyte, B). Protein in the presence of sugars, and C). Protein in the presence of polyols. In the absence of osmolyte (Figure 6.1A), a narrow hydration layer is formed around the protein in both native and denatured states. The hydrophobic residues are usually buried into the interior surface while hydrophilic residues are exposed and often are directly contacted with solvent. However, the enhanced hydration layer was found in the denatured states, because the protein structure is more unstructured and expanded and the denatured states require a much greater number of water molecules for hydration as its solvent accessible surface area is greater than that of the native state.

Preferential hydration by a surface tension effect was found in the stabilisation mechanism of sugars (trehalose and sucrose). When the surface tension of the solvent water increases, sugar concentration near a solvated protein decreases (Lee and Timasheff 1981). Sugars are thus preferentially excluded from the protein surface and the concentration of sugar near the protein surface is lower than in the bulk solution. In the sugar solution, therefore, hydration layer around the protein surface was increased. The compactness of the protein can be increased from this phenomenon, resulting to higher protein stability (Arakawa and Timasheff 1982, Timasheff 1993, Lin and Timasheff 1996), as shown in Figure 6.1B.

The preferential hydration by the solvophobic effect (Gekko and Timasheff 1981a) was found in the stabilisation mechanism of polyols (glycerol). As seen in Figure 6.1C, glycerol molecules are in the solvation layer, bulk solution and on the protein surface. In addition, the hydration layer of protein with glycerol is smaller than for a protein in the absence of the osmolytes, which is different from the sugar mechanism. This is because glycerol, which is a small polar molecule, can favourably interact with both water and hydrophilic residues on the protein surface, suggesting that glycerol molecules might penetrate into the solvation shell. However, glycerol will be preferentially repelled from the nonpolar residues on the protein surface, leading to a redistribution of water and glycerol molecules around nonpolar groups to minimise unfavourable contacts. Therefore, glycerol might have effects on protein molecules due to both preferential exclusion and a direct interaction through hydrogen bonding to the protein surface.

All of the osmolytes used in this thesis showed different efficiencies of preferential hydration and protection. The effectiveness of stabilisation in Im9 and HSA also showed a different order. Our findings reveal that within the series of osmolytes studied, trehalose is a strong stabiliser for HSA, but has nearly the same efficiency as sucrose for Im9. Glycerol has a weak effect on the stabilising effectiveness for both HSA and Im9. These results can be related to earlier research (Kumar, Attri and Venkatesu 2012). Glycerol has usually been found to be less effective in stabilising proteins than the other osmolytes due to its small size. Both trehalose and sucrose are non-reducing disaccharides, but trehalose tends to interact with other sugars (trehalose-trehalose interaction) more than sucrose does, resulting in a better ability to stabilise proteins (Kaushik and Bhat 2003).

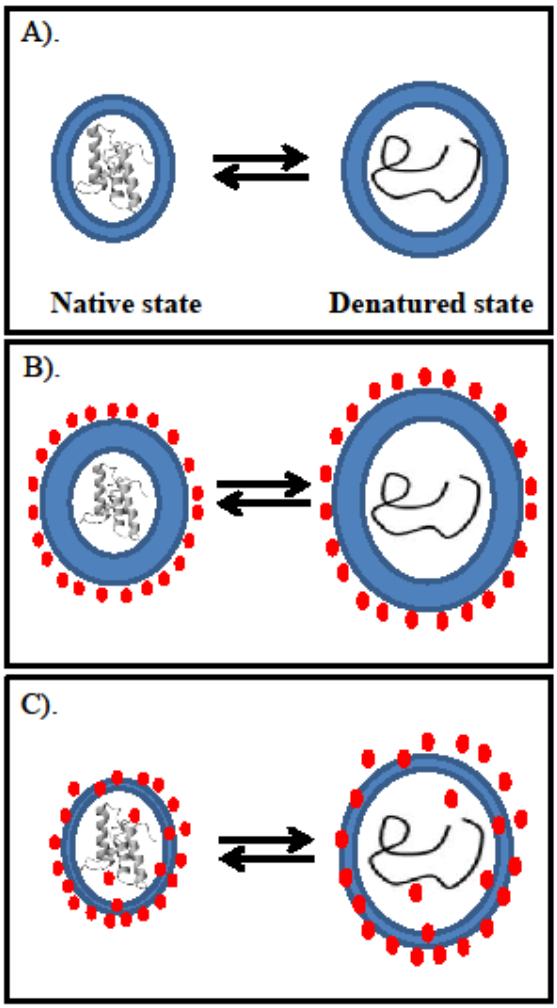

Figure 6.1 Schematic diagram of protein stabilisation mechanism by osmolytes in both native and unfolded states. A). Protein in the absence of osmolyte, B). Preferential hydration by surface tension effect (trehalose and sucrose), C). Preferential hydration by solvophobic interaction (glycerol). The blue circle around protein molecules present hydration layer and red filled circles indicate osmolyte molecules.

References

Adams, P. A. & M. C. Berman (1980) Kinetics and mechanism of the interaction between human serum albumin and monomeric haemin. *Biochemical Journal,* 191**,** 95-102.

Ahmad, B., M. Khursheed, A. Khan, S. K. Haq & R. H. Khan (2004) Intermediate formation at lower urea concentration in 'B' isomer of human serum albumin: a case study using domain specific ligands. *Biochemical and Biophysical Research Communications,* 314**,** 166-173.

Almagor, A., S. Yedgar & B. Gavish (1992) Viscous cosolvent effect on the ultrasonic absorption of bovine serum albumin. *Biophysical Journal,* 61**,** 480-486.

Anraku, M., Y. Tsurusaki, H. Watanabe, T. Maruyama, U. Kragh-Hansen & M. Otagiri (2004) Stabilizing mechanisms in commercial albumin preparations: octanoate and N-acetyl-l-tryptophanate protect human serum albumin against heat and oxidative stress. *Biochimica et Biophysica Acta (BBA) - Proteins and Proteomics,* 1702**,** 9-17.

Anraku, M., K. Yamasaki, T. Maruyama, U. Kragh-Hansen & M. Otagiri (2001) Effect of oxidative stress on the structure and function of human serum albumin. *Pharmaceutical Research,* 18**,** 632-639.

Arakawa, T., R. Bhat & S. N. Timasheff (1990) Why preferential hydration does not always stabilize the native structure of globular proteins. *Biochemistry,* 29**,** 1924-1931.

Arakawa, T. & S. N. Timasheff (1982) Stabilisation of protein-structure by sugars. *Biochemistry,* 21**,** 6536-6544.

Arakawa, T. (1984) Protein stabilization and destabilization by guanidinium salts. *Biochemistry,* 23**,** 5924-5929.

Auton, M., D. W. Bolen & J. Rosgen (2008) Structural thermodynamics of protein preferential solvation: Osmolyte solvation of proteins, aminoacids, and peptides. *Proteins-Structure Function and Bioinformatics,* 73**,** 802-813.

Auton, M., L. M. F. Holthauzen & D. W. Bolen (2007) Anatomy of energetic changes accompanying urea-induced protein denaturation. *Proceedings of the National Academy of Sciences of the United States of America,* 104**,** 15317-15322.

Baptista, R. P., S. Pedersen, G. J. M. Cabrita, D. E. Otzen, J. M. S. Cabral & E. P. Melo (2008) Thermodynamics and mechanism of cutinase stabilization by trehalose. *Biopolymers,* 89**,** 538-547.

Beaven, G. H., S. H. Chen, A. Dalbis & W. B. Gratzer (1974) A spectroscopic study of the haemin–human-serum-slbumin system. *European Journal of Biochemistry,* 41**,** 539-546.

Bell, K. L. & H. C. Brenner (1982) Phosphorescence and optically detected magnetic resonance study of the tryptophan residue in human serum albumin. *Biochemistry,* 21**,** 799-804.

Bennion, B. J. & V. Daggett (2003) The molecular basis for the chemical denaturation of proteins by urea. *Proceedings of the National Academy of Sciences of the United States of America,* 100**,** 5142-5147.

Bijelic, A. 2004. Exploring the unfolding pathways of E colicins and their immunity proteins. In *School of Chemical Sciences and Pharmacy,* 217. Norwich: University of East Anglia.

Boetzel, R., E. S. Collins, N. J. Clayden, C. Kleanthous, R. James & G. R. Moore (2003) Structural dynamics of the receptor-binding domain of colicin E9. *Faraday Discussions,* 122**,** 145-162.

Brekke, O. H. & I. Sandlie (2003) Therapeutic antibodies for human diseases at the dawn of the twenty-first century. *Nature Reviews Drug Discovery,* 2**,** 52-62.

Chalikian, T. V., J. Volker, D. Anafi & K. J. Breslauer (1997) The native and the heat-induced denatured states of α-chymotrypsinogen A: thermodynamic and spectroscopic studies. *Journal of Molecular Biology,* 274**,** 237-252.

Chi, E. Y., S. Krishnan, T. W. Randolph & J. F. Carpenter (2003) Physical stability of proteins in aqueous solution: Mechanism and driving forces in nonnative protein aggregation. *Pharmaceutical Research,* 20**,** 1325-1336.

Cistola, D. P. & D. M. Small (1991) Fatty acid distribution in systems modeling the normal and diabetic human circulation: A 13C Nuclear magnetic resonance study. *Journal of Clinical Investigation,* 87**,** 1431-1441.

Cobos, E. S. & S. E. Radford (2006) Sulfate-induced effects in the on-pathway intermediate of the bacterial immunity protein Im7. *Biochemistry,* 45**,** 2274-2282.

Cranz-Mileva, S., C. T. Friel & S. E. Radford (2005) Helix stability and hydrophobicity in the folding mechanism of the bacterial immunity protein Im9. *Protein Engineering Design & Selection,* 18**,** 41-50.

Creighton, T. E. 1997. *Protein Structure - A practical approach*. Oxford University Press.

Curry, S., H. Mandelkow, P. Brick & N. Franks (1998) Crystal structure of human serum albumin complexed with fatty acid reveals an asymmetric distribution of binding sites. *Nature structural biology,* 5**,** 827-835.

Faber-Barata, J. & M. Sola-Penna (2005) Opposing effects of two osmolytes - trehalose and glycerol - on thermal inactivation of rabbit muscle 6-phosphofructo-1-kinase. *Molecular and Cellular Biochemistry,* 269**,** 203-207.

Farruggia, B. & G. A. Pico (1999) Thermodynamic features of the chemical and thermal denaturations of human serum albumin. *International Journal of Biological Macromolecules,* 26**,** 317-323.

Fasano, M., S. Curry, E. Terreno, M. Galliano, G. Fanali, P. Narciso, S. Notari & P. Ascenzi (2005) The extraordinary ligand binding properties of human serum albumin. *Iubmb Life,* 57**,** 787-796.

Ferguson, N., A. P. Capaldi, R. James, C. Kleanthous & S. E. Radford (1999) Rapid folding with and without populated intermediates in the homologous four-helix proteins Im7 and Im9. *Journal of Molecular Biology,* 286**,** 1597-1608.

Ferguson, N., W. Li, A. P. Capaldi, C. Kleanthous & S. E. Radford (2001) Using chimeric immunity proteins to explore the energy landscape for alpha-helical protein folding. *Journal of Molecular Biology,* 307**,** 393-405.

Fersht, A. 1999. Protein stability. In *Structure and Mechanism in protein science: A guide to enzyme catalysis and protein folding,* 508-539. W.H. Freeman and company.

Frank, H. S. & F. Franks (1968) Structural approach to the solvent power of water for hydrocarbons: urea as a structure breaker. *Journal of Chemical Physics,* 48**,** 4746-&.

Friel, C. T., A. P. Capaldi & S. E. Radford (2003) Structural analysis of the rate-limiting transition states in the folding of lm7 and lm9: Similarities and differences in the folding of homologous proteins. *Journal of Molecular Biology,* 326**,** 293-305.

Galantini, L., C. Leggio, P. V. Konarev & N. V. Pavel (2010) Human serum albumin binding ibuprofen: A 3D description of the unfolding pathway in urea. *Biophysical Chemistry,* 147**,** 111-122.

Galantini, L., C. Leggio & N. V. Pavel (2008) Human Serum Albumin Unfolding: A Small-Angle X-ray Scattering and Light Scattering Study. *The Journal of Physical Chemistry B,* 112**,** 15460-15469.

Gast, K., D. Zirwer, M. Muller-Frohne & G. Damaschun (1998) Compactness of the kinetic molten globule of bovine alpha-lactalbumin: A dynamic light scattering study. *Protein Science,* 7**,** 2004-2011.

Gekko, K. & S. N. Timasheff (1981a) Mechanism of protein stabilization by glycerol: preferential hydration in glycerol-water mixtures. *Biochemistry,* 20**,** 4667-4676.

Gekko, K. (1981b) Thermodynamic and kinetic examination of protein stabilization by glycerol. *Biochemistry,* 20**,** 4677-4686.

Gonzalez-Jimenez, J. & M. Cortijo (2002) Urea-induced denaturation of human serum albumin labeled with acrylodan. *Journal of Protein Chemistry,* 21**,** 75-79.

Gorski, S. A., A. P. Capaldi, C. Kleanthous & S. E. Radford (2001) Acidic conditions stabilise intermediates populated during the folding of Im7 and Im9. *Journal of Molecular Biology,* 312**,** 849-863.

Gounarides, J. S., A. Chen & M. J. Shapiro (1999) Nuclear magnetic resonance chromatography: applications of pulse field gradient diffusion NMR to mixture analysis and ligand-receptor interactions. *Journal of Chromatography B: Biomedical Sciences and Applications,* 725**,** 79-90.

Greene, R. F. & C. N. Pace (1974) Urea and guanidine hydrochloride denaturation of Ribonuclease, Lysozyme, a-Chymotrypsin, and β-Lactoglobulin. *Journal of Biological Chemistry,* 249**,** 5388-5393.

Habib, S., M. A. Khan & H. Younus (2007) Thermal destabilization of stem bromelain by trehalose. *Protein Journal,* 26**,** 117-124.

He, X. M. & D. C. Carter (1992) Atomic structure and chemistry of human serum albumin. *Nature,* 358**,** 209-215.

Hofmeister, F. (1888) Zur Lehre von der Wirkung der Salze. *Archiv fur experimentelle Pathologie und Pharmakologie,* 24**,** 247-260.

Hua, L., R. H. Zhou, D. Thirumalai & B. J. Berne (2008) Urea denaturation by stronger dispersion interactions with proteins than water implies a 2-stage unfolding. *Proceedings of the National Academy of Sciences of the United States of America,* 105**,** 16928-16933.

ICH. 2003. ICH harmonised tripartite guideline: Stability testing of new drug substances and products Q1A(R2). In *International Conference on Harmonisation of Technical Requirements for Registration of Pharmaceuticals for Human Use, http://www.ich.org*.

Ikeda, K., Y. Kurono, Y. Ozeki & T. Yotsuyanagi (1979) Effects of drug bindings on esterase activity of human serum albumin. Dissociation constants of the complexes between the protein and drugs such as N-Arylanthranilic acids, coumarin derivatives and prostaglandins. *Chemical & Pharmaceutical Bulletin,* 27**,** 80-87.

Jackson, S. E. (1998) How do small single-domain proteins fold? *Folding & Design,* 3**,** R81-R91.

Jacob, M. & F. X. Schmid (1999) Protein Folding as a Diffusional Process. *Biochemistry,* 38**,** 13773-13779.

Johnson, C. M. & A. R. Fersht (1995) Protein stability as a function of denaturant concentration: The thermal stability of Barnase in the presence of urea. *Biochemistry,* 34**,** 6795-6804.

Jokiel, M., B. Klajnert & M. Bryszewska (2006) Use of a spectrofluorimetric method to monitor changes of human serum albumin thermal stability in the presence of polyamidoamine dendrimers. *Journal of Fluorescence,* 16**,** 149-152.

Jones, J. A., D. K. Wilkins, L. J. Smith & C. M. Dobson (1997) Characterisation of protein unfolding by NMR diffusion measurements. *Journal of Biomolecular Nmr,* 10**,** 199-203.

Kamal, J. K. A., L. Zhao & A. H. Zewail (2004) Ultrafast hydration dynamics in protein unfolding: Human serum albumin. *Proceedings of the National Academy of Sciences of the United States of America,* 101**,** 13411-13416.

Kamerzell, T. J., R. Esfandiary, S. B. Joshi, C. R. Middaugh & D. B. Volkin (2011) Protein-excipient interactions: Mechanisms and biophysical characterization applied to protein formulation development. *Advanced Drug Delivery Reviews,* 63**,** 1118-1159.

Kaszuba, M., D. McKnight, M. Connah, F. McNeil-Watson & U. Nobbmann (2008) Measuring sub nanometre sizes using dynamic light scattering. *Journal of Nanoparticle Research,* 10**,** 823-829.

Katayama, D. S., R. Nayar, D. K. Chou, J. J. Valente, J. Cooper, C. S. Henry, D. G. Vander Velde, L. Villarete, C. P. Liu & M. C. Manning (2006) Effect of buffer species on the thermally induced aggregation of interferon-tau. *Journal of Pharmaceutical Sciences,* 95**,** 1212-1226.

Kato, H., T. Saito, M. Nabeshima, K. Shimada & S. Kinugasa (2006) Assessment of diffusion coefficients of general solvents by PFG-NMR: Investigation of the sources error. *Journal of Magnetic Resonance,* 180**,** 266-273.

Kaushik, J. K. & R. Bhat (1998) Thermal stability of proteins in aqueous polyol solutions: Role of the surface tension of water in the stabilizing effect of polyols. *The Journal of Physical Chemistry B,* 102**,** 7058-7066.

Kaushik, J. K. (2003) Why is trehalose an exceptional protein stabilizer?: AN ANALYSIS OF THE THERMAL STABILITY OF PROTEINS IN THE PRESENCE OF THE COMPATIBLE OSMOLYTE TREHALOSE. *Journal of Biological Chemistry,* 278**,** 26458-26465.

Kendrick, B. S., B. S. Chang, T. Arakawa, B. Peterson, T. W. Randolph, M. C. Manning & J. F. Carpenter (1997) Preferential exclusion of sucrose from recombinant interleukin-1 receptor antagonist: Role in restricted conformational mobility and compaction of native ‰state. *Proceedings of the National Academy of Sciences,* 94**,** 11917-11922.

Kleanthous, C., U. C. Kuhlmann, A. J. Pommer, N. Ferguson, S. E. Radford, G. R. Moore, R. James & A. M. Hemmings (1999) Structural and mechanistic basis of immunity toward endonuclease colicins. *Nature structural biology,* 6**,** 243-252.

Kraghhansen, U. (1981) Molecular aspects of ligand-binding to serum albumin. *Pharmacological Reviews,* 33**,** 17-53.

Kumar, A., P. Attri & P. Venkatesu (2012) Effect of polyols on the native structure of alpha-chymotrypsin: A comparable study. *Thermochimica Acta,* 536**,** 55-62.

Kumar, R. (2009) Role of naturally occurring osmolytes in protein folding and stability. *Archives of Biochemistry and Biophysics,* 491**,** 1-6.

Kunz, W., J. Henle & B. W. Ninham (2004) '˜Zur Lehre von der Wirkung der Salze' (about the science of the effect of salts): Franz Hofmeister's historical papers. *Current Opinion in Colloid & Interface Science,* 9**,** 19-37.

Kurono, Y., I. Kushida, H. Tanaka & K. Ikeda (1992) Esterase-like activity of human serum albumin. VIII. Reaction with amino acid para-nitrophenyl esters. *Chemical & Pharmaceutical Bulletin,* 40**,** 2169-2172.

Kurono, Y., T. Maki, T. Yotsuyanagi & K. Ikeda (1979) Esterase-like activity of human serum albumin: Structure activity relationships for the reactions with phenyl acetates and para-nitrophenyl esters. *Chemical & Pharmaceutical Bulletin,* 27**,** 2781-2786.

Lakowicz, J. R. 2006a. Quenching of fluorescence. In *Principles of Fluorescence Spectroscopy,* ed. J. R. Lakowicz, 278-330. Springer.

Lakowicz, J. R. 2006b. Solvent and environmental effects. In *Principles of Fluorescence Spectroscopy,* ed. J. R. Lakowicz, 205-235. Springer.

Lapham, J., J. P. Rife, P. B. Moore & D. M. Crothers (1997) Measurement of diffusion constants for nucleic acids by NMR. *Journal of Biomolecular Nmr,* 10**,** 255-262.

Le Duff, C. S., S. B. M. Whittaker, S. E. Radford & G. R. Moore (2006) Characterisation of the conformational properties of urea-unfolded Im7: Implications for the early stages of protein folding. *Journal of Molecular Biology,* 364**,** 824-835.

Lee, J. C. & S. N. Timasheff (1981) The stabilization of proteins by sucrose. *Journal of Biological Chemistry,* 256**,** 7193-7201.

Leggio, C., L. Galantini, P. V. Konarev & N. V. Pavel (2009) Urea-induced denaturation process on defatted human serum albumin and in the presence of palmitic acid. *J Phys Chem B,* 113**,** 12590-602.

Lerbret, A., P. Bordat, F. Affouard, A. Hedoux, Y. Guinet & M. Descamps (2007) How do trehalose, maltose, and sucrose influence some structural and dynamical properties of lysozyme? Insight from molecular dynamics simulations. *Journal of Physical Chemistry B,* 111**,** 9410-9420.

Lide, D. R. 1990. *CRC handbook of chemistry and physics (70th Edn.)*. Boca Raton, FL: CRC PRESS.

Lin, J. J., J. D. Meyer, J. F. Carpenter & M. C. Manning (2009) Aggregation of human serum albumin during a thermal viral inactivation step. *International Journal of Biological Macromolecules,* 45**,** 91-96.

Lin, T. Y. & S. N. Timasheff (1996) On the role of surface tension in the stabilization of globular proteins. *Protein Science,* 5**,** 372-381.

Liu, Y. F. & D. W. Bolen (1995) The peptide backbone plays a dominant role in protien stabilisation by naturally-occurring osmolytes. *Biochemistry,* 34**,** 12884-12891.

Mackay, M. E. & N. H. Martin (1957) The stabilization of purified human albumin to heat. *Biochemical Journal,* 65**,** 284-288.

Marcus, Y. (2009) Effect of ions on the structure of water: Structure making and breaking. *Chemical Reviews,* 109**,** 1346-1370.

Matsushita, S., Y. Isima, V. T. G. Chuang, H. Watanabe, S. Tanase, T. Maruyama & M. Otagiri (2004) Functional analysis of recombinant human serum albumin domains for pharmaceutical applications. *Pharmaceutical Research,* 21**,** 1924-1932.

Means, G. E. & M. L. Bender (1975) Acetylation of human serum albumin by p-nitrophenyl acetate. *Biochemistry,* 14**,** 4989-4994.

Mehrabi, M., S. Hosseinkhani & S. Ghobadi (2008) Stabilization of firefly luciferase against thermal stress by osmolytes. *International Journal of Biological Macromolecules,* 43**,** 187-191.

Melo, E. P., L. Chen, J. M. S. Cabral, P. Fojan, S. B. Petersen & D. E. Otzen (2003) Trehalose favors a cutinase compact intermediate off-folding pathway. *Biochemistry,* 42**,** 7611-7617.

Moriyama, Y., D. Ohta, K. Hachiya, Y. Mitsui & K. Takeda (1996) Fluorescence behavior of tryptophan residues of bovine and human serum albumins in ionic surfactant solutions: A comparative study of the two and one tryptophan(s) of bovine and human albumins. *Journal of Protein Chemistry,* 15**,** 265-272.

Morton, V. L., C. T. Friel, L. R. Allen, E. Paci & S. E. Radford (2007) The effect of increasing the stability of non-native interactions on the folding landscape of the bacterial immunity protein Im9. *Journal of Molecular Biology,* 371**,** 554-568.

Muzammil, S., Y. Kumar & S. Tayyab (2000) Anion-induced stabilization of human serum albumin prevents the formation of intermediate during urea denaturation. *Proteins-Structure Function and Genetics,* 40**,** 29-38.

Myers, J. K., C. N. Pace & J. M. Scholtz (1995) Denaturant m values and heat capacity changes: Relation to changes in accessible surface areas of protein unfolding. *Protein Science,* 4**,** 2138-2148.

O'Brien, E. P., R. I. Dima, B. Brooks & D. Thirumalai (2007) Interactions between hydrophobic and ionic solutes in aqueous guanidinium chloride and urea solutions: Lessons for protein denaturation mechanism. *Journal of the American Chemical Society,* 129**,** 7346-7353.

O'Brien, E. P., G. Ziv, G. Haran, B. R. Brooks & D. Thirumalai (2008) Effects of denaturants and osmolytes on proteins are accurately predicted by the molecular transfer model. *Proceedings of the National Academy of Sciences,* 105**,** 13403-13408.

O'Connor, T. F., P. G. Debenedetti & J. D. Carbeck (2004) Simultaneous determination of structural and thermodynamic effects of carbohydrate solutes on the thermal stability of ribonuclease A. *Journal of the American Chemical Society,* 126**,** 11794-11795.

O'Connor, T. F. (2007) Stability of proteins in the presence of carbohydrates; experiments and modeling using scaled particle theory. *Biophysical Chemistry,* 127**,** 51-63.

Oliveira, A. C., L. P. Gaspar, A. T. Dapoian & J. L. Silva (1994) Arc repressor will not denature under pressure in the absence of water. *Journal of Molecular Biology,* 240**,** 184-187.

Osborne, M. J., A. L. Breeze, L. Y. Lian, A. Reilly, R. James, C. Kleanthous & G. R. Moore (1996) Three-dimensional solution structure and C-13 nuclear magnetic resonance assignments of the colicin E9 immunity protein Im9. *Biochemistry,* 35**,** 9505-9512.

Osborne, M. J., L. Y. Lian, R. Wallis, A. Reilly, R. James, C. Kleanthous & G. R. Moore (1994) Sequential assignments and identification of secondary structure elements of the Colicin E9 Immunity protein in solution by homonuclear and heteronuclear NMR. *Biochemistry,* 33**,** 12347-12355.

Pace, C. N., D. V. Laurents & J. A. Thomson (1990) pH dependence of the urea and guanidine hydrochloride denaturation of Ribonuclease A and Ribonuclease T1. *Biochemistry,* 29**,** 2564-2572.

Pace, C. N. & K. L. Shaw (2000) Linear extrapolation method of analyzing solvent denaturation curves. *Proteins-Structure Function and Genetics***,** 1-7.

Pace, C. N., F. Vajdos, L. Fee, G. Grimsley & T. Gray (1995) How to measure and predict the molar absorption coefficient of a protein. *Protein Science,* 4**,** 2411-2423.

Peresada, S., A. Tonielli, R. Morici & C. S. Johnson (1999) Diffusion ordered nuclear magnetic resonance spectroscopy: principles and applications. *Progress in Nuclear Magnetic Resonance Spectroscopy,* 34**,** 203-256.

Price, W. S. 2009. Diffusion and its measurement. In *NMR studies of translational motion*, 1-68. Cambridge University Press.

Priev, A., A. Almagor, S. Yedgar & B. Gavish (1996) Glycerol decreases the volume and compressibility of protein interior. *Biochemistry,* 35**,** 2061-2066.

Roberto, D. L., S. P. Cristina & H. H. Philippe (2004) Trehalose-protein interaction in aqueous solution. *Proteins: Structure, Function, and Bioinformatics,* 55**,** 177-186.

Rosenfeld, M. & D. M. Surgenor (1950) Interaction between human serum albumin and ferriprotoporphyrin-IX. *Journal of Biological Chemistry,* 183**,** 663-677.

Rowe, R. C. S., Marian E. 2009. *Handbook of Pharmaceutical Excipients*. London: Pharmaceutical Press.

Ruiz, L., N. Reyes, K. Aroche, R. Báez, R. Aldana & E. Hardy (2006) Some factors affecting the stability of interferon alpha 2b in solution. *Biologicals,* 34**,** 15-19.

Salahuddin, P. (2008) Urea and acid induced unfolding of fatted and defatted human serum albumin. *Protein and Peptide Letters,* 15**,** 826-833.

Scharnagl, C., M. Reif & J. Friedrich (2005) Stability of proteins: Temperature, pressure and the role of the solvent. *Biochimica et Biophysica Acta (BBA) - Proteins and Proteomics,* 1749**,** 187-213.

Shukla, D., C. P. Schneider & B. L. Trout (2011) Molecular level insight into intra-solvent interaction effects on protein stability and aggregation. *Advanced Drug Delivery Reviews,* 63**,** 1074-1085.

Simard, J. R., P. A. Zunszain, J. A. Hamilton & S. Curry (2006) Location of high and low affinity fatty acid binding sites on human serum albumin revealed by NMR drug-competition analysis. *Journal of Molecular Biology,* 361**,** 336-351.

Stark, G. R., W. H. Stein & S. Moore (1960) Reactions of the Cyanate Present in Aqueous Urea with Amino Acids and Proteins. *Journal of Biological Chemistry,* 235**,** 3177-3181.

Stumpe, M. C. & H. Grubmuller (2007) Interaction of urea with amino acids: Implications for urea-induced protein denaturation. *Journal of the American Chemical Society,* 129**,** 16126-16131.

Sugio, S., A. Kashima, S. Mochizuki, M. Noda & K. Kobayashi (1999) Crystal structure of human serum albumin at 2.5 angstrom resolution. *Protein Engineering,* 12**,** 439-446.

Tadeo, X., B. Lopez-Mendez, D. Castano, T. Trigueros & O. Millet (2009) Protein stabilization and the Hofmeister effect: The role of hydrophobic solvation. *Biophysical Journal,* 97**,** 2595-2603.

Tanford, C. (1962) Contribution of hydrophobic interactions to the stability of the globular conformation of proteins. *Journal of the American Chemical Society,* 84**,** 4240-4247.

Tanford, C. (1964) Isothermal unfolding of globular proteins in aqueous urea solutions. *Journal of the American Chemical Society,* 86**,** 2050-2059.

Tezuka-Kawakami, T., C. Gell, D. J. Brockwell, S. E. Radford & D. A. Smith (2006) Urea-induced unfolding of the immunity protein Im9 monitored by spFRET. *Biophysical Journal,* 91**,** L42-L44.

Timasheff, S. N. (1993) The control of protein stability and association by weak interactions with water: How do solvents affects these processes? *Annual Review of Biophysics and Biomolecular Structure,* 22**,** 67-97.

Timasheff, S. N. (2002) Protein-solvent preferential interactions, protein hydration, and the modulation of biochemical reactions by solvent components. *Proceedings of the National Academy of Sciences of the United States of America,* 99**,** 9721-9726.

Timasheff, S. N., Arakawa, T. 1997. Stabilisation of protein structure by solvents. In *Protein structure: A practical approach,* ed. T. E. Crieighton, 349-364. Oxford University Press.

Timasheff, S. N., D. S. E. Frederic M. Richards & S. K. Peter. 1998. Control of protein stability and reactions by weakly interacting cosolvents: The simplicity of the complicated. In *Advances in protein chemistry,* 355-432. Academic Press.

TiradoRives, J., M. Orozco & W. L. Jorgensen (1997) Molecular dynamics simulations of the unfolding of barnase in water and 8 M aqueous urea. *Biochemistry,* 36**,** 7313-7329.

Uribe, S. & J. Sampedro (2003) Measuring solution viscosity and its effect on enzyme activity. *Biological Procedures Online,* 5**,** 108-115.

Vagenende, V., M. G. S. Yap & B. L. Trout (2009) Mechanisms of protein stabilization and prevention of protein aggregation by glycerol. *Biochemistry,* 48**,** 11084-96.

Varshney, A., B. Ahmad & R. H. Khan (2008) Comparative studies of unfolding and binding of ligands to human serum albumin in the presence of fatty acid: Spectroscopic approach. *International Journal of Biological Macromolecules,* 42**,** 483-490.

Vivian, J. T. & P. R. Callis (2001) Mechanisms of tryptophan fluorescence shifts in proteins. *Biophysical Journal,* 80**,** 2093-2109.

Wallevik, K. (1973) Reversible denaturation of Human serum albumin by pH, temperature, and guanidine hydrochloride followed by optical rotation. *Journal of Biological Chemistry,* 248**,** 2650-2655.

Wallis, R., K. Y. Leung, M. J. Osborne, R. James, G. R. Moore & C. Kleanthous (1998) Specificity in protein-protein recognition: Conserved Im9 residues are the major determinants of stability in the colicin E9 DNase-Tm9 complex. *Biochemistry,* 37**,** 476-485.

Wallis, R., G. R. Moore, R. James & C. Kleanthous (1995) Protein-protein interactions in colicin E9 DNase-immunity protein complexes. 1. Diffusion-controlled association and femtomolar binding for the cognate complex. *Biochemistry,* 34**,** 13743-13750.

Wallis, R., G. R. Moore, C. Kleanthous & R. James (1992a) Molecular analysis of the protein-protein interaction between the E9-immunity protein and colicin-E9. *European Journal of Biochemistry,* 210**,** 923-930.

Wallis, R., A. Reilly, A. Rowe, G. R. Moore, R. James & C. Kleanthous (1992b) In vivo and in vitro characterization of overproduced colicin E9 immunity protein. *European Journal of Biochemistry,* 207**,** 687-695.

Wallqvist, A., D. G. Covell & D. Thirumalai (1998) Hydrophobic interactions in aqueous urea solutions with implications for the mechanism of protein denaturation. *Journal of the American Chemical Society,* 120**,** 427-428.

Wang, A. J. & D. W. Bolen (1997) A naturally occurring protective system in urea-rich cells: Mechanism of osmolyte protection of proteins against urea denaturation. *Biochemistry,* 36**,** 9101-9108.

Wang, W. (1999) Instability, stabilization, and formulation of liquid protein pharmaceuticals. *International Journal of Pharmaceutics,* 185**,** 129-188.

Wardell, M., Z. Wang, J. X. Ho, J. Robert, F. Ruker, J. Ruble & D. C. Carter (2002) The Atomic Structure of Human Methemalbumin at 1.9 A. *Biochemical and Biophysical Research Communications,* 291**,** 813-819.

Watanabe, H., S. Tanase, K. Nakajou, T. Maruyama, U. Kragh-Hansen & M. Otagiri (2000) Role of Arg-410 and Tyr-411 in human serum albumin for ligand binding and esterase-like activity. *Biochemical Journal,* 349**,** 813-819.

Wilkins, D. K., S. B. Grimshaw, V. Receveur, C. M. Dobson, J. A. Jones & L. J. Smith (1999) Hydrodynamic radii of native and denatured proteins measured by pulse field gradient NMR techniques. *Biochemistry,* 38**,** 16424-16431.

Xie, G. F. & S. N. Timasheff (1997) The thermodynamic mechanism of protein stabilization by trehalose. *Biophysical Chemistry,* 64**,** 25-43.

Yang, Z. X., P. Xiu, B. Y. Shi, L. Hua & R. H. Zhou (2012) Coherent microscopic picture for urea-induced denaturation of proteins. *Journal of Physical Chemistry B,* 116**,** 8856-8862.

Yao, M. & D. W. Bolen (1995) How valid are denaturant-induced unfolding free energy measurements? Level of conformance to common assumptions over an extended range of ribonuclease A Stability. *Biochemistry,* 34**,** 3771-3781.

Zhang, Y. & P. S. Cremer (2006) Interactions between macromolecules and ions: the Hofmeister series. *Current Opinion in Chemical Biology,* 10**,** 658-663.

Zou, Q., B. J. Bennion, V. Daggett & K. P. Murphy (2002) The molecular mechanism of stabilization of proteins by TMAO and its ability to counteract the effects of urea. *Journal of the American Chemical Society,* 124**,** 1192-1202.

Zunszain, P. A., J. Ghuman, T. Komatsu, E. Tsuchida & S. Curry (2003) Crystal structural analysis of human serum albumin complexed with hemin and fatty acid. *BMC structural biology,* 3**,** 6.

Appendix A

Pulsed-field gradient NMR (PFG-NMR) experiment

Pulsed-field gradient NMR (PFG-NMR) technique is used for measuring the translational diffusion coefficients (D_t) which are inversely proportional to hydrodynamic radius as described by the Stoke-Einstein equation:

$$\mathbf{D_t = kT / 6\pi\eta R_h} \qquad \textit{Equation 2.7}$$

In practice, the pulsed-field gradients are generated by passing current through the gradient coils in the NMR probe and normally applied along the z-axis. The different gradient strengths were applied, and a series of 1D H NMR with varied pulsed-filed gradient was obtained as shown in the Figure A.1 A.

The percentages of diffusion gradients were optimized for each sample to give a total decay in the protein signal of between 80 % and 90 %. Each measurement was repeated many scans to improve the signal to noise ratio. Over the series of the diffusion experiment, the intensities of protein and osmolytes will decay exponentially with the square of the gradient area according to Equation 2.8. The decay rates of the exponential curves for the protein and osmolytes are proportional to their diffusion coefficient. By taking the natural log of both sides of Equation 2.8, a linear equation results, and D is calculated from the slope as displayed in Figure A.1 B and C.

$$\mathbf{I = I_o \exp [-D (\gamma\delta G)^2 (\Delta - \delta/3)]} \qquad \textit{Equation 2.8}$$

where,

I_o = Intensity without magnetic field gradient;

I = Intensity with magnetic field gradient;

D = Diffusion coefficient;

γ = Gyromagnetic ratio;

δ = Pulse field gradient duration;

G = Gradient strength;

Δ = Time between the pulse field gradient pulses.

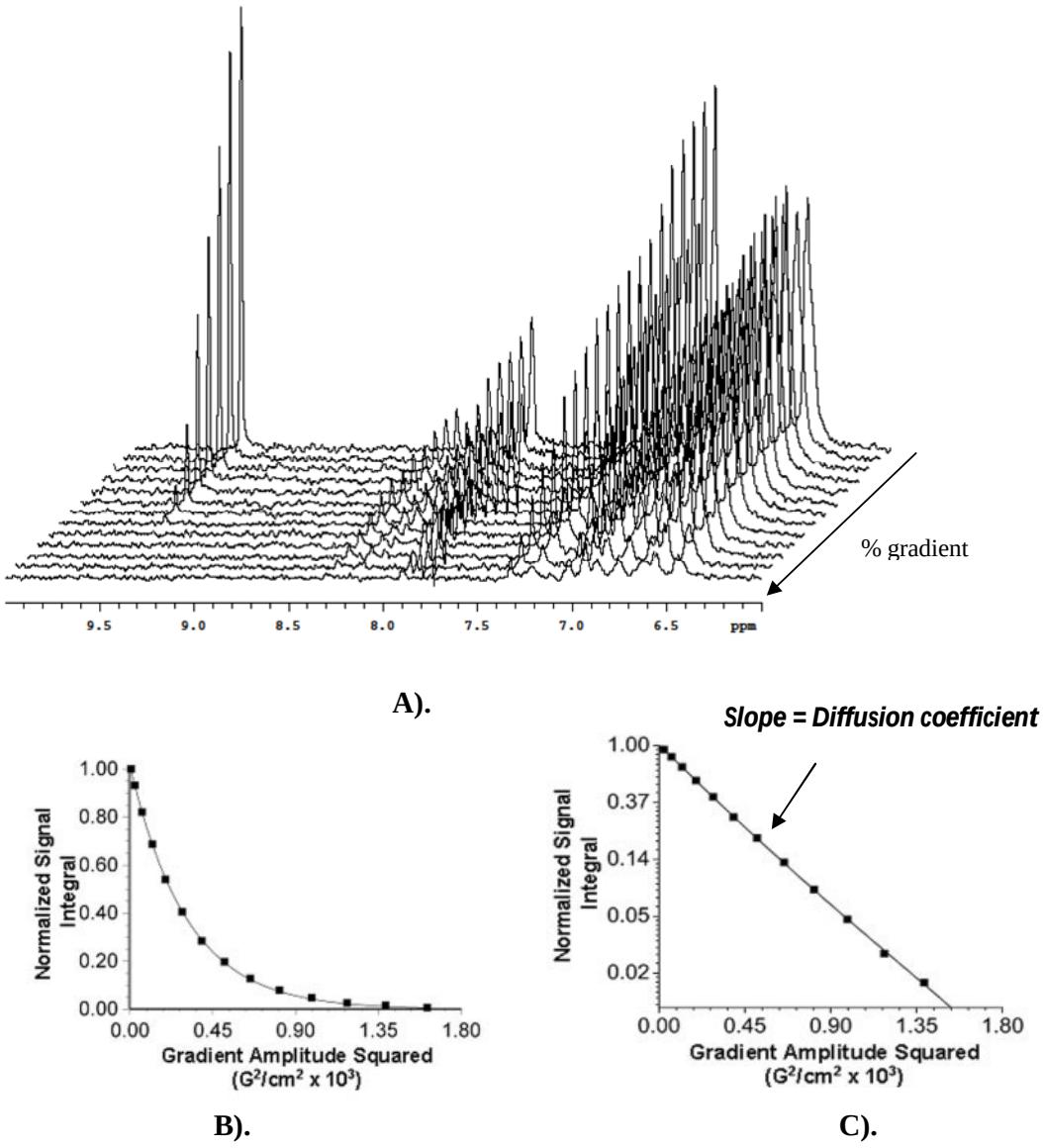

Figure A.1 Effect of pulse-field gradients on NMR spectra in a diffusion experiment. A). A series of 1D ^{1}H NMR diffusion spectra obtained from Im9 in the presence of acetaldehyde. Im9 solution (1 mM) was prepared in deuterated phosphate buffer solution pH 7.0 with 40 µl of 1 % acetaldehyde and measured by Unity*Inova* 500 MHz spectrometer at 25 °C. The diffusion gradients were varied from minimum to maximum strength. B). The signal integral of the Im9 protein as a function of the gradient amplitude squared. From the Equation 2.8, the NMR data can be shown in the exponential fit. C). By taking the natural log of both sides of Equation 2.8, the data in B. (exponential fit) transform to the linear fit of Equation 2.8. The diffusion coefficient can be determined from the slope of the line.

As displayed in Equation 2.7, viscosity of the solution is an important parameter in diffusion coefficient interpretation. In order to overcome this, an internal radius standard was chosen to use as a viscosity probe by adding to the protein solution, so protein and internal radius standard were placed in the measurement solution together. The measured diffusion coefficient for the protein was obtained by integrating the aromatic region and aliphatic region and converted to hydrodynamic radius by comparing with internal radius standard. The hydrodynamic radius for the protein can be calculated relative to known hydrodynamic radius of internal radius standard and the ratio between the measured diffusion coefficient of internal radius standard and protein, as in this Equation 2.9 (Wilkins et al. 1999).

$$\mathbf{R_{h\ protein}} = \frac{\mathbf{D_{ref}}}{\mathbf{D_{Protein}}} \mathbf{x}\ \mathbf{R_{h\ ref}} \qquad \textit{Equation 2.9}$$

where,

$\mathbf{R_{h\ protein}}$ = the hydrodynamic radius of the protein;

$\mathbf{R_{h\ ref}}$ = the hydrodynamic radius of the internal radius standard;

$\mathbf{D_{Protein}}$ = the diffusion coefficient of the protein;

$\mathbf{D_{ref}}$ = the diffusion coefficient of the internal radius standard.

In general, dioxane is the best choice of internal radius standard in PFG-NMR experiment ($R_{h\ dioxane}$=2.12 Å), because it is an inert substance and has low interaction with biological products. However, in some cases, dioxane cannot be used in the experiment, the interaction between protein and internal radius standard needs to be studied by using the diffusion rate constant experiment (Lapham et al. 1997).

An alternative data processing of PFG-NMR experiment is pseudo two dimensional (2D) DOSY (Diffusion ordered spectroscopy). The data can be shown in a two dimensional (2D) NMR spectrum with chemical shift in x-axis and calculated diffusion coefficients in y-axis as displayed in Figure A.2. Therefore, average diffusion coefficients can be calculated from the chosen protein signals and transformed to hydrodynamic radius as in this Equation 2.9.

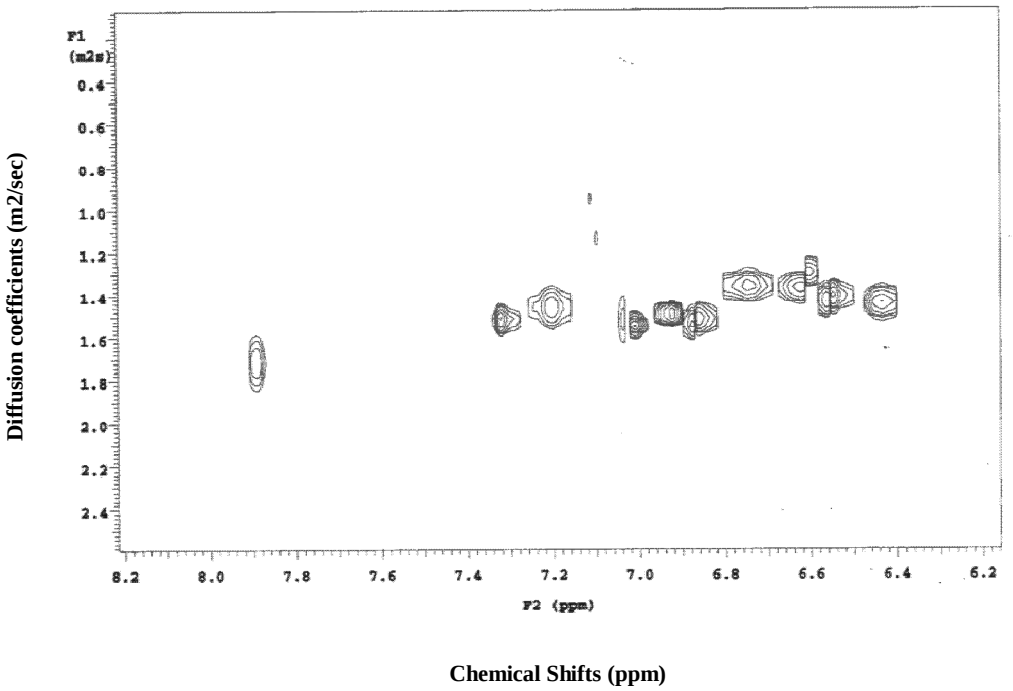

Figure A.2 DOSY (Diffusion ordered spectroscopy) displayed for a solution of Im9 protein were plotted between diffusion coefficients (m^2/sec) (y-axis) versus chemical shift (ppm) (x-axis).